

## **INFORMATION TO USERS**

**This manuscript has been reproduced from the microfilm master. UMI films the text directly from the original or copy submitted. Thus, some thesis and dissertation copies are in typewriter face, while others may be from any type of computer printer.**

**The quality of this reproduction is dependent upon the quality of the copy submitted. Broken or indistinct print, colored or poor quality illustrations and photographs, print bleedthrough, substandard margins, and improper alignment can adversely affect reproduction.**

**In the unlikely event that the author did not send UMI a complete manuscript and there are missing pages, these will be noted. Also, if unauthorized copyright material had to be removed, a note will indicate the deletion.**

**Oversize materials (e.g., maps, drawings, charts) are reproduced by sectioning the original, beginning at the upper left-hand corner and continuing from left to right in equal sections with small overlaps.**

**Photographs included in the original manuscript have been reproduced xerographically in this copy. Higher quality 6" x 9" black and white photographic prints are available for any photographs or illustrations appearing in this copy for an additional charge. Contact UMI directly to order.**

**ProQuest Information and Learning  
300 North Zeeb Road, Ann Arbor, MI 48106-1346 USA  
800-521-0600**

**UMI<sup>®</sup>**



UNIVERSITY OF CALIFORNIA

SANTA BARBARA

**High-Speed Optical Systems  
Based on Electroabsorption Modulators**

A Dissertation submitted in partial satisfaction  
of the requirements for the degree of

Doctor of Philosophy

in

Electrical and Computer Engineering

by

Volkan Kaman

Committee in Charge:

Professor John E. Bowers, Chairperson

Professor Dan J. Blumenthal

Professor Nadir Dagi

Professor Michael Melliari-Smith

December 2000

UMI Number: 3020284

Copyright 2000 by  
Kaman, Volkan

All rights reserved.

UMI<sup>®</sup>

---

UMI Microform 3020284

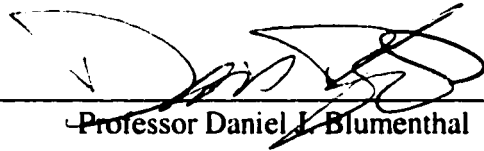
Copyright 2001 by Bell & Howell Information and Learning Company.

All rights reserved. This microform edition is protected against  
unauthorized copying under Title 17, United States Code.

---

Bell & Howell Information and Learning Company  
300 North Zeeb Road  
P.O. Box 1346  
Ann Arbor, MI 48106-1346

The dissertation of Volkan Kaman is approved



---

Professor Daniel L. Blumenthal



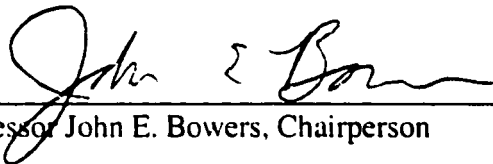
---

Professor Nadir Dagli



---

Professor Michael Melliar-Smith



---

Professor John E. Bowers, Chairperson

December 2000

**High-Speed Optical Systems**  
**Based on Electroabsorption Modulators**

Copyright © by  
Volkan Kaman  
All rights reserved  
December 2000

Department of Electrical and Computer Engineering  
University of California, Santa Barbara  
Santa Barbara, CA 93106

*Dedicated to my parents and Lisa...*

## ACKNOWLEDGEMENTS

The five years I spent at the University of California, Santa Barbara has been a memorable, stimulating, challenging and a great learning experience. I consider myself very fortunate for being a part of this university and for interacting with various brilliant people.

I am first of all grateful to my advisor Professor John E. Bowers for giving me the opportunity to be a part of his research group. Without his guidance, support and experience in this field, none of this work would have been possible. I would also like to acknowledge my committee members, Professors Daniel J. Blumenthal, Nadir Dagli and Michael Melliari-Smith for accepting to be on my committee and for their valuable discussions and suggestions.

Tom Reynolds deserves a lot of credit for not only his help and guidance even after he left the university, but also for being a good friend. I owe Anders Petersen for teaching me the art of microwave packaging and introducing me to basic system measurements. I am also grateful to Adrian Keating for his friendship and valuable discussions on optical systems. Shengzhong Zhang and Yi-Jen Chiu are two key and brilliant people who have made this dissertation possible by designing and fabricating the electroabsorption modulators.

There are several other people who have not only helped me in various aspects throughout the years, but also have been good friends. These include Hsu-Feng Chou, Siegfried Fleischer, Aaron Hawkins, Adil Karim, Chris LaBounty, Daniel Lasaosa, Thomas Liljeberg, Bin Liu, Peter Ohlen, Bengt-Eric Olsson, Joachim Piprek, Rajeev Ram, Lavanya Rau, Gerry Robinson, Holger Schmidt and Kehl Sink. I would also like to thank Vickie Edwards, Christina Loomis, Diana Thurman, and Cortney Wagner for their continuous help.

Finally, I would like to thank my family for their continuous support and love. My years spent here in Santa Barbara could never have been the same without the friendship, love and support of Lisa Porras.



## VITA

**August 1991 –  
June 1995**      **B. S. Electrical Engineering,  
Cornell University, Ithaca, New York**

**September 1995 –  
June 1997**      **M. S. Electrical and Computer Engineering,  
University of California, Santa Barbara**

**June 1998 –  
September 1998**      **Technical Consultant,  
Terabit Technology, Goleta, California**

**June 1997 –  
December 2000**      **Ph. D. Electrical and Computer Engineering,  
University of California, Santa Barbara**

## PUBLICATIONS

1. V. Kaman, Y. J. Chiu, T. Liljeberg, S. Z. Zhang and J. E. Bowers, "A compact 40 Gbit/s demultiplexing receiver based on integrated tandem electroabsorption modulators," to be published in *Electron. Lett.*, 2000.
2. Y. J. Chiu, V. Kaman, S. Z. Zhang and J. E. Bowers, "Distributed effects model for traveling-wave electroabsorption modulator design," submitted to *Photonics Tech. Lett.*, 2000.
3. Y. J. Chiu, V. Kaman, P. Abraham, S. Z. Zhang and J. E. Bowers, "Low-bias and high-saturation-power traveling-wave electroabsorption modulator by using InGaAsP/InGaAsP MQW," to be presented at *LEOS '00*, paper TuX4, 2000.
4. V. Kaman, Y. J. Chiu, T. Liljeberg, S. Z. Zhang and J. E. Bowers, "Integrated tandem traveling-wave electroabsorption modulators for > 100 Gbit/s OTDM applications," *IEEE Photonics Tech. Lett.*, vol. 12, November 2000.
5. V. Kaman, and J. E. Bowers, "120 Gbit/s OTDM system using electroabsorption transmitter and demultiplexer operating at 30 GHz," *Electron. Lett.*, vol. 36, pp. 1477-1479, 2000.
6. V. Kaman, Y. J. Chiu, T. Liljeberg, S. Z. Zhang and J. E. Bowers, "Integrated tandem electroabsorption modulators for high-speed OTDM applications," *MWP '00 Technical Digest*, paper , 2000.
7. V. Kaman, A. J. Keating, S. Z. Zhang and J. E. Bowers, "Electroabsorption modulator as a compact OTDM demultiplexing receiver," *ECOC '00 Technical Digest*, paper 9.4.6, 2000.
8. D. J. Blumenthal, B. E. Olsson, G. Rossi, T. Dimmick, L. Rau, M. Masanovic, O. Lavrova, R. Doshi, O. Jerphagnon, J. E. Bowers, V. Kaman, L. A. Coldren, and J. Barton, "All-optical label swapping networks and technologies," submitted to *IEEE J. of Lightwave Tech.*, Invited paper, 2000.
9. V. Kaman, Y. J. Chiu, S. Z. Zhang, and J. E. Bowers, "3.7 ps pulse generation at  $\geq 30$  GHz by dual-drive electroabsorption modulator," *Electron. Lett.*, vol. 36, pp. 1130-1132, 2000.
10. V. Kaman, A. J. Keating, S. Z. Zhang and J. E. Bowers, "Simultaneous OTDM demultiplexing and detection using an electroabsorption modulator," *IEEE Photonics Tech. Lett.*, vol. 12, pp. 711-713, 2000.
11. B. E. Olsson, P. Ohlen, L. Rau, G. Rossi, O. Jerphagnon, R. Doshi, D. S. Humphries, D. J. Blumenthal, V. Kaman and J. E. Bowers, "Wavelength routing of 40 Gbit/s packets with 2.5 Gbit/s header erasure/rewriting using an all-fiber wavelength converter," *Electron. Lett.*, vol. 36, pp. 345-347, 2000.
12. B. Mason, G. A. Fish, V. Kaman, J. Barton, L. A. Coldren, S. P. DenBaars and J. Bowers, "Characteristics of sampled grating DBR lasers with integrated semiconductor amplifiers and electroabsorption modulators," *OFC '00 Technical Digest*, pp. 193-195, 2000.
13. Y. J. Chiu, S. Z. Zhang, V. Kaman, J. P. Ibbetson, J. E. Bowers and U. K. Mishra, "Bias dependent performance of 1.55  $\mu\text{m}$  absorption high-speed n-i-n photodetectors using low-temperature grown GaAs," *LEOS '99 Technical Digest*, pp. 868-869, 1999.

14. V. Kaman, T. Reynolds, A. Petersen and J. E. Bowers, "A 100-kHz to 50-GHz traveling-wave amplifier IC module," *IEEE Microwave and Guided Wave Lett.*, vol. 9, pp. 416-418, 1999.
15. B. E. Olsson, P. Ohlen, L. Rau, G. Rossi, O. Jerphagnon, R. Doshi, D. S. Humphries, D. J. Blumenthal, V. Kaman and J. E. Bowers, "Wavelength routing of 40 Gbit/s packets with 2.5 Gbit/s header erasure/rewriting using an all-fiber wavelength converter," *ECOC '99 Technical Digest*, post-deadline, pp. 52-53, 1999.
16. V. Kaman, S. Z. Zhang, A. J. Keating and J. E. Bowers, "High-speed operation of traveling-wave electroabsorption modulator," *Electron. Lett.*, vol. 35, pp. 993-995, 1999.
17. S. Z. Zhang, V. Kaman, A. Keating, Y. J. Chiu, P. Abraham and J. E. Bowers, "30 Gbit/s operation of a traveling-wave electroabsorption modulator," *OFC '99 Technical Digest*, pp. 290-292, 1999.
18. J. Piprek, K. Takiguchi, A. Black, P. Abraham, A. Keating, V. Kaman, S. Zhang and J. E. Bowers, "Analog modulation of 1.55  $\mu\text{m}$  vertical-cavity lasers," *Proc. SPIE*, vol. 3627, pp. 119-129, 1999.
19. J. E. Bowers, S. Z. Zhang, P. Abraham, Y. J. Chiu and V. Kaman, "Low drive voltage, high speed traveling-wave electroabsorption modulators," *Photonic Systems for Antenna Applications Symposium*, PSAA-9, 1999.
20. Y. J. Chiu, V. Kaman, S. Z. Zhang, J. E. Bowers and U. K. Mishra, "A novel 1.54  $\mu\text{m}$  n-i-n photodetector based on low-temperature grown GaAs," *LEOS '98 Technical Digest*, pp. 155-156, 1998.
21. L. Samoska, R. Pallela, B. Agarwal, D. Mensa, Q. Lee, V. Kaman, J. Guthrie and M. J. Rodwell, "InP heterojunction bipolar transistor decision circuits," *IEEE MTT-S Technical Digest*, pp. 1843-1846, 1998.
22. K. Kiziloglu, M. W. Yung, S. Hsiang-Chi, S. Thomas, M. B. Kardos, R. H. Walden, J. J. Brown, W. E. Stanchina, V. Kaman and M. J. W. Rodwell, "InP-based high sensitivity pin/HEMT/HBT monolithic integrated optoelectronic receiver," *IPRM '98 Technical Digest*, pp. 443-446, 1998.

## ABSTRACT

### **High-Speed Optical Systems Based on Electroabsorption Modulators**

by

Volkan Kaman

Due to the explosive demand for Internet access and traffic, research in high-capacity optical fiber transmission has accelerated all over the world. Wavelength division multiplexing (WDM) has emerged in the past decade with over 6 Tbit/s transmission demonstrations. However, there is still considerable research in extending the capacity of a single wavelength system by time division multiplexing (TDM), which allows for an increased spectral efficiency for future WDM systems. For high-speed TDM systems, electroabsorption (EA) modulators, with their high-speed, low drive voltage, high extinction ratio and potential for monolithic integration with other opto-electronic components, have become very significant devices.

This thesis investigates and demonstrates various transmitter and receiver subsystems based on EA modulators for future high-speed electrical and optical TDM systems. A 30 Gbit/s electrical TDM system is described, where the EA modulators are used as high-speed data encoding transmitters. The EA modulators are then demonstrated for a variety of functions required in optical TDM systems. A novel simultaneous optical demultiplexer and detector operation is proposed and implemented, which is suitable as a channel add/drop multiplexer and as a compact OTDM demultiplexing receiver. The high-speed switching capability of these devices is also demonstrated with sub-4 ps optical short pulse generation at frequencies  $\geq 30$  GHz by a dual-drive scheme of a high-saturation power EA modulator. Also, integrated tandem EA modulators, which achieve an extinction ratio of 50 dB, are investigated for  $> 100$  Gbit/s OTDM applications. Finally, these devices are employed at 30 GHz to demonstrate a 120 Gbit/s ( $4 \times 30$  Gbit/s) OTDM system, with error-free operation and an average 120 Gbit/s sensitivity of -22.6 dBm.

# CONTENTS

<b>1</b>	<b>Introduction</b>	<b>1</b>
1.1	Overview of TDM Optical Communication Systems	3
1.1.1	Electrical Time Division Multiplexed Systems	3
1.1.2	Optical Time Division Multiplexed Systems	4
1.1.3	Optical Fiber Transmission Demonstrations	6
1.2	External Intensity Modulators in Optical Communication Systems	11
1.2.1	External Intensity Optical Modulators	12
1.2.2	Optical Processing using EA Modulators	13
1.3	Traveling-Wave Electroabsorption Modulators	13
1.3.1	Design and Fabrication	14
1.3.2	Static Characteristics	15
1.3.3	Dynamic Characteristics	16
1.3.4	Chirp Characteristics	17
1.4	Outline of the Dissertation	19
	References	20
<b>2</b>	<b>High-Speed Electrical Time Division Multiplexed Optical Systems</b>	<b>29</b>
2.1	Introduction	29
2.2	Overview of 40 Gbit/s Electrical TDM Systems	30
2.2.1	Research in 40 Gbit/s Integrated Circuit Technology	30
2.2.2	Research in 40 Gbit/s Opto-Electronic Technology	34
2.2.3	40 Gbit/s Electrical TDM System Demonstrations	35
2.3	30 Gbit/s Electrical Time Division Multiplexed System Set-Up	38
2.3.1	30 Gbit/s Electrical Components	39
2.3.2	30 Gbit/s Operation of Electroabsorption Modulator	47
2.3.3	30 Gbit/s Operation of LiNbO <sub>3</sub> Modulator	55
2.4	Discussion and Analysis of the 30 Gbit/s Electrical TDM System	56
2.4.1	Optical Demultiplexing using EA Modulator	57
2.4.2	Investigation of Optical Power Penalties	60
2.4.3	Future Improvements and Conclusions	67

2.5	Summary and Conclusions	69
	References	69
3	Optical Processing using Electroabsorption Modulators	77
3.1	Introduction	77
3.2	Optical Gating using EA Modulators	78
3.2.1	Optical Short Pulse Generation	80
3.2.2	Experimental 10 GHz Optical Switching	85
3.2.3	Simulated 10 GHz Optical Switching	91
3.2.4	Optical Demultiplexing	92
3.3	Integrated 40 Gbit/s Demultiplexer/Photodetector	93
3.3.1	Integrated Tandem EA Modulator Characteristics	93
3.3.2	Experimental Set-Up and Results	94
3.4	Simultaneous Demultiplexing and Detection	98
3.4.1	Operation Principle	101
3.4.2	Device Set-Up	102
3.4.3	Experimental Set-Up and Results	105
3.4.4	Discussion of Current Issues	110
3.4.5	Potential Future Applications	118
3.5	Summary and Conclusions	121
	References	122
4	Optical Time Division Multiplexed Systems Beyond 100 Gbit/s	127
4.1	Introduction	127
4.2	OTDM System Requirements	128
4.2.1	OTDM Transmitter Subsystem	129
4.2.2	OTDM Receiver Subsystem	132
4.2.3	Beyond 100 Gbit/s OTDM Demonstrations	133
4.3	High-Speed Optical Switching using EA Modulators	135
4.3.1	Optical Short Pulse Demonstrations Beyond 30 GHz	136
4.3.2	Dual-Drive Modulation	136
4.3.3	Integrated Tandem EA Modulators	142

4.4	Single Wavelength 120 Gbit/s (4 x 30 Gbit/s) OTDM System	147
4.4.1	Experimental Set-Up	148
4.4.2	Experimental Results and Discussion	151
4.5	Summary and Conclusions	153
	References	154
5	Conclusions and Future Work	159
5.1	Summary	159
5.2	Electroabsorption Modulator Improvements	161
5.3	Next-Generation Traveling-Wave Electroabsorption Modulator	164
5.4	High-Speed TDM for High-Capacity WDM	166
	References	168
A	Microwave Packaging Technology for 40 Gbit/s Applications	171
	References	175
B	Design of 20-kHz to 50-GHz Amplifier IC Modules	177
B.1	IC Characteristics	177
B.2	Package Design	178
B.3	Drain Bias Circuit Design	180
B.4	Performance of Packaged Amplifiers	181
	References	181
C	High-Speed Microwave Package Examples	183
C.1	20-kHz to 46-GHz Bias-Tees	183
C.2	Microwave Low-Pass Filters	185
C.3	20 Gbit/s 2:1 Multiplexer	185
C.4	100-kHz to 30-GHz Receiver	186
C.5	Electroabsorption Modulator Modules	187
	References	188

## CHAPTER 1

### Introduction

Optical fiber communication has rapidly evolved in the last decade from single-wavelength 16 Gbit/s transmission [1] to the recent single-channel 1.28 Tbit/s [2] and over 6 Tbit/s multi-wavelength transmission demonstrations [3, 4]. While technological advancements in optical fibers, optical amplifiers, passive and active optical components as well as electronic and opto-electronic devices have allowed for the recent high-capacity demonstrations, the concurrent explosive growth and demand for Internet access and traffic has accelerated the research for these novel technologies.

The introduction of the erbium-doped fiber amplifier (EDFA) with a gain-band of 1530-1565 nm is a major technological breakthrough for optical fiber communications. The EDFA extended the range of loss-limited transmission and reduced the need for electrical repeaters. Fiber transmission length was then limited by chromatic dispersion induced pulse broadening at 1.55  $\mu\text{m}$  according to [5],

$$B^2 |\beta_2| L < \frac{1}{16} \quad (1.1)$$

where  $B$  is the bit rate,  $\beta_2$  is the group-velocity dispersion, and  $L$  is the fiber length. For conventional single-mode fiber (SMF) with a dispersion of 17 ps/nm/km, the dispersion-limited transmission at 1.55  $\mu\text{m}$  for 10 and 40 Gbit/s are 60 and 4 km, respectively. This prompted several technological solutions such as transmission in dispersion-shifted fiber (DSF) and dispersion compensating techniques including signal pre-chirping [6], dispersion-compensating fiber (DCF) [7], dispersion-compensating devices [8], and transmission employing mid-span spectral inversion



(MSSI) [9]. Concurrently, soliton transmission over thousands of kilometers of fiber became a reality due to optical amplification by EDFA's [10].

The EDFA also allowed for the simultaneous amplification of multi-wavelength channels, which consequently lead to an immediate commercial deployment of wavelength division multiplexing (WDM). While the capacity of transmitted information was drastically increased by WDM, non-linear channel interactions, such as four-wave mixing (FWM) and cross-phase modulation (XPM) induced by the Kerr effect during fiber propagation, posed a severe limitation for WDM fiber transmission [11]. FWM-induced propagation degradation is especially pronounced in DSF (at dispersion-zero), which conflicted with single channel high bit rate (dispersion-limited) and WDM (non-linearity-limited) transmission. This problem was solved by the proposal of dispersion-managed optical links, in which fiber non-linearities are suppressed by a high local dispersion while the total average dispersion of the link is kept low [12]. The crucial inventions for dispersion-managed systems were the nonzero dispersion-shifted fiber (NZDSF), which has a dispersion-zero around 1520 nm, as well as the deployment of DCF [13].

The capacity of WDM systems were further increased by employing the L-band (1570-1610 nm) transmission window [14] as well as increasing the spectral efficiency through dense-WDM (DWDM). The spectral efficiency of DWDM systems can be further improved by increasing the capacity of a single channel by time division multiplexing (TDM). The guard bandwidth number between adjacent wavelength channels as well as the amount of WDM transmitters can be reduced by a factor proportional to the increase in the TDM bit rate, which allows for a better system management of high-capacity point-to-point links. High-speed TDM systems can be realized by multiplexing tributary channels either in the electrical (ETDM) or the optical time domain (OTDM). Over the past decade, intense

research effort for both TDM techniques has focused on the development of advanced electronic, opto-electronic and all-optical technologies for various transmitter and receiver subsystems. The outcome of these developments has allowed for the demonstration of single-channel 40 Gbit/s ETDM [15, 16] and 1.28 Tbit/s OTDM systems [2] as well as ultra high-capacity 6.4 Tbit/s ETDM/WDM [3] and 3.04 Tbit/s OTDM/WDM systems [17].

## **1.1 Overview of TDM Optical Communication Systems**

### ***1.1.1 Electrical Time Division Multiplexed Systems***

A typical 40 Gbit/s ETDM based optical system is shown in Figure 1.1. The 40 Gbit/s electrical data stream is generated by multiplexing four tributary 10 Gbit/s channels using a high-speed electrical multiplexer. This data stream is then amplified to satisfy the drive voltage requirements of the high-speed optical modulator and encoded onto a CW light to generate a 40 Gbit/s non-return-to-zero (NRZ) optical signal. It is also possible to generate a 40 Gbit/s return-to-zero (RZ) optical signal by using an optical short pulse source, such as a mode-locked laser [18, 19] or a modulator [20], at 40 GHz instead of a CW source. In this case, the 40 Gbit/s electrical NRZ signal is synchronized to the 40 GHz optical pulse generator such that the data is encoded onto the pulse train. At the expense of a wider optical bandwidth, the RZ modulation format exhibits an improved optical sensitivity [21] as well as reduced impact of fiber non-linearities compared to the NRZ format [22-25]. Multi-level signal modulation [26-28] at 40 Gbit/s by electrical processing techniques has also been demonstrated for reducing the optical spectral width, which decreases dispersion-induced broadening [26] as well as increasing the spectral efficiency of DWDM systems [27].

On the receiver side, a low-noise optical pre-amplifier EDFA and an optical bandpass filter are used to boost the 40 Gbit/s (NRZ or RZ) optical signal into a

40 GHz photodetector. The optical-to-electrical (O/E) converted signal is then usually electrically amplified before a high-speed demultiplexer extracts the four 10 Gbit/s tributary channels. Synchronization of the incoming 40 Gbit/s signal is achieved by a clock-recovery circuit, which extracts the 40 GHz clock signal from the high-speed data stream. Since the 40 GHz spectral component is available in the RZ format, clock-recovery can be achieved using a high-Q bandpass filter. On the other hand, the NRZ format requires a non-linear circuit to generate the 40 GHz clock signal.

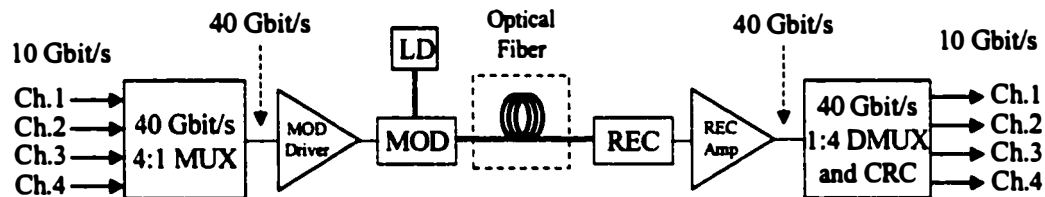


**Figure 1.1** Schematic diagram of a 40 Gbit/s electrical TDM based optical system. MUX: multiplexer; MOD: modulator; REC: receiver; DMUX: demultiplexer; CRC: clock-recovery circuit.

The major drawback of 40 Gbit/s ETDM systems are the high bandwidth (> 30 GHz) and constant phase response requirements for all of the electronic and opto-electronic components in the transmitter and receiver subsystems. Even though electrical multiplexers and demultiplexers operating at speeds of 80 Gbit/s [29] and 60 Gbit/s [30], respectively, have been achieved, optical fiber transmission demonstrations employing full ETDM have been limited to 40 Gbit/s [15, 16].

### ***1.1.2 Optical Time Division Multiplexed Systems***

The transmitter and receiver bandwidth limitations of a 40 Gbit/s system can be eliminated by optical multiplexing and demultiplexing of four 10 Gbit/s tributary channels in an OTDM system (Figure 1.2). The OTDM transmitter consists of a 10 GHz short pulse source that is synchronized to the 10 Gbit/s tributary channels. The optical pulse train is fed into an optical multiplexer with

four separate paths, where the 10 Gbit/s channels are encoded and delayed before recombining into a 40 Gbit/s OTDM data stream. The 40 Gbit/s data stream is usually of the RZ format; however, a 40 Gbit/s NRZ data stream can be realized by employing time and polarization multiplexing of adjacent channels.

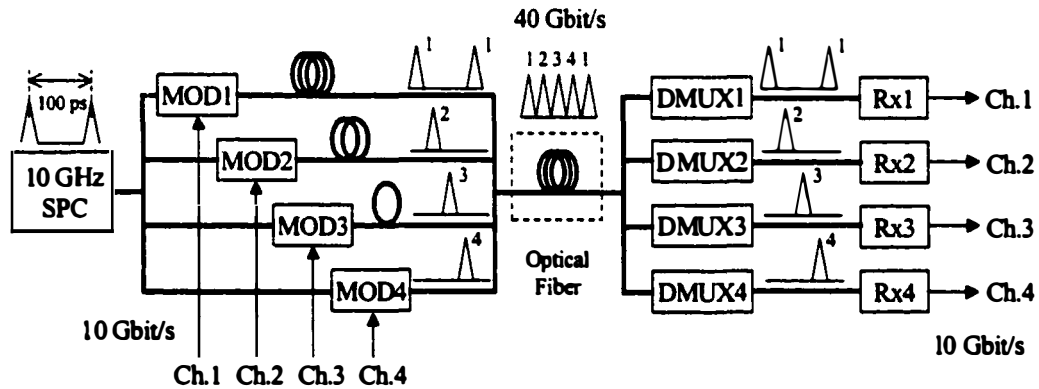


**Figure 1.2** Schematic diagram of a 40 Gbit/s OTDM based optical system. SPC: short pulse source; MOD: modulator; DMUX: demultiplexer; Rx: receiver.

The 40 Gbit/s OTDM receiver can be realized by RF-driven modulators as shown in Figure 1.2. The 40 Gbit/s data stream is optically pre-amplified before it is split into four branches. At each branch, the RF-driven modulator selects one of the tributary channels by suppressing the other channels. The demultiplexed 10 Gbit/s optical channels are then O/E converted using 10 Gbit/s receivers.

OTDM systems have the advantage of only requiring electronic and opto-electronic component bandwidths at the tributary rate since the optical multiplexing and demultiplexing are performed in the optical domain. Depending on the optical pulse source and the demultiplexer, OTDM data rates as high as 1.28 Tbit/s can be realized with an electrical base rate of 10 Gbit/s [2]. Currently, OTDM transmitter and receiver subsystem technologies are widely used in laboratory demonstrations; however, they are yet to be commercially deployed due to cost, size and stability issues.

### ***1.1.3 Optical Fiber Transmission Demonstrations***

To date, several 40 Gbit/s single-wavelength and WDM laboratory and field trial experiments have been demonstrated using the TDM transmitter and receiver subsystem technologies described in the preceding sections. In this section, optical fiber transmission experiments based on (1) single-channel 40 Gbit/s ETDM or OTDM, (2) single-channel OTDM with bit rates beyond 40 Gbit/s, and (3) WDM systems with Terabit/s capacity based on 40 Gbit/s or higher TDM are described.

(1) *Single-Channel 40 Gbit/s TDM*: The first 40 Gbit/s optical fiber transmission experiments were conducted using OTDM techniques as early as 1992 due to the lack of high-speed devices [10, 31]. While over 560 km DSF transmission was achieved with 40 Gbit/s OTDM [32], the use of DCF allowed for 80 km [33] and 150 km [34] of SMF transmission. A polarization multiplexed 40 Gbit/s OTDM signal achieved 240 km of SMF transmission in conjunction with DCF [35]. Dispersion-compensation by MSSI using FWM in semiconductor optical amplifiers increased 40 Gbit/s OTDM transmission distances to over 406 km [9] and 434 km [36] of SMF. Recently, a record distance of 1,220 km dispersion-compensated error-free SMF transmission of a single-polarization 40 Gbit/s RZ data stream was achieved through careful dispersion management [37]. Soliton transmission at 40 Gbit/s over 8,600 km of DSF using periodic dispersion-compensation without in-line control [38], 10,000 km of DSF using electroabsorption (EA) modulators for in-line control [39], and over 70,000 km in a 250-km DSF loop using in-line modulation and optical filtering [40] have also been demonstrated. On the other hand, the first 40 Gbit/s optical transmission using high-speed ETDM were demonstrated concurrently in 1997 over 300 km of DSF and RZ format [15], and 148 km of DSF and NRZ format [16]. It should be emphasized that the 30 Gbit/s ETDM system assembled entirely at the *University of California, Santa Barbara* (this work) predates the aforementioned 40 Gbit/s demonstrations (Chapter 2).

The NRZ and RZ modulation formats have been extensively investigated at 40 Gbit/s for dispersion-managed SMF optical links. Theoretical studies and computer simulations predict an advantage for the low duty cycle RZ format due to its robustness to self-phase modulation (SPM) [22, 23]. For lower duty cycles, pulse broadening and peak power reduction due to dispersion is enhanced in comparison to the NRZ format. Therefore, SPM influence during fiber propagation is reduced and higher optical input power levels are allowed, which was verified experimentally using standard SMF and linear dispersion-compensation for 40 Gbit/s transmission lengths of 432 and 218 km for the RZ and NRZ formats, respectively [24]. In another experiment, 2.5 ps RZ pulses (10% duty cycle) were employed to minimize SPM effects by rapid pulse dispersion, and achieve 800 km of SMF transmission [25]. In contrast to the conventional dispersion-managed systems where span-by-span compensation allows fiber non-linearity to act in each span, the dispersion compensation was performed at the end of the 800-km fiber link.

(2) *Beyond 40 Gbit/s Single-Channel OTDM*: Single-channel OTDM transmission at an aggregate bit rate of 80 Gbit/s has been demonstrated over 80 km of DSF as early as 1993 [41]. However, most of the long-haul 80 Gbit/s transmission experiments have been demonstrated since 1999 (Table 1.1) [41-49]. The longest transmission distance achieved at 80 Gbit/s is 1,100 km in a dispersion-managed recirculating loop [49]. Figure 1.3 shows a historical progression of single wavelength OTDM experiments with capacities beyond 100 Gbit/s [2, 50-62], where the circle and triangle symbols correspond to single and alternate polarization multiplexing, respectively. The most notable of these experiments are the 120 Gbit/s (4 x 30 Gbit/s) OTDM system demonstration (this work) [53], the next generation bit rate of 160 Gbit/s OTDM transmission over 200 km of DSF [54], 300 km of NZDSF [55], and 160 km of standard SMF [56]. The 640 Gbit/s

Company, Year	OTDM Bit Rate (Gbit/s)	ETDM Base Rate (Gbit/s)	Transmitter & Receiver Type	Pattern Length (PRBS)	Fiber Link	Ref.
NTT, 1993	80*	10	GS-LD, 2 LN MOD	$2^7-1$	80 km DSF	[41]
BT, 1997	80	10	2 EA MOD, EA MOD	$2^7-1$	-	[42]
Chalmers U., 1999	80*	10	ML-FRL, NOLM	$2^{15}-1$	172 km DSF	[43]
H. -H. Inst., 1999	80	10	ML-FRL, all-optical	$2^7-1$	250 km SMF	[44]
NTT, 2000	80*	40	ML-LD, EA MOD	$2^7-1$	168 km DF-fiber	[45]
Oki, 1998	80*	20	EA MOD, EA MOD	$2^{15}-1$	160 km NZDSF	[46]
Aston U., 1999	80*	10	ML-FRL, EA MOD	$2^{31}-1$	523 km SMF	[47]
Kansai, 1999	80*	10	ML-LD, 2 EA MOD	$2^{15}-1$	800 km DSF	[48]
NRL, 2000	80	10	ML-FRL, all-optical	$2^7-1$	1,100 km DM-fiber	[49]

**Table 1.1** Chronological summary of single-wavelength 80 Gbit/s OTDM system and transmission demonstrations. OTDM channels with alternate polarization multiplexing are denoted by (\*). GS-LD: gain-switched laser diode; LN: LiNbO<sub>3</sub>; ML-FRL: mode-locked fiber ring laser; ML-LD: mode-locked laser diode; DSF: dispersion-shifted fiber; SMF: standard single mode fiber; DF: dispersion-flattened; NZDSF: nonzero dispersion-shifted fiber; DM: dispersion-managed.

OTDM experiment was over 40 km of DSF [62] while the recent 1.28 Tbit/s OTDM data stream transmission was over 70 km of dispersion-flattened (DF) fiber [2]. The experimental details of the beyond 100 Gbit/s OTDM demonstrations (Table 4.1) and the 120 Gbit/s OTDM system experiment [53] are reviewed in detail in Chapter 4.

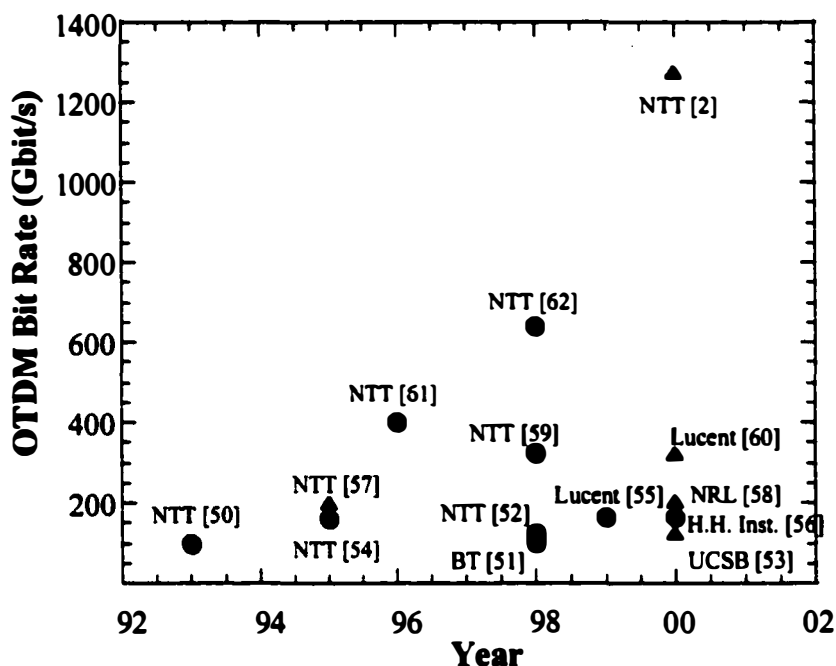


**Figure 1.3** Historical progression of > 100 Gbit/s OTDM demonstrations. Circle and triangle symbols correspond to single and alternate polarization multiplexing of adjacent channels.

(3) *Terabit/s WDM based on  $\geq 40$  Gbit/s TDM*: Increasing the channel rate of next generation WDM systems to 40 Gbit/s or higher is a definite means of satisfying the demand for high-capacity transmission. Since the first four-channel 40 Gbit/s ETDM based 160 Gbit/s WDM demonstration over 320 km of DSF in 1996 [63], several beyond 1 Tbit/s capacity WDM experiments with 40 Gbit/s line rates have been achieved (Table 1.2) [3, 4, 64-73]. The first demonstration was based on 40 Gbit/s (polarization-multiplexed) NRZ format OTDM channels with an aggregate capacity of 1.4 Tbit/s [64]. The most notable of these experiments include 1.28 Tbit/s transmission (ETDM/RZ) over 1,000 km of NZDSF [68], 3.28 Tbit/s transmission (ETDM/NRZ) over 300 km of NZDSF [72], 5.12 Tbit/s transmission (ETDM/NRZ) of polarization-interleaved adjacent wavelength channels over 300 km of NZDSF [73], 6.4 Tbit/s transmission (ETDM/NRZ) with a spectral efficiency of 0.8 bit/s/Hz over 186 km of dispersion-flattened optical link



[3], and 7.04 Tbit/s bi-directional transmission (ETDM/NRZ) over 50 km of NZDSF [4]. Several important techniques employed for these demonstrations were the use of a 40 Gbit/s channel rate, transmission in the C- and L-bands over NZDSF, distributed Raman amplification, and polarization-interleaving of adjacent wavelength channels to reduce coherent crosstalk and to increase spectral efficiency.

Company, Year	WDM Bit Rate (Tbit/s)	TDM Channel Number & Format	$\lambda$ Range (nm)	$\lambda$ Spacing (GHz) & Spectral Efficiency (bit/s/Hz)	Fiber Link	Ref.
Lucent, 1999	1	25, OTDM/NRZ <sup>(1)</sup>	1536.7-1560.7	125, 0.32	342 km NZDSF	[64]
NTT, 2000	1.2	30, ETDM/NRZ	1560.6-1609.2	200, 0.4	375 km DF-fiber	[65]
Alcatel, 2000	1.28	32, ETDM/NRZ	1529.9-1555.4	100, 0.4	300 km NZDSF	[66]
Alcatel, 2000	1.28	32, ETDM/NRZ	1542.9-1567.9	100, 0.4	250 km SMF	[67]
Nortel, 2000	1.28	32, ETDM/NRZ	1535.0-1559.8	100, 0.4	1,000 km NZDSF	[68]
Lucent, 1998	1.4	35, OTDM/NRZ <sup>(1)</sup>	1529.5-1563.5	125, 0.32	85 km SMF	[69]
Lucent, 1999	1.6	40, ETDM/NRZ	1530.7-1561.8	100, 0.4	400 km NZDSF	[70]
Siemens, 1999	3.2	80, ETDM/NRZ	1531.1-1562.2 1568.8-1601.4	100 <sup>(2)</sup> , 0.4	40 km SMF	[71]
Lucent, 2000	3.28	82, ETDM/NRZ	1530.7-1561.8 1570.4-1604.9	100, 0.4	300 km NZDSF	[72]
Alcatel, 2000	5.12	128, ETDM/NRZ	1529.9-1561.2 1569.6-1692.5	50 & 75 <sup>(3)</sup> , 0.64	300 km NZDSF	[73]
NEC, 2000	6.4	160, ETDM/NRZ	1529.5-1561.0 1570.4-1603.6	50 <sup>(3)</sup> , 0.8	186 km DF-fiber.	[3]
Siemens, 2000	7.04	176, ETDM/NRZ	1528.8-1563.5 1568.4-1604.9	50 <sup>(2)</sup> , 0.8	50 km NZDSF	[4]

**Table 1.2** Summary of Terabit/s WDM demonstrations with line rates of 40 Gbit/s based on electrical or optical multiplexing. Notes: <sup>(1)</sup> Polarization multiplexing of adjacent OTDM channels employed; <sup>(2)</sup> polarization-interleaving of adjacent wavelength channels employed; <sup>(3)</sup> bi-directional propagation of wavelength channels constitutes total capacity.

Several Terabit/s WDM transmission experiments based on greater than 40 Gbit/s OTDM channels have also been demonstrated [17, 74-76]. The four experiments, which are summarized in Table 1.3, were limited to transmission distances of less than 100 km of DSF while the highest spectral efficiency of 0.4 was achieved by polarization multiplexing of two 40 Gbit/s ETDM/RZ channels [75].

Company, Year	WDM Bit Rate (Tbit/s)	TDM Channel Number & Format	$\lambda$ Range (nm)	$\lambda$ Spacing (GHz) & Spectral Efficiency (bit/s/Hz)	Fiber Link	Ref.
NTT, 1996	1	10 x 100 Gbit/s (10 x 10 Gbit/s)	1533.6-1562.0	400, 0.25	40 km DSF	[74]
NTT, 1998	1.08	13 x 80 Gbit/s, (2 x 40 Gbit/s)*	1542.9-1562.2	200, 0.4	89 km DF-fiber	[75]
NTT, 1997	1.4	7 x 200 Gbit/s (20 x 10 Gbit/s)	1529.4-1557.7	600, 0.33	50 km DSF	[76]
NTT, 1999	3.04	19 x 160 Gbit/s (16 x 10 Gbit/s)	1540.0-1566.0 1570.0-1609.0	480, 0.33	40 km DSF	[17]

**Table 1.3** Summary of Terabit/s WDM demonstrations based on OTDM channels with line rates beyond 40 Gbit/s. OTDM channels with alternate polarization multiplexing are denoted by (\*).

## 1.2 External Intensity Modulators in Optical Communication Systems

Optical fiber transmission distance for 10 Gbit/s and higher bit rates are predominantly limited by chromatic dispersion (Eq. (1.1)). The dispersion-induced pulse broadening is enhanced with a chirped optical source [77], which is detrimental for high-speed data transmission. Due to their high chirping characteristics, directly modulated 1.55  $\mu\text{m}$  semiconductor lasers are therefore unsuitable for high-speed and long-haul data transmission. On the other hand, external intensity modulators with their high-speed and low-chirp characteristics are ideal for high-speed data modulation and transmission [78].

### ***1.2.1 External Intensity Optical Modulators***

(1) *Electro-Optic Modulators*: Electro-optic (EO) modulators are based on the linear electro-optic effect, or Pockel's effect, which is the change in the index of refraction of a material under an applied electric field. In a Mach-Zehnder interferometer configuration, the optical phase modulation from the change of the refractive index results in an intensity modulation. Traveling-wave EO modulators based on LiNbO<sub>3</sub> are the most common and commercialized types. The highest electrical 3-dB bandwidth achieved is 44 GHz [79], and the lowest drive voltage required for 40 Gbit/s modulation is 1.95 V using a push-pull type modulator [80].

(2) *Electroabsorption Modulators*: Electroabsorption (EA) modulators are based on the Franz-Keldysh or the Quantum Confined Stark Effect (QSCE) in bulk and quantum-well materials, respectively, which is the change of material absorption under an applied electric field. The highest electrical bandwidth achieved with EA modulators is 50 GHz [81] while the lowest drive voltage requirement is 0.9 V<sub>pp</sub> for 40 Gbit/s modulation [82].

A comparison of general characteristics of LiNbO<sub>3</sub> Mach-Zehnder and EA modulators requires investigation of the drive voltage requirements for a given bandwidth (modulation efficiency), optical insertion loss, dynamic extinction ratio, chirp, polarization dependence, and the potential for monolithic integration. The drawback of LiNbO<sub>3</sub> modulators are the (1) high drive voltage requirement (typically 3-6 V), (2) high polarization dependence, (3) unsuitability for monolithic integration, (4) and bias point drift due to temperature. On the other hand, EA modulators have the advantage of (1) low drive voltage requirement (typically 1-3 V) due to non-linear absorption, (2) a high maximum extinction ratio, (3) polarization insensitivity, and (4) potential for monolithic integration. However, the insertion loss of EA modulators (8-12 dB) is quite high compared to LiNbO<sub>3</sub> modulators (4-6 dB). Also, while EA modulators have a fixed chirp, LiNbO<sub>3</sub>

modulators can have tunable or fixed as well as zero chirp. On the other hand, for high data rate modulation, due to their higher modulation efficiency, EA modulators typically have a much higher dynamic extinction ratio.

### ***1.2.2 Optical Processing using EA Modulators***

EA modulators were primarily intended for high-speed data modulation as an alternative to LiNbO<sub>3</sub> modulators. However, due to their highly non-linear absorption characteristic as a function of reverse bias, EA modulators have found extensive applications for optical processing, especially in OTDM systems. These applications include optical short pulse generation [20, 83, 84], optical demultiplexing [85, 86], clock-recovery [87], optical regeneration [88, 89], wavelength conversion [90, 91], and add/drop multiplexing [92, 93]. These optical processing techniques in conjunction with simple, stable and compact operation make EA modulators well suited for high-speed OTDM transmitter and receiver subsystems [53].

## **1.3 Traveling-Wave Electroabsorption Modulators**

Conventional EA modulators are typically based on a lumped electrode structure, which are intrinsically bandwidth-limited by the total  $RC$  time constant. Therefore, the device has to be very short (less than 100  $\mu\text{m}$ ) in order to achieve high-speed operation [81]. However, at the expense of high-speed operation, the extinction ratio and power saturation of the device are reduced while the drive voltage requirement as well as difficulty in handling and packaging are increased. On the other hand, longer devices with traveling-wave electrodes can overcome the  $RC$  limitation while potentially having lower drive voltages and higher extinction ratios [94-97].

The 25-GHz polarization-insensitive traveling-wave EA modulators [96, 97] described in this section were employed as the fundamental opto-electronic device for the demonstration of various transmitter [20, 98] and receiver subsystems [92, 99-101] for the 30 Gbit/s ETDM [102] and the 120 Gbit/s OTDM systems [53] in this dissertation. The 30 Gbit/s ETDM transmission experiment using the traveling-wave EA modulator is the first ETDM experiment over 20 Gbit/s demonstrated by any university while it is also the first modulation experiment for any traveling-wave EA modulator. Similarly, the 120 Gbit/s OTDM experiment is the first demonstration of the feasibility of using EA modulators as optical pulse generators and demultiplexers beyond 20 GHz in conjunction with high-speed ETDM.

### ***1.3.1 Design and Fabrication***

The traveling-wave EA modulators are based on a coplanar waveguide (CPW) electrode structure, which is employed for both the 500- $\mu\text{m}$  long microwave feed lines and the 300- $\mu\text{m}$  long optical waveguide region (Figure 1.4). The ridge is formed by a  $\text{CH}_4/\text{H}_2/\text{Ar}$  reactive ion etch (RIE), which is followed by a  $\text{HCl}:\text{H}_3\text{PO}_4$  wet etch to reduce the RIE damage. In order to passivate the side-walls and to reduce the capacitance due to the p-electrode on the optical waveguide, PMGI bridges connecting the grounds from the sides of the optical waveguide are formed on both ends. The material structure consists of 0.5- $\mu\text{m}$   $\text{n}^+\text{-InP}$  bottom contact layer, 0.3- $\mu\text{m}$   $\text{n-InP}$  cladding layer, 10 strain-compensated MOCVD-grown InGaAsP quantum wells (10.4 nm, 0.37% tensile strain) and InGaAsP barrier (7.6 nm, 0.5% compressive strain), 1.5- $\mu\text{m}$   $\text{p-InP}$  cladding layer and 0.1  $\mu\text{m}$   $\text{p}^+\text{-InGaAs}$  top contact layer on the semi-insulating InP substrate. The room temperature photoluminescence peak of the material is at 1495 nm.

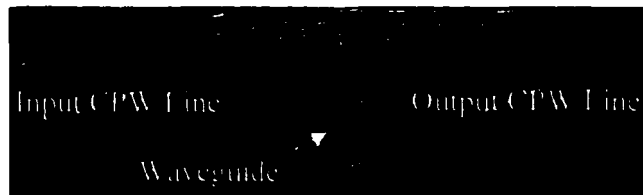


**Figure 1.4** Top-view photograph of the 2- $\mu\text{m}$  wide, 300- $\mu\text{m}$  long traveling-wave EA modulator [96].

### **1.3.2 Static Characteristics**

The static fiber transmission characteristics of a 2- $\mu\text{m}$  wide, 300- $\mu\text{m}$  EA modulator were measured using a lens pair to couple the CW light in and out of the device to fiber. High-frequency microwave probes were employed to supply the reverse bias as well as RF signal for dynamic characterization to be described in the next section. The fiber-to-fiber transmission as a function of reverse bias is shown in Figure 1.5 for several wavelengths and the TE and TM polarization states. At 1.55  $\mu\text{m}$ , the drive voltage requirements for 10 and 20 dB extinction ratios are 0.8 V and 1.2 V, respectively, for the TE polarization. The 20-dB extinction ratio requirement for the TM mode is 1.28 V, which demonstrates the low polarization dependence of the device as a result of proper bandgap engineering. It should be noted that for these initial measurements, the facets were not antireflection (AR)-coated, and the fiber-to-fiber insertion loss of the device for the TM mode was 13.6 dB at 1.57  $\mu\text{m}$ . In the high-speed transmission experiments described later in this dissertation, all the devices were AR-coated and in conjunction with a better coupling scheme, insertion losses as low as 10 dB were achieved at 1.55  $\mu\text{m}$ . The static fiber-to-fiber transmission characteristics of the EA modulators used for these experiments are presented within their respective sections.

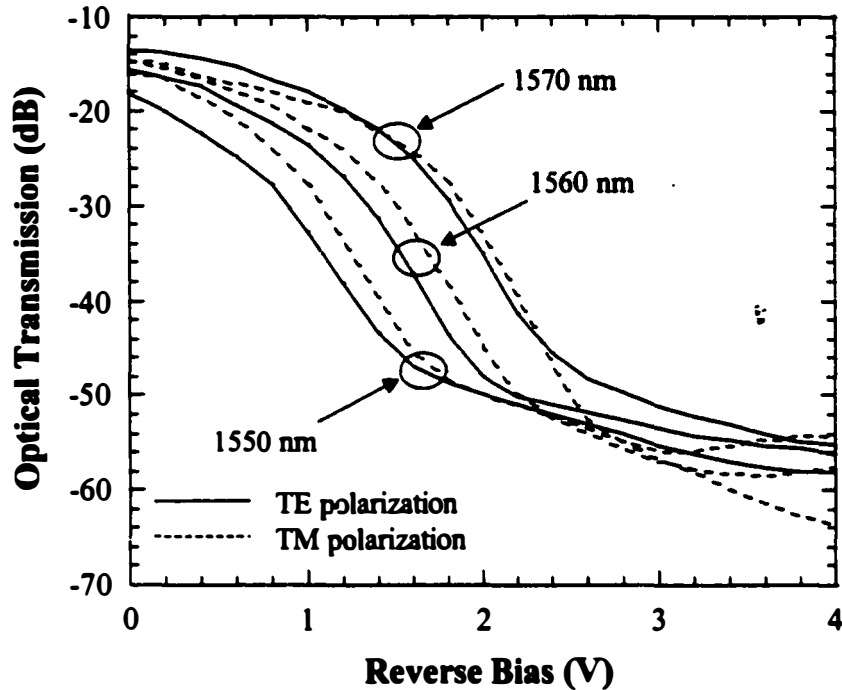


**Figure 1.5** Fiber-to-fiber transmission characteristics of a 300- $\mu\text{m}$  long traveling-wave EA modulator as a function of applied reverse bias for several wavelengths and TE and TM polarization states. The device facets are not antireflection-coated.

### 1.3.3 Dynamic Characteristics

The electro-optic frequency response of the EA modulator is shown in Figure 1.6 for three different terminations, which are realized by ribbon-bonded thin-film resistors. The 3-dB bandwidths are 10.7, 18, and 25 GHz for no termination, 50  $\Omega$ , and 32  $\Omega$ , respectively. From the 0.4 pF capacitance and 4.6  $\Omega$  series resistance of the device deduced from the  $S_{11}$  measurements, the  $RC$ -limited bandwidths are 7.3, 13.4, and 15.8 GHz, respectively, which confirms that the traveling-wave electrode structure improves the device bandwidth. The reason for the bandwidth improvement for reduced load terminations is due to the interplay of multiple microwave reflections between the optical waveguide and the feed lines as well as between the feed lines and the source and load terminations. Since the characteristic impedances of the waveguide and the feed lines are about 25 and

42  $\Omega$ , respectively, the reflections become weaker for a 50  $\Omega$  termination (in comparison to no termination), and negative for a 32  $\Omega$  load. This leads to a cancellation of the reflections between the optical waveguide and feed lines, and consequently to an enhancement of the response at high frequencies. Further measurements also revealed that the microwave propagation loss was 2 dB at 20 GHz for the 300- $\mu\text{m}$  long device.

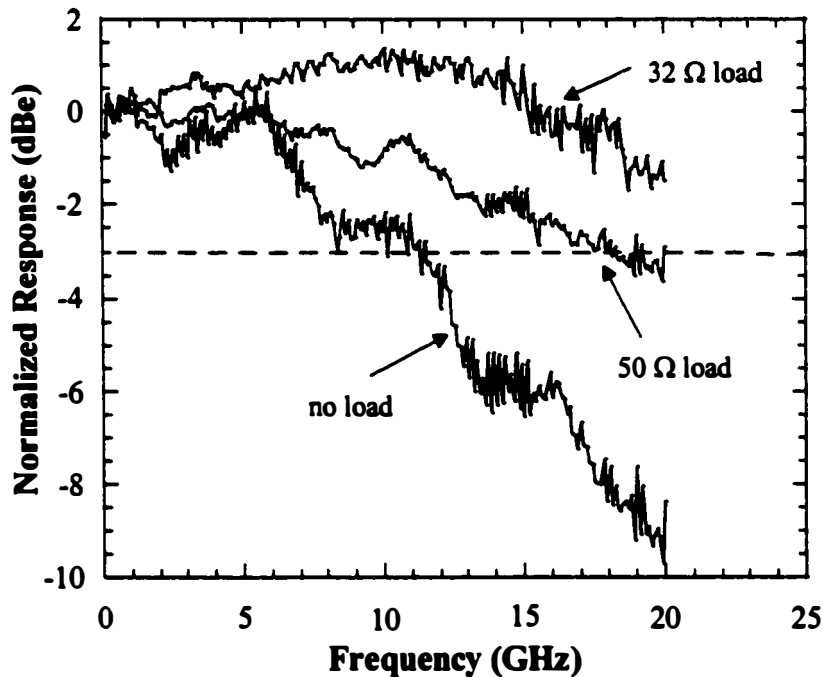


**Figure 1.6** Electro-optic frequency response of a 2- $\mu\text{m}$  wide, 300- $\mu\text{m}$  long traveling-wave EA modulator. The 3-dBe bandwidths are 10.7, 18, and 25 GHz for no termination, 50  $\Omega$  load, and 32  $\Omega$  load, respectively.

#### **1.3.4 Chirp Characteristics**

For long-haul fiber transmission, it is desirable that the chirp-induced pulse broadening is low. The small-signal chirp parameter, or the linewidth enhancement factor  $\alpha$ , of the traveling-wave EA modulator was investigated using the fiber response peak method [103], and the details of this measurement can be found in



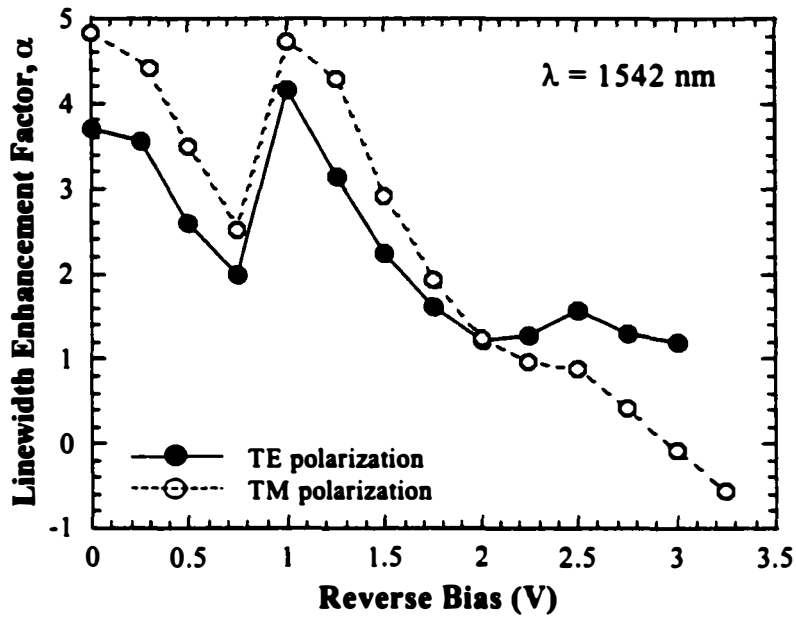


Figure 1.7 Measured linewidth enhancement factor,  $\alpha$ , of the 2- $\mu\text{m}$  wide, 300- $\mu\text{m}$  long traveling-wave EA modulator as a function of reverse bias at a wavelength of 1542 nm.

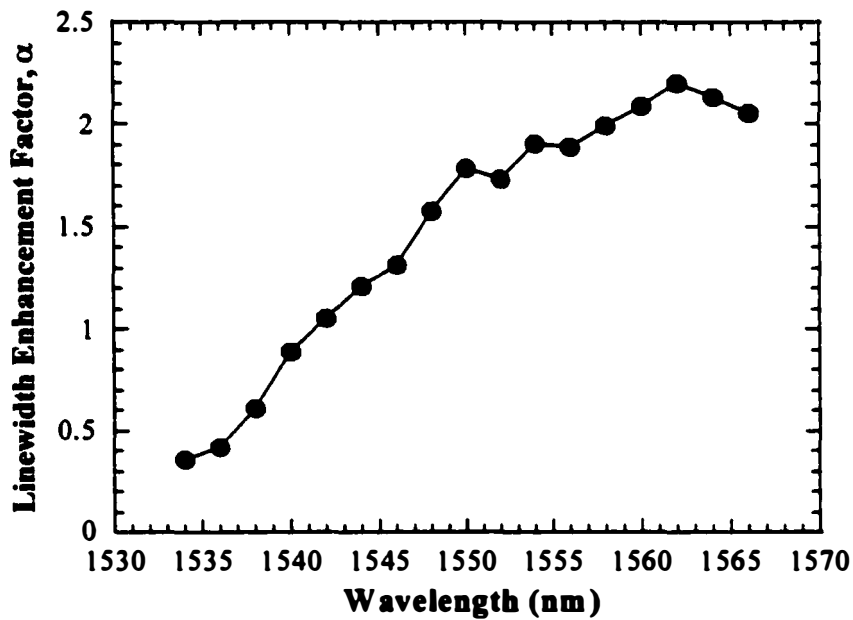


Figure 1.8 Measured linewidth enhancement factor,  $\alpha$ , of the 2- $\mu\text{m}$  wide, 300- $\mu\text{m}$  long traveling-wave EA modulator as a function of wavelength at a reverse bias of -2 V.

[97]. The chirp factor as a function of reverse bias at 1542 nm is shown in Figure 1.7. The measured chirp of 1.2 at a reverse bias of -2 V limited the transmission distance to less than 25 km of SMF at 10 Gbit/s. Figure 1.8 shows the chirp parameter as a function of wavelength (EDFA C-band) at a reverse bias of -2 V. The chirp parameter decreases as the wavelength is decreased.

#### **1.4 Outline of the Dissertation**

This dissertation is intended to investigate and demonstrate high-speed electrical and optical TDM systems, and the underlying transmitter and receiver subsystem technologies by using high-speed traveling-wave EA modulators for compact and stable future applications.

Chapter 2 focuses on high-speed ETDM systems beyond 20 Gbit/s. A 30 Gbit/s ETDM optical system assembled at the *University of California, Santa Barbara*, with full electrical multiplexing and demultiplexing is presented. This high-speed optical system predates all of the eventual 40 Gbit/s ETDM transmission demonstrations. A traveling-wave EA modulator, which is also fabricated at the *University of California, Santa Barbara*, is investigated at 30 Gbit/s as a high-speed data encoder, and overall problems and improvements for future high-speed electrical transmitter and receiver subsystems are analyzed. This demonstration is also the first high-speed modulation of a traveling-wave EA modulator.

Chapter 3 is devoted to experimentally demonstrating various optical processing techniques using EA modulators, primarily intended for high-speed OTDM system applications. Optical gating of these devices for optical short pulse generation and demultiplexing is investigated in detail at a modulation frequency of 10 GHz. Novel packaged integrated tandem EA modulators are also presented as compact and stable 40 Gbit/s OTDM receiver subsystems, with applications up to

80 Gbit/s. The chapter concludes with a novel idea of using an EA modulator for simultaneous demultiplexing and detection of a single channel from a high-speed OTDM data stream, with future applications to compact add/drop multiplexers as well as OTDM demultiplexing receivers.

Chapter 4 investigates next generation high-speed OTDM systems with aggregate and tributary channel bit rates of over 100 and 20 Gbit/s, respectively. Dual-drive and integrated tandem EA modulators are investigated for short pulse generation and optical demultiplexing at modulation frequencies higher than 30 GHz. Sub-4 ps optical pulses are achieved at these frequencies, which are the shortest pulse widths demonstrated to date using sinusoidally driven EA modulators. Using these devices, a 120 Gbit/s (4 x 30 Gbit/s) OTDM system with error-free operation is demonstrated.

The dissertation is summarized and concluded in Chapter 5.

## References

- [1] A. H. Gnauck, R. M. Jopson, C. A. Burrus, S. J. Wang, and N. K. Dutta, "16 Gbit/s transmission experiments using a directly modulated 1.3  $\mu\text{m}$  DFB laser," *IEEE Photonics Tech. Lett.*, vol. 1, pp. 337-339, 1989.
- [2] M. Nakazawa, T. Yamamoto, and K. R. Tamura, "1.28 Tbit/s – 70 km OTDM transmission using third- and fourth-order simultaneous dispersion compensation with a phase modulator," *ECOC '00 Technical Digest*, PD 2.6, 2000.
- [3] T. Ito, K. Fukuchi, K. Sekiya, D. Ogasahara, R. Ohhira, and T. Ono, "6.4 Tb/s (160 x 40 Gb/s) WDM transmission experiment with 0.8 bit/s/Hz spectral efficiency," *ECOC '00 Technical Digest*, PD 1.1, 2000.
- [4] A. Farbert, G. Mohs, S. Spalter, J. P. Elbers, C. Furst, A. Schopflin, E. Gottwald, C. Scheerer, and C. Glingener, "7 Tb/s (176 x 40 Gb/s) bidirectional interleaved transmission with 50 GHz channel spacing," *ECOC '00 Technical Digest*, PD 1.3, 2000.
- [5] G. P. Agrawal, *Fiber-Optic Communication Systems*, John Wiley & Sons, Inc., 1992.
- [6] N. Henmi, T. Saito, and T. Ishida, "Prechirp technique as a linear dispersion compensation for ultrahigh speed long span intensity modulation directed detection optical communication systems," *IEEE J. of Lightwave Tech.*, vol. 12, 1706-1719, 1994.

- [7] G. Ishigawa, M. Sekiya, H. Onaka, H. Nishimoto, and T. Chikama, "Optimization of pre-chirping and dispersion compensation for 10 Gbit/s, repeaterless transmission using standard single mode fiber," *ECOC '94 Technical Digest*, pp. 693-696, 1994.
- [8] F. Ouellette, "Dispersion cancellation using linearly chirped Bragg grating filters in optical waveguide," *Optics Lett.*, vol. 12, pp. 847-849, 1987.
- [9] D. D. Marcenac, D. Nisset, A. E. Kelly, M. Brierley, A. D. Ellis, D. G. Moodie, and C. W. Ford, "40 Gbit/s transmission over 406 km of NDSF using mid-span spectral inversion by four-wave-mixing in a 2 mm long semiconductor optical amplifier," *Electron. Lett.*, vol. 33, pp. 879-880, 1997.
- [10] K. Iwatsuki, K. Suzuki, S. Nishi, and M. Saruwatari, "40 Gbit/s optical soliton transmission over 65 km," *Electron. Lett.*, vol. 28, pp. 1821-1822, 1992.
- [11] A. R. Chraplyvy, "Limitations on lightwave communications imposed by optical fiber nonlinearities" *IEEE J. of Lightwave Tech.*, vol. 8, pp. 1548-1557, 1990.
- [12] C. Kurtzke, "Suppression of fiber nonlinearities by appropriate dispersion management," *IEEE Photonics Tech. Lett.*, vol. 5, pp. 1250-1252, 1993.
- [13] L. Clark, A. A. Klein, and D. W. Peckham, "Impact of fiber selection and nonlinear behavior on network upgrade strategies for optically amplified long interoffice routes," *NFOEC '94 Proceedings*, pp. 123-132, 1994.
- [14] M. Jinno, T. Sakamoto, J. Kani, S. Aisawa, K. Oda, M. Fukui, H. Ono, and K. Oguchi, "First demonstration of 1580 nm wavelength band WDM transmission for doubling usable bandwidth and suppressing FWM in DSF," *Electron. Lett.*, vol. 33, pp. 882-883, 1997.
- [15] M. Yoneyama, A. Sano, T. Kataoka, A. Hirano, T. Otsuji, K. Sato, H. Miyazawa, and K. Hagimoto, "40 Gbit/s optical repeater circuit using InAlAs/InGaAs HEMT digital IC modules," *Electron. Lett.*, vol. 33, pp. 1977-1978, 1997.
- [16] W. Bogner, E. Gottwald, A. Schopflin, and C. J. Weiske, "40 Gbit/s unrepeated optical transmission over 148 km by electrical time division multiplexing and demultiplexing," *Electron. Lett.*, vol. 33, pp. 2136-2137, 1997.
- [17] S. Kawanishi, H. Takara, K. Uchiyama, I. Shake, and K. Mori, "3 Tbit/s (160 Gbit/s\*19 channel) optical TDM and WDM transmission experiment," *Electron. Lett.*, vol. 35, pp. 826-827, 1999.
- [18] K. Sato, A. Hirano, and H. Ishii, "Chirp-compensated 40-GHz mode-locked lasers integrated with electroabsorption modulators and chirped gratings," *IEEE J. of Selected Topics in Quantum Electron.*, vol. 5, pp. 590-595, 1999.
- [19] A. D. Ellis, R. J. Manning, I. D. Phillips, and D. Nisset, "1.6 ps pulse generation at 40 GHz in phase-locked ring laser incorporating highly nonlinear fibre for application to 160 Gbit/s OTDM networks," *Electron. Lett.*, vol. 35, pp. 645-646, 1999.
- [20] V. Kaman, Y. J. Chiu, S. Z. Zhang, and J. E. Bowers, "3.7 ps pulse generation at  $\geq 30$  GHz by dual-drive electroabsorption modulator," *Electron. Lett.*, vol. 36, pp. 1130-1132, 2000.
- [21] L. Boivin, M. C. Nuss, J. Shah, D. A. B. Miller, and H. A. Haus, "Receiver sensitivity improvement by impulsive coding," *IEEE Photonics Tech. Lett.*, vol. 9, pp. 684-686, 1997.
- [22] S. Zhang, R. Nagarajan, A. Petersen, and J. Bowers, "40 Gbit/s fiber optic transmission systems: are solitons needed?," *Proc. of the SPIE*, p.182-185, 1996.

- [23] D. Breuer, and K. Petermann, "Comparison of NRZ- and RZ-modulation format for 40-Gb/s TDM standard-fiber systems," *IEEE Photonics Tech. Lett.*, vol. 9, pp. 398-400, 1997.
- [24] R. Ludwig, U. Feiste, E. Dietrich, H. G. Weber, D. Breuer, M. Martin, and F. Kuppers, "Experimental comparison of 40 Gbit/s RZ and NRZ transmission over standard singlemode fibre," *Electron. Lett.*, vol.35, pp. 2216-2218, 1999.
- [25] A. H. Gnauck, S. G. Park, J. M. Wiesenfeld, and L. D. Garrett, "Highly dispersed pulses for 2\*40 Gbit/s transmission over 800 km of conventional singlemode fibre," *Electron. Lett.*, vol.35, pp. 2218-2219, 1999.
- [26] K. Yonenaga, A. Hirano, M. Yoneyama, Y. Miyamoto, K. Hagimoto, and K. Noguchi, "Expansion of tolerable dispersion range in a 40 Gbit/s optical transmission system using an optical duobinary signal," *Electron. Lett.*, vol. 34, pp. 385-386, 1998.
- [27] K. Yonenaga, M. Yoneyama, Y. Miyamoto, K. Hagimoto, and K. Noguchi, "160 Gbit/s WDM transmission experiment using four 40 Gbit/s optical duobinary channels," *Electron. Lett.*, vol. 34, pp. 1506-1507, 1998.
- [28] W. Idler, B. Franz, D. Schlump, B. Wedding, and A. J. Ramos, "Field trial at 40 Gbit/s over 28.6 and 86 km of standard singlemode fibre using quaternary dispersion supported transmission," *Electron. Lett.*, vol. 34, pp. 2425-2426, 1998.
- [29] T. Otsuji, K. Murata, T. Enoki, and Y. Umeda, "80 Gbit/s multiplexer IC using InAlAs/InGaAs/InP HEMTs," *Electron. Lett.*, vol. 34, pp. 113-114, 1998.
- [30] A. Felder, M. Moller, M. Wurzer, M. Rest, T. F. Meister, and H. -M. Rein, "60 Gbit/s regenerating demultiplexer in SiGe bipolar technology," *Electron. Lett.*, vol. 33, pp. 1984-1986, 1997.
- [31] A. D. Ellis, T. Widdowson, X. Shan, G. E. Wickens, and D. M. Spirit, "Transmission of a true single polarisation 40 Gbit/s soliton data signal over 205 km using a stabilised erbium fibre ring laser and 40 GHz electronic timing recovery.," *Electron. Lett.*, vol.29, pp. 990-992, 1993.
- [32] W. S. Lee, G. Pettitt, D. Garthe, and A. Hadjifotiou, "40 Gbit/s OTDM transmission over a distance of 560 km: System implementation and performance evaluation," *Electron. Lett.*, vol. 32, pp. 1685-1686, 1996.
- [33] A. D. Ellis, and D. M. Spirit, "Unrepeated transmission over 80km standard fibre at 40Gbit/s," *Electron. Lett.*, vol. 30, pp. 72-74, 1994.
- [34] R. Ludwig, W. Pieper, H. G. Weber, D. Breuer, K. Petermann, F. Kuppers, and A. Mattheus, "Unrepeated 40 Gbit/s RZ single channel transmission over 150 km of standard singlemode fibre at 1.55  $\mu\text{m}$ ," *Electron. Lett.*, vol. 33, pp. 76-77, 1997.
- [35] K. I. Suzuki, N. Ohkawa, M. Murakami, and K. Aida, "Unrepeated 40 Gbit/s RZ signal transmission over 240 km conventional singlemode fibre," *Electron. Lett.*, vol. 34, pp. 799-800, 1998.
- [36] U. Feiste, R. Ludwig, E. Dietrich, S. Diez, H. J. Ehrke, Dz. Razic, and H. G. Weber, "40 Gbit/s transmission over 434 km standard fibre using polarisation independent mid-span spectral inversion," *Electron. Lett.*, vol. 34, pp. 2044-2045, 1998.
- [37] S. B. Alleston, P. Harper, I. S. Penketh, I. Bennion, and N. J. Doran, "1220 km propagation of 40 Gbit/s single channel RZ data over dispersion managed standard (non-dispersion shifted) fibre," *OFC '99 Technical Digest*, PD3/1-3, 1999.

- [38] I. Morita, K. Tanaka, N. Edagawa, S. Yamamoto, and M. Suzuki, "40 Gbit/s single-channel soliton transmission over 8600 km using periodic dispersion compensation," *Electron. Lett.*, vol. 34, pp. 1863-1865, 1998.
- [39] G. Aubin, T. Montalant, J. Moulou, F. Pirio, J. B. Thomine, and F. Devaux, "40 Gbit/s OTDM soliton transmission over transoceanic distances," *Electron. Lett.*, vol. 32, pp. 2188-2189, 1996.
- [40] K. Suzuki, H. Kubota, A. Sahara, and M. Nakazawa, "40 Gbit/s single channel optical soliton transmission over 70000 km using in-line synchronous modulation and optical filtering," *Electron. Lett.*, vol. 34, pp. 98-100, 1998.
- [41] K. Iwatsuki, K. Suzuki, S. Nishi, and M. Saruwatari, "80 Gb/s optical soliton transmission over 80 km with time/polarization division multiplexing," *IEEE Photonics Tech. Lett.*, vol. 5, pp. 245-247, 1993.
- [42] D. D. Marcenac, A. D. Ellis, and D. G. Moodie, "80 Gbit/s OTDM using electroabsorption modulators," *Electron. Lett.*, vol. 34, pp. 101-103, 1998.
- [43] J. Hansryd, B. Bakhshi, B. E. Olsson, P. A. Andrekson, J. Brentel, and E. Kolltveit, "80 Gbit/s single wavelength soliton transmission over 172 km installed fibre," *Electron. Lett.*, vol. 35, pp. 313-315, 1999.
- [44] U. Feiste, R. Ludwig, C. Schmidt, E. Dietrich, S. Diez, H. J. Ehrke, E. Patzak, H. G. Weber, and T. Merker, "80-Gb/s transmission over 106-km standard-fiber using optical phase conjugation in a Sagnac-interferometer," *IEEE Photonics Tech. Lett.*, vol. 11, pp. 1063-1065, 1999.
- [45] K. Yonenaga, A. Hirano, S. Kuwahara, Y. Miyamoto, H. Toba, K. Sato, and H. Miyazawa, "Temperature-independent 80 Gbit/s OTDM transmission experiment using zero-dispersion-flattened transmission line," *Electron. Lett.*, vol. 36, pp. 343-345, 2000.
- [46] H. T. Yamada, H. Murai, A. R. Pratt, and Y. Ozeki, "Scaleable 80 Gbit/s OTDM using a modular architecture based EA modulators," *ECOC '00 Technical Digest*, paper 1.3.5, 2000.
- [47] I. Yamashita, K. Shimoura, K. Inoguchi, and S. Seikai, "Single channel 80 Gbit/s OTDM transmission through a 800 km dispersion shifted fiber," *ECOC '00 Technical Digest*, paper 6.1.5, 2000.
- [48] P. Harper, S. B. Alleston, and N. J. Doran, "80 Gbit/s RZ transmission over 523km using dispersion compensated standard fiber," *ECOC '00 Technical Digest*, paper 6.1.6, 2000.
- [49] M. L. Dennis, J. W. Lou, T. F. Carruthers, and I. N. Duling, "Dense-dispersion-managed transmission of 80-Gb/s time-division-multiplexed data over 1000 km," *ECOC '00 Technical Digest*, PD 1.9, 2000.
- [50] S. Kawanishi, H. Takara, K. Uchiyama, M. Saruwatari, and T. Kitoh, "Fully time-division-multiplexed 100 Gbit/s optical transmission experiment," *Electron. Lett.*, vol. 29, pp. 2211-2212, 1993.
- [51] A. D. Ellis, J. K. Lucek, D. Pitcher, D. G. Moodie, and D. Cotter, "Full 10\*10 Gbit/s OTDM data generation and demultiplexing using electroabsorption modulators," *Electron. Lett.*, vol. 34, pp.1766-1767, 1998.

- [52] S. Kawanishi, Y. Miyamoto, H. Takara, M. Yoneyama, K. Uchiyama, I. Shake, and Y. Yamabayashi, "120 Gbit/s OTDM system prototype," *ECOC '98 Technical Digest*, pp. 43-45, 1998.
- [53] V. Kaman, and J. E. Bowers, "120 Gbit/s OTDM system using electroabsorption transmitter and demultiplexer operating at 30 GHz," *Electron. Lett.*, vol. 36, pp. 1477-1479, 2000.
- [54] M. Nakazawa, K. Suzuki, E. Yoshido, E. Yamada, T. Kitoh, and M. Kawachi, "160 Gbit/s soliton transmission over 200 km," *Electron. Lett.*, vol. 31, pp. 565-566, 1995.
- [55] B. Mikkelsen, G. Raybon, R. J. Essiambre, K. Dreyer, Y. Su, L. E. Nelson, J. E. Johnson, G. Shtengel, A. Bond, D. G. Moodie and A. D. Ellis, "160 Gbit/s single-channel transmission over 300 km nonzero-dispersion fiber with semiconductor based transmitter and demultiplexer", *ECOC '99 Technical Digest*, PD2-3, 1999.
- [56] R. Ludwig, U. Feiste, S. Diet, C. Schubert, C. Schmidt, H. J. Ehrke, and H. G. Weber, "Unrepeated 160 Gbit/s RZ single-channel transmission over 160 km of standard fibre at 1.55  $\mu\text{m}$  with hybrid MZI optical demultiplexer," *Electron. Lett.*, vol. 36, pp. 1405-1406, 2000.
- [57] S. Kawanishi, H. Takara, T. Morioka, O. Kamatani, and M. Saruwatari, "200 Gbit/s, 100 km time-division-multiplexed optical transmission using supercontinuum pulses with prescaled PLL timing extraction and all-optical demultiplexing," *Electron. Lett.*, vol. 31, pp. 816-817, 1995.
- [58] W. I. Kaechele, M. L. Dennis, T. F. Carruthers, and I. N. Duling, "Dispersion-managed 200 Gb/s polarization-multiplexed transmission over 160 km," *ECOC '00 Technical Digest*, paper 6.1.4, 2000.
- [59] E. Yoshida, T. Yamamoto, A. Sahara, and M. Nakazawa, "320 Gbit/s TDM transmission over 120 km using 400 fs pulse train," *Electron. Lett.*, vol. 34, pp. 1004-1005, 1998.
- [60] G. Raybon, B. Mikkelsen, R. J. Essiambre, A. J. Stentz, T. N. Nielsen, K. Dreyer, J. E. Johnson, L. Hsu, D. W. Peckham, and L. Gruner-Nielsen, "320 Gbit/s single-channel pseudo-linear transmission over 200 km non-zero-dispersion fiber", *OFC '00 Technical Digest*, PD29, 2000.
- [61] S. Kawanishi, H. Takara, T. Morioka, O. Kamatani, K. Takiguchi, T. Kitoh, and M. Saruwatari, "Single channel 400 Gbit/s time-division-multiplexed transmission of 0.98 ps pulses over 40 km employing dispersion slope compensation," *Electron. Lett.*, vol. 32, pp. 916-918, 1996.
- [62] M. Nakazawa, E. Yoshida, T. Yamamoto, E. Yamada, and A. Sahara, "TDM single channel 640 Gbit/s transmission experiment over 60 km using 400 fs pulse train and walk-off free, dispersion flattened nonlinear optical loop mirror," *Electron. Lett.*, vol. 34, pp. 907-908, 1998.
- [63] S. Kuwano, N. Takachio, K. Iwashita, T. Otsuji, Y. Imai, T. Enoki, K. Yoshino, and K. Wakita, "160-Gbit/s (4-ch\*40-Gbit/s electrically multiplexed data) WDM transmission over 320-km dispersion-shifted fiber," *OFC '96 Technical Digest*, pp. 427-430 1996.
- [64] C. D. Chen, I. Kim, O. Mizuhara, T. V. Nguyen, K. Ogawa, R. E. Tench, L. D. Tzeng, and P. D. Yeates, "40 Gbit/s\*25 ch (1 Tbit/s aggregate capacity) WDM transmission over 342 km of fibre," *Electron. Lett.*, vol. 35, pp. 648-649, 1999.

- [65] Y. Miyamoto, K. Yonenaga, S. Kuwahara, M. Tomizawa, A. Hirano, H. Toba, K. Murata, Y. Tada, Y. Umeda, and H. Miyazawa, "1.2 Tbit/s (30\*42.7 Gbit/s ETDM channel) WDM transmission over 3\*125 km with forward error correction," *Electron. Lett.*, vol. 36, pp. 812-813, 2000.
- [66] S. Bigo, E. Lach, Y. Frignac, D. Hamoir, P. Sillard, W. Idler, S. Gauchard, A. Bertaina, S. Borne, L. Lorcy, N. Torabi, B. Franz, P. Nouchi, P. Guenot, L. Fleury, G. Wien, G. Le Ber, R. Fritschi, B. Junginger, M. Kaiser, D. Bayart, G. Veith, J. P. Hamaide, and J. L. Beylat, "1.28 Tbit/s WDM transmission of 32 ETDM channels at 40 Gbit/s over 3x100 km distance," *ECOC '00 Technical Digest*, paper 10.1.3, 2000.
- [67] E. Brandon, J. P. Blondel, F. Boubal, L. Buet, V. Havard, A. Hugbart, L. Labrunie, P. Le Roux, D. Toullier, and R. Uhel, "1.28 Tbit/s (32 x 40 Gbit/s) unrepeated transmission over 250 km," *ECOC '00 Technical Digest*, paper 10.1.4, 2000.
- [68] Y. Zhu, W. S. Lee, C. Scahill, C. Fludger, D. Watley, M. Jones, J. Homan, B. Shaw, and A. Hadjifotiou, "1.28 Tbit/s (32x40 Gbit/s) transmission over 1000 km with only 6 spans," *ECOC '00 Technical Digest*, PD 1.4, 2000.
- [69] C. D. Chen, I. Kim, O. Mizuhara, T. V. Nguyen, K. Ogawa, R. E. Tench, L. D. Tzeng, and P. D. Yeates, "40 Gbit/s\*35 ch (1.4 Tbit/s aggregate capacity) WDM transmission over 85 km standard singlemode fibre," *Electron. Lett.*, vol. 34, pp. 2370-2371, 1998. *Electronics Letters*, vol.34, 1998.
- [70] T. N. Nielsen, A. J. Stentz, P. B. Hansen, Z. J. Chen, D. S. Vengsarkar, T. A. Strasser, K. Rottwitz, J. H. Park, S. Stulz, S. Cabot, K. S. Feder, P. S. Westbrook, and K. G. Kosinski, "1.6 Tb/s (40\*40 Gb/s) transmission over 4\*100 km nonzero-dispersion fiber using hybrid Raman/Er-doped inline amplifiers," *ECOC '99 Technical Digest*, pp. 26-27, 1999.
- [71] C. Scheerer, C. Glingener, A. Farbert, J. P. Elbers, A. Schopflin, E. Gottwald, and G. Fischer, "3.2 Tbit/s (80\*40 Gbit/s) bidirectional WDM/ETDM transmission over 40 km standard singlemode fibre," *Electron. Lett.*, vol. 35, pp. 1752-1753, 1999.
- [72] T. N. Nielsen, A. J. Stentz, K. Rottwitz, D. S. Vengsarkar, L. Hsu, P. B. Hansen, Z. J. Chen, J. H. Park, K. S. Feder, T. A. Strasser, S. Cabot, S. Stulz, C. K. Kan, A. F. Judy, S. Y. Park, L. E. Nelson, and L. Gruner-Nielsen, "3.28 Tb/s (82\*40 Gb/s) transmission over 3\*100 km nonzero-dispersion fiber using dual C- and L-band hybrid Raman/Erbiium-doped inline amplifiers," *OFC '00 Technical Digest*, PD23, 2000.
- [73] S. Bigo, A. Bertaina, Y. Frignac, S. Borne, L. Lorcy, D. Hamoir, D. Bayart, J. P. Hamaide, W. Idler, E. Lach, B. Franz, G. Veith, P. Sillard, L. Fleury, P. Guenot, and P. Nouchi, "5.12 Tbit/s (128x40 Gbit/s WDM) transmission over 3x100 km of Terlight fibre," *ECOC '00 Technical Digest*, PD 1.2, 2000.
- [74] T. Morioka, H. Takara, S. Kawanishi, O. Kamatani, K. Takiguchi, K. Uchiyama, M. Saruwatari, H. Takahashi, M. Yamada, T. Kanamori, and H. Ono, "1 Tbit/s (100 Gbit/s\*10 channel) OTDM/WDM transmission using a single supercontinuum WDM source," *Electron. Lett.*, vol. 32, pp. 906-907, 1996.
- [75] Y. Miyamoto, K. Yonenaga, A. Hirano, N. Shimizu, M. Yoneyama, H. Takara, K. Noguchi, and K. Tsuzuki, "1.04-Tbit/s DWDM transmission experiment based on alternate polarization 80-Gbit/s OTDM signals," *ECOC '98 Technical Digest*, pp. 55-57, 1998.



- [76] S. Kawanishi, H. Takara, K. Uchiyama, I. Shake, O. Kamatani, and H. Takahashi, "1.4 Tbit/s (200 Gbit/s\*7 ch) 50 km optical transmission experiment," *Electron. Lett.*, vol. 33, pp. 1716-1717, 1997.
- [77] G. P. Agrawal, *Fiber-Optic Communication Systems*, John Wiley & Sons, Inc., 1992.
- [78] K. Wakita, K. Yoshino, I. Kotaka, S. Kondo, and Y. Noguchi, "High speed, high efficiency modulator module with polarisation insensitivity and very low chirp," *Electron. Lett.*, vol. 31, pp. 2041-2042, 1995.
- [79] D. W. Dolfi, and T. R. Ranganath, "50 GHz velocity-matched broad wavelength LiNbO<sub>3</sub> modulator with multimode active section," *Electron. Lett.*, vol. 28, pp. 1197-1198, 1992.
- [80] K. Noguchi, O. Mitomi, and H. Miyazawa, "Push-pull type ridged Ti:LiNbO<sub>3</sub> optical modulator," *IEICE Trans. on Electronics*, vol. E79-C, pp. 27-31, 1996.
- [81] T. Ido, S. Tanaka, M. Suzuki, and H. Inoue, "MQW electroabsorption optical modulator for 40 Gbit/s modulation," *Electron. Lett.*, vol. 31, pp. 2124-2125, 1995.
- [82] K. Yoshino, K. Wakita, I. Kotaka, S. Kondo, Y. Noguchi, S. Kuwano, N. Takachio, T. Otsuji, Y. Imai, and T. Enoki, "40-Gbit/s operation of InGaAs/InAlAs MQW electroabsorption modulator module with very low driving-voltage," *ECOC '96 Technical Digest*, pp. 203-206, 1996.
- [83] M. Suzuki, H. Tanaka, K. Utaka, N. Edagawa, and Y. Matsushima, "Transform-limited 14 ps optical pulse generation with 15 GHz repetition rate by InGaAsP electroabsorption modulator," *Electron. Lett.*, vol. 28, pp. 1007-1008, 1992.
- [84] K. Wakita, K. Yoshino, A. Hirano, S. Kondo, and Y. Noguchi, "Very-high-speed and low driving-voltage modulator modules for a short optical pulse generation," *IEICE Trans. on Electron.*, vol. E81-C, pp. 175-179, 1998.
- [85] M. Suzuki, H. Tanaka, and Y. Matsushima, "10 Gbit/s optical demultiplexing and switching by sinusoidally driven InGaAsP electroabsorption modulators," *Electron. Lett.*, vol. 28, pp. 934-935, 1992.
- [86] I. D. Phillips, A. Gloag, D. G. Moodie, N. J. Doran, I. Bennion, and A. D. Ellis, "Simultaneous two-channel OTDM demultiplexing using a single electroabsorption modulator in a novel bi-directional configuration," *Electron. Lett.*, vol. 33, pp. 1811-1812, 1997.
- [87] I. D. Phillips, A. Gloag, D. G. Moodie, N. J. Doran, I. Bennion, and A. D. Ellis, "Simultaneous demultiplexing and clock recovery using a single electroabsorption modulator in a novel bi-directional configuration," *Optics Comm.*, vol. 150, pp. 101-105, 1998.
- [88] T. Miyazaki, N. Edagawa, M. Suzuki and S. Yamaoto, "Novel optical-regenerator using electroabsorption modulator", *OFC '99 Technical Digest*, pp. 350-352, 1999.
- [89] Y. Kisaka, A. Hirano, M. Yoneyama and N. Shimizu, "Simple 2R repeater based on EA modulator directly driven by uni-travelling-carrier photodiode", *Electron. Lett.*, vol. 35, pp. 1016-1017, 1999.
- [90] N. Edagawa, M. Suzuki, and S. Yamamoto, "Novel wavelength converter using an electroabsorption modulator," *IEICE Trans. on Electron.*, vol. E81-C, pp. 1251-1257, 1998.

- [91] L. K. Oxenloewe, A. T. Clausen, and H. N. Poulsen, "Wavelength conversion in an electroabsorption modulator," *ECOC '00 Technical Digest*, paper 9.4.4, 2000.
- [92] V. Kaman, A. J. Keating, S. Z. Zhang, and J. E. Bowers, "Simultaneous OTDM demultiplexing and detection using an electroabsorption modulator," *IEEE Photonics Tech. Lett.*, vol. 12, pp. 711-713, 2000.
- [93] I. D. Phillips, A. Gloag, D. G. Moodie, N. J. Doran, I. Bennion and A.D Ellis, "Drop and insert multiplexing using an electroabsorption modulator," *IEEE Photonics Tech. Lett.*, vol. 10, pp. 291-293, 1998.
- [94] K. Kawano, M. Kohtoku, M. Ueki, T. Ito, S. Kondoh, Y. Noguchi, and Y. Hasumi, "Polarisation-insensitive travelling-wave electrode electroabsorption (TW-EA) modulator with bandwidth over 50GHz and driving voltages less than 2 V," *Electron. Lett.*, vol. 33, pp. 1580-1581, 1997.
- [95] D. Jager, A. Stohr, and R. Heinzlmann, "Advanced microwave photonic devices for analog optical links," *MWP '98 Technical Digest*, pp. 153-156, 1998.
- [96] S. Z. Zhang, Y. J. Chiu, P. Abraham, J. E. Bowers, "25 GHz polarization-insensitive electroabsorption modulators with traveling-wave electrodes", *IEEE Photonics Tech. Lett.*, vol. 11, pp. 191-193, 1999.
- [97] S. Z. Zhang, "Traveling-wave electroabsorption modulators," *ECE Technical Report*, Ph. D. Dissertation, University of California, Santa Barbara, 1999.
- [98] S. Z. Zhang, V. Kaman, A. Keating, Y. J. Chiu, P. Abraham, and J. E. Bowers, "30 Gbit/s operation of a traveling-wave electroabsorption modulator," *OFC '99 Technical Digest*, pp. 290-292, 1999.
- [99] V. Kaman, Y. J. Chiu, T. Liljeberg, S. Z. Zhang and J. E. Bowers, "Integrated tandem traveling-wave electroabsorption modulators for > 100 Gbit/s OTDM applications", *IEEE Photonics Tech. Lett.*, vol. 12, November 2000.
- [100] V. Kaman, A. J. Keating, S. Z. Zhang, and J. E. Bowers, "Electroabsorption modulator as a compact OTDM demultiplexing receiver," *ECOC '00 Technical Digest*, paper 9.4.6, 2000.
- [101] V. Kaman, Y. J. Chiu, T. Liljeberg, S. Z. Zhang, and J. E. Bowers, "A compact 40 Gbit/s demultiplexing receiver based on integrated tandem electroabsorption modulators," to be published in *Electron. Lett.*, 2000.
- [102] V. Kaman, S. Z. Zhang, A. J. Keating, and J. E. Bowers, "High-speed operation of travelling-wave electroabsorption modulator," *Electron. Lett.*, vol. 35, pp. 993-995, 1999.
- [103] F. Devaux, Y. Sorel, and J. F. Kerdiles, " Simple measurement of fiber dispersion and of chirp parameter of intensity modulated light emitter," *J. of Lightwave Tech.*, vol. 11, pp. 1937-1940, 1993.



## CHAPTER 2

### **High-Speed Electrical Time Division Multiplexed Optical Systems**

#### **2.1 Introduction**

The speed of optical fiber communication systems based on electrical time division multiplexing (ETDM) has increased rapidly over the last decade. Wavelength division multiplexed (WDM) systems operating at 10 Gbit/s are presently widely deployed while the expected next generation of 40 Gbit/s-per-wavelength optical communication systems have already been demonstrated in various laboratory experiments [1-3], in field trials [4], and are currently being planned for commercial installation [5]. Whether the goal is to upgrade an existing 10 Gbit/s system to 40 Gbit/s or to install a new 40 Gbit/s system, the requirements for the transmitter and receiver subsystems are quite similar. The most apparent requirement is to deploy a novel set of very high-speed and broadband electronic and opto-electronic devices that can accommodate not only 40 Gbit/s data streams, but also very long pattern lengths. The consequent challenge for each device then becomes their packaging into high-speed modules that can handle these frequencies without degrading device performance. Even though broad bandwidth is essential, from a subsystem perspective, low cost and low power consumption as well as compactness become the driving force behind novel device technology. A good example to this is the traveling-wave electroabsorption (EA) modulator [6] introduced in the preceding chapter, which reduces the microwave power requirement while maintaining high-speed operation and offering the option of integration with other system components.

In this chapter, the assembly and investigation of a 30 Gbit/s ETDM system, with special emphasis on the high-speed transmitter and receiver subsystems technologies will be described. This research predates most of the

subsequent demonstrations at 40 Gbit/s and higher. The 30 Gbit/s system also forms the basis of the advanced experiments described in Chapter 4. The chapter concludes with a general analysis of 40 Gbit/s optical transmission systems based on electrical multiplexing and demultiplexing, and an investigation of future ETDM systems beyond 40 Gbit/s.

## **2.2 Overview of 40 Gbit/s Electrical TDM Systems**

This section reviews various published device technologies for 40 Gbit/s ETDM systems, including high-speed electrical multiplexers, electrical demultiplexers, broadband amplifiers (modulator drivers and baseband amplifiers), 40 GHz photoreceivers as well as optical modulators with bandwidths exceeding 30 GHz. Published 40 Gbit/s optical transmission systems employing these technologies will also be reviewed.

### ***2.2.1 Research in 40 Gbit/s Integrated Circuit Technology***

The electrical time division multiplexer is the key component for the transmitter subsystem of high-speed ETDM systems. Since 1994, there has been several demonstrations of 40 Gbit/s and higher multiplexers in various device technologies such as AlGaAs/GaAs heterojunction bipolar transistors (HBT) [7, 8], Si-bipolar [9], InAlAs/InGaAs/InP high electron mobility transistors (HEMT) [10, 14, 15], GaAs HEMT [12, 16, 19], Si/Ge-bipolar [13, 21], InP/InGaAs HBT [17, 18, 20], and GaAs MESFET [22]. Table 2.1 summarizes the important characteristics, such as maximum bit rate of operation, multiplexing configuration, power consumption and output voltage swing of these multiplexers. The maximum bit rate achieved is 80 Gbit/s on-wafer [15] and 60 Gbit/s in a high-speed test-fixture [12], which are both 2:1 multiplexers. On the other hand, the highest operating speed achieved for a 4:1 multiplexer is 50 Gbit/s [20].

Company, Year	Bit Rate (Gbit/s)	IC Technology	MUX Scheme	Power (W)	Output Swing (V)	Measurement	Ref.
Toshiba, 1994	40	AlGaAs/GaAs HBT	4:1	0.70	0.80	on-wafer	[7]
Rockwell, 1995	40	AlGaAs/GaAs HBT	4:1	3.50	0.40	on-wafer	[8]
Siemens, 1995	50	Si-bipolar	2:1	0.30	0.60	packaged	[9]
NTT, 1996	46	InAlAs/InGaAs /InP HEMT	2:1	1.70	0.80	packaged	[10]
Fraunhofer Inst., 1997	45	AlGaAs/GaAs HEMT	2:1	0.50	1	on-wafer	[11]
Siemens, 1997	60	Si/Ge-bipolar	2:1		0.50	test fixture	[12]
NTT, 1997	44	GaAs MESFET	2:1	0.91		on-wafer	[13]
NTT, 1997	64	InAlAs/InGaAs /InP HEMT	2:1	2.40	0.90	on-wafer	[14]
NTT, 1998	80	InAlAs/InGaAs /InP HEMT	2:1	2.70	1	on-wafer	[15]
Fraunhofer Inst., 1998	44	AlGaAs/GaAs HEMT	4:1		0.70	on-wafer	[16]
	55		2:1	1.50	0.70		
Hitachi, 1998	40	InP/InGaAs HBT	2:1	2.30	0.70	packaged	[17]
CNET, 1998	40	InP HBT	2:1	1	0.40	packaged	[18]
Philips, 1998	44	GaAs HEMT	2:1	0.50	1	on-wafer	[19]
Lucent, 1999	50	InP HBT	4:1	0.80	0.15	on-wafer	[20]
Hitachi, 1999	40	Si/Ge HBT	2:1	0.87	0.6	on-wafer	[21]
NTT, 2000	70	GaAs MESFET	2:1	0.19	0.13	on-wafer	[22]

**Table 2.1** Chronological summary of published electrical time division multiplexers with operation at or higher than 40 Gbit/s. MUX: multiplexer.

The electrical time division demultiplexer is the key component at the receiver subsystem of high-speed ETDM systems. The device technologies for 40 Gbit/s and higher demultiplexers as well as decision circuits based on D-type flip-flops (DFF) include InAlAs/InGaAs/InP HEMT [10, 25, 26], Si-bipolar [23], GaAs MESFET [24, 28], Si/Ge-bipolar [21, 27, 33], InP HBT [19, 29, 32], GaAs HEMT [20, 31], GaAs HBT [30], and InAlAs/InGaAs HBT [34]. Table 2.2 summarizes the important characteristics, such as maximum bit rate of operation, demultiplexing configuration, power consumption and input voltage swing requirements of these demultiplexers. The maximum bit rate of operation achieved is 60 Gbit/s for a 1:2 demultiplexer configuration in a measuring socket [27] while 40 Gbit/s operation was achieved for 4:1 demultiplexers [32-34]. It should be noted that some of the listed devices in Table 2.2 are DFF's, which when driven at 10 GHz are capable of 40-to-10 Gbit/s demultiplexing. Since the DFF has only one output, individual channels can be selected by varying the phase of the clock signal.

In 40 Gbit/s ETDM systems, high-power modulator drivers become very significant for satisfying the voltage drive requirements of optical modulators by amplifying the electrical multiplexer output. Modulator drivers with 40 Gbit/s output voltage swings of about  $3 V_{pp}$  in various technologies including SiGe-bipolar [35], InP/InGaAs HBT [18], GaAs HEMT [36], and AlGaAs/InGaAs HEMT [37] have been demonstrated. Recently, a 40 Gbit/s modulator driver was developed using GaAs p-HEMT technology, which is capable of an output voltage swing greater than  $5 V_{pp}$  [38]. A variety of packaged baseband amplifiers that are suitable for various 40 Gbit/s applications have also been demonstrated since 1995 [39-43].

Company, Year	Bit Rate (Gbit/s)	IC Technology	IC Type	Power (W)	Input Swing (V)	Measurement	Ref.
NTT, 1996	40	InAlAs/InGaAs /InP HEMT	1:2	1.90	0.80	packaged	[10]
Siemens, 1996	46	Si-bipolar	1:2	0.83	0.40	packaged	[23]
NTT, 1997	40	GaAs MESFET	DFF		0.40	on-wafer	[24]
NTT, 1997	40	InAlAs/InGaAs /InP HEMT	1:2	3.90		on-wafer	[25]
NTT, 1997	46	InAlAs/InGaAs /InP HEMT	DFF	1.70	0.1	on-wafer	[26]
Siemens, 1997	60	Si/Ge-bipolar	1:2	1.20	0.30	test fixture	[27]
CNET, 1998	40	InP HBT	1:2	2.50		packaged	[18]
Philips, 1998	44	GaAs HEMT	1:2			on-wafer	[19]
NTT, 1998	40	GaAs MESFET	DFF		0.80	on-wafer	[28]
Hitachi, 1999	40	Si/Ge HBT	1:2			on-wafer	[21]
NTT, 1999	40	InP/InGaAs HBT	DFF	0.94		on-wafer	[29]
NEC, 1999	40	GaAs HBT	DFF			packaged	[30]
Fraunhofer Inst., 1999	40	GaAs HEMT	1:2	3.20		on-wafer	[31]
NTT, 1999	40	InP/InGaAs HBT	1:4	2.97		on-wafer	[32]
Hitachi, 2000	40	Si/Ge HBT	1:4	3.20	0.40	on-wafer	[33]
Lucent, 2000	40	InP HBT	1:4	1.10	0.30	on-wafer	[34]

**Table 2.2** Chronological summary of published electrical time division demultiplexers and DFF's with operation at or higher than 40 Gbit/s. DFF: D-type flip-flop.



### ***2.2.2 Research in 40 Gbit/s Opto-Electronic Technology***

The receiver subsystem of 40 Gbit/s ETDM systems requires photoreceivers that are capable of performing efficient high-speed optical-to-electrical (O/E) conversion. Several monolithically integrated receiver modules operating at 40 Gbit/s have been demonstrated in various technologies [44-50]. Recently, a 40 Gbit/s optical receiver was realized by directly driving the decision circuit with a  $1 V_{pp}$  voltage swing generated from an untraveling-carrier photodetector [51].

High-speed optical modulators can be classified into electro-optic (EO) and electroabsorption (EA) modulators. Traveling-wave EO modulators with greater than 30 GHz bandwidth suitable for 40 Gbit/s modulation at  $1.55 \mu\text{m}$  have been demonstrated using  $\text{LiNbO}_3$  [52-56], and GaAs/AlGaAs [57].  $\text{LiNbO}_3$  based EO modulators have reached optical bandwidths of 75 GHz [53] and electrical bandwidths of 44 GHz [52]. On the other hand, the lowest drive voltage of 2.9 V has been achieved for a 30 GHz device [55] while a push-pull type ridged  $\text{Ti:LiNbO}_3$  optical modulator required a half-wave voltage of 1.95 V in push-pull operation [54]. In the past decade, EA modulators have emerged as alternative external modulators due to their high bandwidth and low drive voltage requirements [58-67]. Table 2.3 summarizes the bandwidth, optical insertion loss, and extinction ratio of these EA modulators. The highest electrical bandwidth achieved is 50 GHz [60] while the lowest drive voltage required for 40 Gbit/s modulation is  $0.9 V_{pp}$  [61]. These EA modulators are also suitable for integration with other optical devices, such as DFB lasers [63] and semiconductor optical amplifiers (SOA) [66] resulting in low optical insertion loss.

Company, Year	Material System	$f_{3\text{dBc}}$ (GHz)	Insertion Loss (dB)	Static Extinction Ratio	Dynamic Extinction Ratio	Ref.
CNET, 1995	InGaAs/InAlAs	42	10	20 dB @ 2.4 V		[58]
Alcatel, 1995	InGaAsP	42		16 dB @ 2.5 V		[59]
Hitachi, 1995	InGaAs/InAlAs	50	8	15 dB @ 2.8 V		[60]
NTT, 1996	InGaAs/InAlAs	40	9	> 15 dB @ 2.5 V		[61]
CNET, 1997	InGaAsP	42				[62]
NTT*, 1998	InGaAsP	> 30	$P_{\text{out}} = -3\text{ dBm}$	23 dB @ 4 V	14 dB @ 3 V <sub>pp</sub>	[63]
NTT, 1998	InGaAs/InAlAs	42	8	20 dB @ 1 V	> 15 dB @ 3 V <sub>pp</sub>	[64]
Lucent, 1999	InGaAsP	43	15	20 dB @ 6 V	6 dB @ 3 V <sub>pp</sub>	[65]
OPTO+, 2000	InGaAsP	36	0	> 18 dB @ 4.5 V	10 dB @ 2 V <sub>pp</sub>	[66]
Hitachi, 2000	InGaAs/InAlAs	40	11.5	15 dB @ 1.7 V	11 dB @ 2.3 V <sub>pp</sub>	[67]

**Table 2.3** Chronological summary of published electroabsorption (EA) modulators with bandwidths higher than 30 GHz. (\*) indicates integrated EA modulator with DFB laser.  $f_{3\text{dBc}}$ : 3-dB electrical bandwidth.

### 2.2.3 40 Gbit/s Electrical TDM System Demonstrations

Single-channel and multi-wavelength optical fiber transmission experiments based on 40 Gbit/s line rates have been extensively investigated and demonstrated in the past decade (Chapter 1). In these experiments, various transmitter and receiver subsystems have been employed, including electrical or optical multiplexing and demultiplexing for the optical transmission of 40 Gbit/s non-return-to-zero (NRZ) and return-to-zero (RZ) modulation schemes. In this section,

40 Gbit/s optical systems with the following specific characteristics will be reviewed: 1) 40 Gbit/s electrical transmitter employing either EA or LiNbO<sub>3</sub> modulators, and 2) receiver subsystems based on 40 Gbit/s electrical or optical demultiplexing [1-3, 68-76]. Table 2.4 summarizes the transmitter and receiver subsystem characteristics of 40 Gbit/s electrically multiplexed TDM systems in chronological order. References are provided for the electrical IC's and modulators used (refer to Tables 2.1-2.3).

The first 40 Gbit/s optical transmission using full electrical time division multiplexing and demultiplexing was demonstrated in 1997 at *Siemens*, Germany [1]. In this experiment, the electrical 40 Gbit/s  $2^7-1$  data stream of 7 V<sub>pp</sub> was applied to a 20 GHz LiNbO<sub>3</sub> Mach-Zehnder modulator, and error-free transmission over 148 km of dispersion shifted fiber (DSF) with an average receiver sensitivity of -23.2 dBm was achieved. Concurrently, at *NTT Laboratories*, Japan, an electrically multiplexed 40 Gbit/s  $2^7-1$  data stream of 3.3 V<sub>pp</sub> was applied to a Ti:LiNbO<sub>3</sub> modulator, and electrically demultiplexed using a DFF selector with an average receiver sensitivity of -24.3 dBm [68]. Recently, a 40 Gbit/s ETDM system prototype based on 40 Gbit/s electrical multiplexer and demultiplexer was demonstrated, which achieved a receiver sensitivity of -25.1 dBm for a pseudo random bit stream (PRBS) of  $2^7-1$  [72]. An automatic bias controller was used to compensate for the DC drift of the LiNbO<sub>3</sub> modulator. A 3-dB optical power penalty was acquired for longer pattern lengths ( $2^{15}-1$ ), which was attributed to (1) the degraded input sensitivity of the decision circuit, (2) accumulation of pattern jitter, and (3) intersymbol interference in the process of E/O conversion in the transmitter and O/E conversion in the receiver.

Company, Year	Electrical Multiplexer (MUX)	Optical Modulator, $V_{drive}$	Demultiplexer (DMUX)	Pattern Length (PRBS)	Sensitivity (dBm) @ BER = $10^{-9}$	Ref.
NTT, 1996	2:1 MUX [10]	EA 26 GHz 2 V <sub>pp</sub>	optical DMUX	2 <sup>7</sup> -1	-26	[2]
Siemens, 1997	4:1 MUX [12]	LN 20 GHz 7 V <sub>pp</sub>	1:2 DMUX [23]	2 <sup>7</sup> -1	-23.3	[1]
NTT, 1997	2:1 MUX [14]	LN [53] 3.3 V <sub>pp</sub>	DFF [26]	2 <sup>7</sup> -1	-24.8	[68]
NTT, 1998	2:1 MUX [14]	LN [54] 3 V <sub>pp</sub>	optical DMUX	2 <sup>7</sup> -1	-26	[69]
Alcatel, 1999	2:1 SiGe MUX	EA [59] 3 V <sub>pp</sub>	DFF	2 <sup>7</sup> -1	-23.2	[70]
NEC, 1999	2:1 MUX	LN [56]	DFF [30]	2 <sup>7</sup> -1	-24.6	[71]
NTT, 2000	2:1 MUX [15]	LN [55] 3 V <sub>pp</sub>	1:2 DMUX [10]	2 <sup>7</sup> -1 2 <sup>15</sup> -1	-24.1 -21	[72]
NTT, 2000	2:1 MUX [14]	LN [55]	DFF [26]	2 <sup>23</sup> -1	-24	[73]
Nortel, 2000	GaAs HBT MUX	LN	optical DMUX	2 <sup>31</sup> -1	Q > 7	[74]
Lucent, 2000	electrical MUX	LN	optical DMUX	2 <sup>31</sup> -1	< 10 <sup>-10</sup>	[3]
Oki, 2000	electrical MUX	EA 3 V <sub>pp</sub>	optical DMUX	2 <sup>15</sup> -1		[75]
Alcatel, 2000	2:1 SiGe MUX	LN 5-6 V <sub>pp</sub>	DFF	2 <sup>15</sup> -1		[76]
Hitachi, 2000	2:1 MUX [17]	EA [67] 2.3 V <sub>pp</sub>	DFF	2 <sup>7</sup> -1	-25	[67]

**Table 2.4** Chronological summary of published 40 Gbit/s ETDM optical transmission experiments. MUX: multiplexer; DMUX: demultiplexer; LN: LiNbO<sub>3</sub> modulator; PRBS: pseudo random bit stream; BER: bit error rate.

As it can be seen from Table 2.4, both LiNbO<sub>3</sub> and EA modulators were employed as 40 Gbit/s optical modulators. The lowest drive voltage requirements were 2 V<sub>pp</sub> for an EA modulator [2] and 3 V<sub>pp</sub> for a LiNbO<sub>3</sub> modulator [69]. Most of the recent very high capacity WDM experiments employed LiNbO<sub>3</sub> modulators

since they exhibit less wavelength dependence in comparison to EA modulators. It should be noted that in these WDM laboratory experiments, typically a single modulator is used to encode data onto all the wavelength channels, which puts stringent requirements on the modulator. In a real communication system, each wavelength channel would require separate optical modulators.

The receiver subsystems in the 40 Gbit/s experiments listed in Table 2.4 consist of high-speed 40 Gbit/s electrical demultiplexers, 40 Gbit/s DFF's employed as channel selectors, and optical demultiplexing techniques. It is interesting to note that only two research groups have employed a full 40 Gbit/s electrically multiplexed and demultiplexed system [1, 72]. Both systems were limited to pattern lengths of  $2^7-1$ . The longest pattern length of  $2^{31}-1$  was employed only in optically demultiplexed systems [3, 74]. On the other hand, the 40 Gbit/s WDM field trial operated at a PRBS of  $2^{23}-1$ , which employed a DFF as the electrical demultiplexer [73].

In the next section, a 30 Gbit/s electrically multiplexed and demultiplexed optical system with both EA and LiNbO<sub>3</sub> modulators will be described. The requirements and operation of the 30 Gbit/s subsystem technologies are comparable to 40 Gbit/s systems.

### **2.3 30 Gbit/s Electrical Time Division Multiplexed System Set-up**

This research began in 1995 when no electronic or opto-electronic devices were available for bit rates greater than 20 Gbit/s. The 30 Gbit/s ETDM set-up was entirely assembled using electronic integrated circuits (IC) from *Rockwell Science Center* and opto-electronic devices from the *University of California, Santa Barbara*. These devices in chip form were packaged into modules using the microwave packaging technology described in Appendix A. Recently, some of these devices have become commercially available. The system was then used to

investigate the high-speed operation of the traveling-wave EA modulator introduced in Chapter 1. A commercially available LiNbO<sub>3</sub> modulator was also used to compare the performance of the EA modulator. The current problems and future improvements for the 30 Gbit/s ETDM link are discussed in the next section.

### ***2.3.1 30 Gbit/s Electrical Components***

The 30 Gbit/s ETDM system requires a variety of high-speed electrical components. The most significant of these devices include the 30 Gbit/s 4:1 multiplexer [8], the 20-kHz to 50-GHz amplifiers [43], the 30 GHz optical receiver [77], and the 30 Gbit/s 1:4 demultiplexer and clock-recovery circuit [78]. It is imperative for repeatable and stable system demonstrations that all of these devices are packaged in modules with high-speed connector interfaces. Therefore, a high-speed microwave packaging technology was established [79], which was also applied to the design and fabrication of bias-tees and low-pass filters as well as prototype EA modulator modules (Appendix C).

The microwave packages were designed to accommodate 40 Gbit/s digital circuits with minimized microwave insertion losses at 40 GHz. For such high frequencies, the right choice of microwave connectors as well as transmission line designs are required to provide a high-speed interface between the electronic circuits and subsequent modules. A coplanar waveguide (CPW) transmission line was chosen for ease of providing a low-inductance ground between the chip and the surface ground of the substrate. In order to minimize CPW radiation and skin losses, quartz substrates with a low dielectric constant ( $\epsilon_r = 3.92$ ) were used. Cavity resonances and microstrip modes were suppressed by suspending the quartz substrate over an air gap with a microwave absorber. A detailed discussion and design of these packages are presented in Appendix A.

(1) *30 Gbit/s Electrical 4:1 Multiplexer*: The building point of any high-speed TDM system is the electrical time division multiplexer, which multiplexes 2 or more tributary data channels in the electrical time domain into one high-speed data stream. The most common multiplexing configurations are 2:1 and 4:1 multiplexing (Table 2.1) with the former having a relative simplicity and high-speed potential. Since most system applications require a four-fold capacity increase, three separate 2:1 multiplexer modules would be required to accomplish this task, which would potentially increase the cost, size and the power consumption of the transmitter subsystem. Therefore, a 4:1 multiplexing scheme is a key approach for a compact and cost-effective transmitter.

The 30 Gbit/s 4:1 multiplexer IC used in the system experiments were fabricated at the *Rockwell Science Center* on MOCVD grown epitaxial wafers using a self-aligned AlGaAs/GaAs HBT technology [8]. The 4:1 multiplexer circuit occupies an area of  $1 \times 2 \text{ mm}^2$ , and dissipates 3.5 W for a power supply voltage of -7.5 V. The device operates at a maximum bit rate of 30 Gbit/s, with data input levels of  $150 \text{ mV}_{pp}$  per channel and a differential clock input of  $500 \text{ mV}_{pp}$ . The multiplexer is capable of handling four simultaneous single-ended data channels while the system clock is half of the bit rate.

The 30 Gbit/s multiplexer IC's were packaged in a hexagonal module using the technology described in Appendix A. A hexagonal design was used to equalize the package delays for each of the 10 RF interconnections (four 7.5 Gbit/s tributary data inputs, two complementary 15 GHz clock inputs, two complementary 7.5 GHz clock outputs and two complementary 30 Gbit/s data outputs). Figure 2.1 shows a picture of the packaged multiplexer. The CPW transmission line length from the IC to the K-connector interface is 1" long. Figure 2.2 is a close-up picture of the packaged multiplexer IC. In order to achieve low inductance interconnections, very short ribbon bonds were used for the chip-to-substrate interface (Appendix A).

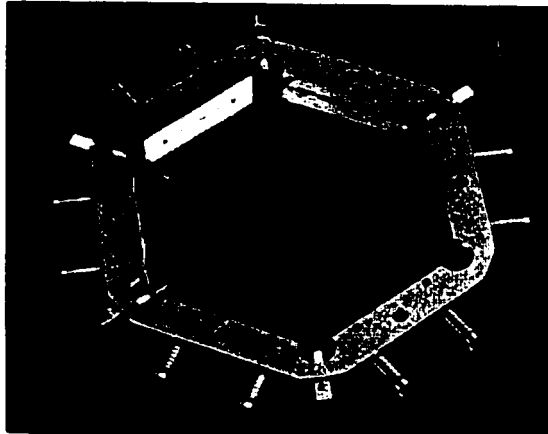


**Figure 2.1** Picture of the hexagonal 30 Gbit/s 4:1 electrical multiplexer module. The multiplexer IC is mounted in a brass package and surrounded by a quartz substrate.

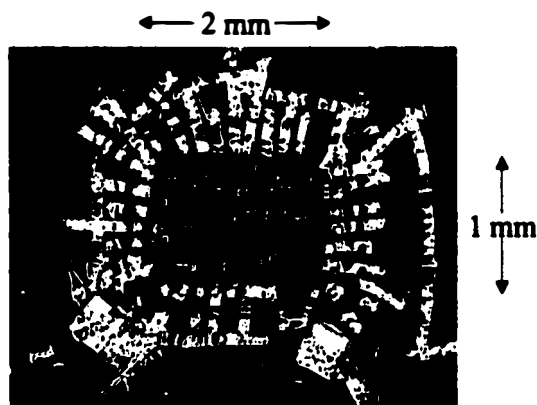


**Figure 2.2** Close-up picture of the packaged 30 Gbit/s 4:1 electrical multiplexer IC. The multiplexer IC is ribbon-bonded to the quartz substrate transmission lines.

The 30 Gbit/s multiplexer set-up used in the optical transmission experiments is schematically shown in Figure 2.3. A 12 Gbit/s pattern generator was used to generate the 7.5 Gbit/s data pattern. This data pattern was split four times and delayed with respect to each other using different cable lengths in order to ensure decorrelation between the four input data channels. Sufficient decorrelation between the four channels is necessary in order to preserve a true PRBS multiplexed output with the right spectral content. At the input to the



multiplexer, 1-dB electrical attenuators were employed to minimize the effects of possible reflections, which could deteriorate device operation. Similarly, a 15 GHz RF source, which was generated either by an external RF synthesizer or by the frequency multiplied 7.5 GHz clock output of the pattern generator, was used to drive the multiplexer. Electrical phase shifters were employed for the alignment of the data inputs and the complementary clock inputs for best operation. Figure 2.4(a)-(e) show the four 7.5 Gbit/s input data patterns to the multiplexer as well as the multiplexed 30 Gbit/s output. Each channel was delayed by at least 10 bits (or by 1.33 ns) with respect to each other. The complementary 30 Gbit/s eye diagrams are shown in Figure 2.5. The slight eye closure on every other channel is believed to be due to an on-chip clock-phase alignment problem in the electrical multiplexer.

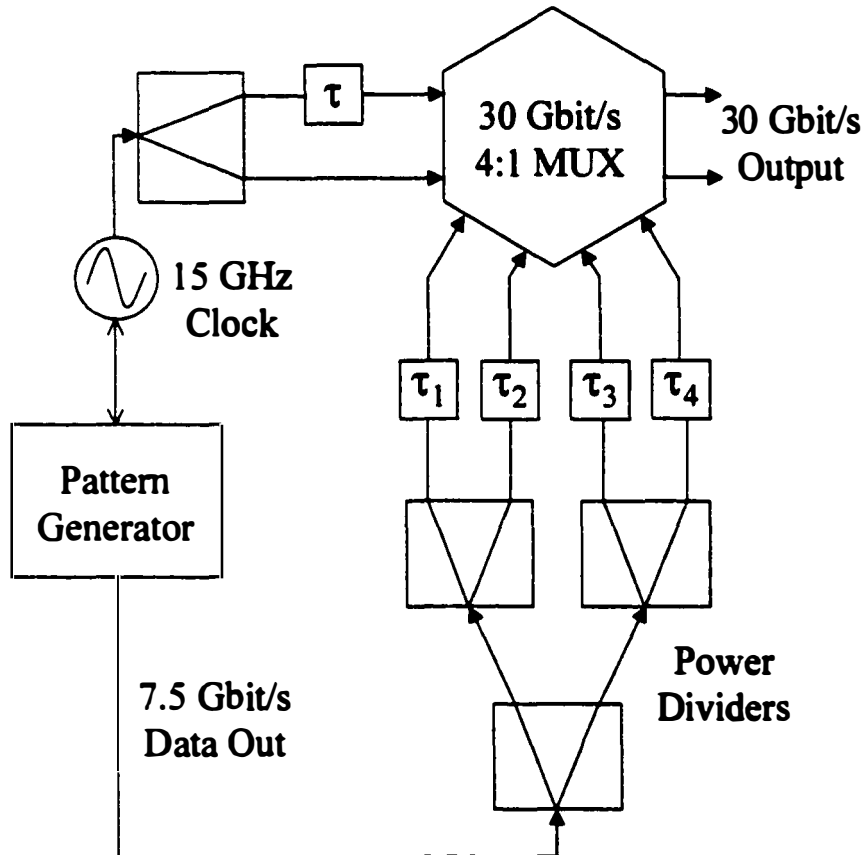
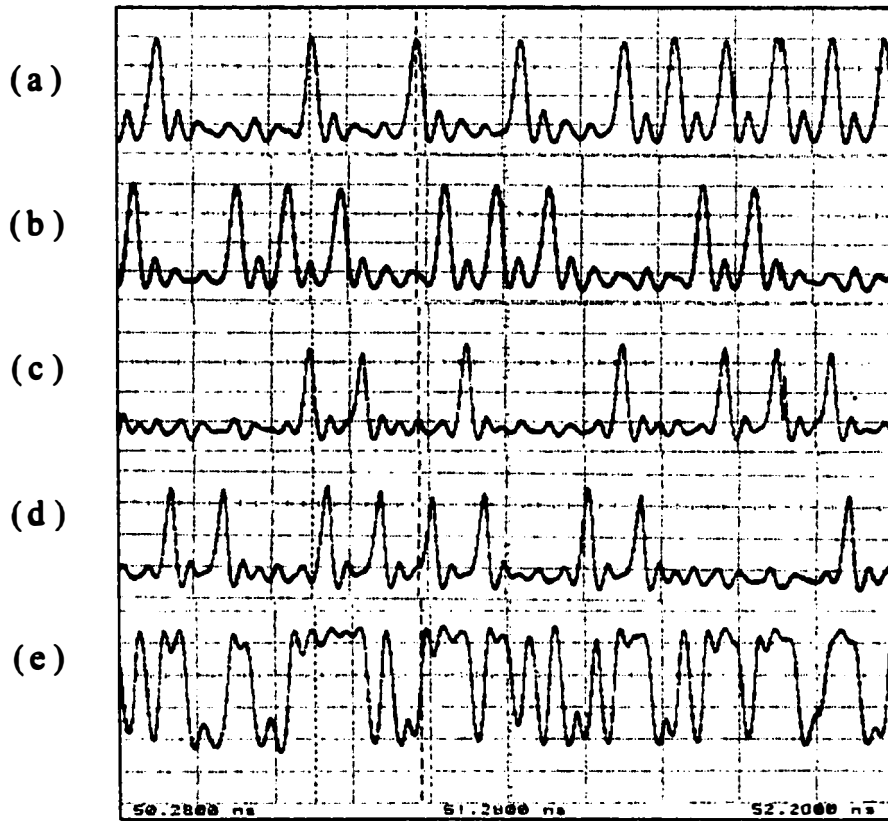
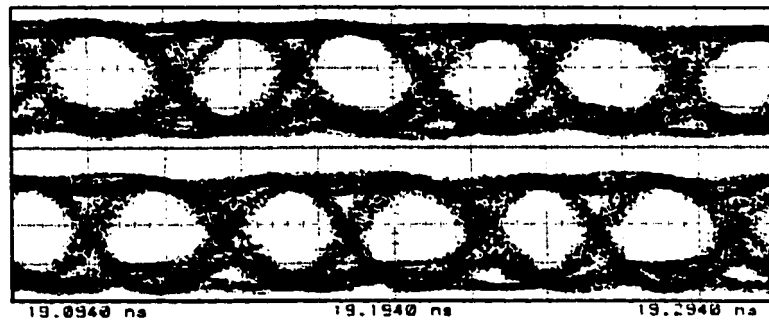


Figure 2.3 Schematic diagram of the 30 Gbit/s multiplexer set-up.



**Figure 2.4** Data patterns of (a)–(d) the four 7.5 Gbit/s input channels to the multiplexer, and (e) the 30 Gbit/s multiplexed output (200 ps/div).

The voltage level of the multiplexer output was typically 300 mV<sub>pp</sub>. Amplifiers are required to boost the drive signal and also to amplify the detected signal. The packaged amplifiers are described in the next section.



**Figure 2.5** The 30 Gbit/s eye diagrams of the complementary outputs of the multiplexer (20 ps/div).

(2) *20-kHz to 50-GHz Amplifiers*: Electrical amplifiers play a very significant role in various parts of high-speed electrical links. In the transmitter subsystem, high power modulator drivers amplify the electrical multiplexer output to satisfy the drive voltage requirements of the optical modulator. In the receiver subsystem, amplifiers are deployed as low-noise electrical pre-amplifiers and receiver post-amplifiers. These receiver amplifiers are responsible for providing enough voltage swing input to the decision circuit without introducing excess noise to the received photodetector output. For all three applications, a linear response with little magnitude variation and a constant group delay over a broad bandwidth is essential for low bit error rates with long pattern lengths.

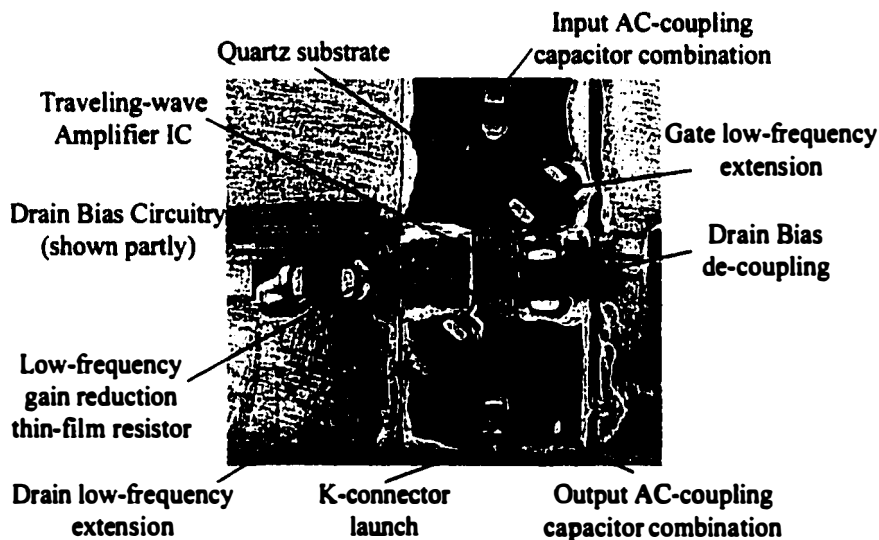


Figure 2.6 Close-up picture of the packaged 50 GHz amplifier [43].

In order to satisfy both the transmitter and the receiver amplification applications in the 30 Gbit/s ETDM set-up, a commercially available medium-power traveling-wave amplifier with an on-chip bandwidth of 2-50 GHz was employed [80]. The packaged amplifier modules were designed to reduce the overall microwave insertion losses and to extend the low-frequency cut-off of the amplifier to 20 kHz while maintaining gain-flatness over a broad bandwidth [43].

Figure 2.6 shows a photograph of the packaged IC while extensive detail of the amplifier module design is given in Appendix B.

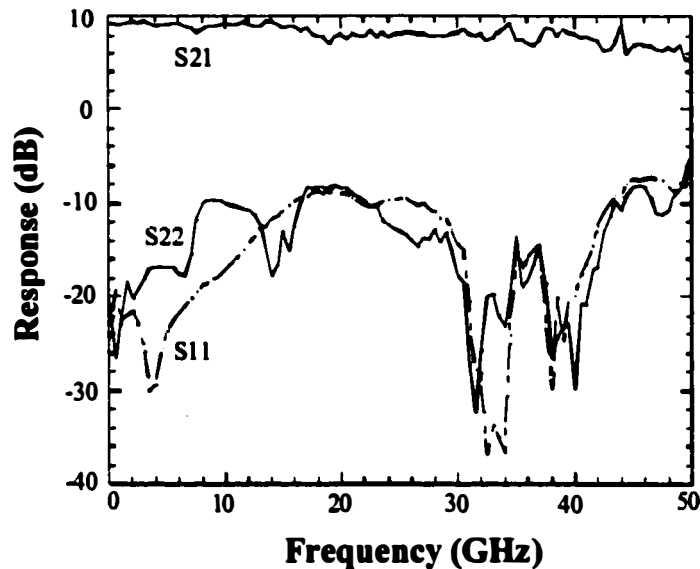


Figure 2.7 Measured frequency response of the packaged 50 GHz amplifier module.

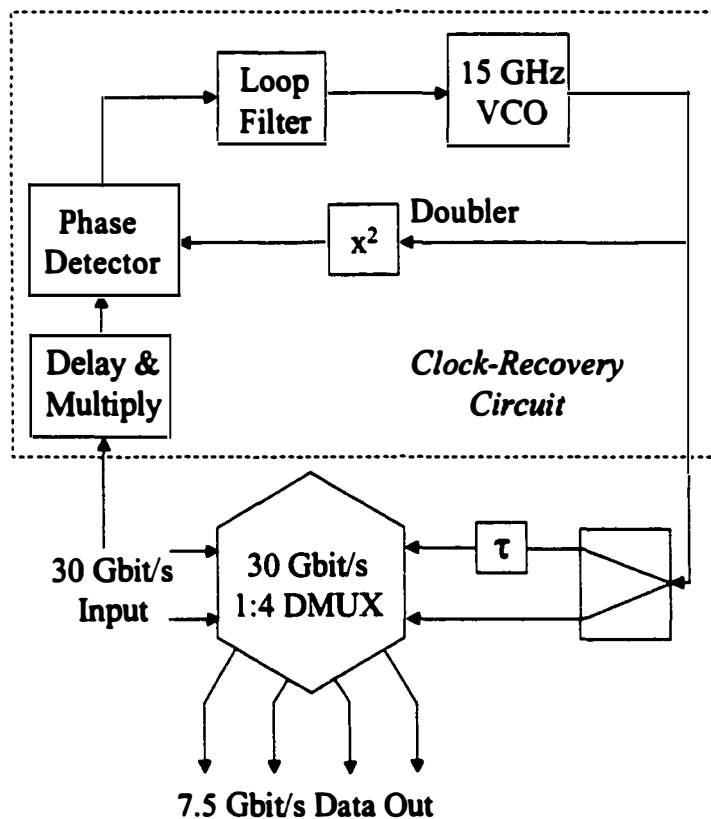


Figure 2.8 Eye diagrams of (a) the 30 Gbit/s input (100 mV/div; 13 ps/div), and (b) the 3 Vpp output of three cascaded amplifiers (750 mV/div; 20 ps/div).

Figure 2.7 shows a typical frequency response of the packaged amplifiers with an average gain of 8.5 dB and a gain-flatness within  $\pm 1.5$  dB from 20 kHz to 50 GHz. The packaged amplifier's response is in good agreement with the chip performance with the exception of some deterioration of the return losses, which is believed to be due to the ac-coupling capacitors. Figure 2.8 shows (a) the 30 Gbit/s

input and (b) the  $3 V_{pp}$  output of three cascaded amplifier modules. No significant degradation of the eye is observed. These amplifiers were also used as receiver post-amplifiers in the 30 Gbit/s ETDM set-up.

(3) *30 Gbit/s 1:4 Demultiplexer and Clock-Recovery Circuit*: As the electrical multiplexer is the starting point for a high-speed optical system, the electrical demultiplexer at the receiver subsystem is the final high-speed section. The electrical demultiplexer separates the high-speed electrical data stream back into the tributary channels while the clock-recovery circuit recovers the clock from the incoming data stream for re-timing and decision purposes. Figure 2.9 schematically describes the demultiplexer and clock-recovery circuit set-up.



**Figure 2.9** Schematic diagram of the 30 Gbit/s demultiplexer and clock-recovery circuit set-up.

Similar to the electrical multiplexer, a 1:2 or 1:4 demultiplexing configuration is most common for high-speed demultiplexers (Table 2.2). The 30 Gbit/s 1:4 demultiplexer IC's [78] used in the system experiments were fabricated using the AlGaAs HBT technology at Rockwell Science Center as described in the multiplexer section. The 1:4 demultiplexer circuit occupies an area of  $1 \times 2 \text{ mm}^2$ , and dissipates 3.1 W for a power supply voltage of -7.7 V. The device operates at a maximum bit rate of 30 Gbit/s, with complementary data input levels of  $250 \text{ mV}_{pp}$  and a differential clock input of  $500 \text{ mV}_{pp}$ . The device outputs four simultaneous single-ended data channels while the system clock is half of the bit rate. The demultiplexer IC's were packaged in a similar hexagonal package as the electrical multiplexer. An automatic gain control (AGC) amplifier [81] was used to ensure complementary data input to the demultiplexer.

The clock signal required for the demultiplexer was extracted using a 30 GHz clock-recovery circuit based on a phase-locked loop (PLL) [78]. A non-linear delay and multiply circuit was employed to recover the spectral clock component from the incoming 30 Gbit/s NRZ data stream. The PLL consists of a phase detector that functions as a high-speed mixer, a loop filter and a 15 GHz voltage controlled oscillator (VCO). The 15 GHz output of the VCO was fed into the 30 Gbit/s demultiplexer as well as a microwave doubler that generated a 30 GHz clock signal into the phase detector. Bit error rate measurements at 30 Gbit/s, which are presented in Section 2.3.2, revealed that there was only 0.3 dB receiver sensitivity degradation with the clock recovery circuit operating compared to using a clock signal directly from a synthesizer to drive the demultiplexer.

### ***2.3.2 30 Gbit/s Operation of Electroabsorption Modulator***

Electroabsorption modulators with their low driving voltage requirement, high modulation efficiency, polarization insensitivity and potential for integration

with lasers make them an attractive transmitter for 40 Gbit/s applications. EA modulators employing a traveling-wave electrode structure potentially have an increased extinction ratio with lower drive voltages by overcoming the bandwidth limiting  $RC$  time constant [6]. The high-speed operation of the 26 GHz traveling-wave EA modulator, fabricated at the *University of California, Santa Barbara*, was investigated by employing the 30 Gbit/s ETDM system components described in the preceding section. The fiber-to-fiber transmission characteristics of the 2- $\mu\text{m}$  wide, 300- $\mu\text{m}$  long traveling-wave EA modulator used in the 30 Gbit/s ETDM system is shown in Figure 2.10. The insertion loss was 15 dB at 1542 nm while a maximum extinction ratio of 25 dB at a reverse bias of -3.8 V was achieved for the TE mode. The traveling-wave electrode was terminated by a 32  $\Omega$  thin-film resistor, which extended the bandwidth of the device to 26 GHz (Figure 2.11).

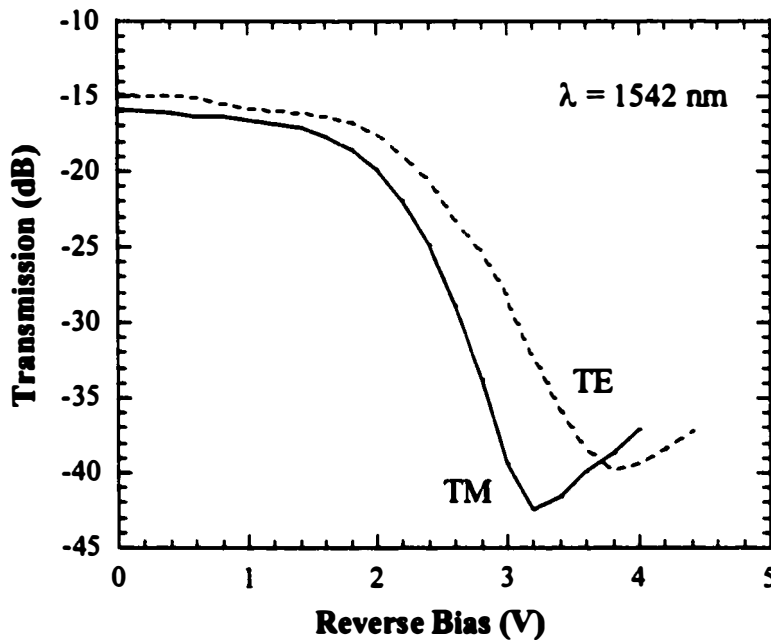


**Figure 2.10** Fiber-to-fiber transmission characteristic of the EA modulator used in the 30 Gbit/s ETDM experiment as a function of reverse bias at a wavelength of 1542 nm for both TE (dashed line) and TM (solid line) polarization modes.

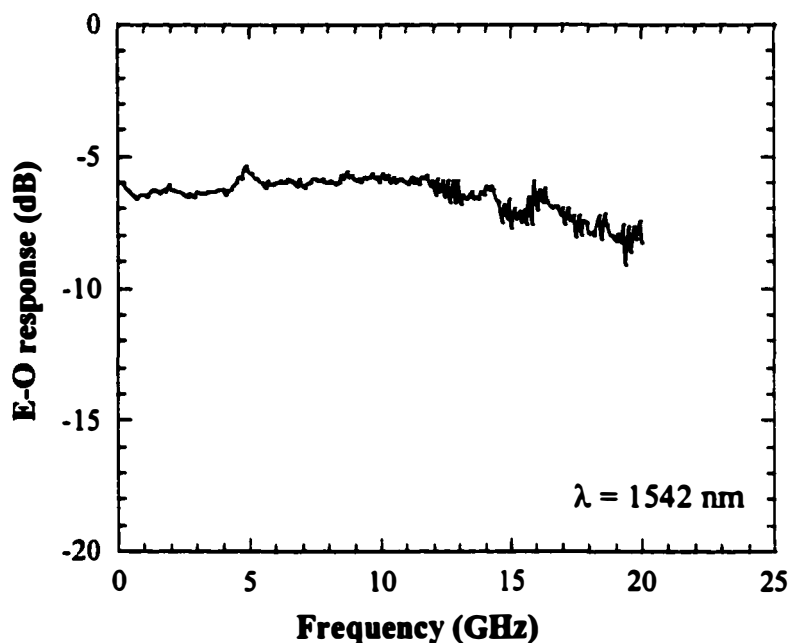


**Figure 2.11** Electro-optic frequency response of the EA modulator used in the 30 Gbit/s ETDM experiment at 1542 nm.

Transmission experiments at 30 Gbit/s were carried out using the set-up shown in Figure 2.12 [82]. The 30 Gbit/s NRZ electrical data stream was generated by multiplexing four 7.5 Gbit/s  $2^7-1$  PRBS delayed by 10 bits from each other using the 30 Gbit/s 4:1 multiplexer. A voltage swing of  $2 V_{pp}$  was applied to the EA modulator by high-speed probes. A DFB laser operating at 1542 nm followed by a polarization controller was used as the light source into the EA modulator. Two lens pairs were used to couple the light in and out of the modulator. The output signal from the EA modulator was amplified by a booster erbium-doped fiber amplifier (EDFA) before it was launched into 50 km of DSF with a zero-dispersion wavelength at 1540 nm.



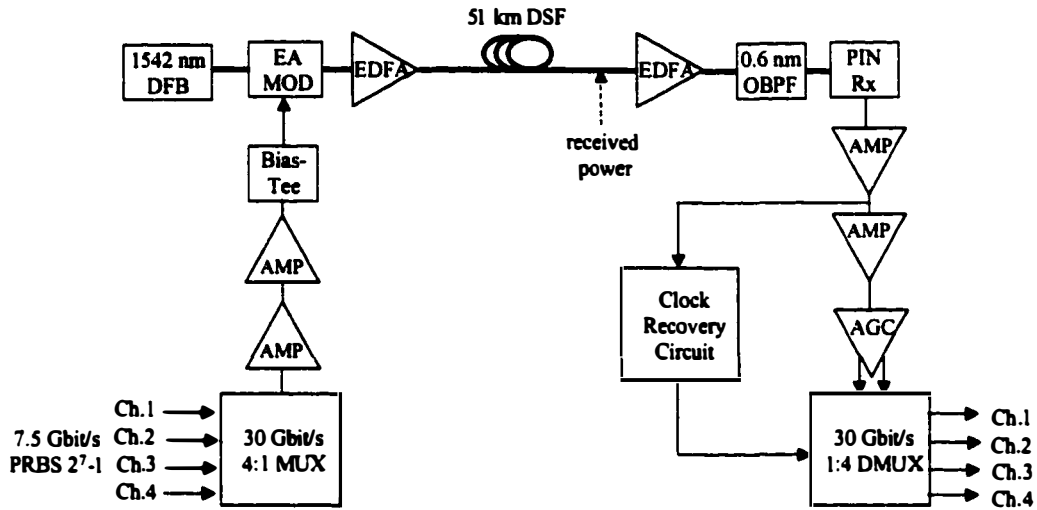


**Figure 2.12** Set-up for the 30 Gbit/s ETDM transmission experiment. MUX: multiplexer; AMP: 50 GHz amplifier; DSF: dispersion-shifted fiber; OBPF: optical bandpass filter; PIN Rx: pin-based receiver; AGC: automatic gain control amplifier; DMUX: demultiplexer.

At the receiver end, an EDFA followed by a 0.6 nm optical filter was used as an optical pre-amplifier into the packaged receiver with a 30 GHz bandwidth [77]. Broadband electrical amplifiers followed the optical receiver before the signal was electrically demultiplexed. The high-speed signal was fed into the 30 Gbit/s 1:4 demultiplexer and the clock-recovery circuit. A 15 GHz VCO was phase-locked to the incoming 30 Gbit/s NRZ data stream. The output voltage swing of 300 mV<sub>pp</sub> at 7.5 Gbit/s from the demultiplexer was then fed into the bit-error rate tester.

Figure 2.13 shows (a) the 30 Gbit/s output of the 4:1 multiplexer, (b) the received 30 Gbit/s signal after back-to-back transmission, and (c) after transmission over 50 km of DSF (mean dispersion of 0.16 ps/nm/km). In the case of back-to-back transmission, the booster EDFA was not used. The  $\alpha$  parameter of the modulator was +1.2 at the operating bias of -2 V. The extra noise on the eye diagram after 50 km transmission is due to the high noise figure of the booster EDFA. No pulse shape degradation is observed after the transmission. Figure

2.13(d) shows the demultiplexer output at 7.5 Gbit/s after 50 km of DSF transmission.

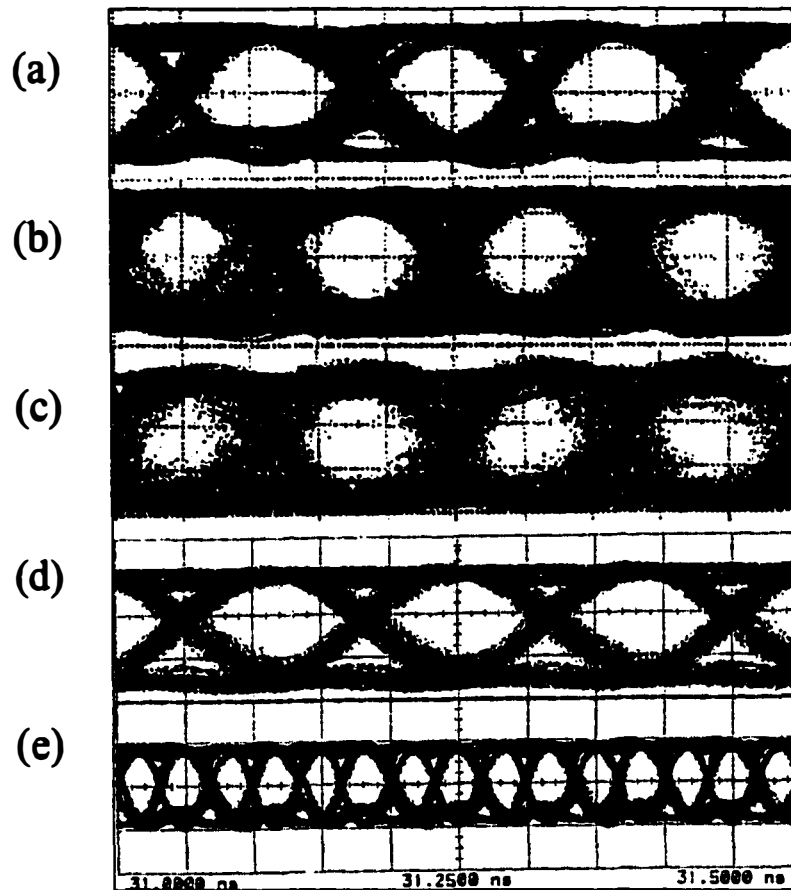


**Figure 2.13** Measured eye diagrams of (a) the 30 Gbit/s electrical output from the multiplexer (13 ps/div), (b) the received 30 Gbit/s signal after back-to-back transmission (13 ps/div) and (c) after transmission over 50 km of DSF (13 ps/div), (d) the demultiplexed 7.5 Gbit/s channel after transmission (150 ps/div), and (e) the 30 Gbit/s multiplexer output (150 ps/div).

The bit error rate (BER) performance of the traveling-wave EA modulator is shown in Figure 2.14. BER measurements in the back-to-back measurement revealed that there was only 0.3-dB receiver sensitivity degradation with the clock-recovery circuit operating compared to using a clock signal directly from a synthesizer. A 30 Gbit/s receiver sensitivity of -20.2 dBm and -16.5 dBm were

achieved for back-to-back and over 50 km of DSF transmission, respectively, for the best demultiplexed channel. In the back-to-back measurement, the booster EDFA was not used and error-free operation was achieved. However, a 3.7 dB power penalty and an error floor were observed in the fiber transmission using the booster EDFA. The optical input power to the booster EDFA was -18.3 dBm, which is within 3 dB of the back-to-back system sensitivity. In a separate back-to-back measurement including the booster EDFA, the same power penalty and error floor were observed (Figure 2.14). This verified that the penalty and the error floor are due to the high noise figure and the low optical input power to the booster EDFA. The EA modulator insertion loss was approximately 20 dB at the bias point including the fiber coupling losses, which is the major contributor to the low input power into the booster EDFA, and hence the lower optical sensitivity.

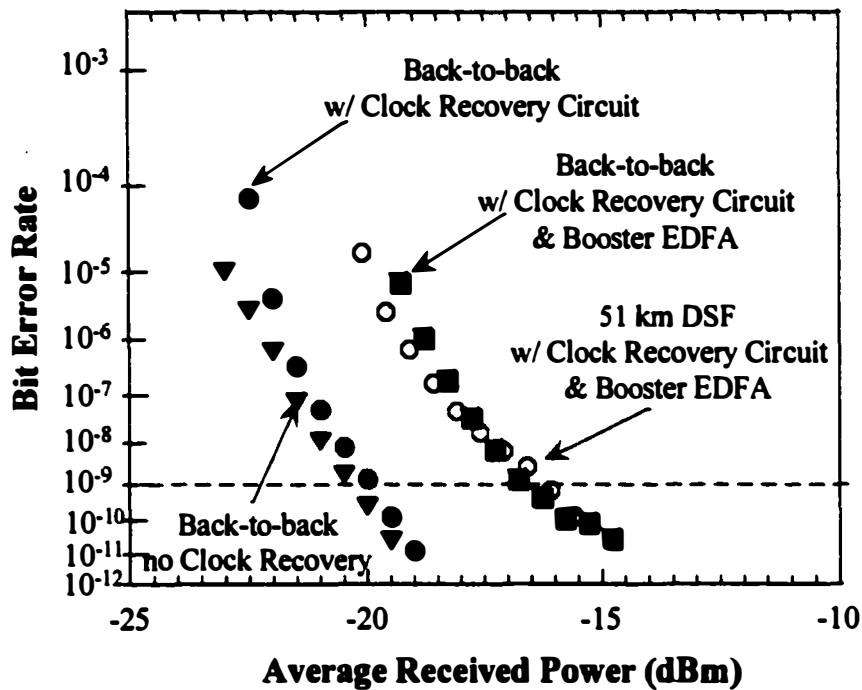


**Figure 2.14** BER measurements at 30 Gbit/s. Triangles: Back-to-back with no clock-recover circuit; filled circles: back-to-back with 30 GHz clock-recovery circuit; squares: back-to-back with clock-recovery circuit and booster EDFA; open circles: 51 km of DSF transmission with clock-recovery circuit and booster EDFA.

Transmission experiments using the traveling-wave EA modulator were also carried out at 10 Gbit/s ( $2^{31}-1$  pattern length) using commercially available components. Figure 2.15 shows the schematic diagram of the 10 Gbit/s experimental set-up. A DFB laser operating at 1542 nm followed by a polarization controller was used as the light source into the EA modulator. The input to the modulator was 3.4 dBm. The output signal from the EA modulator was amplified by an EDFA before it was launched into 150 km of DSF with a mean dispersion of  $-0.93$  ps/nm/km.

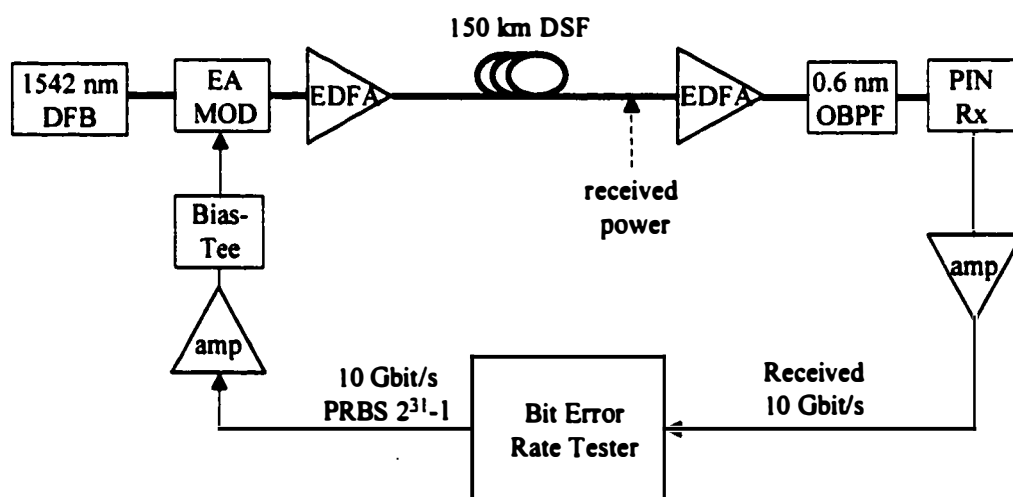


**Figure 2.15** Experimental set-up for the 10 Gbit/s transmission using the EA modulator. DSF: dispersion-shifted fiber; OBPF: optical bandpass filter; PIN Rx: pin-based receiver.

Figure 2.16 shows the BER performance of the EA modulator for back-to-back and over 150 km of DSF transmission. In the back-to-back measurements, error-free operation and a receiver sensitivity of  $-31.2$  dBm were achieved for both the TM and the TE polarizations without changing the operating conditions of the modulator. This indicates that the polarization-dependence of the EA modulator is very low. An improved sensitivity of  $-32.8$  dBm was observed after 150 km of DSF transmission due to the interplay between the positive chirp of the modulator and the slightly negative dispersion of the fiber. Contrary to its effect in the

30 Gbit/s transmission, the booster EDFA did not degrade the system performance since the optical output power from the EA modulator was significantly higher than the 10 Gbit/s system sensitivity.

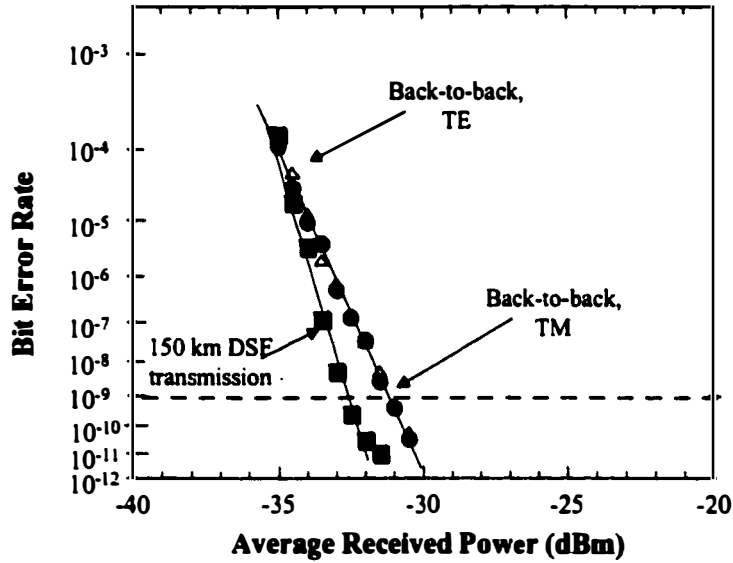


Figure 2.16 BER measurements at 10 Gbit/s. Triangles: Back-to-back TE polarization; circles: back-to-back TM polarization; squares: 150 km of DSF transmission TM polarization.

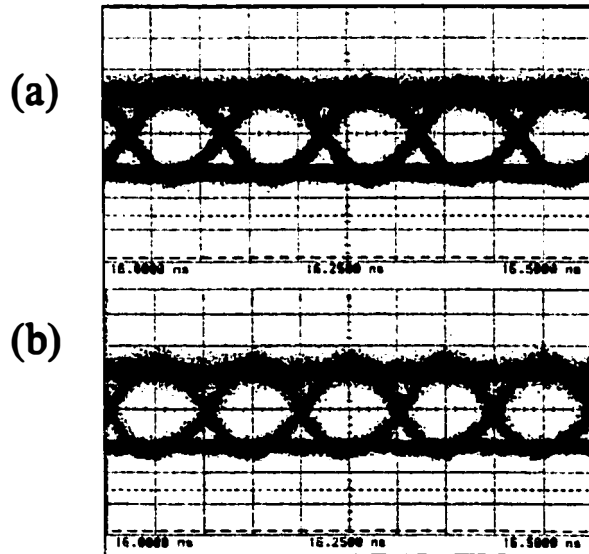
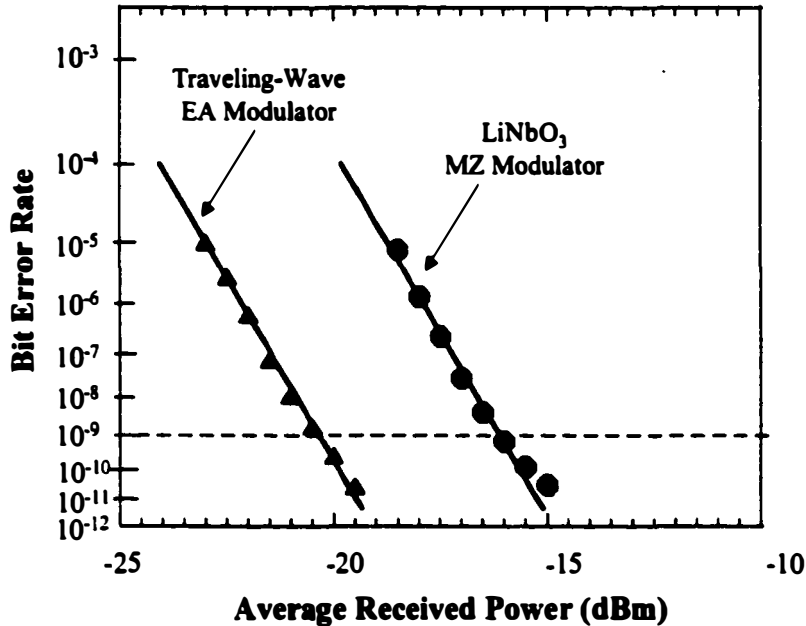


Figure 2.17 Measured 10 Gbit/s eye diagrams for (a) back-to-back and (b) after 150 km of DSF transmission (20 ps/div).

Figure 2.17 shows the received eye diagrams for (a) back-to-back, and (b) after transmission over 150 km of DSF. The long pattern length used in this transmission experiment indicates good low-frequency characteristics for this modulator. This is also a good indication that the pattern length limitation in the 30 Gbit/s transmission is due to the ETDM system, which is investigated in the next sections.

### ***2.3.3 30 Gbit/s Operation of LiNbO<sub>3</sub> Modulator***

In order to evaluate the performance of the EA modulator, the same 30 Gbit/s experimental set-up (Figure 2.12) was employed using a commercially available fiber-coupled LiNbO<sub>3</sub> modulator with a 3-dB electrical bandwidth of 20 GHz [83]. The device reaches a maximum extinction of 35.5 dB for a static  $V_{\pi}$  of 4.65 V while the optical insertion loss is 6 dB at 1542 nm. A 30 Gbit/s drive voltage of  $3 V_{pp}$ , generated by the electrical multiplexer and the cascade of amplifiers, was applied to the LiNbO<sub>3</sub> modulator biased at -2.64 V. The polarization of the optical input light was optimized and back-to-back BER measurements at 30 Gbit/s were performed using the same receiver subsystem as in Figure 2.13. The 30 Gbit/s BER measurements for the LiNbO<sub>3</sub> modulator performance are shown in Figure 2.18. A receiver sensitivity of -16.4 dBm for a BER of  $10^{-9}$  was achieved. Also shown in Figure 2.18 for comparative purposes is the back-to-back BER measurement using the EA modulator. The optical power penalty incurred with the LiNbO<sub>3</sub> modulator is 3.8 dB for a BER of  $10^{-9}$ . This penalty is predominantly due to the lower bandwidth and the high drive voltage requirement of the commercial LiNbO<sub>3</sub> modulator, which confirms that the traveling-wave EA modulator is a good candidate for future high-speed optical communication systems.



**Figure 2.18** BER measurements at 30 Gbit/s for the traveling-wave EA modulator (triangles) and the LiNbO<sub>3</sub> modulator (circles).

#### 2.4 Discussion and Analysis of the 30 Gbit/s Electrical TDM System

In the previous two sections, the high-speed performance of the traveling-wave EA modulator was investigated and determined to be superior over a commercially available LiNbO<sub>3</sub> modulator. A better receiver sensitivity for the EA modulator was achieved due to its nonlinear absorption characteristic, lower drive voltage requirement and higher bandwidth. Also, the EA modulator's low polarization dependence as well as its potential for integration provides additional advantages over the LiNbO<sub>3</sub> modulator. However, the overall 30 Gbit/s optical system exhibited two significant problems: (1) a high experimental receiver sensitivity of -20.2 dBm, and (2) a poor performance for long pattern lengths ( $2^{31}-1$ ). Therefore, an investigation and characterization of the overall 30 Gbit/s system performance is required.

### 2.4.1 Optical Demultiplexing using EA Modulator

In order to assess the performance of the 30 Gbit/s receiver subsystem, optical demultiplexing using an EA modulator, which will be described in detail in Chapter 3, was employed. The EA modulator was driven at 7.5 GHz and an optical transparency gate for the selection of any of the four channels was generated. The main advantage of this demultiplexing scheme in comparison to its ETDM counterpart is that the receiver subsystem requires a bandwidth of less than 7.5 GHz. Therefore, this technique eliminates any bandwidth-dependent penalty that might occur from the 30 Gbit/s receiver subsystem and can be constructed with commercially available 10 Gbit/s components.

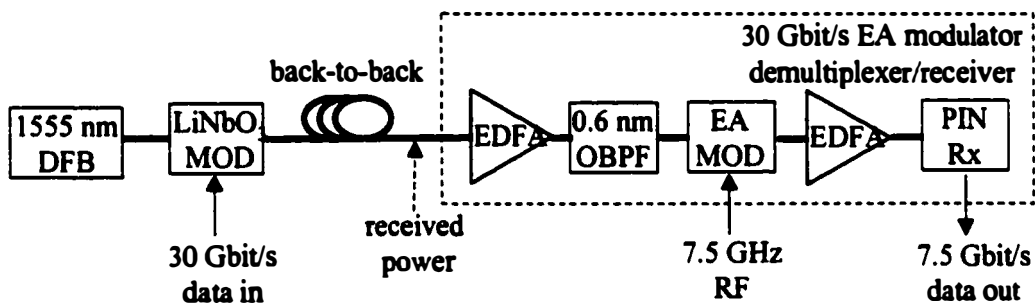


**Figure 2.19** Schematic of the 30 Gbit/s experimental set-up using an EA modulator as the optical demultiplexer. OBPF: optical bandpass filter; PIN Rx: pin-based receiver.

A schematic diagram of the experimental set-up including the EA modulator based receiver is shown in Figure 2.19. A low-noise EDFA (noise figure of 4 dB) was used as the optical pre-amplifier input to the EA demultiplexer while the receiver sensitivity was measured at the input of the pre-amplifier EDFA. For ease of experimental set-up, the fiber-coupled LiNbO<sub>3</sub> modulator was used as the optical data modulator in this experiment. This allowed for a direct comparison of 30 Gbit/s receiver sensitivities. The EA modulator was reverse biased at -4.5 V and driven with a 6 V<sub>pp</sub> 7.5 GHz RF signal to generate the optical demultiplexing window. Any of the four input channels can be selected by using an electrical



phase delay. Due to the optical insertion loss of the EA modulator, the demultiplexed optical channel was then amplified by an EDFA before detected by a commercial 10 Gbit/s receiver. The O/E converted signal was then electrically amplified for BER measurements.

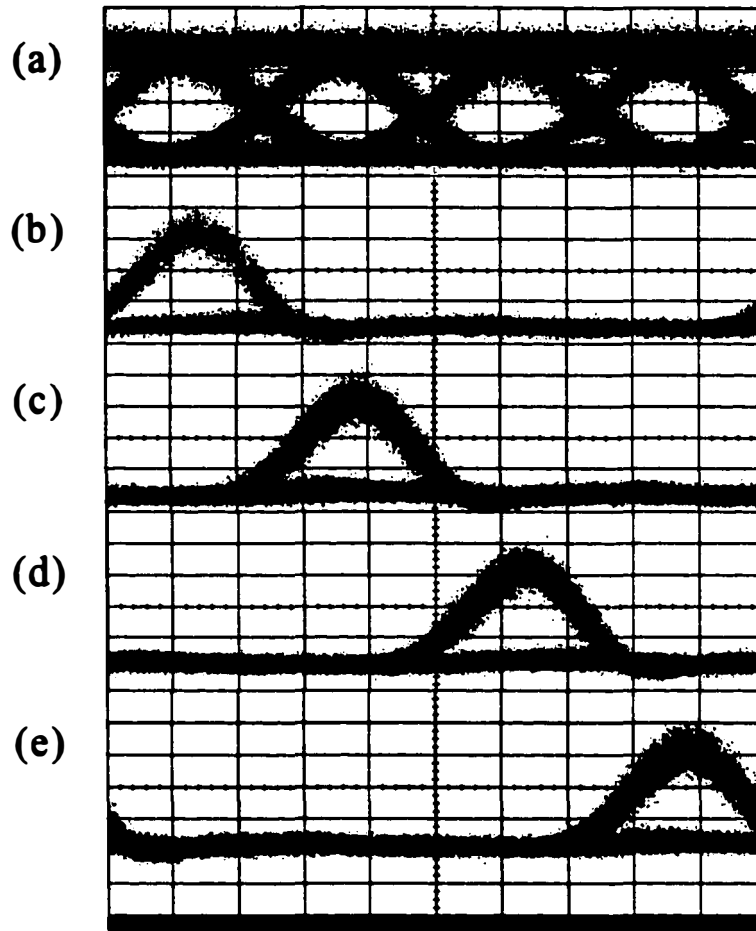


**Figure 2.20** Measured eye diagrams of (a) the 30 Gbit/s optical signal and (b)–(e) the four demultiplexed 7.5 Gbit/s optical channels (13.3 ps/div).

Figure 2.20 shows (a) the 30 Gbit/s optical eye diagram and (b)–(e) the four demultiplexed 7.5 Gbit/s optical channels measured with a 30 GHz photodetector. Clear eye opening is observed for all four channels. The demultiplexed and O/E converted 7.5 Gbit/s tributary channel is simultaneously shown with the 30 Gbit/s optical eye diagram in Figure 2.21.

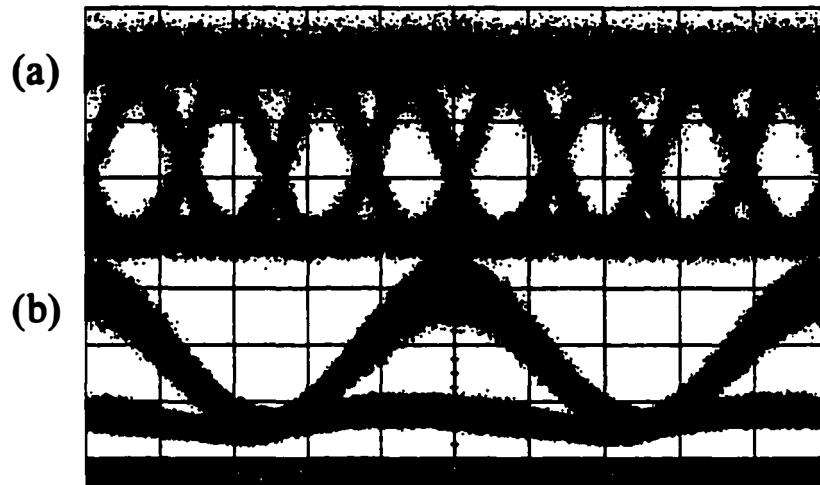


Figure 2.21 Measured eye diagrams of (a) the 30 Gbit/s optical signal and (b) the demultiplexed and O/E converted 7.5 Gbit/s electrical channel (26.6 ps/div).

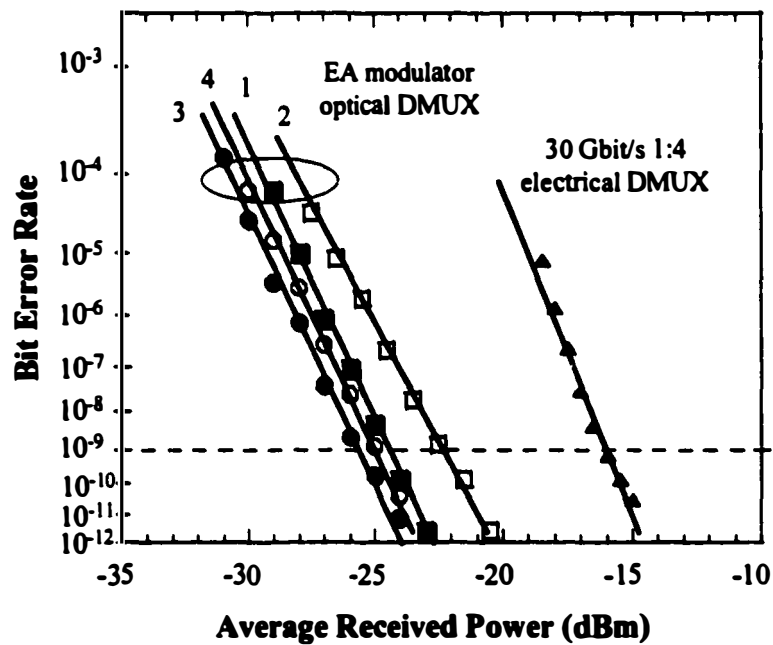


Figure 2.22 BER measurements at 30 Gbit/s for all four channels using the EA modulator based optical demultiplexer. Also shown is the 30 Gbit/s BER measurement using the 30 Gbit/s ETDM receiver subsystem (triangles).

The 30 Gbit/s BER measurements for all four channels are presented in Figure 2.22 for a pattern length of  $2^7-1$ . Error-free operation is achieved for all four channels with an average 30 Gbit/s receiver sensitivity of -25 dBm for three of the channels. Channel 2 exhibited a comparatively higher sensitivity (-22.2 dBm), which is attributed to a change in the operating conditions of the system during BER measurements. Also shown in Figure 2.22 is the BER measurement using the 30 Gbit/s ETDM receiver subsystem (Section 2.4.3). An average improvement of 8.6 dB in 30 Gbit/s receiver sensitivity is observed using the EA modulator based optical demultiplexer.

#### 2.4.2 Investigation of Optical Power Penalties

The receiver sensitivities obtained from the 10 and 30 Gbit/s back-to-back experiments using the EA and LiNbO<sub>3</sub> modulators as well as different set-ups were compared to assess the optical power penalties (Table 2.5). The BER can be obtained by,

$$BER = \frac{1}{2} \operatorname{erfc} \left( \frac{Q}{\sqrt{2}} \right) \quad (2.1)$$

where the  $Q$ -factor is given by,

$$Q = \frac{I_1 - I_2}{\sigma_1 + \sigma_2} \quad (2.2)$$

The signal current  $I_x$  for an optically pre-amplified receiver is given by,

$$I_x = RGP_x \quad (x = 0,1) \quad (2.3)$$

	Bit Rate (Gbit/s)	Modulator	Transmitter	EDFA (NF)	Receiver	sensitivity @ $10^{-9}$ (dBm)	Section
(a)	10	EA	commercial	7	commercial	-31.2 -32.8*	2.3.2
(b)	30	EA	30 Gbit/s	7	30 Gbit/s	-20.2	2.3.2
(c)	10	LiNbO <sub>3</sub>	commercial	4 7	commercial	-36 -33	
(d)	30	LiNbO <sub>3</sub>	30 Gbit/s	7	30 Gbit/s	-16.4	2.3.3
(e)	30	LiNbO <sub>3</sub>	30 Gbit/s	7	EA DMUX	-25	2.4.1

**Table 2.5** Summary of 10 and 30 Gbit/s system sensitivities using different transmitter and receiver subsystem configurations. (\*) denotes chirp compensated transmission.

where  $G$  is the optical amplifier gain and  $R$  is the responsivity of the photodetector. Neglecting the photodetector thermal noise ( $\sigma_{th}$ ), shot noise ( $\sigma_s$ ), and spontaneous-shot beat noise ( $\sigma_{s-sp}$ ), the noise current contributions are signal-spontaneous ( $\sigma_{sig-sp}$ ) and spontaneous-spontaneous ( $\sigma_{sp-sp}$ ) beat noises given by,

$$\sigma_{sp-sp}^2 = (q\eta GF_n)^2 \Delta v_{opt} \Delta f \quad (2.4a)$$

$$\sigma_{sig-sp}^2 = \frac{2(q\eta G)^2}{h\nu} F_n P_x \Delta f \quad (2.4b)$$

where  $\eta$  is the photodetector quantum efficiency,  $F_n$  is the optical amplifier noise figure,  $\Delta v_{opt}$  is the optical filter bandwidth, and  $\Delta f$  is the electrical bandwidth. Assuming infinite extinction ratio and balanced photodetection, Eq. (2.3) and (2.4) can be written as,

$$I_1 = 2RG\bar{P}_{rec} \text{ and } I_0 = 0 \quad (2.5a)$$

$$\sigma_1^2 = \sigma_{sig-sp}^2 + \sigma_{sp-sp}^2 \quad \text{and} \quad \sigma_0 = \sigma_{sp-sp} \quad (2.5b)$$

The receiver sensitivity  $P_{rec}$  is obtained by substituting Eq. (2.5) in Eq. (2.2) and solving for  $P_{rec}$ :

$$\bar{P}_{rec} = h\nu F_n \Delta f \left( Q^2 + Q \sqrt{\frac{\Delta v_{opt}}{\Delta f}} \right) \quad (2.6)$$

(1) *Optical Pre-Amplifier EDFA*: From Eq. (2.6), it can be seen that the noise figure of the optical pre-amplifier is directly proportional to the received power. An optical power penalty,  $\delta_{EDFA}$ , due to the EDFA noise figure can be defined as,

$$\delta_{EDFA} = 10 \log(F_n) \quad (2.7)$$

From the measurements in Table 2.5(b), a 3-dB noise figure difference in the 10 Gbit/s measurements resulted in a 3-dB optical power penalty. Therefore, a 3-dB improvement in receiver sensitivity would be expected in the measurements of (a), (b), and (d) (Table 2.5). This would result in an improved 30 Gbit/s receiver sensitivity of -23.2 dBm and -19.4 dBm for the EA and the LiNbO<sub>3</sub> modulators, respectively.

(2) *30 Gbit/s Electrical Receiver Subsystem*: The 30 Gbit/s BER measurements employed with the LiNbO<sub>3</sub> modulator using the 30 Gbit/s electrical receiver subsystem (d) and the optical demultiplexer (e) allow for a direct assessment of the electrical receiver subsystem performance. By subtracting the power penalty incurred from the optical pre-amplifier EDFA, a power penalty ( $\delta_{RX}$ ) of 5.6 dB is observed for the 30 Gbit/s receiver subsystem. This penalty is believed to be due to

several factors: (1) the microwave reflections between the receiver and the post-amplifiers, (2) the added extra noise and microwave reflections within the cascade of three post-amplifiers, and (3) the decision capability of the 30 Gbit/s demultiplexer. The 30 Gbit/s receiver sensitivity of the EA modulator in Table 2.5(b) would therefore increase to -25.8 dBm (only  $\delta_{RX}$ ) and -28.8 dBm ( $\delta_{RX}$  &  $\delta_{EDFA}$ ).

(3) *30 Gbit/s Electrical Transmitter Subsystem*: When the 30 Gbit/s experiment in Section 2.4.1 using the LiNbO<sub>3</sub> modulator and the optical demultiplexer was repeated for a pattern length of  $2^{31}-1$ , an error floor was observed at a BER of  $10^{-8}$ . Since the commercial receiver and amplifier have low-frequency cut-offs below 100 kHz, this indicates that the pattern-dependent effect is due to the transmitter, which consists of the 30 Gbit/s 4:1 electrical multiplexer, a cascade of broadband amplifiers and the LiNbO<sub>3</sub> modulator. It is informative to look at the electrical 30 Gbit/s eye diagrams at the input to the modulator, which are shown in Figure 2.23 for (a)  $2^7-1$  and (b)  $2^{31}-1$  pattern lengths. The noise build-up is clearly more apparent for the longer pattern length. This is attributed to (1) the 4:1 multiplexer operation and timing alignment, (2) microwave reflections within the amplifier

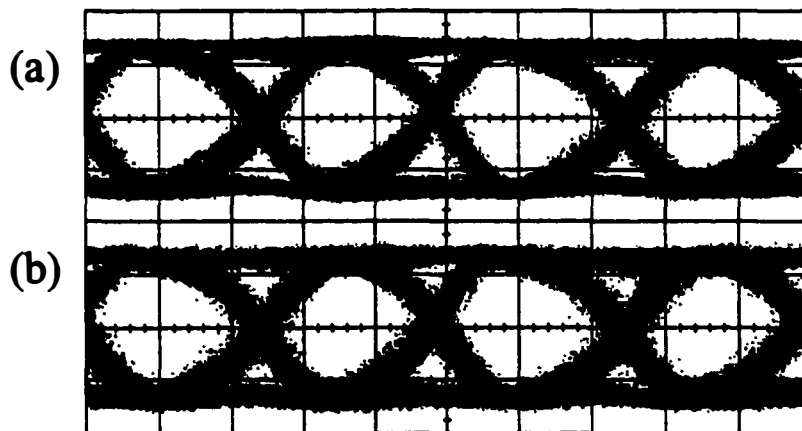


Figure 2.23 Measured eye diagrams at 30 Gbit/s at the output of the transmitter amplifier cascade for pattern lengths of (a)  $2^7-1$  and (b)  $2^{31}-1$  (13.3 ps/div).

cascade as in the receiver subsystem, and (3) the saturated operation of the last amplifier in the cascade.

(4) *Modulator Extinction Ratio*: The performance of optically pre-amplified systems can be significantly degraded by the finite extinction ratio ( $r_{ex}$ ) of the input optical signal. Extinction ratio is defined as,

$$r_{ex} = P_0 / P_1 \quad (2.8)$$

The signal currents and the noise current contributions (neglecting  $\sigma_{sp-sp}$ ) for a finite extinction ratio are given by,

$$I_1 = \left( \frac{2}{1+r_{ex}} \right) RG \bar{P}_{rec} \quad \text{and} \quad I_0 = r_{ex} I_1 \quad (2.9a)$$

$$\sigma_1^2 = \left( \frac{4}{1+r_{ex}} \right) \frac{(q\eta G)^2}{h\nu} F_n \Delta f \bar{P}_{rec} \quad \text{and} \quad \sigma_0 = \sqrt{r_{ex}} \sigma_1 \quad (2.9b)$$

The receiver sensitivity is obtained by substituting Eq. (2.9) in Eq. (2.2) and solving for  $P_{rec}$ :

$$\bar{P}_{rec} = \left( \frac{1+r_{ex}}{1-r_{ex}} \right) \left( \frac{1+\sqrt{r_{ex}}}{1-\sqrt{r_{ex}}} \right) h\nu F_n \Delta f Q^2 \quad (2.10)$$

An optical power penalty,  $\delta_{ex}$ , due to the finite extinction ratio can be defined as,

$$\delta_{ex} = 10 \log \left[ \left( \frac{1+r_{ex}}{1-r_{ex}} \right) \left( \frac{1+\sqrt{r_{ex}}}{1-\sqrt{r_{ex}}} \right) \right] \quad (2.11)$$

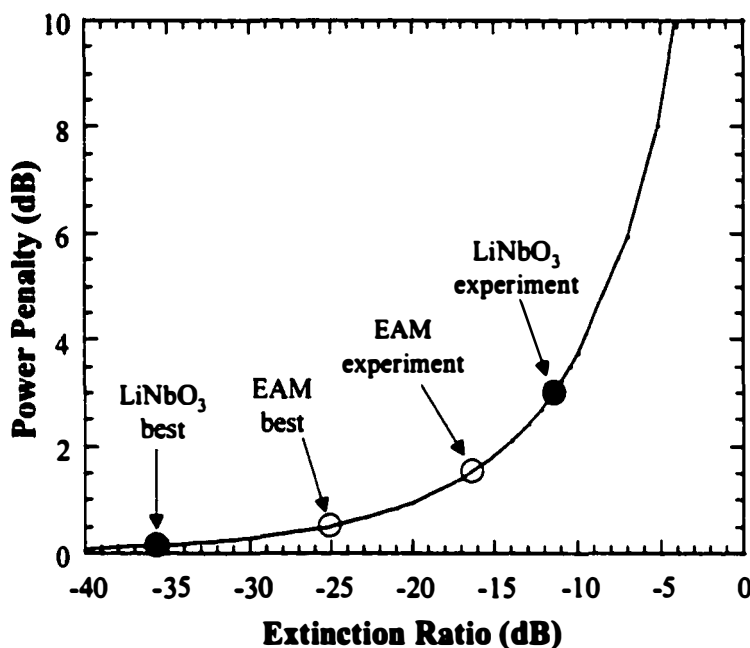


**Figure 2.24** Simulated optical power penalties for a BER of  $10^{-9}$  as a function of finite transmitter extinction ratio for an optically pre-amplified receiver. Also shown are experimental and predicted best operating points for the EA and LiNbO<sub>3</sub> modulators used in the 30 Gbit/s experiments.

Figure 2.24 demonstrates how the power penalty increases for degraded extinction ratios in an optically pre-amplified system. Also shown in the plot are the predicted power penalties for both of the modulators from their maximum static extinction ratios. A power penalty of less than 0.15 dB and 0.5 dB would be expected if the drive voltage swing corresponded to the maximum static extinction ratios of 35.5 dB for the LiNbO<sub>3</sub> modulator and 25 dB for the EA modulator, respectively. However, the modulation efficiency is degraded for high-speed operation due to the bandwidth limitations of the modulator. From the 20 GHz 3-dBe bandwidth of the LiNbO<sub>3</sub> modulator, the applied 3 V<sub>pp</sub> drive voltage is reduced to 1.68 V<sub>pp</sub> at 30 Gbit/s. At the bias point of -2.64 V, the attenuated voltage swing corresponds to an extinction ratio of 11.4 dB resulting in a power penalty of 3.4 dB (Figure 2.24). A similar analysis for the EA modulator would yield an extinction



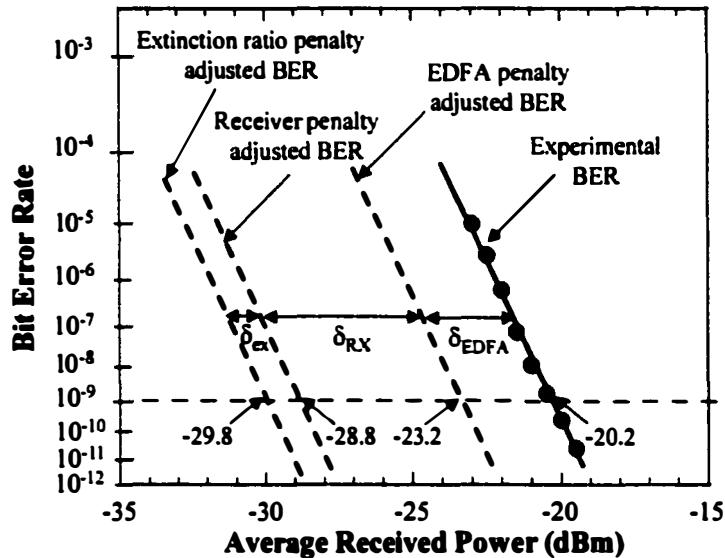


**Figure 2.25** Predicted 30 Gbit/s BER curves with respect to the measured BER for the traveling EA modulator by taking into account the EDFA, 30 Gbit/s ETDM receiver subsystem, and finite transmitter extinction ratio optical power penalties.

ratio of 16.3 dB and a power penalty of 1.5 dB for a 2 V<sub>pp</sub> voltage swing. Since the best achievable extinction ratio results in a power penalty of 0.5 dB, the real power penalty due to the finite extinction ratio of this device is 1 dB.

The overall effects of the power penalties due to the EDFA,  $\delta_{EDFA}$ , the 30 Gbit/s receiver subsystem,  $\delta_{RX}$ , and the finite extinction ratio,  $\delta_{ex}$ , are summarized in Figure 2.25 together with the 30 Gbit/s BER measurements. A 30 Gbit/s receiver sensitivity of -29.8 dBm would be expected by using the traveling-wave EA modulator after elimination of the power penalties.

In a different analysis, the obtained sensitivity using the EA modulator at 10 Gbit/s is -34.2 dBm when the EDFA penalty of 3 dB is subtracted from the measured result (Table 2.5 (a)). For a 10 Gbit/s and 30 Gbit/s signal to achieve the same BER, an extra amount of 4.6 dB optical power is required at 30 Gbit/s (by Eq. (2.6)). This would mean that the predicted 30 Gbit/s sensitivity from the 10 Gbit/s

BER measurements would be -29.6 dBm, which is in very good agreement with the sensitivity obtained in the preceding analysis.

### ***2.4.3 Future Improvements and Conclusions***

The 30 Gbit/s experimental results using the LiNbO<sub>3</sub> and EA modulators as well as the optical power penalty analysis in the preceding section allow for the generalization of several improvements and requirements for future 40 Gbit/s transmitter and receiver subsystems:

**(1) 40 Gbit/s Transmitter Subsystem:** The major problem with the electrical transmitter subsystem was its poor performance for long pattern lengths. One of the reasons for this is the contradicting demand of high-speed operation and high voltage drive requirement of the modulator, which leads to the saturated operation of the electrical amplifiers. Also, microwave reflections due to improper impedance matching between the electrical components as well as the modulator cause double reflections and increased intersymbol interference and timing jitter. A cascade of electrical amplifiers should be avoided and replaced by a single high-power amplifier. However, this does not alleviate the reflections between the amplifier and the modulator. For a 20-cm long cable used in the 30 Gbit/s experiments, double reflections occurring at the modulator and the driver results in a 2 ns (61 bits) time delay. Therefore, the modulator driver [35] or a power multiplexer [84] should be directly bonded to the device, which would not only eliminate any external components such as K-connector interfaces, but also reduce the reflection induced time delay to less than 1 ps. Monolithic integration of an EA modulator with a modulator driver or a multiplexer would be the ideal solution.

**(2) 40 Gbit/s Receiver Subsystem:** The 30 Gbit/s experimental analysis showed that an optical pre-amplifier EDFA with very low noise figure is essential for improved sensitivities. The high receiver power penalty induced by the electrical components

(as in the transmitter subsystem) reveal that external electronic amplification should be avoided. A high-gain optical pre-amplifier coupled with a very high-efficiency (high output voltage) photodetector could be used to directly drive the electrical demultiplexer [51], which would avoid the signal distortions and excess noise added by electrical amplifiers. This concept could be implemented either by directly bonding the photodetector to the demultiplexer or by monolithically integrating the receiver [50].

A schematic diagram of the ideal 40 Gbit/s transmitter and receiver subsystems is shown in Figure 2.26. Note that the external 40 Gbit/s high-speed interfaces are completely removed. This implementation could also allow for the realization of future 160 Gbit/s ETDM systems based on 40 Gbit/s base rate.

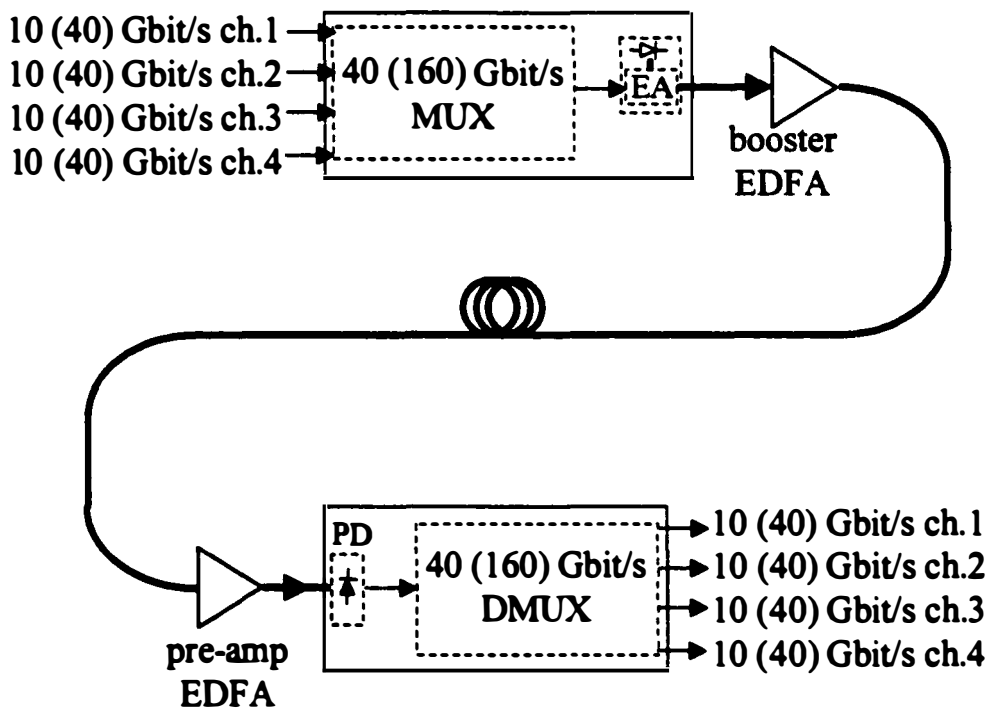


**Figure 2.26** The ideal 40 Gbit/s (and 160 Gbit/s) ETDM based optical system with integrated transmitter and receiver subsystems. The outer interfaces are at the tributary channel speed of 10 Gbit/s (40 Gbit/s). MUX: multiplexer; DMUX: demultiplexer; PD: photodetector; EA: modulator.

## 2.5 Summary and Conclusions

In this chapter, an electrically multiplexed and demultiplexed 30 Gbit/s TDM system was introduced while the application of EA and LiNbO<sub>3</sub> modulators for high-speed TDM systems were discussed. It was experimentally identified that electrical TDM systems suffer optical power penalties and pattern length limitations due to microwave reflections between E/O and O/E interfaces, long electrical amplifier chains, and saturated operation of modulator drivers. The traveling-wave EA modulator with its non-linear attenuation characteristic showed superior operation over a commercial LiNbO<sub>3</sub> modulator due to its high bandwidth, low drive voltage requirement, low polarization sensitivity, and potential for integration. The 30 Gbit/s experimental analysis revealed that monolithic integration of various electronic and opto-electronic devices would improve system performance and result in compact size as well as low power consumption.

Future 160 Gbit/s ETDM systems will require novel device technologies that can overcome the problems observed in 40 Gbit/s subsystems. It is quite likely that at 160 Gbit/s, the transmitter and receiver subsystems will require complete monolithic integration between the electrical tributary channels and the multiplexed high-speed optical channel. This will eliminate any high-speed electrical connections with the benefit of reduced microwave reflections and system degradation while the only interfaces would be at the tributary speed. For the future integrated high-speed electrical TDM system, EA modulators will be strong candidates due to their potential for monolithic integration.

## References

- [1] W. Bogner, E. Gottwald, A. Schopflin, and C. J. Weiske, "40 Gbit/s unrepeated optical transmission over 148 km by electrical time division multiplexing and demultiplexing," *Electron. Lett.*, vol. 33, pp. 2136-2137, 1997.

- [2] S. Kuwano, N. Takachio, K. Iwashita, T. Otsuji, Y. Imai, T. Enoki, K. Yoshino, and K. Wakita, "160-Gbit/s (4-ch\*40-Gbit/s electrically multiplexed data) WDM transmission over 320-km dispersion-shifted fiber," *OFC '96 Technical Digest*, pp. 427-430 1996.
- [3] T. N. Nielsen, A. J. Stentz, K. Rottwitz, D. S. Vengsarkar, L. Hsu, P. B. Hansen, Z. J. Chen, J. H. Park, K. S. Feder, T. A. Strasser, S. Cabot, S. Stulz, C. K. Kan, A. F. Judy, S. Y. Park, L. E. Nelson, and L. Gruner-Nielsen, "3.28 Tb/s (82\*40 Gb/s) transmission over 3\*100 km nozero-dispersion fiber using dual C- and L-band hybrid Raman/Erbium-doped inline amplifiers," *OFC '00 Technical Digest*, PD23, 2000.
- [4] G. Veith, "European 40 Gbit/s field tests," *ECOC '99 Technical Digest*, pp. 82-83, 1999.
- [5] "Manufacturers and carriers prepare for OC-768," *Lightwave*, pp.74-80, June 2000.
- [6] S. Z. Zhang, Y. J. Chiu, P. Abraham, J. E. Bowers, "25 GHz polarization-insensitive electroabsorption modulators with traveling-wave electrodes", *IEEE Photonics Tech. Lett.*, vol. 11, pp. 191-193, 1999.
- [7] Y. Kuriyama, M. Asaka, T. Sugiyama, N. Iizuka, and M. Obara, "Over 40 Gbit/s ultrahigh-speed multiplexer IC implemented with high  $f_{max}$  AlGaAs/GaAs HBTs," *Electron. Lett.*, vol. 30, pp. 401-402, 1994.
- [8] K. Runge, R. L. Pierson, P. J. Zampardi, P. B. Thomas, J. Yu, and K. C. Wang, "40 Gbit/s AlGaAs/GaAs HBT 4:1 multiplexer IC," *Electron. Lett.*, vol. 31, pp. 876-877, 1995.
- [9] M. Moller, H. M. Rein, A. Felder, J. Popp, and J. Bock, "50 Gbit/s time-division multiplexer in Si-bipolar technology," *Electron. Lett.*, vol. 31, pp. 1431-1433, 1995.
- [10] T. Otsuji, M. Yoneyama, Y. Imai, S. Yamaguchi, T. Enoki, Y. Umeda, and E. Sano, "46 Gbit/s multiplexer and 40 Gbit/s demultiplexer IC modules using InAlAs/InGaAs/InP HEMTs," *Electron. Lett.*, vol. 32, pp. 685-686, 1996.
- [11] Z. Lao, U. Nowotny, A. Thiede, V. Hurm, G. Kaufel, M. R. Motzer, W. Bronner, J. Seibel, and A. Hulsmann, "45 Gbit/s AlGaAs/GaAs HEMT multiplexer IC", *Electron. Lett.*, vol. 33, pp. 589-590, 1997.
- [12] M. Moller, H. M. Rein, A. Felder, and T. F. Meister, "60 Gbit/s time-division multiplexer in SiGe-bipolar technology with special regard to mounting and measuring technique," *Electron. Lett.*, vol. 33, pp. 679-680, 1997.
- [13] K. Sano, K. Murata, and K. Nishimura, "44 Gbit/s GaAs MESFET selector IC," *Electron. Lett.*, vol. 33, pp. 1377-1378, 1997.
- [14] T. Otsuji, M. Yoneyama, Y. Imai, T. Enoki, and Y. Umeda, "64 Gbit/s multiplexer IC using InAlAs/InGaAs/InP HEMTs," *Electron. Lett.*, vol. 33, pp. 1488-1489, 1997.
- [15] T. Otsuji, K. Murata, T. Enoki, and Y. Umeda, "80 Gbit/s multiplexer IC using InAlAs/InGaAs/InP HEMTs," *Electron. Lett.*, vol. 34, pp. 113-114, 1998.
- [16] U. Nowotny, Z. Lao, A. Thiede, H. Lienhart, J. Hornung, G. Kaufel, K. Kohler, and K. Glorer, "44 Gbit/s 4:1 multiplexer and 50 Gbit/s 2:1 multiplexer in pseudomorphic AlGaAs/GaAs-HEMT technology," *Proc. of ISCAS '98*, pp. 201-203, 1998.
- [17] H. Suzuki, K. Watanabe, K. Ishikawa, H. Masuda, K. Ouchi, T. Tanoue, and R. Takeyari, "Very-high-speed InP/InGaAs HBT IC's for optical transmission systems," *IEEE J. of Solid-State Circuits*, vol. 33, pp. 1313-1327, 1998.

- [18] P. Andre, J. L. Benchimol, P. Desrousseaux, A. M. Duchenois, J. Godin, A. Konczykowska, M. Meghelli, M. Riet, and A. Scavennec, "InP DHBT technology and design methodology for high-bit-rate optical communication circuits," *IEEE J. of Solid-State Circuits*, vol. 33, pp. 1328-1335, 1998.
- [19] J. Hourany, J. Bellaiche, J. P. Andre, and E. Delhaye, "Recent advances in 40 Gb/s digital functions for high bit rate telecommunication applications," *Proc. of ICECS '98*, pp. 389-392, 1998.
- [20] J. P. Mattia, R. Pallela, G. Georgieu, Y. Baeyens, H. S. Tsai, Y. K. Chen, C. Dorschky, W. von Mohrenfels, M. Reinhold, C. Groepper, M. Sokolich, L. Nguyen, and W. Stanchina, "High-speed multiplexers: a 50 Gb/s 4:1 MUX in InP HBT technology," *GaAs IC Symposium*, pp. 189-192, 1999.
- [21] K. Washio, "SiGe HBTs and ICs for optical-communication systems," *Solid-State Electronics*, vol. 43, pp. 1619-1625, 1999.
- [22] K. Murata, T. Otsuji, Y. Imai and S. Sugitani, "A distributed selector IC using MESFETs with multilayer-interconnection structure," *IEEE J. of Solid-State Circuits*, vol. 35, pp. 1527-1535, 2000.
- [23] A. Felder, M. Moller, J. Popp, J. Bock, and H. M. Rein, "46 Gb/s DEMUX, 50 Gb/s MUX, and 30 GHz static frequency divider in silicon bipolar technology," *IEEE J. of Solid-State Circuits*, vol. 31, pp. 481-486, 1996.
- [24] K. Murata, T. Otsuji, M. Yoneyama, and M. Tokumitsu, "A 40 Gbit/s super-dynamic decision IC using 0.15- $\mu$ m GaAs MESFETs," *IEEE MTT-S Digest*, pp. 465-468, 1997.
- [25] T. Otsuji, M. Yoneyama, Y. Imai, T. Enoki, and Y. Umeda, "40 Gbit/s, fully-integrated 1:2 demultiplexer IC using InAlAs/InGaAs HEMTs," *Electron. Lett.*, vol. 33, pp. 1409-1410, 1997.
- [26] M. Yoneyama, T. Otsuji, Y. Imai, S. Yamaguchi, T. Enoki, Y. Umeda, and K. Hagimoto, "46 Gbit/s super-dynamic decision circuit module using InAlAs/InGaAs HEMTs," *Electron. Lett.*, vol. 33, pp. 1472-1474, 1997.
- [27] A. Felder, M. Moller, M. Wurzer, M. Rest, T. F. Meister, and H. -M. Rein, "60 Gbit/s regenerating demultiplexer in SiGe bipolar technology," *Electron. Lett.*, vol. 33, pp. 1984-1986, 1997.
- [28] K. Murata, T. Otsuji, M. Yoneyama, and M. Tokumitsu, "A 40 Gbit/s super-dynamic decision IC fabricated with 0.12- $\mu$ m GaAs MESFETs," *IEEE J. of Solid-State Circuits*, vol. 33, pp. 1527-1535, 1998.
- [29] E. Sano, H. Nakajima, N. Watanabe, and S. Yamahata, "40 Gbit/s decision IC using InP/InGaAs composite-collector heterojunction bipolar transistors," *Electron. Lett.*, vol. 35, pp. 1194-1195, 1999.
- [30] K. Emura, "Technologies for making full use of high-speed IC performance in the development of 40-Gb/s optical receivers," *Solid-State Electronics*, vol. 43, pp. 1613-1618, 1999.
- [31] M. Lang, Z. G. Wang, A. Thiede, H. Lienhart, T. Jakobus, W. Bronner, J. Hornung, and A. Hulsmann, "A complete GaAs HEMT single chip data receiver for 40 Gbit/s data rates," *IEEE GaAs IC Symposium*, pp. 55-58, 1998.

- [32] E. Sano, H. Nakajima, N. Watanabe, S. Yamahata, and Y. Ishii, "40 Gbit/s 1:4 demultiplexer IC using InP-based heterojunction bipolar transistors," *Electron. Lett.*, vol. 35, pp. 2116-2117/1984-1986, 1999.
- [33] T. Masuda, K. I. Ohhata, F. Arakawa, N. Shiramizu, E. Ohue, K. Oda, R. Hayami, M. Tanabe, H. Shimamoto, M. Kondo, T. Harada, and K. Washio, "45 GHz transimpedance, 32 dB limiting amplifier and 40 Gb/s 1:4 high-sensitivity demultiplexer with decision circuit using SiGe HBTs for 40 Gb/s optical receiver," *IEEE Int. Solid-State Circuits Conf. 2000*, pp. 60-61, 2000.
- [34] J. P. Mattia, R. Pullela, Y. Baeyens, Y. K. Chen, T. Huan-Shang, G. Georgiou, T. W. von Mohrenfels, M. Reinhold, C. Groepper, C. Dorschky, and C. Schulien, "A 1:4 demultiplexer for 40 Gb/s fiber-optic applications," *IEEE Int. Solid-State Circuits Conf. 2000*, pp. 64-65, 2000.
- [35] R. Schmid, T. F. Meister, M. Rest, and H. -M Rein, "40 Gbit/s EAM driver IC in SiGe bipolar technology," *Electron. Lett.*, vol.34, pp. 1095-1097, 1998.
- [36] A. Thiam, E. Legros, S. Vuye, P. Andre, E. Wawrzykowski, and C. Joly, "40 Gbit/s GaAs P-HEMT driver module for optical communications," *Electron. Lett.*, vol. 34, pp. 2232-2234, 1998.
- [37] L. Zhibao, A. Thiede, U. Nowotny, H. Lienhart, V. Hurm, M. Schlechtweg, J. Hornung, W. Bronner, K. Kohler, A. Hulsmann, B. Raynor, and T. Jakobus, "40-Gb/s high-power modulator driver IC for lightwave communication systems," *IEEE J. of Solid-State Circuits*, vol.33, pp. 1520-1526, 1998.
- [38] M. Leich, M. Ludwig, A. Hulsmann, V. Hurm, F. Steinhagen, A. Thiede, and M. Schlechtweg, "40 Gbit/s high voltage modulator driver in P-HEMT technology," *Electron. Lett.*, vol. 35, pp. 1842-1844, 1999.
- [39] S. Kimura, Y. Imai, and Y. Miyamoto, "Direct-coupled distributed baseband amplifier IC's for 40-Gb/s optical communication," *IEEE J. of Solid-State Circuits*, vol. 31, pp. 1374-1379, 1995.
- [40] J. Mullrich, T. F. Meister, M. Rest, W. Bogner, A. Schopflin, and H. M. Rein, "40 Gbit/s transimpedance amplifier in SiGe bipolar technology for the receiver in optical-fibre TDM links," *Electron. Lett.*, vol. 34, pp. 452-453, 1998.
- [41] R. Ohhira, Y. Amamiya, T. Niwa, N. Nagano, T. Takeuchi, C. Kurioka, T. Chuzenji, and K. Fukuchi, "AlGaAs-InGaAs HBT IC modules for 40-Gb/s optical receiver," *IEICE Trans. on Electronics*, vol. E82-C, pp. 448-455, 1999.
- [42] H. Kikuchi, H. Tsunetsugu, M. Hirano, S. Yamaguchi, and Y. Imai, "Ultra-high-speed GaAs MESFET IC modules using flip chip bonding," *IEICE Trans. on Electronics*, vol. E82-C, pp. 475-482, 1999.
- [43] V. Kaman, T. Reynolds, A. Peterson, and J. E. Bowers, "A 100-kHz to 50-GHz traveling-wave amplifier IC module," *IEEE Microwave and Guided Wave Lett.*, vol. 9, pp. 416-418, 1999.
- [44] E. Legros, T. Barrou, S. Vuye, L. Giraudet, C. Joly, F. Blache, T. Ducellier, and M. Goix, "High-sensitivity high-gain SOA-filter-PIN-PHEMT 40-Gb/s photoreceiver," *ECOC '98 Technical Digest*, pp.69-70, 1998.

- [45] V. Hurm, W. Benz, W. Bronner, A. Hulsmann, T. Jakobus, K. Kohler, A. Leven, M. Ludwig, B. Raynor, J. Rosenzweig, M. Schlechtweg, and A. Thiede, "40 Gbit/s 1.55  $\mu\text{m}$  pin-HEMT photoreceiver monolithically integrated on 3 in GaAs substrate," *Electron. Lett.*, vol. 34, pp. 2060-2062, 1998.
- [46] K. Takahata, Y. Miyamoto, Y. Muramoto, H. Fukano, and Y. Matsuoka, "Ultrafast monolithic receiver OEIC module operating at over 40 Gbit/s," *Electron. Lett.*, vol. 35, pp. 322-324, 1999.
- [47] G. G. Mekonnen, W. Schlaak, H. G. Bach, R. Steingruber, A. Seeger, Th. Enger, W. Passenberg, A. Umbach, C. Schramm, G. Unterborsch, and S. van Waasen, "37 GHz bandwidth InP-based photoreceiver OEIC suitable for data rates up to 50 Gb/s," *IEEE Photonics Tech. Lett.*, vol.11, pp. 257-259, 1999.
- [48] A. Huber, D. Huber, T. Morf, H. Jackel, C. Bergamaschi, V. Hurm, M. Ludwig, and M. Schlechtweg, "Monolithic, high transimpedance gain (3.3 k  $\Omega$ ), 40 Gbit/s InP-HBT photoreceiver with differential outputs," *Electron. Lett.*, vol. 35, pp. 897-898, 1999.
- [49] M. Bitter, R. Bauknecht, W. Hunziker, and H. Melchior, "Monolithic InGaAs-InP p-i-n/HBT 40-Gb/s optical receiver module," *IEEE Photonics Tech. Lett.*, vol.12, pp. 74-76, 2000.
- [50] N. Shimizu, K. Murata, A. Hirano, Y. Miyamoto, H. Kitabayashi, Y. Umeda, T. Akeyoshi, T. Furuta, and N. Watanabe, "40 Gbit/s monolithic digital OEIC composed of untravelling-carrier photodiode and InP HEMTs," *Electron. Lett.*, vol. 36, pp. 1220-1221, 2000.
- [51] Y. Miyamoto, M. Yoneyama, K. Hagimoto, T. Ishibashi, and N. Shimizu, "40 Gbit/s high sensitivity optical receiver with uni-travelling-carrier photodiode acting as decision IC driver," *Electron. Lett.*, vol. 34, pp. 214-215, 1998.
- [52] D. W. Dolfi, and T. R. Ranganath, "50 GHz velocity-matched broad wavelength LiNbO<sub>3</sub> modulator with multimode active section," *Electron. Lett.*, vol. 28, pp. 1197-1198, 1992.
- [53] K. Noguchi, H. Miyazawa, and O. Mitomi, "75 GHz broadband Ti:LiNbO<sub>3</sub> optical modulator with ridge structure," *Electron. Lett.*, vol. 30, pp. 949-951, 1994.
- [54] K. Noguchi, O. Mitomi, and H. Miyazawa, "Push-pull type ridged Ti:LiNbO<sub>3</sub> optical modulator, IEICE Trans. on Electronics, vol. E79-C, pp. 27-31, 1996.
- [55] K. Noguchi, H. Miyazawa, and O. Mitomi, "40-Gbit/s Ti:LiNbO<sub>3</sub> optical modulator with a two-stage electrode," *IEICE Trans. on Electronics*, vol. E81-C, pp. 1316-1320, 1998.
- [56] R. Madabhushi, Y. Uematsu, K. Fukuchi, A. Noda, "Wide-band, low driving voltage Ti:LiNbO<sub>3</sub> optical modulators for 40 Gb/s applications," *ECOC '98 Technical Digest*, pp.547-548, 1998.
- [57] R. Spickermann, S. R. Sakamoto, M. G. Peters, and N. Dagli, "GaAs/AlGaAs travelling wave electro-optic modulator with an electrical bandwidth >40 GHz," *Electron. Lett.*, vol. 32, pp. 1095-1096, 1996.
- [58] F. Devaux, S. Chelles, J. C. Harmand, N. Bouadma, F. Huet, M. Carre, and M. Foucher, "Polarization independent InGaAs/InAlAs strained MQW electroabsorption modulator with 42 GHz bandwidth," *IOOC '95 Technical Digest*, pp. 56-57, 1995.
- [59] K. Satzke, D. Baums, U. Cebulla, H. Haisch, D. Kaiser, E. Lach, E. Kuhn, J. Weber, R. Weinmann, P. Wiedemann, and E. Zielinski, "Ultrahigh-bandwidth (42 GHz) polarisation-



- independent ridge waveguide electroabsorption modulator based on tensile strained InGaAsP MQW," *Electron. Lett.*, vol. 31, pp.2030-2032, 1995.
- [60] T. Ido, S. Tanaka, M. Suzuki, and H. Inoue, "MQW electroabsorption optical modulator for 40 Gbit/s modulation," *Electron. Lett.*, vol. 31, pp. 2124-2125, 1995.
- [61] K. Yoshino, K. Wakita, I. Kotaka, S. Kondo, Y. Noguchi, S. Kuwano, N. Takachio, T. Otsuji, Y. Imai, and T. Enoki, "40-Gbit/s operation of InGaAs/InAlAs MQW electroabsorption modulator module with very low driving-voltage," *ECOC '96 Technical Digest*, pp. 203-206, 1996.
- [62] F. Alexandre, D. Jahan, F. Devaux, A. Ougazzaden, F. Huet, E. Vergnol, and E. V. K. Rao, "Butt-coupled waveguide-modulators by low temperature embedded CBE regrowth for high speed modulation (42 GHz) or large extinction ratio (>50 db)," *IPRM '97 Technical Digest*, pp. 621-624, 1997.
- [63] H. Takeuchi, K. Tsuzuki, K. Sato, M. Yamamoto, Y. Itaya, A. Sano, M. Yoneyama, and T. Otsuji, "NRZ operation at 40 Gb/s of a compact module containing an MQW electroabsorption modulator integrated with a DFB laser," *IEEE Photonics Tech. Lett.*, vol.9, pp. 572-574, 1997.
- [64] K. Wakita, K. Yoshino, A. Hirano, S. Kondo, and Y. Noguchi, "Very-high-speed and low driving-voltage modulator modules for a short optical pulse generation," *IEICE Trans. on Electronics*, vol. E81-C, pp. 175-179, 1998.
- [65] A. E. Bond, G. Shtengel, Y. Akulova, and C. L. Reynolds, "43 GHz modulation bandwidth packaged InGaAsP MQW EA modulators with integrated mode converters," *ECOC '99 Technical Digest*, pp.14-15, 1999.
- [66] J. R. Burie, F. Dumont, O. le Gouezigou, S. Lamy, D. Cornec, and P. Andre, "50 Gb/s capability of a new zero loss integrated SOA/EA modulator," *ECOC '00 Technical Digest*, paper 1.3.3, 2000.
- [67] M. Shirai, K. Watanabe, T. Ido, K. Ishikawa, H. Suzuki, and R. Takeyari, "Low driving voltage optical modulators for 40-Gbit/s applications," *ECOC '00 Technical Digest*, paper 1.3.4, 2000.
- [68] M. Yoneyama, A. Sano, T. Kataoka, A. Hirano, T. Otsuji, K. Sato, H. Miyazawa, and K. Hagimoto, "40 Gbit/s optical repeater circuit using InAlAs/InGaAs HEMT digital IC modules," *Electron. Lett.*, vol. 33, pp. 1977-1978, 1997.
- [69] K. Yonenaga, A. Matsuura, S. Kuwahara, M. Yoneyama, Y. Miyamoto, K. Hagimoto, and K. Noguchi, "Dispersion-compensation-free 40-Gbit/s x 4-channel WDM transmission experiment using zero-dispersion-flattened transmission line," *OFC '98 Technical Digest*, PD20, 1998.
- [70] E. Lach, M. Kaiser, W. Pohlmann, and G. Veith, "40 Gbit/s ETDM binary NRZ transmission over installed G.652 field fibre with enhanced dispersion tolerance," *ECOC '99 Technical Digest*, pp. 86-87, 1999.
- [71] R. Ohhira, Y. Yano, A. Noda, Y. Suzuki, C. Kurioka, M. Tachigori, S. Moribayashi, K. Fukuchi, T. Ono, and T. Suzuki, "40 Gbit/s\*8-ch NRZ WDM transmission experiment over 80 km\*5-span using distributed Raman amplification in RDF," *ECOC '99 Technical Digest*, pp. 176-177, 1999.

- [72] M. Yoneyama, Y. Miyamoto, T. Otsuji, H. Toba, Y. Yamane, T. Ishibashi, and H. Miyazawa, "Fully electrical 40-Gb/s TDM system prototype based on InP HEMT digital IC technologies," *IEEE J. of Lightwave Tech.*, vol. 18, pp. 34-43, 2000.
- [73] K. Yonenaga, Y. Miyamoto, A. Hirano, A. Sano, S. Kuwahara, H. Kawakami, H. Toba, K. Murata, M. Fukutoku, Y. Yamane, K. Noguchi, T. Ishibashi, and K. Nakajima, "320 Gbit/s WDM field experiment using 40 Gbit/s ETDM channels over 176 km dispersion-shifted fibre with nonlinearity-tolerant signal format," *Electron. Lett.*, vol. 36, pp. 153-155, 2000.
- [74] Y. Zhu, W. S. Lee, G. Pettitt, M. Jones, and A. Hadjifotiou, "Eight-channel 40 Gb/s RZ transmission over four 80 km spans (328 km) of NDSF with a net dispersion tolerance of 180 ps/nm," *OFC '00 Technical Digest*, Paper TuD4, 2000.
- [75] H. Murai, H. T. Yamada, A. R. Pratt, and Y. Ozeki, "8\*40 Gbit/s transmission over 640 km of large-effective-area nonzero-dispersion shifted fibre with an input power tolerance greater than 7 dB," *Electron. Lett.*, vol. 36, pp. 1479-1480, 2000.
- [76] S. Bigo, E. Lach, Y. Frignac, D. Hamoir, P. Sillard, W. Idler, S. Gauchard, A. Bertaina, S. Borne, L. Lorcy, N. Torabi, B. Franz, P. Nouchi, P. Guenot, L. Fleury, G. Wien, G. Le Ber, R. Fritschi, B. Junginger, M. Kaiser, D. Bayart, G. Veith, J. P. Hamaide, and J. L. Beylat, "1.28 Tbit/ WDM transmission of 32 ETDM channels at 40 Gbit/s over 3x100 km distance," *ECOC '00 Technical Digest*, paper 10.1.3, 2000.
- [77] A. K. Petersen, T. Reynolds, R. Nagarajan, Y. G. Wey, J. E. Bowers, and M. Rodwell, "3-MHz-30-GHz traveling-wave optical front-end receiver," *OFC '95 Technical Digest*, pp. 157-158, 1995.
- [78] K. Runge, P. J. Zampardi, R. L. Pierson, P. B. Thomas, S. M. Beccue, R. Yu, and K. C. Wang, "High speed AlGaAs/GaAs HBT circuits for up to 40 Gb/s optical communication," *Technical Digest GaAs IC Symposium*, pp. 211-214, 1997.
- [79] A. K. Petersen, R. Yu, K. Runge, J. E. Bowers, and K. C. Wang, "Microwave packages for 30 Gbit/s analog and digital circuits," *Proc. of EPEP '95*, pp. 152-154, 1995.
- [80] Hewlett Packard Co., "2-50 GHz distributed amplifier technical data," *Communication Components Designer's Catalog*, pp. 6-40-6-46, 1997.
- [81] R. Yu, S. Beccue, P. J. Zampardi, R. L. Pierson, A. Peterson, K. C. Wang, and J. E. Bowers, "A packaged broad-band monolithic variable gain amplifier implemented in AlGaAs/GaAs HBT technology," *IEEE J. of Solid-State Circuits*, vol. 31, pp. 1380-1387, 1996.
- [82] V. Kaman, S. Z. Zhang, A. J. Keating, and J. E. Bowers, "High-speed operation of travelling-wave electroabsorption modulator," *Electron. Lett.*, vol. 35, pp. 993-995, 1999.
- [83] Intensity modulator, T. MZH1, 5-40, Sumitomo Osaka Cement Co. Ltd.
- [84] M. Moller, T. F. Meister, R. Schmid, J. Rupeter, M. Rest, A. Schoplin, and H. M Rein, "SiGe retiming high-gain power MUX for directly driving an EAM up to 50 Gbit/s," *Electron. Lett.*, vol. 34, pp. 1782-1784, 1998.



## CHAPTER 3

### **Optical Processing using Electroabsorption Modulators**

#### **3.1 Introduction**

With the increasing demand for information bandwidth in optical communication systems, the transmission capacity of optical fibers will be utilized to its full extent. Since the speed for electronic signal processing is limited by the well know electronic bottleneck, all-optical solutions have emerged over the past decade. Wavelength division multiplexing (WDM) is already commercially deployed while intense research in optical time division multiplexing (OTDM) provides an alternative upgrade solution for future ultra-high-capacity optical systems. In order to increase the capacity of point-to-point OTDM systems, high-speed optical processing using all-optical and electro-optic techniques has become a key area of research. Optical short pulse generation and optical demultiplexing are the underlying technologies for realizing very high-speed OTDM systems. The point-to-point systems can then be implemented into scalable and reconfigurable OTDM networks [1]. In addition to possessing the point-to-point system technologies, each network node also requires an add/drop multiplexing functionality for dropping channels from the incoming data stream while inserting new channels into the vacant time slots (Figure 3.1). As these OTDM networks are scaled further by WDM, the optical processing technologies have to maintain wavelength and polarization insensitivity.

Optical processing technologies such as short pulse generation, optical demultiplexing, clock-recovery and add/drop multiplexing have been widely demonstrated using all-optical fiber techniques, semiconductor optical amplifiers (SOA) and electroabsorption (EA) modulators. Even though EA modulators were primarily intended for high-speed data modulation (Chapter 2), various optical

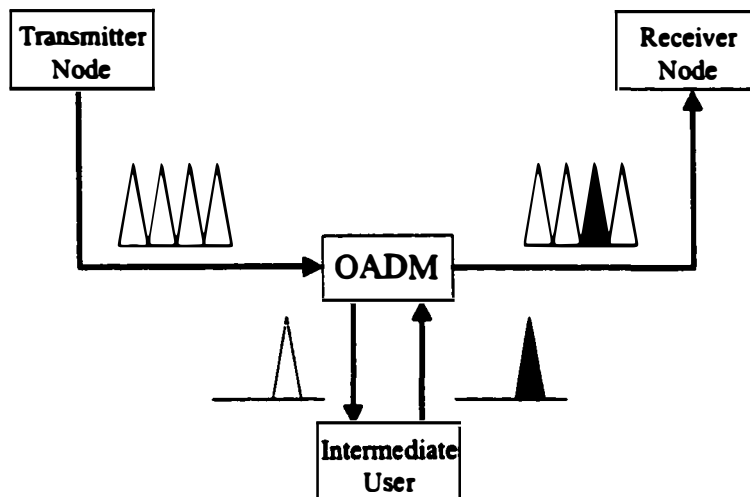


**Figure 3.1** A simple OTDM network architecture with an optical add/drop multiplexing (OADM) node.

processing techniques using compact and stable EA modulators have recently been demonstrated [2-12]. These include optical short pulse generation [2, 3], optical demultiplexing [4, 5], clock-recovery [6], optical regeneration [7, 8], wavelength conversion [9, 10], and add/drop multiplexing [11]. In this chapter, optical gating applications for short pulse generation and demultiplexing as well as a novel simultaneous optical demultiplexing and detection technique for high-speed OTDM transmitter and receiver subsystems using the traveling-wave EA modulator [12] will be described.

### 3.2 Optical Gating using EA Modulators

Over the past decade, EA modulators have attracted a lot of interest for optical gating applications such as optical short pulse generation [2, 3] and optical demultiplexing [4, 5]. Due to the nonlinear attenuation characteristic of the EA modulator, optical transparency gates of different durations can be achieved as a function of the applied sinusoidal RF drive and varied reverse biases. Figure 3.2 shows the operation principle of optical gating using an EA modulator. An optical input (CW light or data stream) is coupled into the modulator and a large sinusoidal

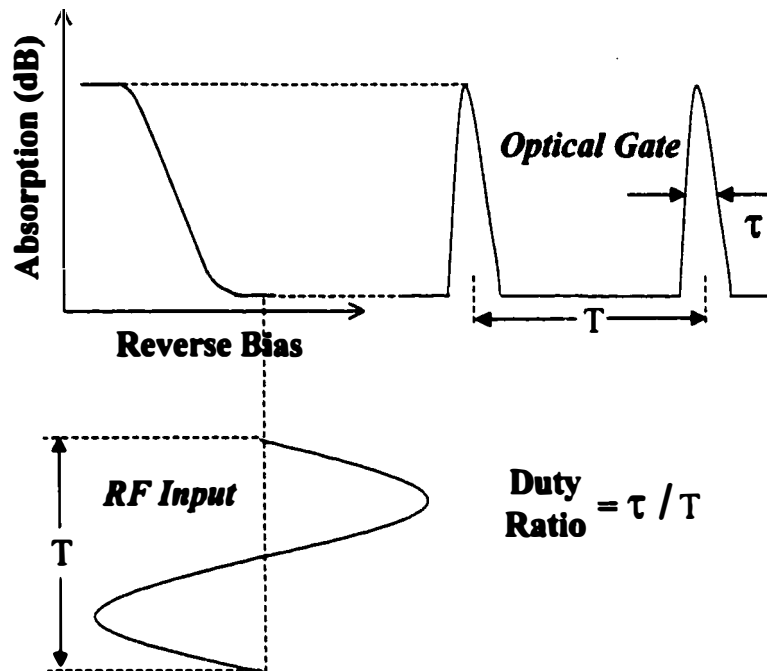


**Figure 3.2** Operation principle of optical gating using EA modulators under sinusoidal RF modulation.

voltage signal under reverse bias drives the device. As a result of the pulse compression due to the nonlinear attenuation characteristic of the EA modulator, optical gates of different duty ratios corresponding to different reverse biases and the sinusoidal modulation can be generated. It is important to note that the optical gating mechanism is independent of the 3-dBe bandwidth of the EA modulator since the nonlinear absorption characteristic dictates the pulse shape and pulse width. Supplying sufficient RF power at the modulation frequency can simply compensate for the drop in frequency response. Typically, extinction ratios of greater than 20 dB can be achieved for the optical gates due to the high absorption characteristic of EA modulators at large reverse biases. Figure 3.3 schematically shows (a) the optical short pulse generation and (b) the optical demultiplexing applications using a sinusoidally driven and reverse biased EA modulator.

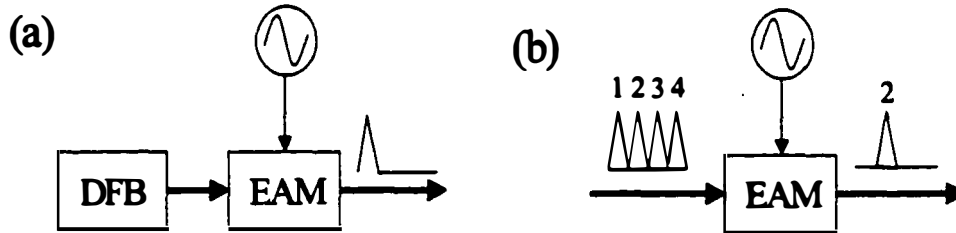


**Figure 3.3** (a) Optical short pulse generation, and (b) optical demultiplexing using sinusoidally driven and reverse biased EA modulators.

### 3.2.1 Optical Short Pulse Generation

Optical short pulses are necessary in the transmitter subsystem of optical or electrical TDM systems employing the return-to-zero (RZ) format. Due to the flexible operation of EA modulators, Gaussian, super-Gaussian or *sech* (for soliton transmission) pulse shapes with different pulse widths can be generated. In order to avoid pulse overlap in OTDM transmitter applications, it is sometimes necessary to generate shorter optical pulses than can be generated using single frequency sinusoidal modulation. Several techniques, which are summarized schematically in Figure 3.4, can be employed to achieve small duty ratio pulse trains.

(1) *Harmonic Modulation*: The optical short pulse generation capability of an EA modulator depends strongly on its nonlinear absorption characteristic. Assuming negligible dependence on the bandwidth of the device, the output pulse width of a sinusoidally driven EA modulator is inversely proportional to the modulation frequency (the bandwidth limitation can be compensated with sufficient RF power). This results in halved pulse width generation at doubled frequency operation. Therefore, an EA modulator driven with a RF modulation source consisting of the fundamental frequency and its higher harmonics can generate shorter pulses at the fundamental repetition rate [13]. The comb-like RF modulation signal can be generated either by an impulse generator or by superimposing the fundamental

sinusoidal frequency and its second harmonic (Figure 3.4(a)). This technique can also be employed in conjunction with the pulse width shortening methods described below.

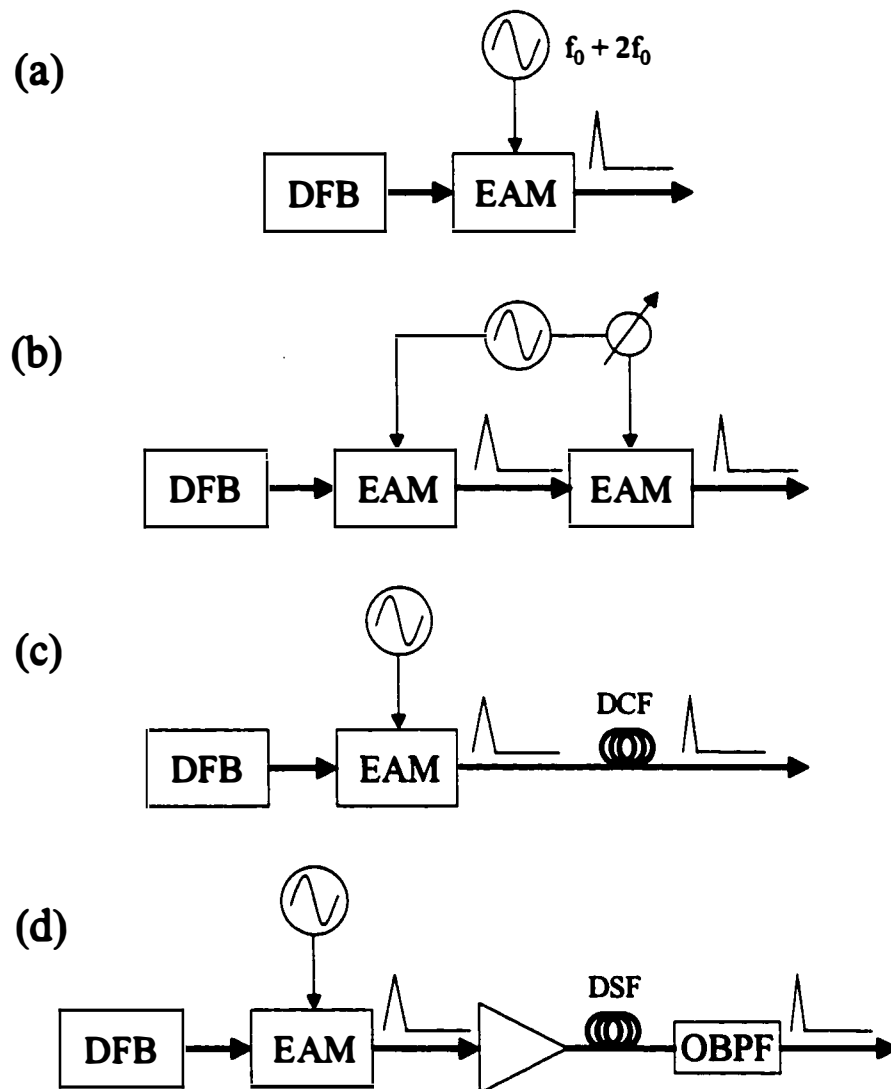


**Figure 3.4** Optical short pulse generation techniques: (a) harmonic RF modulation, (b) tandem EA modulators, (c) linear chirp compensation, and (d) non-linear pulse compression. DCF: dispersion-compensating fiber; DSF: dispersion-shifted fiber; OBPF: optical bandpass filter.



(2) *Tandem Operation*: A series cascade of two or more RF driven EA modulators is another method for generating shorter optical pulses (Figure 3.4(b)) [14-17]. Since each device generates an optical gate, the optical output of the cascade of EA modulators is the logical product of the individual optical gates. The final pulse width depends on the temporal intensity profile of the individual EA modulator switching windows. Assuming identical Gaussian intensity profiles for a cascade of  $N$  EA modulators, a factor of  $\sqrt{N}$  reduction is expected in the overall pulse width, which is illustrated in Figure 3.5 for a tandem. For practical applications, the cascade of EA modulators is typically limited to two devices since the optical insertion loss becomes excessively large. The tandem scheme not only shortens the optical pulse widths, but effectively doubles the dynamic extinction ratio compared to a single device. Using the tandem scheme, even shorter pulses can be realized by offsetting the phases of the two optical gates at the expense of optical output power. For two Gaussian transmission windows, the effect of adjusting the relative phase is to reduce the peak transmitted power while the pulse duration is unaltered compared to the case when both are in phase. However, for a super-Gaussian transmission profile, offsetting the relative phases results in a reduction of pulse width (Figure 3.6(a)). A comparison between a super-Gaussian optical window for a single device, the resultant optical gate from synchronous phase delay, and the shortened optical pulse due to the phase offset is shown in Figure 3.6(b). It should be emphasized that shorter optical pulse widths can be achieved by larger phase offsets at the expense of optical output peak power. The ultimate limit would be determined by the overall system requirement. Finally, the tandem scheme can be realized by integrating the two EA modulators on a single chip [14-16], or by employing two separate fiber-coupled EA modulators and optical amplifiers [17].

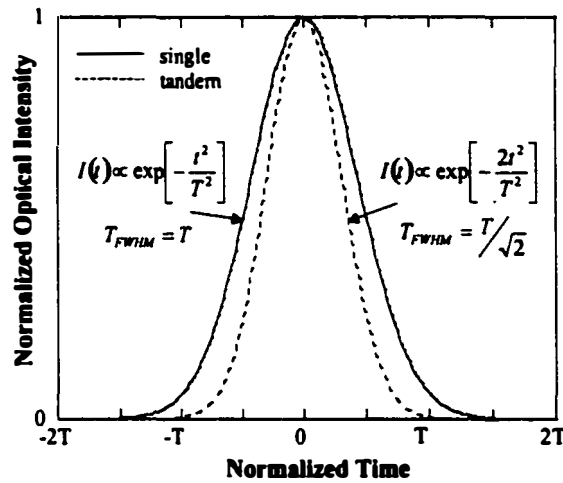


Figure 3.5 Pulse width reduction of a Gaussian pulse in a tandem configuration.

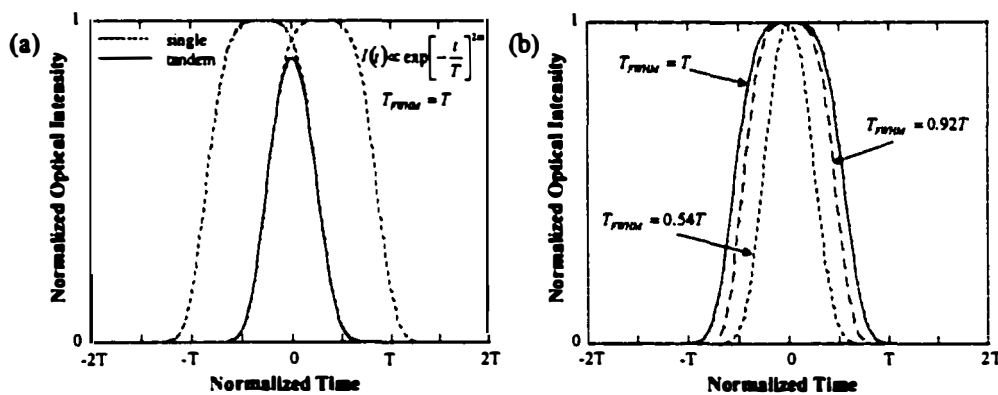


Figure 3.6 (a) Pulse width reduction of a super-Gaussian pulse in a tandem configuration with a  $0.6T$  phase offset, (b) pulse shape and pulse width comparison for normalized single super-Gaussian pulse (solid line), tandem with synchronous phase (long dashed line), and tandem with phase offset (short dashed line).

(3) *Linear Chirp Compensation:* It is desirable for system applications that the generated optical pulses have the narrowest optical spectrum, i.e., the pulses are transform-limited. However, due to the initial frequency chirping,  $C$ , of EA modulators (Chapter 1), the spectral width is enhanced by a factor of  $(1+C^2)^{1/2}$  assuming Gaussian pulses (Figure 3.4(c)). The linear chirp can be compensated by following the EA modulator with dispersion-compensating fiber (DCF) of specific length,  $L$ , given by [18],

$$L = \frac{C}{1 + C^2} \left( \frac{T_0^2}{|\beta_2|} \right) \quad (3.1)$$

where  $T_0$  is the half-width at  $1/e$ -intensity point of the chirped pulse, and  $\beta_2$  is the group-velocity dispersion parameter. Linear pulse compression by Eq. (3.1) is valid only for the condition that  $\beta_2 C < 0$  is satisfied. The minimum pulse width,  $T_{min}$ , is then given by,

$$T_{min} = \frac{T_0}{\sqrt{1 + C^2}} \quad (3.2)$$

(4) *Non-Linear Pulse Compression*: Optical pulses generated by EA modulators can be significantly reduced to short pulse widths by employing non-linear pulse compression techniques using dispersion decreasing fiber [19], or self-phase modulation (SPM) in dispersion shifted fiber (DSF) with subsequent optical filtering (Figure 3.4(d)) [20]. The optical pulses generated by the EA modulator require significant amplification to high optical peak powers to achieve spectral broadening by SPM in a specific length of DSF. The output pulses are transform-limited and the optical pulse widths are determined by the optical filter spectral bandwidth.

There have been several optical short pulse generation demonstrations at modulation frequencies of 10 and 20 GHz by utilizing the preceding pulse compression methods. By employing the dual-frequency technique on a single EA modulator and linear chirp compression, optical pulse widths of 4.1 ps were achieved for a repetition rate of 10 GHz [21]. At 20 GHz modulation, a very small pulse duty ratio of 7.2% was achieved due to the low drive voltage requirement of the EA modulator [22]. On the other hand, 1.8 ps transform-limited pulses were

realized at 20 GHz by nonlinear compression of 7 ps optical pulses generated from an EA modulator [20]. Optical pulse generation demonstrations beyond 20 GHz will be reviewed in Chapter 4.

The major drawback of pulse generation using EA modulators is the high optical loss. The fiber-to-fiber insertion loss, which is mainly due to optical coupling losses, contributes 8-12 dB loss for state-of-the-art EA modulators. On the other hand, the optical loss associated with the pulse shaping process is inherently dependent on the duty ratio of the optical pulses. For very short optical pulses, most of the optical input power is absorbed, which requires compensation by using an external optical amplifier. Even though very short optical pulses can be realized under high reverse bias and large signal modulation, the average optical output power has to exceed the optical system signal-to-noise ratio (SNR) requirement. Therefore, it is imperative that the EA modulator has a high saturation input power. Monolithic integration of the EA modulator with a DFB laser [23, 24] and/or a SOA [25] can also compensate the optical losses by eliminating input or output coupling losses.

### ***3.2.2 Experimental 10 GHz Optical Switching***

The optical switching performance of a 2- $\mu\text{m}$  wide, 300- $\mu\text{m}$  long traveling-wave EA modulator was investigated at a modulation frequency of 10 GHz over the erbium-doped fiber amplifier (EDFA) gain band (1530-1565 nm). The optical transmission characteristics for the device as a function of reverse bias for several wavelengths are shown in Figure 3.7. For these measurements, a tunable laser with an output power of -5.1 dBm in conjunction with a polarization controller was used as the optical source input to the EA modulator while the output was monitored on an optical power meter. At zero bias (on state) for the TE polarization, the device insertion loss ranges from -12.4 dBm to -9.8 dBm for the wavelengths of 1535 to

1565 nm, respectively. The average polarization dependent loss at zero bias is 1 dB over the whole wavelength band. On the other hand, the device achieves a maximum extinction ratio of 39.5 dB at 1535 nm and a minimum of 33.4 dB at 1565 nm.

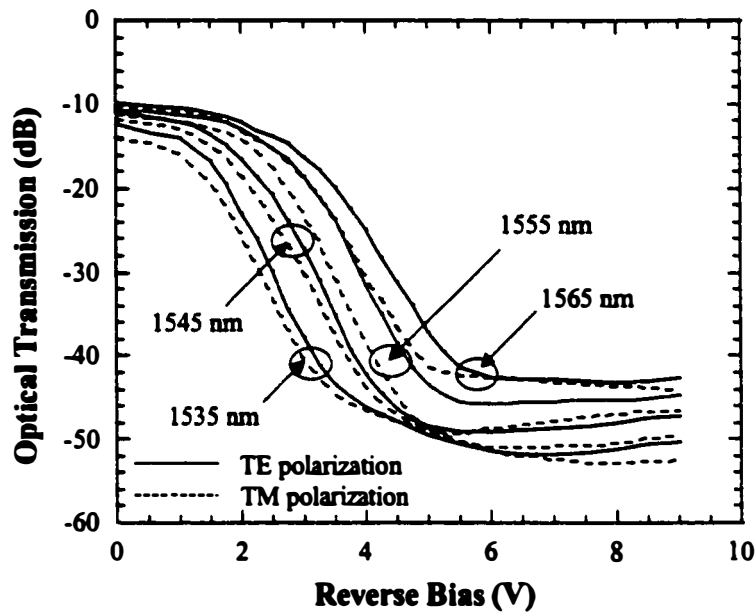


**Figure 3.7** Fiber-to-fiber transmission characteristics as a function of reverse bias of the traveling-wave EA modulator for several wavelengths and polarization modes within the EDFA gain band.

The optical switching performance of the EA modulator was first investigated with an optical input power of +8 dBm at 1555 nm. The device was driven by a 10 GHz sinusoidal 9.5 V<sub>pp</sub> RF modulation signal. The optical output of the EA modulator was monitored using an in-line optical power meter. The optical pulses were then amplified using an EDFA followed by a 2.4 nm optical bandpass filter, and fed into a 40 GHz photodetector and 50 GHz oscilloscope. The impulse response of the detection system was measured to be 12.84 ps for less than 1 ps pulses generated from a femtosecond pulse laser. The measured optical pulse widths were then deconvolved to obtain the actual pulse widths assuming a Gaussian pulse shape. The obtained optical gate width variation as a function of

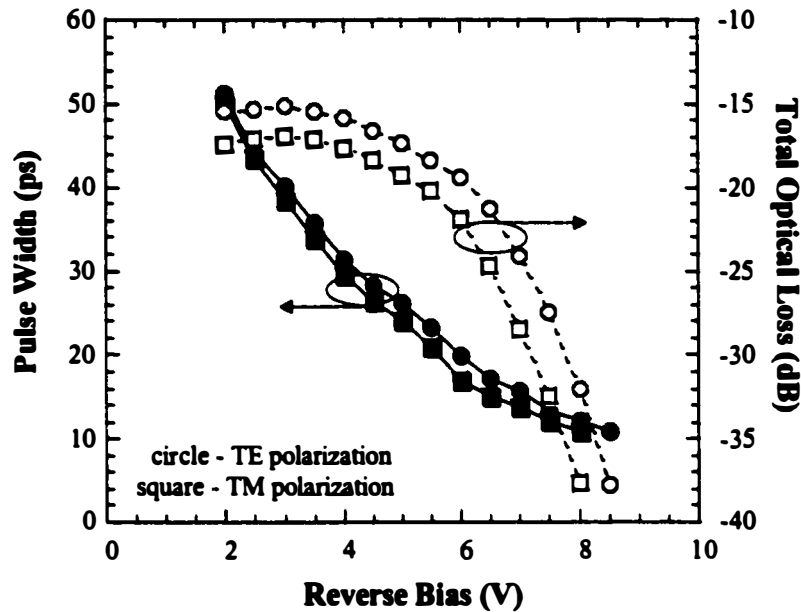


**Figure 3.8** Optical gate widths and corresponding total optical loss for 10 GHz modulation of the EA modulator as a function of reverse bias for a CW light input of +8 dBm at 1555 nm. Closed symbols: pulse width; open symbols: total optical insertion loss.

reverse bias is shown in Figure 3.8 for both polarization states. Optical gates as short as 10.8 ps were achieved at -8.5 V while the duty ratios varied from 50% to 10.8% by varying the reverse bias voltage. As a reference, the total optical loss due to insertion loss and optical pulse shaping is shown in Figure 3.8 as well. As intuitively expected, the optical loss increases quite rapidly at higher reverse biases when shorter optical pulses are generated. For a fixed reverse bias, the TE polarization exhibits only a 2 ps wider optical gate width in comparison to the TM mode. However, it should also be noted that for a 0.5 V higher reverse bias, the TE polarization achieves the same pulse width and total optical insertion loss as the TM mode. This difference is simply due to the faster non-linear response onset of the TM polarization mode for increasing reverse bias (see Figure 3.7). The obtained optical gates as a function of increasing reverse bias (-3 V to -8 V) for the TE polarization are presented in Figure 3.9. The observed satellite peaks are due to electrical reflections within the 40 GHz photodetector. An enhancement in

dynamic extinction ratio can be observed from -3 V to -8 V due to the higher absorption achieved during the negative voltage swing of the sinusoidal modulation.

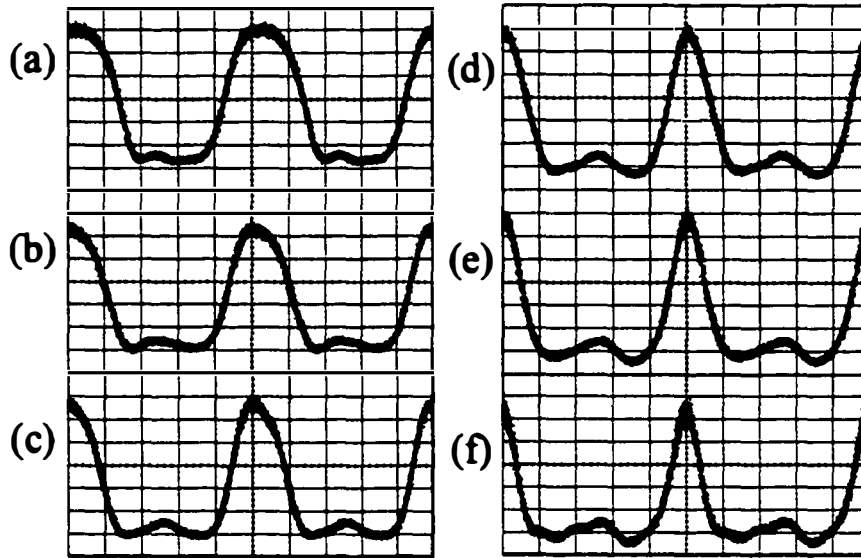


**Figure 3.9** Reverse bias-dependence of measured optical gate shapes for 10 GHz sinusoidal 9.5 V<sub>pp</sub> RF modulation at 1555 nm, (a) -3 V, (b) -4 V, (c) -5 V, (d) -6 V, (e) -7 V, and (f) -8 V (20 ps/div).

The optical gate widths were also measured for varying 10 GHz drive voltages (5 V<sub>pp</sub> to 9 V<sub>pp</sub>) as a function of reverse bias for the TE polarization at 1555 nm (Figure 3.10). For a fixed reverse bias, the optical pulse width widens as the drive voltage is increased. This is expected since the positive swing of the sinusoidal modulation is larger. On the other hand, as the reverse bias is increased for a fixed drive voltage as in Figure 3.8, the optical gate widths get shorter. It is also important to investigate the optical insertion loss behavior as the drive voltage and reverse bias are varied (Figure 3.10). At a reverse bias of -6 V, as the optical pulse width varies from 15 ps to 18 ps for drive voltages of 5 to 9 V<sub>pp</sub>, the optical insertion loss decreases from 37 dB to 24 dB, respectively. An optical power loss difference of 13 dB is detrimental for system performance. Therefore, in order to achieve the shortest optical pulses for acceptable SNR, the EA modulator should be

biased at the largest reverse voltage, and the drive voltage should be chosen accordingly for a trade-off between required optical output power and pulse width.

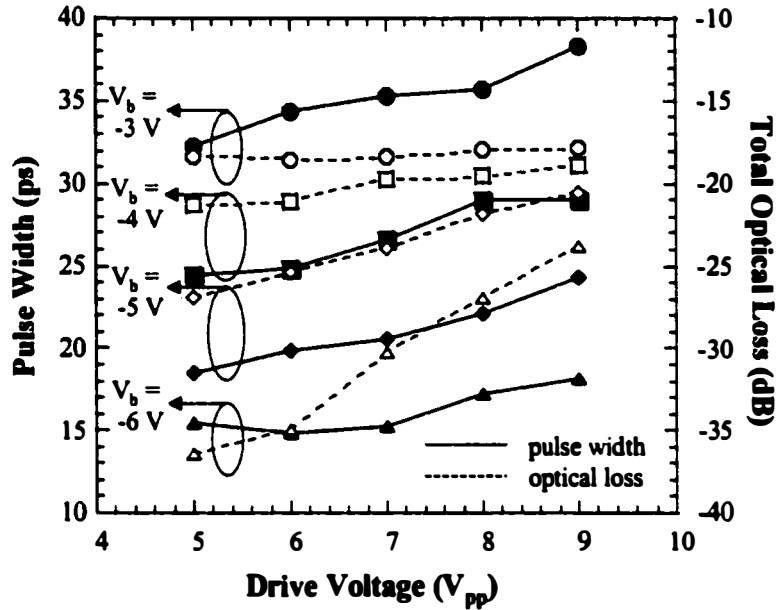


Figure 3.10 Measured optical pulse widths (solid lines) and total optical losses (dashed lines) for varying drive voltages (5 to 9  $V_{pp}$ ) and reverse biases for 10 GHz sinusoidal modulation.

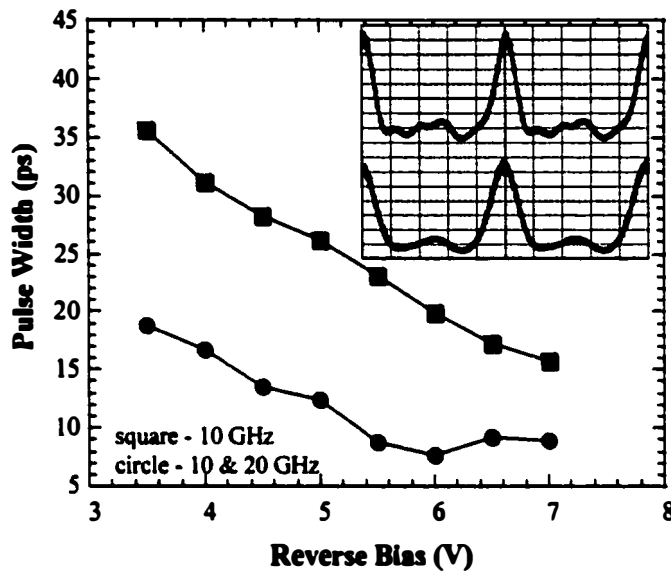
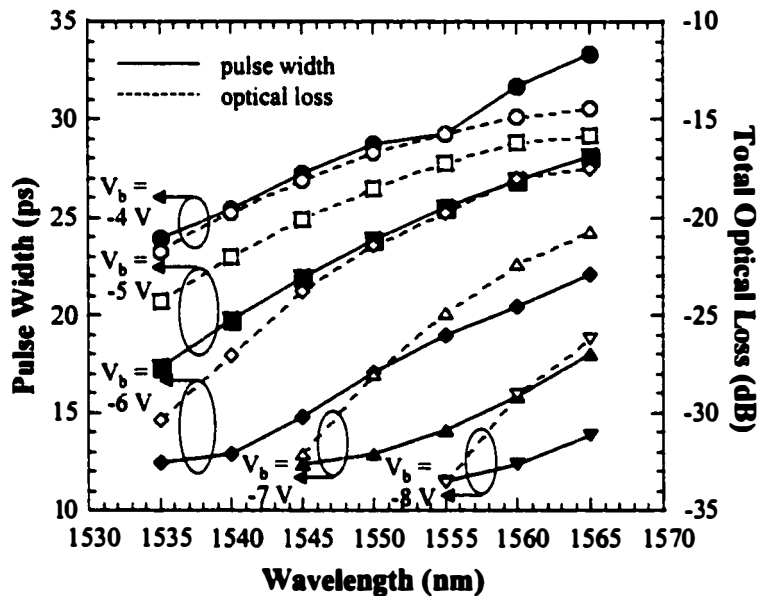


Figure 3.11 Comparison of harmonic (circle) and sinusoidal (square) modulation. Insets: Oscilloscope traces of harmonic (upper) and sinusoidal (lower) pulses (20 ps/div).



Shorter optical pulse generation by employing the dual-frequency modulation technique of the EA modulator was also investigated. A  $9 V_{pp}$  10 GHz signal and a  $6 V_{pp}$  20 GHz signal were phase delayed and combined to generate a  $6.5 V_{pp}$  10 GHz comb-like RF drive, which was fed into the EA modulator. The optical input to the device was +8 dBm at 1555 nm. The obtained optical pulse widths are shown in Figure 3.11 for the TE polarization state. Optical pulse widths as short as 8.8 ps were achieved. As a comparison, the pulse widths obtained with only the 10 GHz sinusoidal RF modulation are presented as well. The optical pulses measured at a reverse bias of -6 V are shown as an inset to Figure 3.11.



**Figure 3.12** Optical switching performance of the EA modulator at 10 GHz sinusoidal modulation for several wavelengths in the EDFA gain band.

The optical switching performance of the EA modulator was also investigated for several wavelengths in the EDFA gain band. A tunable laser followed by an EDFA and a polarization controller were used as the optical input to the EA modulator. The optical input power was adjusted to +7 dBm while the 10 GHz RF drive was  $7 V_{pp}$ . The optical pulse width results as well as the total

optical insertion loss for the TE polarization are shown in Figure 3.12. It can be observed that for a given reverse bias, the shortest optical pulses are achieved at lower wavelengths, which is simply due to the faster onset of nonlinear absorption as a function of reverse bias for shorter wavelengths (see Figure 3.7). However, the total optical loss is also larger for shorter wavelengths due to the higher optical insertion loss and shorter optical pulses at these wavelengths.

### ***3.2.3 Simulated 10 GHz Optical Switching***

The 10 GHz optical switching response of the EA modulator at 1555 nm was simulated using the absorption curves presented in Figure 3.7. For the simulation, dynamic characteristics such as microwave insertion loss or reflections within the device were ignored, and a 10 GHz 9.5 V<sub>pp</sub> sinusoidal modulation was applied. The simulated pulse widths and total optical losses for the TE polarization are plotted in Figure 3.13 in conjunction with the observed experimental results (from Figure 3.8). The simulated results are in close agreement with the experimental measurements in the 5-8 V reverse bias range. Similar agreement was observed for the TM polarization as well. For the experimental results, it should be noted that due to slight microwave losses and reflections, the drive voltage on the EA modulator is less than the applied 9.5 V<sub>pp</sub>, which is the reason for the experimentally observed shorter pulses.

The 10 GHz results could be used to predict the obtainable pulse widths at higher frequencies by the inverse relationship of pulse width and modulation frequency (Section 3.2.2). In that case, for a 9.5 V<sub>pp</sub> 40 GHz modulation drive, optical pulses as short as 3 ps at a reverse bias of -8 V should be expected. However, at these high frequencies, the microwave insertion losses and reflections as well as the walk-off between the optical and microwave pulses need to be considered. The higher speed switching performance of the traveling-wave EA modulator will be discussed in detail in Chapter 4.

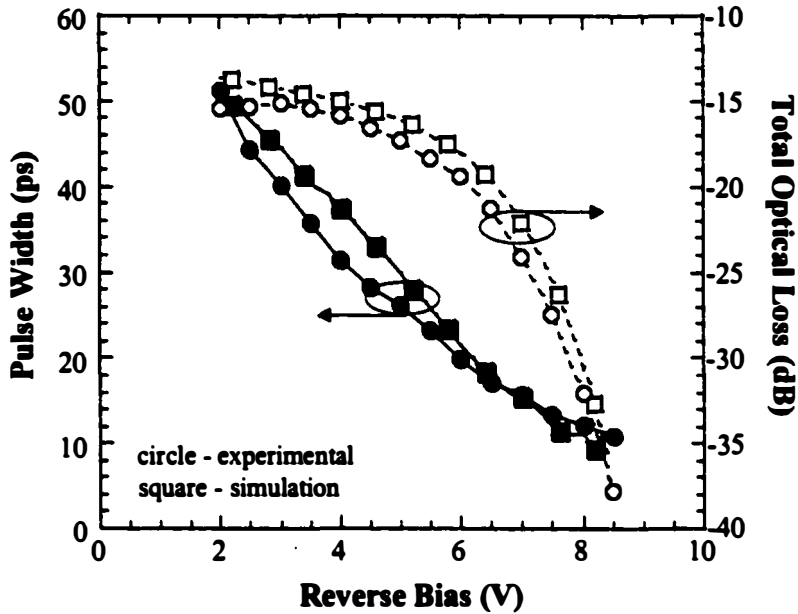


**Figure 3.13** Simulated (square) and experimental (circle) optical switching performance of the EA modulator at 10 GHz modulation of 1555 nm wavelength.

### 3.2.4 Optical Demultiplexing

High-speed demultiplexing is one of the key features in high bit-rate TDM transmission systems. Demultiplexing based on high-speed integrated circuit (IC) technology has been demonstrated at 60 Gbit/s [26]; however, it has been limited to 40 Gbit/s in fiber transmission experiments [27, 28]. On the other hand, optical demultiplexing using a sinusoidally driven EA modulator has emerged as an alternative approach to electrical demultiplexing [4], with demonstrations beyond 100 Gbit/s [20, 29]. The optical data input is coupled into the modulator, and a sinusoidal RF voltage, which is chosen to be at the desired tributary data rate, drives the device. The generated optical transparency gate allows for the selection, or demultiplexing, of any of the TDM channels. The demultiplexed optical channel is then optically amplified and fed into an optical-to-electrical (O/E) converter. In contrast to high-speed electrical demultiplexing which operates at the aggregate data rate, receiver subsystems based on optical demultiplexing using EA

modulators require only the tributary bandwidth. Any of the tributary channels can be selected by synchronizing the optical transparency gate using an electrical phase shifter at the RF drive input. This technique was previously demonstrated in the 30 Gbit/s ETDM system in Chapter 2. The EA modulator was reverse biased at -4.5 V and driven with a 7.5 GHz RF signal allowing error-free operation for all four channels.

### **3.3 Integrated 40 Gbit/s Demultiplexer/Photodetector**

The major drawback of optical demultiplexing using EA modulators is the high optical insertion loss associated with the device. Due to the fiber coupling losses, the demultiplexed optical channel requires external optical amplification before O/E conversion can be performed. There are two consequences to this: (1) each channel to be demultiplexed requires an optical amplifier and a receiver, which increases the cost, size and complexity of the receiver node, and (2) environmentally induced timing jitter between the demultiplexer and the clock-recovery unit can lead to possible SNR deterioration. Therefore, it is desirable to integrate the EA modulator based demultiplexer and the photodetector, which not only allows for a compact receiver, but it also provides efficient coupling without the need for additional optical components. For this purpose, novel integrated tandem EA modulators, fabricated and packaged at the *University of California, Santa Barbara*, were employed and error-free 40 Gbit/s operation was demonstrated [30]. The feasibility of this demultiplexing receiver for 80-to-20 Gbit/s demultiplexing and detection is also investigated [30].

#### ***3.3.1 Integrated Tandem EA Modulators Characteristics***

The demultiplexing receiver consists of 2- $\mu\text{m}$  wide, 300- $\mu\text{m}$  and 400- $\mu\text{m}$  long EA modulators, which were cleaved as a tandem (Figure 3.14(a)) [30]. Since the 400- $\mu\text{m}$  long device achieved a maximum extinction ratio of 38 dB (see Figure

4.10), it was employed as the RF modulated optical demultiplexer. The 300- $\mu\text{m}$  long device was used as a reverse biased photodetector with a responsivity of 0.5 A/W and a photodetection bandwidth of 18 GHz, which is suitable for 20 Gbit/s detection applications. For this application, low microwave crosstalk between the two devices is required since modulation of the photodetector results in decreased absorption of the desired channel. Therefore, the 20- $\mu\text{m}$  long optical waveguide between the two modulators was defined by  $\text{H}^+$  ion implantation. An impedance of 50  $\Omega$  and microwave crosstalk of less than -30 dB between the two devices were measured. However, the ion-implantation also introduced an additional optical insertion loss of about 2.3 dB. Both modulators were terminated in a 50  $\Omega$  thin-film resistor and a dielectric capacitor (Appendix C), which reduced heating effects and allowed for long-term operation of the demultiplexing receiver without any external temperature cooling (Figure 3.14(b)).

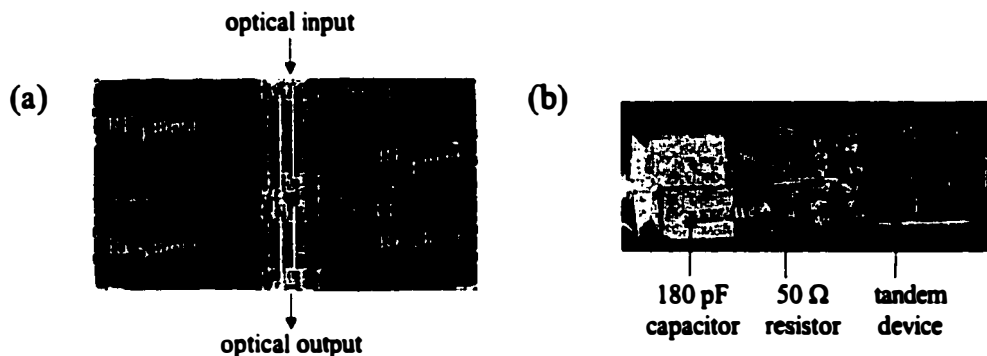


**Figure 3.14** (a) Picture of integrated tandem EA modulators (white dashed region denotes the  $\text{H}^+$  ion-implanted regions), (b) picture of packaged tandem EA modulators [30].

### 3.3.2 Experimental Set-Up and Results

The experimental set-up for the 40 Gbit/s demultiplexing and detection is schematically shown in Figure 3.15. An EA modulator was harmonically driven at 10 GHz to generate 8 ps pulses at 1555 nm. This pulse train was encoded with a 10 Gbit/s data stream ( $2^7-1$  pattern length) using a  $\text{LiNbO}_3$  modulator. The

40 Gbit/s OTDM data stream was realized by passively multiplexing the 10 Gbit/s optical pulses using fiber delay lines. The 40 Gbit/s data stream was then optically pre-amplified before it was coupled into the tandem receiver. The 400- $\mu\text{m}$  EA modulator was reverse biased at -4.8 V and driven by a 6 V<sub>pp</sub> 10 GHz RF signal to generate a 14 ps switching window, which was synchronized to the desired optical channel by an electrical delay line. The demultiplexed optical channel was then detected by the 300- $\mu\text{m}$  device biased at -8 V.

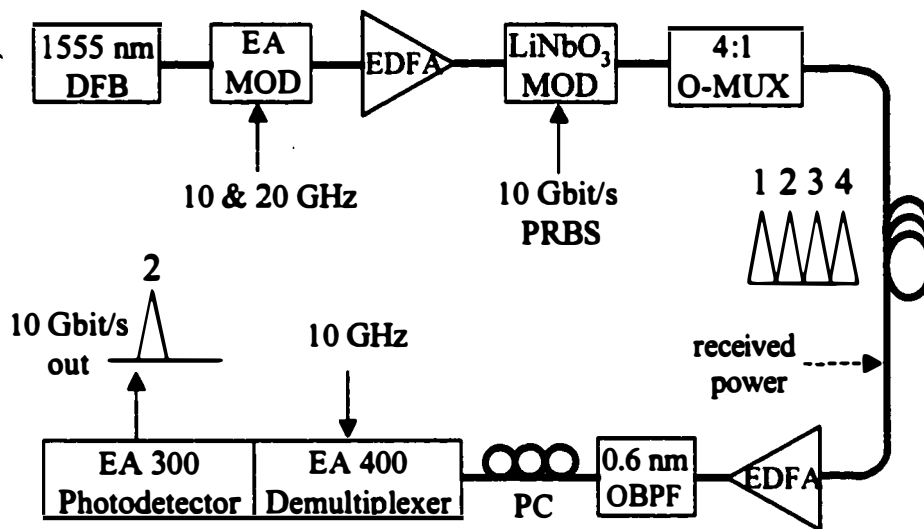


Figure 3.15 Experimental set-up for the integrated 40 Gbit/s demultiplexer/photodetector. O-MUX: optical multiplexer; OBPF: optical bandpass filter; PC: polarization controller.

Single channel 10 Gbit/s bit error rate (BER) measurements were performed in order to determine the photodetection performance of the tandem device, where the average received optical power was determined at the input of the optical pre-amplifier. The plot in Figure 3.16 shows the average received power required for a BER of  $10^{-9}$  as a function of the optical input power into the tandem. Degradation in receiver sensitivity is observed for low input powers due to the low SNR at the photodetector while no power penalty is acquired at higher input powers. It is important to mention that a 2-dB optical power penalty was observed for a pattern

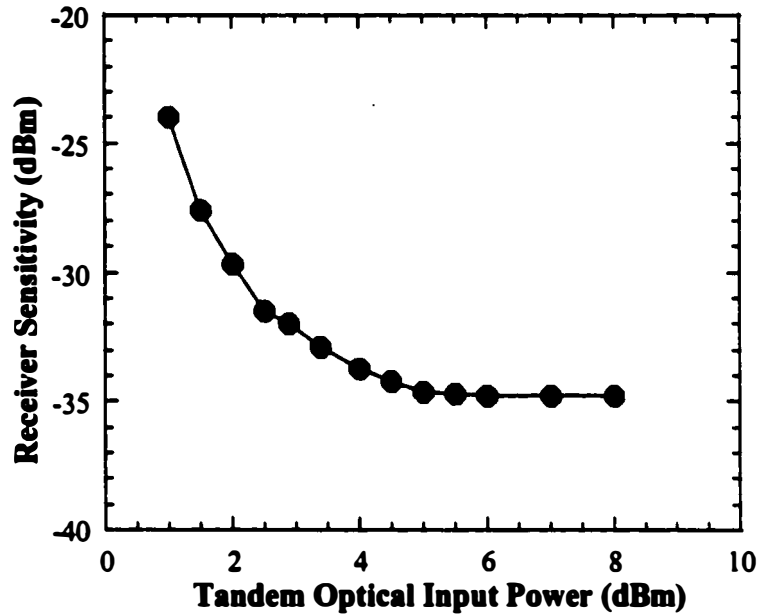


Figure 3.16 Single-channel 10 Gbit/s performance of demultiplexing receiver for a BER of  $10^{-9}$  as a function of optical input power to the integrated receiver.

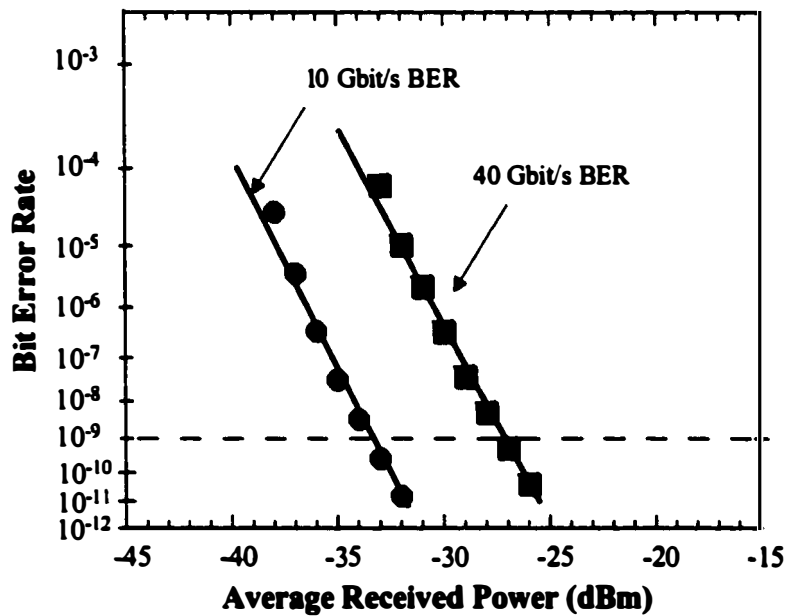
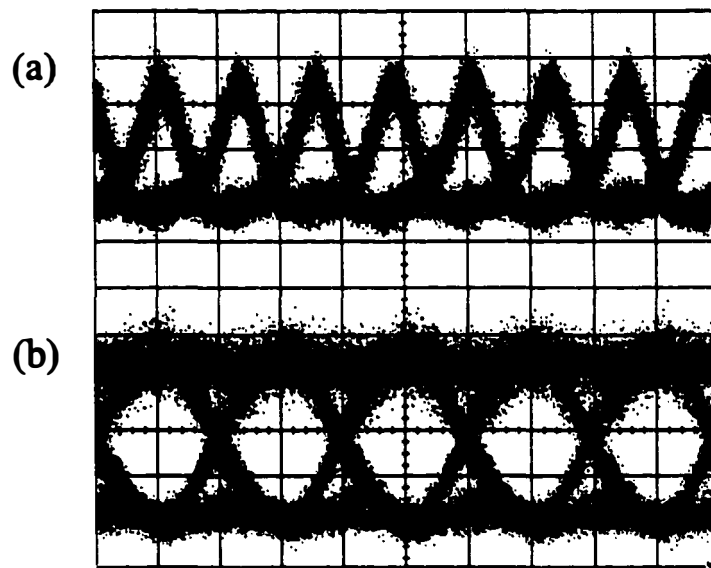


Figure 3.17 BER measurements for 10 Gbit/s single channel (circle) and 40 Gbit/s (square) data stream with a  $2^7-1$  pattern length (9.2 dBm optical input power to the tandem device).

length of  $2^{31}-1$ , which was determined to be due to electrical reflections from the RF termination of the 300- $\mu\text{m}$  photodetector device. Figure 3.17 shows the BER measurements at 10 and 40 Gbit/s, where the average received power was determined at the input of the optical pre-amplifier. Error-free operation with a pattern length of  $2^7-1$  was achieved for 40 Gbit/s operation with a receiver sensitivity of -27 dBm. The 40 Gbit/s optical input data stream and the received electrical 10 Gbit/s channel are shown in Figure 3.18.



**Figure 3.18** Eye diagrams of (a) 40 Gbit/s optical input (20 ps/div), and (b) 10 Gbit/s demultiplexed and received channel (50 ps/div).

In order to investigate the possibility for 80 Gbit/s operation, the 400- $\mu\text{m}$  demultiplexing modulator was driven with a 6.4  $V_{pp}$  20 GHz RF signal. The widths of the optical pulses were measured using a second harmonic generation autocorrelator and deconvolved assuming a Gaussian pulse shape as inferred from the optical spectrum measurements. The obtained pulse widths as a function of reverse bias for a CW input of 1555 nm are presented in Figure 3.19. Pulse widths as short as 6 ps were achieved, which indicates that penalty-free demultiplexing of 80 Gbit/s data stream is possible [21].



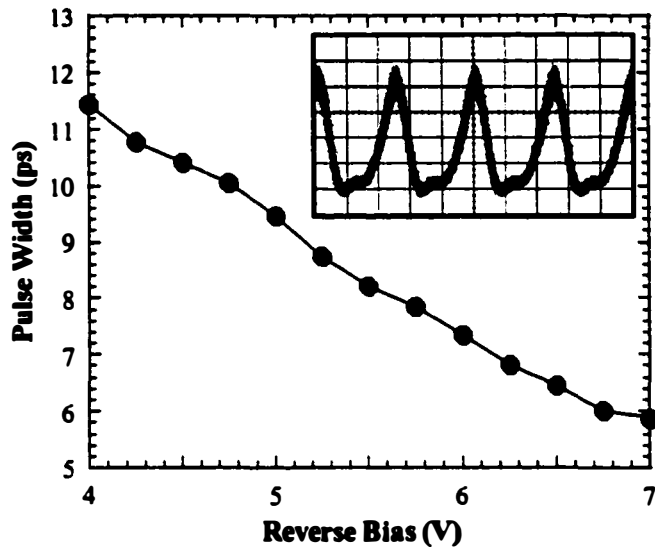


**Figure 3.19** Pulse width as a function of reverse bias at 20 GHz modulation for the 400- $\mu\text{m}$  EA modulator (1555 nm). Inset: Oscilloscope trace of pulses measured using a 40 GHz photodetector (20 ps/div).

### 3.4 Simultaneous Demultiplexing and Detection

The ability to drop a single channel from a high-speed OTDM data stream is significant for future OTDM network nodes since optical demultiplexing is performed while still transmitting the other channels in an optically transparent manner for further optical processing (Figure 3.1). This has the advantage of optical power conservation in contrast to standard optical demultiplexing (for example, using an EA modulator) in which the other channels are suppressed. This ‘complementary’ demultiplexing functionality has been widely demonstrated using all-optical techniques based on wavelength conversion including four-wave mixing in optical fiber [31] and SOA’s [32], and integrated Mach-Zehnder interferometers [33]. This technique requires an optical short pulse source on a different wavelength synchronized to the incoming optical data stream as well as WDM filters and an external photodetector for O/E conversion (Figure 3.20(a)). Electro-optic techniques include using two synchronized LiNbO<sub>3</sub> or EA modulators [34] in

a parallel configuration (Figure 3.20(b)) with complementary gate durations; while one modulator demultiplexes the desired channel, the other performs the drop function and transmits the remaining channels. This technique not only requires an external photodetector, but also a perfect synchronization between the two modulators due to the possible drift in fiber. In order to reduce the cost and complexity of the node, it is desirable to perform the complementary demultiplexing and the O/E conversion of the dropped channel simultaneously. EA modulators are ideal for this application since they can be used as optical switches and photodetectors due to their absorptive characteristic (Figure 3.20(c)).

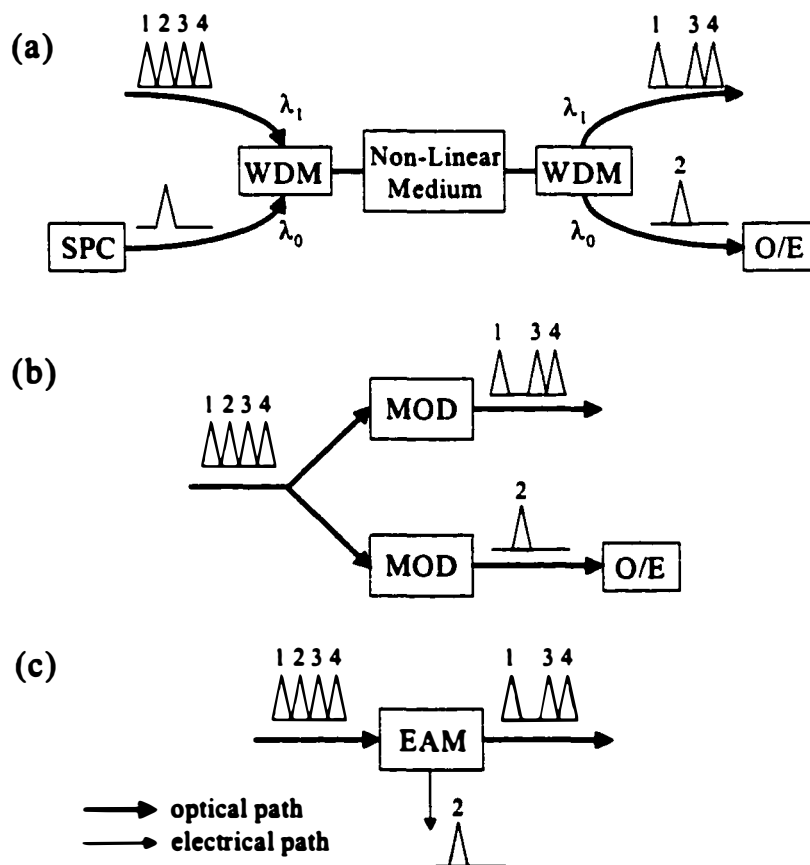


**Figure 3.20** OTDM channel 'drop' techniques. (a) All-optical based on wavelength-conversion, (b) two modulators in parallel configuration with complementary gate durations, and (c) simultaneous drop and detection using an EA modulator. The dropped channel in (c) is also simultaneously optical-to-electrical (O/E) converted. SPC: short pulse source; WDM: WDM coupler.

In consideration of the use of an EA modulator in OTDM drop and detect applications, several crosstalk issues need to be addressed to avoid overall system performance degradation (Figure 3.21). The electrical extinction ratio (defined as the ratio between the responsivity at high reverse bias and zero bias) has to be high enough to prevent absorption of the undropped channels that would interfere with the dropped channel (Figure 3.21(a)). Similarly, the switching window for the drop has to be short enough in order to avoid any crosstalk due to the absorption of the adjacent channels (Figure 3.21(b)). Finally, if a new channel is to be inserted in the available bit slot after a channel is dropped, it is also important to have a high optical extinction ratio to prevent interference between the dropped channel and the channel to be inserted (Figure 3.21(c)).

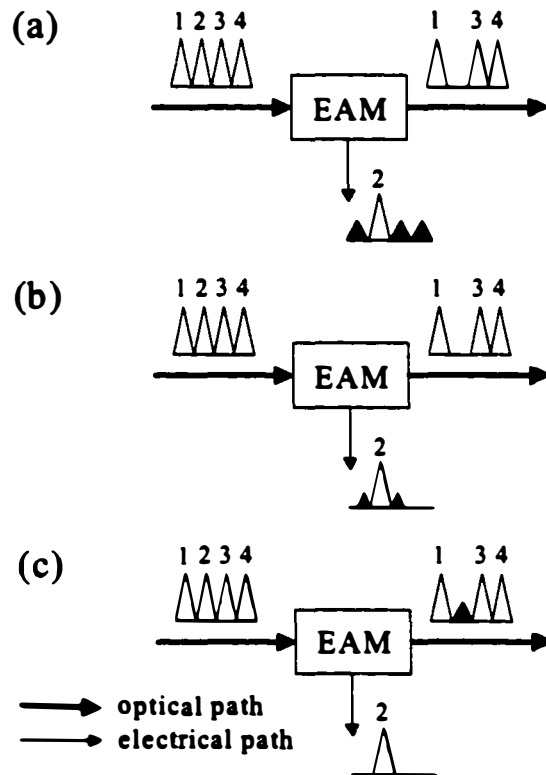


**Figure 3.21** Crosstalk issues using the 'drop and detect' EA modulator. (a) Electrical extinction ratio, (b) absorption switching window, and (c) optical extinction ratio. The dropped channel 2 is of the electrical format.

To date, only the ability of an EA modulator to drop a channel without detection has been demonstrated [35]. This section demonstrates for the first time the use of an EA modulator to simultaneously drop and detect the desired channel from an OTDM data stream while transmitting the other channels in an optically transparent manner [11]. The key advantages of this scheme are the elimination of an external photodetector and any optical wiring within the receiver subsystem. This functionality will be a potential building block of future low-cost and compact add/drop multiplexers and OTDM demultiplexing receivers [36].

### ***3.4.1 Operation Principle***

Due to its compact size as well as simple and stable operation, the EA modulator is well suited for optical demultiplexing applications (Figure 3.3(b)). Its nonlinear attenuation characteristic allows a reverse biased EA modulator with an applied RF signal to produce a switching window for selecting the desired channel from the incoming data stream. While the transmission window provides optical transparency for the demultiplexed channel, the other channels are absorbed in the modulator. The proposed method for simultaneous demultiplexing and detection is quite similar to the conventional optical demultiplexing method (Figure 3.20(c)). The reverse bias and the applied RF signal are chosen such that instead of suppressing the other channels by absorption in the modulator, only the desired channel is absorbed and the remaining channels are transmitted in an optically transparent manner. When the RF drive signal swings negative, the EA modulator is in the high absorption state and any optical signal passing through the modulator is absorbed and converted to photocurrent. On the other hand, when the RF signal swings positive, the EA modulator switches to high optical transparency with low absorption. Either of the two electrical ports can then be used to collect the photogenerated carriers if data '1' is present (in this work, the conventionally terminated port is used as the pulse detector).

### 3.4.2 Device Set-Up

The EA modulator used for the simultaneous OTDM drop and detect application is a 2.5- $\mu\text{m}$  wide, 300- $\mu\text{m}$  long device with traveling-wave electrodes. The device reaches a maximum extinction ratio of 39.7 dB while the fiber-to-fiber insertion loss is 10 dB for the TE polarization at the operating wavelength of 1555 nm (Figure 3.22). A maximum responsivity of 0.66 A/W is achieved at a reverse bias of -5.8 V and the electrical extinction ratio is 13.9 dB. For a 50  $\Omega$  termination, the device modulation bandwidth is 10 GHz while the return loss is less than -13 dB over a 20 GHz bandwidth.

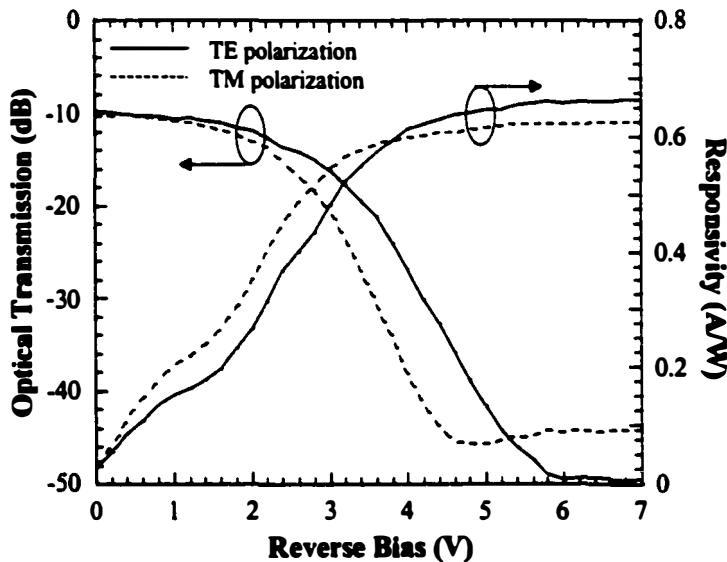


**Figure 3.22** Optical transmission and responsivity characteristics as a function of reverse bias of the EA modulator used in the simultaneous demultiplexing and detection application.

The device set-up for the simultaneous demultiplexing and detection application is schematically shown in Figure 3.23. The traveling-wave modulator is a 4-port device: the optical input and output are shown as port 1 and 3, respectively. The EA device is reverse biased with a 10 GHz driving signal applied at port 2 using a high power amplifier. Port 4 functions as the 10 Gbit/s optical pulse detector. The output at this port consists of photogenerated carriers (if data

'1' is present) as well as the attenuated 10 GHz driving signal. This signal is rejected from the data using a 6.4 GHz low-pass filter (with 60-dB attenuation at 10 GHz), and reflected back into the modulator synchronized with the original drive using an electrical phase shifter. The low-pass filter also converts the RZ data into NRZ format for BER measurements. The alignment of the optical bits to the electrical drive signal is performed using an optical delay line.

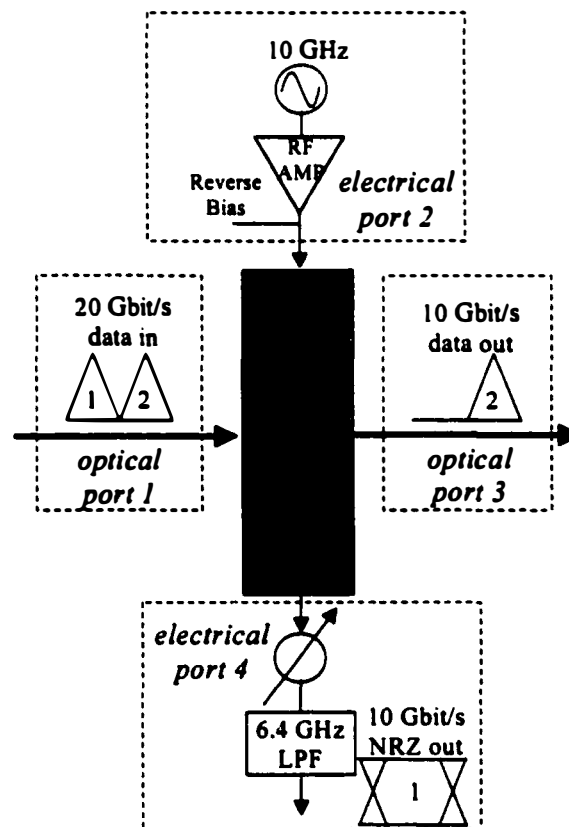


**Figure 3.23** Schematic device set-up for simultaneous demultiplexing and detection application. Port 1: Optical input; port 2: RF modulation input; port 3: transparent optical output; port 4: electrical photodetection output port. LPF: low-pass filter.

Since the EA modulator simultaneously performs optical switching and photodetection, it is imperative to analyze its photodetection behavior. Figure 3.24 shows the photodetection response for several reverse biases when the device is terminated in 50  $\Omega$ . A 10 GHz bandwidth is achieved at a reverse bias of -7 V

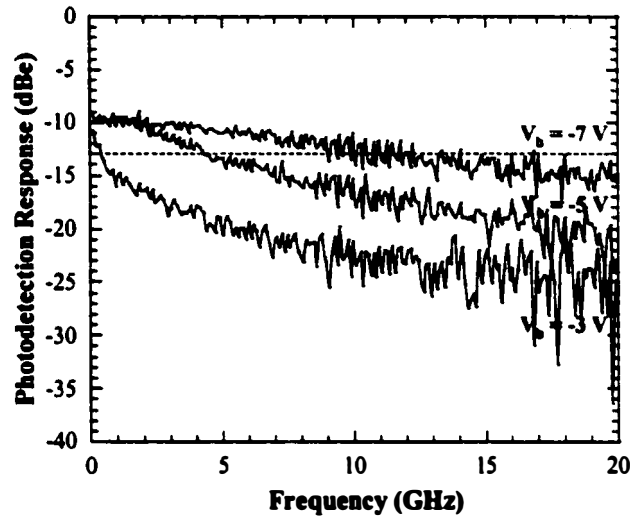


**Figure 3.24** Photodetection response of the 50  $\Omega$  terminated EA modulator for several reverse biases.

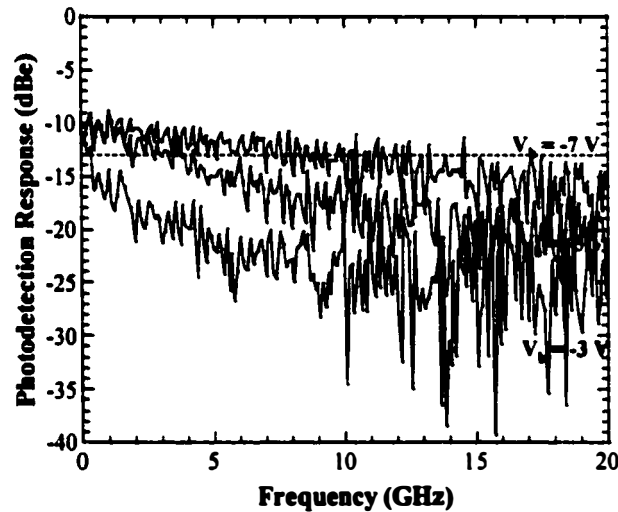


**Figure 3.25** Photodetection response of the EA modulator for several reverse biases when terminated with the output of the high-power RF amplifier at port 2 (Figure 3.23).

while the bandwidth falls to 5 GHz at -5 V. This introduces a fundamental limit on this particular EA modulator since operation at low reverse biases is preferable to achieve the desired optical gates for transparency and absorption. An additional limitation on the overall device performance comes from the high-power amplifier at port 2. When the EA modulator operates as a photodetector, the output

impedance of the high-power RF amplifier (10 MHz – 20 GHz bandwidth) acts as the device termination. Figure 3.25 shows the photodetection response of the device when the 50  $\Omega$  termination is replaced by the high-power amplifier. Even though the 3-dBe bandwidth remains the same, the frequency response is significantly deteriorated due to the poor output impedance of the amplifier. In addition, the amplifier's low frequency cut-off of 10 MHz limited the experiment to a pattern length of  $2^7 - 1$ ; however, this is not a fundamental limitation.

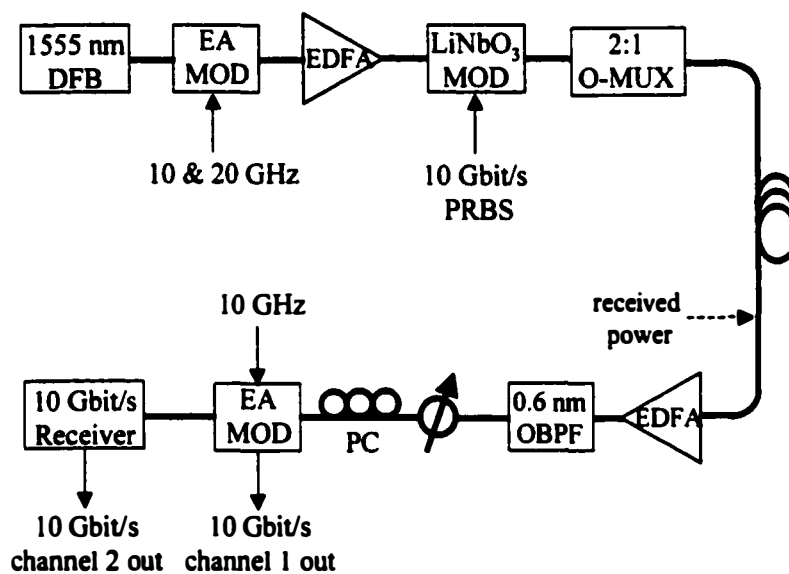


**Figure 3.26** Set-up for the 20 Gbit/s OTDM drop and detect experiment. O-MUX: optical multiplexer; OBPF: optical bandpass filter; PC: polarization controller.

### 3.4.3 Experimental Set-Up and Results

The EA modulator described in the preceding section was used for the simultaneous demultiplexing and electrical detection of a single 10 Gbit/s channel from a 20 Gbit/s OTDM data stream while transmitting the other channel in an optically transparent manner. The experimental set-up for the 20 Gbit/s OTDM simultaneous drop and detect is shown in Figure 3.26. An EA modulator harmonically driven at 10 GHz was used to generate 11 ps pulses at 1555 nm. The



10 Gbit/s data was encoded onto the 10 GHz pulse train by a LiNbO<sub>3</sub> modulator. The 10 Gbit/s RZ data was then passively multiplexed (with 20 bits of delay between channels) to generate a 20 Gbit/s OTDM data stream. The 20 Gbit/s signal was coupled into the drop and detect EA modulator using an optical pre-amplifier followed by a 0.6 nm bandwidth optical filter. A polarization controller was used at the input of the modulator for best operation. The average received power was determined at the input of the optical pre-amplifier to the EA modulator for all BER measurements.

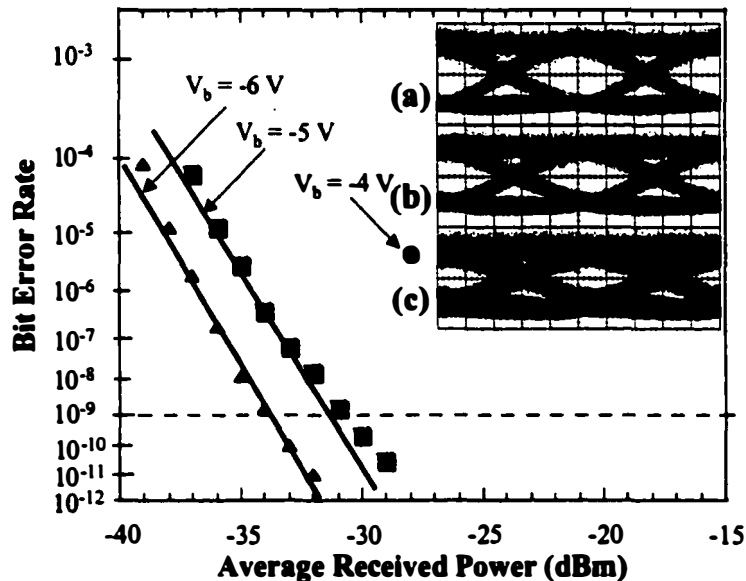


**Figure 3.27** BER measurements for single-channel 10 Gbit/s input when EA modulator is operated as a photodetector with port 2 terminated in a 50  $\Omega$  resistor. Insets: Eye diagrams at reverse biases of (a) -6 V, (b) -5 V, and (c) -4 V (20 ps/div).

(1) *Single-Channel 10 Gbit/s Performance:* In order to determine the electrical photodetection performance of the EA device, single-channel 10 Gbit/s BER measurements were performed by blocking one of the arms of the optical multiplexer. First, the device was terminated with a 50  $\Omega$  resistor at port 2 while the photodetection port 3 was as illustrated in Figure 3.23. BER measurements were then performed at various reverse biases (Figure 3.27). As expected from the

photodetection response in Figure 3.24, error-free operation was achieved for reverse biases higher than -5 V. A receiver sensitivity of -33.5 dBm for a BER of  $10^{-9}$  was obtained at a reverse bias of -6 V. At a bias of -5 V, a 2.5-dB power penalty and a slight error floor were incurred while an error floor at  $10^{-6}$  was observed at -4 V due to the high-frequency limitations of the device.

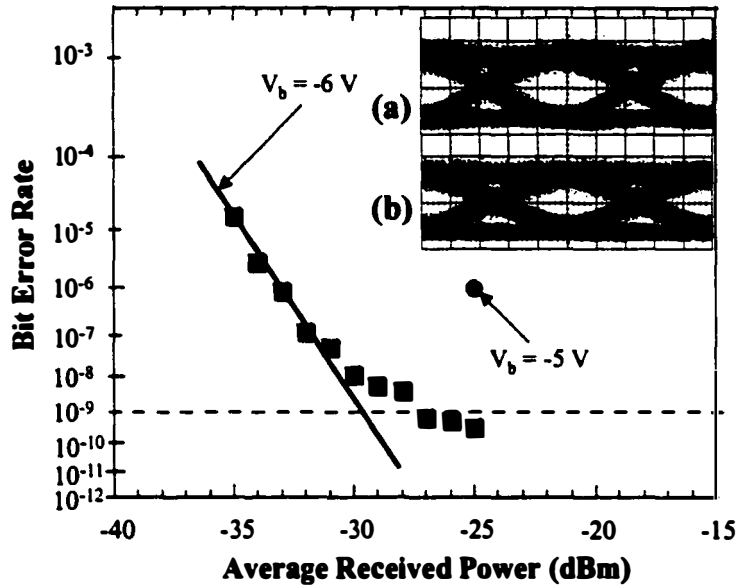


**Figure 3.28** BER measurements for single-channel 10 Gbit/s input when EA modulator is operated as a photodetector with port 2 terminated with the high-power RF amplifier (no RF input). Insets: Eye diagrams at reverse biases of (a) -6 V, and (b) -5 V (20 ps/div).

The  $50 \Omega$  termination at port 2 was then replaced by the high power amplifier (without the RF signal applied) in order to determine the optical power penalty incurred due to the amplifier. The BER measurements in Figure 3.28 reveal that at a reverse bias of -6 V, the sensitivity dropped to -27.5 dBm with a significant error floor. The eye diagrams in Figure 3.28 qualitatively show the degradation in the photodetection process due to the imperfect output impedance as well as the high noise figure of the driving amplifier, which is unacceptable for system applications. Figure 3.29 shows the BER measurements when the 10 GHz 10 Vpp RF signal was applied to the modulator and synchronized to the incoming

10 Gbit/s data stream for absorption. Error-free operation with a receiver sensitivity of -32.5 dBm is achieved at a reverse bias of only -5 V, which is a 1.5 dB improvement in comparison to the 50  $\Omega$  termination case (Figure 3.27). The negative power penalty at -5 V is simply due to the higher average reverse bias, and hence higher photodetection bandwidth, obtained from the negative swing of the 10 GHz signal during the time period of the 10 Gbit/s channel.

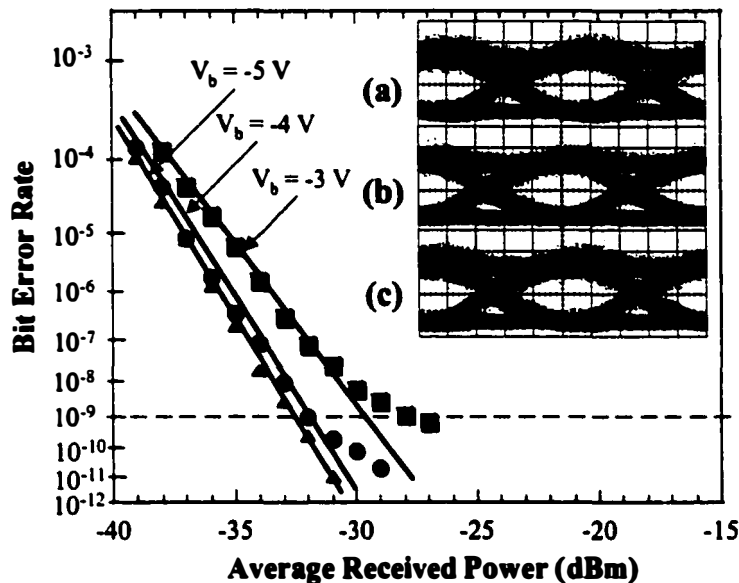


**Figure 3.29** BER measurements for single-channel 10 Gbit/s input when EA modulator is operated as a photodetector with port 2 terminated with the high-power RF amplifier (10 GHz sinusoidal RF input applied). Insets: Eye diagrams at reverse biases of (a) -5 V, (b) -4 V, and (c) -3 V (20 ps/div).

(2) *Two-Channel 20 Gbit/s Performance:* The performance of the simultaneous drop and detect operation was then assessed with a 20 Gbit/s OTDM input (Figure 3.30(a)). Figure 3.30(b) shows the optical gating performed by the modulator at a bias of -5 V with the 10 GHz drive signal (10 V<sub>pp</sub>) aligned to channel 2 for optical transparency. The optical output at port 3 is shown in Figure 3.30(c), where channel 2 is transmitted while channel 1 has been completely removed. The optically transparent channel 2 was then amplified before being detected at a commercial 10 Gbit/s receiver. The simultaneously dropped and detected 10 Gbit/s

NRZ converted channel 1 is shown in Figure 3.30(d). Sufficient eye opening is achieved with most of the noise due to the residual absorption of channel 2.

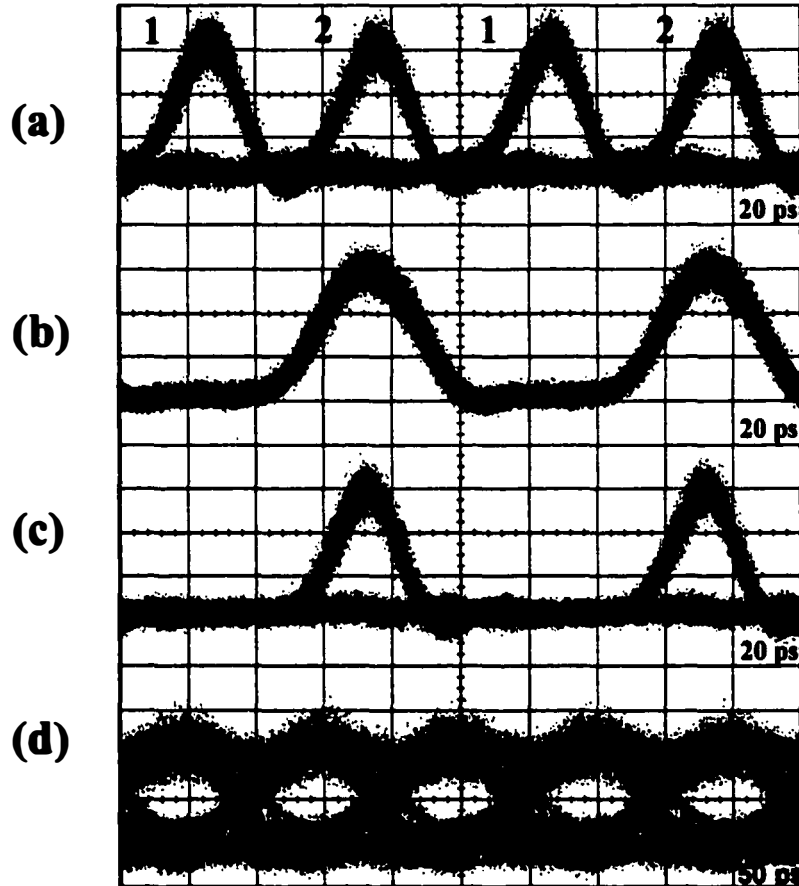


**Figure 3.30** Eye diagrams of (a) the 20 Gbit/s OTDM input at port 1 (20 ps/div), (b) the optical transparency gate of the EA modulator aligned to channel 2 (20 ps/div), (c) the 10 Gbit/s channel 2 transmitted in an optically transparent manner at port 3 (20 ps/div), and (d) the simultaneously demultiplexed and O/E converted 10 Gbit/s channel 1 at port 4 (50 ps/div).

20 Gbit/s BER measurements were then performed with the EA modulator operated as a simultaneous demultiplexer and O/E converter at a bias of -5 V (Figure 3.31). The optically transparent channel 2 operated error-free with a 20 Gbit/s sensitivity of -33.5 dBm and a 10 Gbit/s sensitivity (when channel 1 was blocked) of -36.5 dBm (not shown). This result indicates the good optical extinction of the modulator as verified in the eye diagram (Figure 3.30(c)). On the

other hand, the simultaneously dropped and O/E converted channel 1 exhibited a 20 Gbit/s sensitivity of -28.5 dBm and an error floor. From the single channel 10 Gbit/s sensitivity of -32.5 dBm (Figure 3.29), one can expect a 20 Gbit/s sensitivity of -29.5 dBm for the same channel if there is no power penalty. However, our measurements indicate that there is a power penalty of 1 dB and an error floor, which is investigated and discussed in the next section.

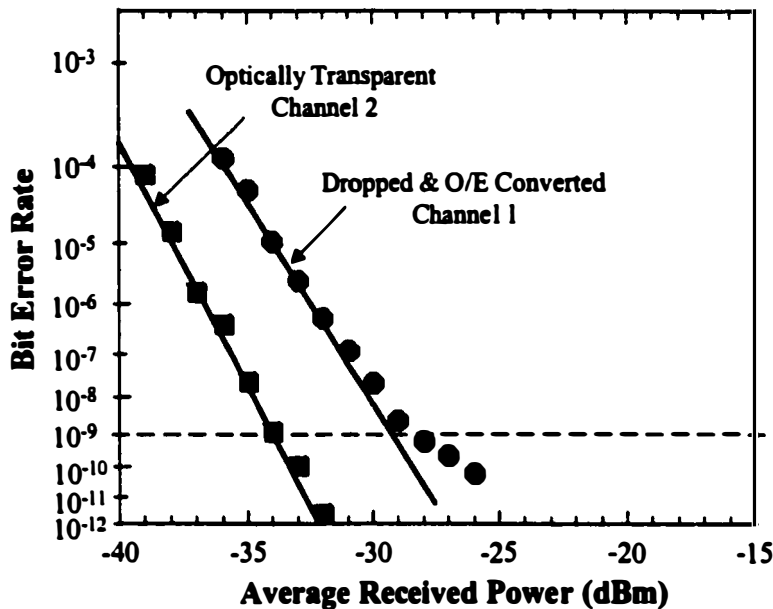


**Figure 3.31** BER measurements at 20 Gbit/s for the demultiplexed and O/E converted channel 1 (circle) and the optically transparent channel 2 (square).

#### 3.4.4 Discussion of Current Issues

The measurements for the simultaneous demultiplexing and detection experiment revealed that there are several significant issues, such as pattern length dependence and residual absorption, which can be classified into two categories:

(1) *External Electronics*: The simultaneous demultiplexing and detection was limited to a pattern length of  $2^7-1$ , which was determined to be due to the high-power amplifier at port 2 (Figure 3.23). When the EA modulator acts as a

photodetector, the output impedance of the amplifier acts as the termination to the device. The high-power amplifier not only has a low-frequency limit of about 10 MHz, but its  $S_{22}$  response over the 10 GHz bandwidth of interest is poor (Figure 3.25). The effect of the amplifier was seen to degrade the EA photodetector performance in the 10 Gbit/s single-channel experiment (Figure 3.28).

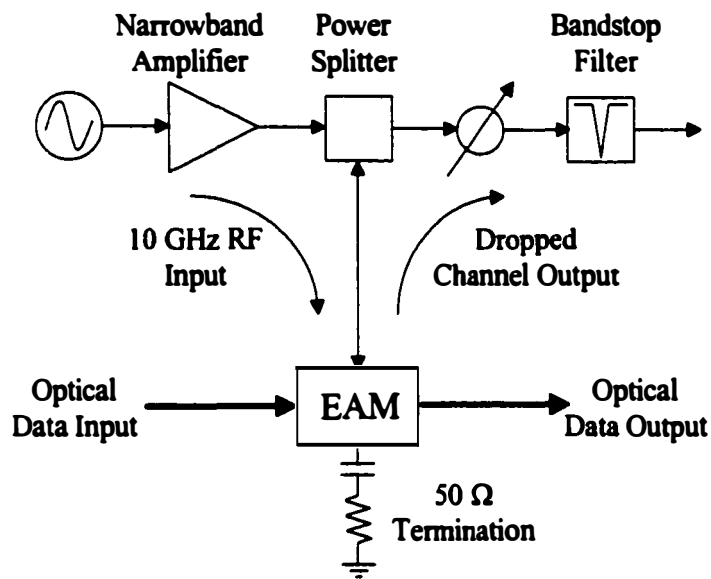


**Figure 3.32** Schematic diagram of the EA modulator set-up for eliminating the negative impacts of the high-power RF amplifier on system performance.

The amplifier's negative impact can be eliminated by using a single port for both modulation and photodetection separated by a splitter while terminating the other port in a  $50\ \Omega$  thin-film or on-chip resistor as shown schematically in Figure 3.32. The  $50\ \Omega$  termination would ensure broadband modulation and photodetection operation, which would allow for  $2^{31}-1$  pattern lengths. This scheme would also eliminate the broad bandwidth requirement for the amplifier; therefore, a high power narrowband 10 GHz amplifier could be employed to reduce the cost of the set-up. However, the splitter in port 2 would result in a 6-dB power

loss on the detected channel, which would need to be compensated by optical amplification of the input signal.

(2) *EA Modulator Limitations:* The simultaneous demultiplexing and detection experiment was limited to two-channel 20 Gbit/s operation as well as residual absorption of the transparent channel, which are due to the particular EA modulator characteristics. The most apparent problem is the insufficient photodetection response due to carrier transit time limitation for reverse biases lower than -5 V, which leads to a trade-off between bandwidth and electrical extinction ratio. As will be shown below, it is desirable to operate at lower reverse biases, which not only allows for lower residual absorption, but also for a longer optical transparency window and a shorter absorption (detection) window. This would be ideal for the simultaneous demultiplexing and detection of a single channel from a four-channel 40 Gbit/s OTDM data stream.

From the two-channel 20 Gbit/s BER measurements in Figure 3.31, it was determined that there was a 1-dB power penalty and an error floor on the demultiplexed and detected channel. In order to investigate the power penalty,  $\delta_X$ , incurred due to residual crosstalk from the transparent channel, an analysis was performed. Crosstalk due to residual absorption,  $X$ , is defined as the ratio of the residual power from the unwanted channels ( $P_k$ ) to the target channel power ( $P_i$ ):

$$X = \frac{\sum_{k \neq i} P_k}{P_i} \quad (3.3)$$

The receiver sensitivity  $P_{rec}$  is obtained by substituting Eq. (3.3) in Eq. (2.3)-(2.4) and solving for  $P_{rec}$  using Eq. (2.2):

$$\bar{P}_{rec} = \frac{h\nu F_n \Delta f}{(1-X)^2} \left( (1+X)Q^2 + Q \sqrt{(1-X)^2 \frac{\Delta v_{opt}}{\Delta f} + 4Q^2 X} \right) \quad (3.4)$$

For a system with negligible crosstalk, Eq. (3.4) reduces to Eq. (2.6). The power penalty is then defined by the ratio of the received power due to crosstalk and in the absence of crosstalk:

$$\delta_x = 10 \log \left[ \frac{(1+X)Q^2 + Q \sqrt{(1-X)^2 \frac{\Delta v_{opt}}{\Delta f} + 4Q^2 X}}{(1-X)^2 \left( Q^2 + Q \sqrt{\frac{\Delta v_{opt}}{\Delta f}} \right)} \right] \quad (3.5)$$

The power penalty due to crosstalk contributions is plotted in Figure 3.33 for various  $Q$  values. Since the maximum electrical extinction ratio for the EA modulator is 13.9 dB, a minimum power penalty of 0.74 dB would be expected for a BER of  $10^{-9}$ . However, for a real assessment of the power penalty, the effects of the switching window shape as well as the input optical pulses need to be considered.

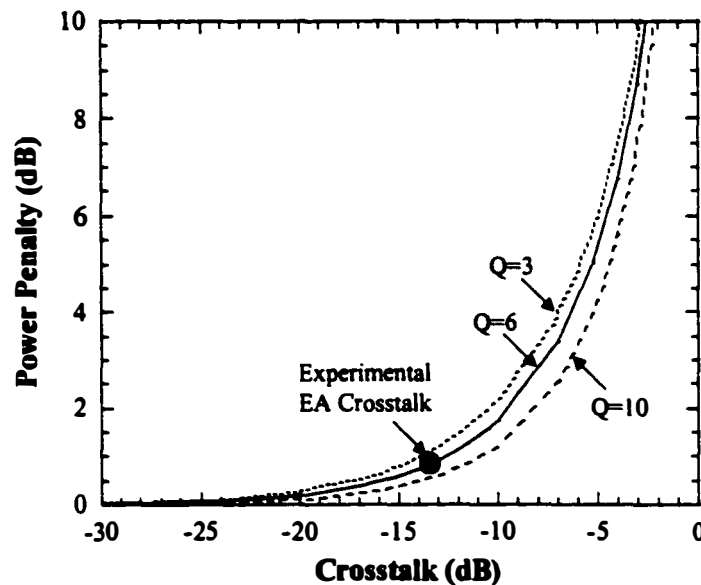


**Figure 3.33** Simulated power penalties due to crosstalk from insufficient electrical extinction ratio for various  $Q$ -values in optically pre-amplified receivers.



The TE mode absorption (responsivity) curve in Figure 3.22 was employed to simulate achievable absorption windows (assuming no bandwidth limitations) for various reverse biases at 10 GHz modulation of the EA modulator. The simulated absorption profiles for an applied 10 V<sub>pp</sub> sinusoidal modulation are shown in Figure 3.34. As the reverse bias is decreased to forward bias, the absorption window decreases while the optical transparency window widens. At the experimental operating bias of -5 V, a simulated absorption width of 65 ps is observed, which agrees with the experimental width in Figure 3.30(b).

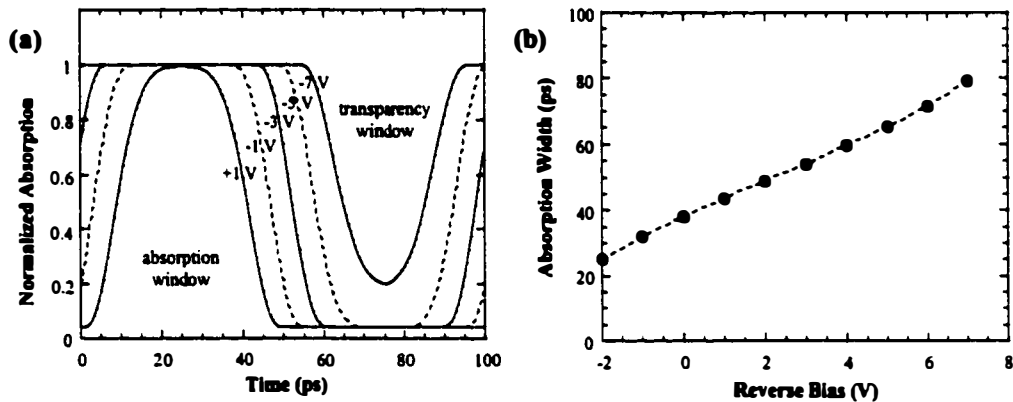


**Figure 3.34** Simulated (a) absorption profiles and (b) absorption widths for an applied 10 GHz 10 V<sub>pp</sub> sinusoidal modulation of the EA modulator as a function of various reverse biases (the measured TE polarization responsivity curve in Figure 3.22 is used).

The crosstalk due to the residual absorption of the transparent channel was simulated by taking into account the shape of the switching window and the optical input pulses. The input pulses were assumed to be Gaussian with a pulse width of 11 ps. The simulated crosstalk and the power penalty are shown as a function of reverse bias in Figure 3.35. The power penalty increases at high reverse biases due to the high absorption of the transparent channel and at forward biases due to the lower absorption of the demultiplexed channel. The best operating region is between zero and -4 V, assuming the bandwidth of the device is constant and the input sinusoidal signal is 10 V<sub>pp</sub>. At the experimental reverse bias of -5 V, the

crosstalk and power penalty for a BER of  $10^{-9}$  are -13.4 dB and 0.83 dB, respectively, which agrees well with the experimentally observed penalty.

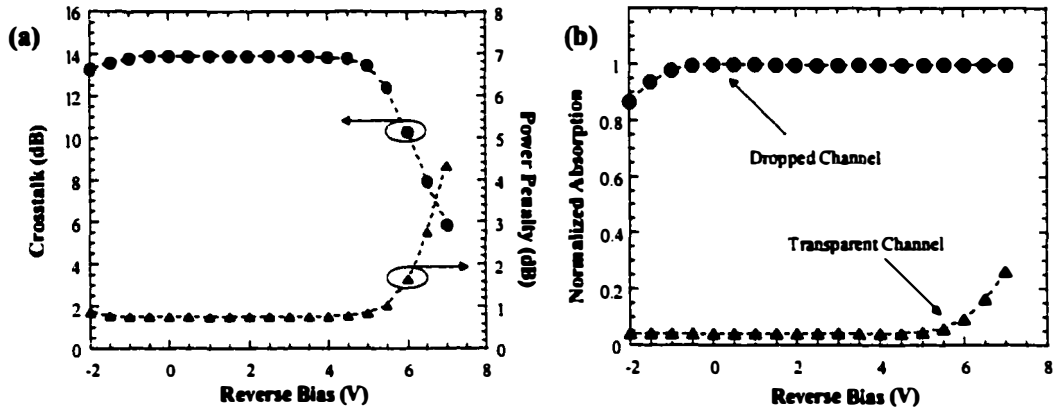


Figure 3.35 Simulated (a) crosstalk (circle) and power penalty (triangle), and (b) normalized absorption for dropped (circle) and optically transparent (triangle) channels for a 20 Gbit/s OTDM input with 11 ps Gaussian pulses.

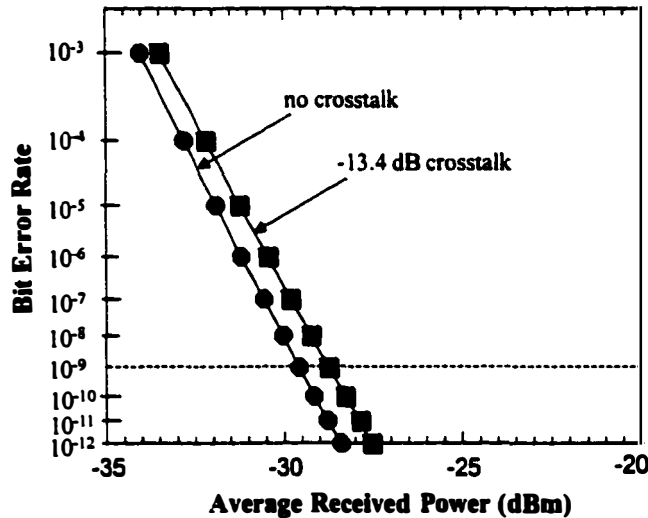


Figure 3.36 Simulated 20 Gbit/s BER curves for the simultaneous drop and detect experiment with no crosstalk (circle) and -13.4 dB crosstalk (square).

Figure 3.36 shows the simulated 20 Gbit/s BER plots for the simultaneously demultiplexed and detected channel with zero and -13.4 dB crosstalk. The reference curve (no crosstalk) is normalized to the experimental 10 Gbit/s results

from Figure 3.29 for a reverse bias of -5 V. The error floor, which had incurred in the experiment, is not observed in the simulated BER curves. This can be simply understood from Eq. (3.5), which reduces to Eq. (3.6) for infinite  $Q$  values,

$$\delta_x \stackrel{Q \rightarrow \infty}{=} 20 \log \left[ \frac{1}{1 - \sqrt{X}} \right] \quad (3.6)$$

From Eq. (3.6), it can be inferred that power penalty due to crosstalk is independent of the  $Q$ -factor for very low BER's. Therefore, the demultiplexing induced crosstalk will only result in power penalties without error floors. The error floor is believed to be due to the saturation of the EA modulator when operated as a photodetector. In order to achieve the same BER at 10 and 20 Gbit/s, the received power has to be increased by 3 dB to accommodate for the optical power in the second channel. This results in a 3-dB additional optical power input to the EA modulator at 20 Gbit/s (about +9 dBm). Power saturation is caused at high input power levels due to hole pile-up at the valence band discontinuity of the heterointerfaces [37], and electric field screening [38]. Due to the accumulation of trapped holes, the induced potential drop at the heterointerface reduces the electric field, which results in a more optically transparent waveguide. Similarly, the space charge generated in the waveguide due to the electric field screening effect during the electroabsorption process reduces the applied bias. These two effects not only attenuate the modulator absorption, but also degrade the bandwidth of the device.

Power saturation of the EA modulator results in a pattern dependent power penalty and an error floor. When an optical input with bit '1' saturates the device, the absorption of the immediately following '1's are decreased. The saturation is pronounced in the presence of long strings of '1's. If the saturating '1' is followed by '0's, the absorption of the modulator recovers to its original state before another '1' saturates the device. Obviously, the power saturation induced penalty increases

with higher optical input powers, which results in an error floor at low BER's. Optical power saturation in an EA modulator can be relieved by inserting a graded interface between the cladding layer and the barrier, or by a hole pile-up buffer layer [37].

From the preceding discussion and analysis, there are three basic requirements the EA modulator has to satisfy for the simultaneous demultiplexing and detection functionality to operate with low power penalties. These include (1) a high photodetection bandwidth (about 6 GHz) at low reverse biases, (2) very low absorption at zero bias (or high electrical extinction ratio), and (3) a high saturation input power. Additionally, the device requires good electrical characteristics for a forward bias condition during part of the driving cycle.

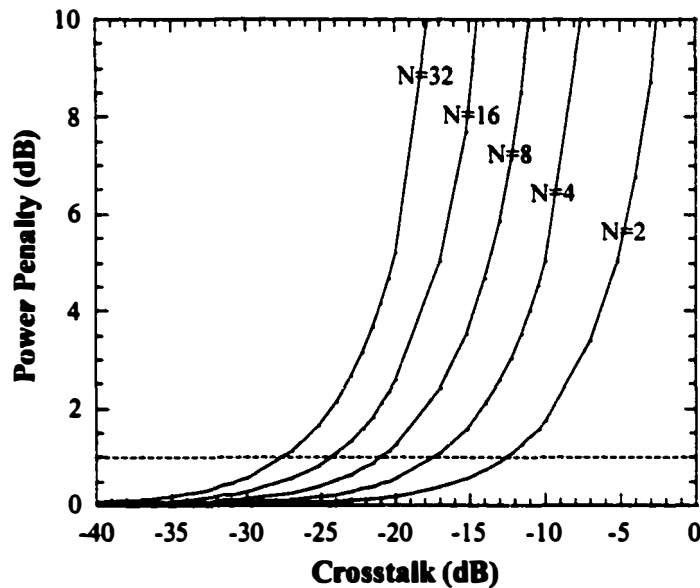


**Figure 3.37** Simulated power penalties for a BER of  $10^{-9}$  due to relative channel crosstalk from insufficient electrical extinction ratio for higher capacity OTDM systems, where  $N$  is the number of optically multiplexed channels. For a 1-dB optical power penalty, the extinction ratio has to be higher than 18 dB for a four-channel system.

For larger number of channels operation, the EA modulator requires a higher electrical extinction ratio since the number of transparent channels is

increased. Figure 3.37 shows the amount of electrical extinction required in N-channel systems in order to obtain a BER of  $10^{-9}$ . For 40 Gbit/s operation, since there are 3 times as many channels to be avoided from absorption in comparison to 20 Gbit/s, an extra electrical extinction ratio of 4.77 dB is required. Additional power penalty can also arise from the residual absorption of the adjacent channels due to the absorption window at 40 Gbit/s. Therefore, the absorption window can not exceed the bit slot of the channel to be demultiplexed. A 25-ps window can easily be achieved by either single or harmonic modulation of the EA modulator at low reverse biases. Satisfaction of these absorption criteria as well as high optical power saturation would be ideal for the simultaneous demultiplexing and detection of a single channel from a four-channel 40 Gbit/s OTDM data stream.

#### ***3.4.5 Potential Future Applications***

The simultaneous demultiplexing and photodetection operation of EA modulators introduces two potential low-cost and compact future OTDM network applications. These include add/drop multiplexers and integrated OTDM demultiplexing receivers.

(1) *Add/Drop Multiplexer*: As discussed in the introductory section, future OTDM network nodes will require a high-speed optical processing feature for dropping the desired channels from an incoming TDM data stream while inserting new channels into the available time slots. These add/drop multiplexers will require high speed, small size, and low cost. The simultaneous demultiplexing and detection operation using an EA modulator is ideal for performing the drop function (Figure 3.38). A new channel can be inserted by a synchronized optical source and multiplexer.

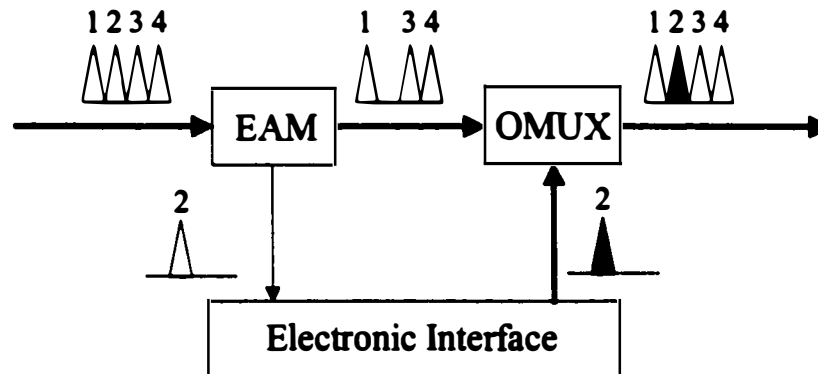


**Figure 3.38** A compact add/drop multiplexer for high-speed OTDM applications using the simultaneous drop and detect EA modulator. The 'add' operation is performed using a synchronized optical source and multiplexer.

(2) *Compact OTDM Demultiplexing Receiver:* Current 40 Gbit/s receiver subsystems based on ETDM techniques using high-speed O/E converters and electrical demultiplexers are in the process of commercial realization (Figure 3.39(a)). As it was discussed in Chapter 2, the main drawbacks of ETDM are the high bandwidth requirements and scalability to higher speeds. On the other hand, the relaxed bandwidth requirement and simple operation of optical demultiplexing based on EA modulators has made this approach into one of the most widely used laboratory tools for high-speed TDM experiments (Figure 3.39(b)). However, this technique has significant disadvantages from a commercial implementation perspective. The demultiplexed channel is usually followed by an optical amplifier, which compensates for the losses in the modulator, and an O/E converter. In this configuration, each channel to be demultiplexed requires separate demultiplexing paths resulting in a complex and expensive receiver node. As it was demonstrated in Section 3.3, it is possible to integrate the modulator, the optical amplifier and the O/E converter on a single chip. However, due to the nature of the demultiplexing method, in a 1:4 demultiplexing scheme, 75% of the incoming optical data stream is suppressed by absorption in the modulator in addition to multiple fiber-coupling losses. As a result of the optical power

inefficiency, the number of fiber-to-device interfaces, and cost of the individual components, the EA modulator based optical demultiplexing scheme is quite impractical for commercial applications.

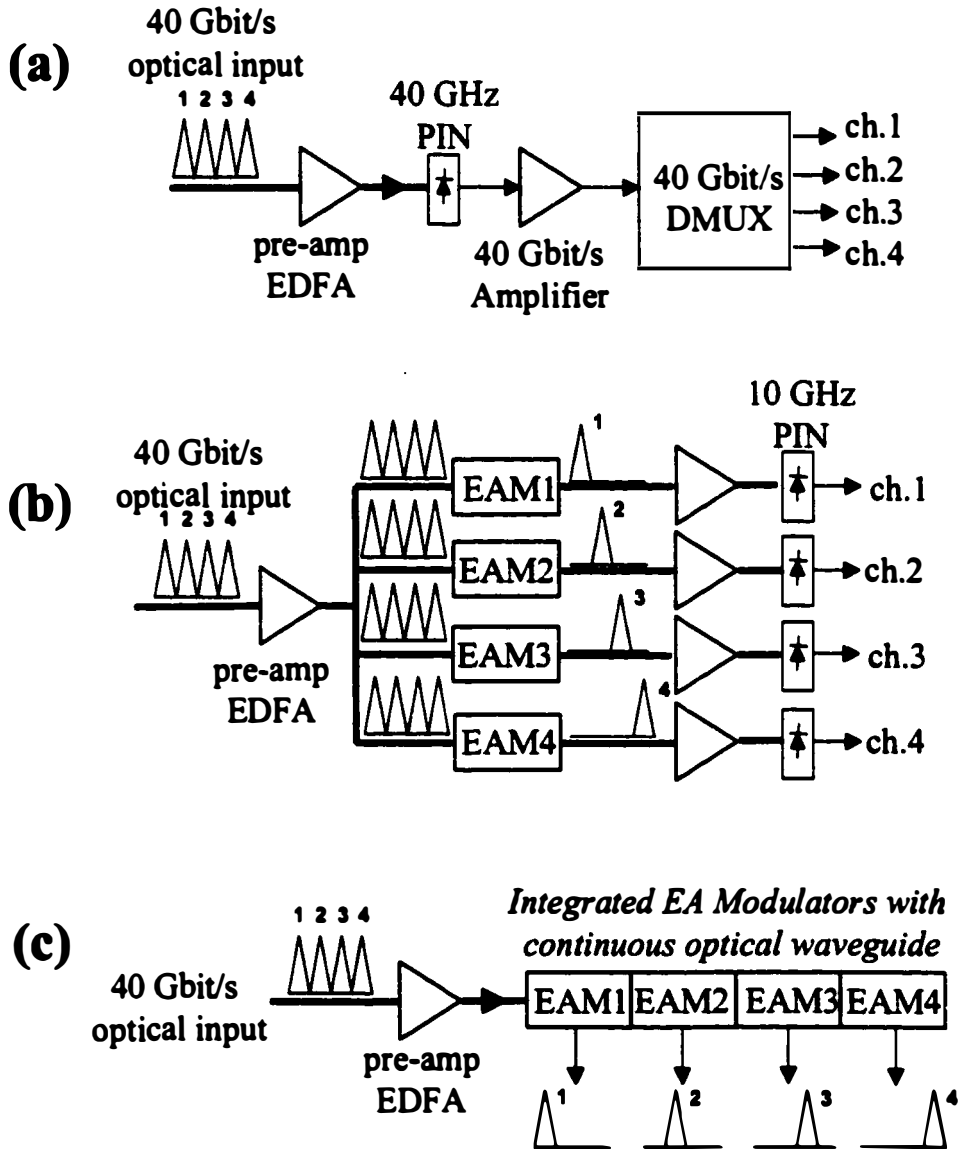


**Figure 3.39** Schematically shown 40 Gbit/s receiver subsystems based on (a) high-speed electrical TDM, (b) conventional parallel EA demultiplexers, and (c) proposed compact demultiplexing receiver based on integrated EA modulators. DMUX: demultiplexer; PIN: photodetector.

On the other hand, the proposed simultaneous demultiplexing and detection technique using an EA modulator achieves optical power conservation through complementary optical demultiplexing. A compact 40 Gbit/s demultiplexing receiver can be realized by cascading four EA modulators integrated on a single chip (with a continuous optical waveguide) as shown in Figure 3.39(c). This receiver scheme has the potential for serial-optical to direct parallel-electrical conversion. One of the major advantages of this demultiplexing receiver is that the complexity, size and cost of the conventional optical demultiplexer is reduced drastically into a single package with a single fiber-to-device interface requirement. The scheme essentially mimics a high-speed ETDM receiver subsystem with the added benefit of operation at the tributary base rate.

### **3.5 Summary and Conclusions**

In this chapter, various optical processing techniques using simple sinusoidal modulation of EA modulators were presented and investigated. These features include optical short pulse generation, optical demultiplexing as well as simultaneous demultiplexing and detection with the advantage of simple and stable operation, compact size and low polarization sensitivity. Optical pulses with duty ratios less than 10% and extinction ratios greater than 20 dB were easily achieved while the EA modulator's high-speed OTDM demultiplexing capability was demonstrated. The biggest drawback of EA modulators was determined to be the high insertion loss, which requires compensation with external optical amplifiers. Therefore, integrated tandem EA modulators were investigated and demonstrated as efficient and compact OTDM receiver subsystems. The demultiplexing feature of the EA modulator was further augmented by simultaneously detecting the demultiplexed channel while transmitting the remaining channels in an optically transparent manner. This experiment and the subsequent analysis revealed that four-channel 40 Gbit/s operation of the simultaneous demultiplexer and O/E



converter is realizable with applications to future high-speed add/drop multiplexers and compact OTDM demultiplexing receivers.

The various optical processing demonstrations using EA modulators indicate that these devices will be key elements in future OTDM systems. For successful commercial implementation of EA modulators in OTDM system applications, a reduction in the optical insertion loss and an increase in the optical input power saturation need to be accomplished. These improvements will require that high extinction ratio, low drive voltage, and low polarization and wavelength sensitivity characteristics are retained.

## References

- [1] A. D. Ellis, T. Widdowson, I. D. Phillips, and W. A. Pender, "High speed OTDM networks employing electro-optic modulators," *IEICE Trans. on Electron.*, vol. E81-C, pp. 1301-1308, 1998.
- [2] M. Suzuki, H. Tanaka, K. Utaka, N. Edagawa, and Y. Matsushima, "Transform-limited 14 ps optical pulse generation with 15 GHz repetition rate by InGaAsP electroabsorption modulator," *Electron. Lett.*, vol. 28, pp. 1007-1008, 1992.
- [3] V. Kaman, Y. J. Chiu, S. Z. Zhang, and J. E. Bowers, "3.7 ps pulse generation at  $\geq 30$  GHz by dual-drive electroabsorption modulator," *Electron. Lett.*, vol. 36, pp. 1130-1132, 2000.
- [4] M. Suzuki, H. Tanaka, and Y. Matsushima, "10 Gbit/s optical demultiplexing and switching by sinusoidally driven InGaAsP electroabsorption modulators," *Electron. Lett.*, vol. 28, pp. 934-935, 1992.
- [5] I. D. Phillips, A. Gloag, D. G. Moodie, N. J. Doran, I. Bennion, and A. D. Ellis, "Simultaneous two-channel OTDM demultiplexing using a single electroabsorption modulator in a novel bi-directional configuration," *Electron. Lett.*, vol. 33, pp. 1811-1812, 1997.
- [6] I. D. Phillips, A. Gloag, D. G. Moodie, N. J. Doran, I. Bennion, and A. D. Ellis, "Simultaneous demultiplexing and clock recovery using a single electroabsorption modulator in a novel bi-directional configuration," *Optics Comm.*, vol. 150, pp. 101-105, 1998.
- [7] T. Miyazaki, N. Edagawa, M. Suzuki and S. Yamaoto, "Novel optical-regenerator using electroabsorption modulator", *OFC '99 Technical Digest*, pp. 350-352, 1999.
- [8] Y. Kisaka, A. Hirano, M. Yoneyama and N. Shimizu, "Simple 2R repeater based on EA modulator directly driven by uni-travelling-carrier photodiode", *Electron. Lett.*, vol. 35, pp. 1016-1017, 1999.

- [9] N. Edagawa, M. Suzuki, and S. Yamamoto, "Novel wavelength converter using an electroabsorption modulator," *IEICE Trans. on Electron.*, vol. E81-C, pp. 1251-1257, 1998.
- [10] L. K. Oxenloewe, A. T. Clausen, and H. N. Poulsen, "Wavelength conversion in an electroabsorption modulator," *ECOC '00 Technical Digest*, paper 9.4.4, 2000.
- [11] V. Kaman, A. J. Keating, S. Z. Zhang, and J. E. Bowers, "Simultaneous OTDM demultiplexing and detection using an electroabsorption modulator," *IEEE Photonics Tech. Lett.*, vol. 12, pp. 711-713, 2000.
- [12] S. Z. Zhang, Y. J. Chiu, P. Abraham, J. E. Bowers, "25 GHz polarization-insensitive electroabsorption modulators with traveling-wave electrodes", *IEEE Photonics Tech. Lett.*, vol. 11, pp. 191-193, 1999.
- [13] N. M. Froberg, G. Raybon, A. M. Johnson, Y. K. Chen, T. Tanbun-Ek, R. A. Logan, A. Tate, A. M. Sargent, K. Wecht, and P. F. Sciortino, Jr., "Pulse generation by harmonic modulation of an integrated DBR laser-modulator," *Electron. Lett.*, vol. 30, pp. 650-651, (no.8), 1994.
- [14] H. Tanaka, S. Takagi, M. Suzuki and Y. Matsushima, "Optical short pulse generation by double optical gate operation of tandem connected electroabsorption modulators driven by sinusoidal voltages", *Electron. Lett.*, vol. 29, pp. 1449-1451, 1993.
- [15] F. Devaux, D. Jahan, F. Alexandre, A. Ougazzaden, E. Vergnol and M. Carre, "Tandem of modulators for high on/off pulse generation (-55 dB)", *Electron. Lett.*, vol. 33, pp. 1491-1492, 1997.
- [16] V. Kaman, Y. J. Chiu, T. Liljeberg, S. Z. Zhang and J. E. Bowers, "Integrated tandem traveling-wave electroabsorption modulators for > 100 Gbit/s OTDM applications", *IEEE Photonics Tech. Lett.*, vol. 12, November 2000.
- [17] D. D. Marcenac, A. D. Ellis and D. G. Moodie, "80 Gbit/s OTDM using electroabsorption modulators", *Electron. Lett.*, vol. 34, pp.101-103, 1998.
- [18] G. P. Agrawal, *Fiber-Optic Communication Systems*, John Wiley & Sons, Inc., 1992.
- [19] M. Guy, S. Chernikov, and R. Taylor, "Electroabsorption modulators for high speed ultrashort pulse generation and processing," *IEICE Trans. on Electron.*, vol. E81-C, pp. 169-174, 1998.
- [20] B. Mikkelsen, G. Raybon, R. J. Essiambre, K. Dreyer, Y. Su, L. E. Nelson, J. E. Johnson, G. Shtengel, A. Bond, D. G. Moodie and A. D. Ellis, "160 Gbit/s single-channel transmission over 300 km nonzero-dispersion fiber with semiconductor based transmitter and demultiplexer", *ECOC '99 Technical Digest*, PD2-3, 1999.
- [21] D. G. Moodie, A. D. Ellis, A. R. Thurlow, M. J. Harlow, I. F. Lealman, S. D. Perrin, L. J. Rivers and M. J. Robertson, "Multiquantum well electroabsorption modulators for 80 Gbit/s OTDM systems", *Electron. Lett.*, vol.31, pp.1370-1371, 1995.
- [22] S. Oshiba, K. Nakamura and H. Horikawa, "Low-drive-voltage MQW electroabsorption modulator for optical short-pulse generation", *IEEE J. Quantum Electron.*, vol. 34, pp. 277-281, 1998.
- [23] H. Tanaka, M. Suzuki, and Y. Matsushima, "Optical short pulse generation by DFB laser/EA modulator integrated light source," *IEEE J. of Quantum Electron.*, vol. 29, pp. 1708-1713, 1993.

- [24] H. Takeuchi, K. Tsuzuki, K. Sato, S. Matsumoto, M. Yamamoto and Y. Itaya, "High-speed electroabsorption modulator integrated with DFB laser with bandwidth over 30 GHz and its pulse generation", *MWP '96 Technical Digest*, pp. 301-304, 1996.
- [25] N. Souli, A. Ramdane, F. Devauz, A. Ougazzaden, and S. Slemkes, "Tandem of electroabsorption modulators integrated with a DFB laser and an optical amplifier for short optical pulse generation and coding," *Proc. of Optoelectron.*, vol. 145, pp. 198-200, 1998.
- [26] A. Felder, M. Moller, M. Wurzer, M. Rest, T. F. Meister, and H. M. Rein, "60 Gbit/s regenerating demultiplexer in SiGe bipolar technology," *Electron. Lett.*, vol. 33, pp. 1984-1986, 1997.
- [27] W. Bogner, E. Gottwald, A. Schopflin and C. J. Weiske, "40 Gbit/s unrepeated optical transmission over 148 km by electrical time division multiplexing and demultiplexing," *Electron. Lett.*, vol. 33, pp. 2136-2137, 1997.
- [28] M. Yoneyama, Y. Miyamoto, T. Otsuji, H. Toba, Y. Yamane, T. Ishibashi, and H. Miyazawa, "Fully electrical 40-Gb/s TDM system prototype based on InP HEMT digital IC technologies," *IEEE J. of Lightwave Tech.*, vol. 18, pp. 34-43, 2000.
- [29] V. Kaman, and J. E. Bowers, "120 Gbit/s OTDM system using electroabsorption transmitter and demultiplexer operating at 30 GHz," *Electron. Lett.*, vol. 36, pp. 1477-1479, 2000.
- [30] V. Kaman, Y. J. Chiu, T. Liljeberg, S. Z. Zhang, and J. E. Bowers, "A compact 40 Gbit/s demultiplexing receiver based on integrated tandem electroabsorption modulators," submitted to *Electron. Lett.*, 2000.
- [31] O. Kamatani, Y. Katagiri, and S. Kawanishi, "100-Gbit/s optical TDM add/drop multiplexer based on photonic downconversion and four-wave mixing," *OFC '98 Technical Digest*, pp. 112-113, 1998.
- [32] A. Buxens, H. N. Poulsen, A. T. Clausen, K. S. Jepsen, and P. Jeppesen, "Simultaneous all-optical add-drop multiplexing functionality using bi-directional four wave mixing in a semiconductor optical amplifier," *ECOC '99 Technical Digest*, pp. 248-249, 1999.
- [33] R. Hess, M. Duelk, W. Vogt, E. Gamper, E. Gini, P. A. Besse, H. Melchior, K. S. Jepsen, B. Mikkelsen, M. Vaa, H. N. Poulsen, A. T. Clausen, K. E. Stubkjaer, S. Bouchoule, and F. Devaux, "Simultaneous all-optical add and drop multiplexing of 40 Gbit/s OTDM signals using monolithically integrated Mach-Zehnder interferometer," *Electron. Lett.*, vol. 34, pp. 579-580, 1998.
- [34] A. D. Ellis, T. Widdowson, X. Shan, and D. G. Moodie, "Three-node, 40 Gbit/s OTDM network experiment using electro-optic switches," *Electron. Lett.*, vol. 30, pp. 1333-1334, 1994.
- [35] I. D. Phillips, A. Gloag, D. G. Moodie, N. J. Doran, I. Bennion and A.D Ellis, "Drop and insert multiplexing using an electroabsorption modulator," *IEEE Photonics Tech. Lett.*, vol. 10, pp. 291-293, 1998.
- [36] V. Kaman, A. J. Keating, S. Z. Zhang, and J. E. Bowers, "Electroabsorption modulator as a compact OTDM demultiplexing receiver," *ECOC '00 Technical Digest*, paper 9.4.6, 2000.
- [37] M. Suzuki, H. Tanaka, and S. Akiba, "Effect of hole pile-up at heterointerface on modulation voltage in GaInAsP electroabsorption modulators," *Electron. Lett.*, vol. 25, pp. 88-89, 1989.

- [38] T. H. Wood, J. Z. Pastalan, C. A. Burrus, B. C. Johnson, B. I. Miller, J. L. deMiguel, U. Koren, and M. G. Young, "Electric field screening by photogenerated holes in multiple quantum wells: a new mechanism for absorption saturation," *Appl. Phys. Lett.*, vol. 57, pp. 1081-1083, 1990.



## CHAPTER 4

### **Optical Time Division Multiplexed Systems Beyond 100 Gbit/s**

#### **4.1 Introduction**

Ultra high-speed optical time division multiplexing (OTDM) has recently emerged as an attractive means of constructing very high-capacity optical systems. With the explosive demand for high capacity in optical communication systems, high TDM bit rates have the advantage of an increased spectral efficiency (high bit rate-to-bandwidth ratio) and a potential reduction in cost per bit. High-capacity channel rates also allow for a lower number of wavelength channels, which results in a relaxed control and management of wavelength division multiplexed (WDM) optical networks as well as reduced inter-channel non-linear effects. Due to the aforementioned advantages, fiber transmission systems based on channel rates of 40 Gbit/s are currently being planned for commercial installation [1], and next generation bit rates of 160 Gbit/s per wavelength channel are under investigation in various laboratories [2-5]. Since the speed of electronics is presently limited to 40 Gbit/s, various high-speed OTDM techniques have gained popularity to construct optical systems with bit rates beyond 100 Gbit/s per wavelength channel. In order to realize high-speed OTDM systems, high-speed technologies including optical short pulse generation, optical multiplexing, optical demultiplexing, and timing extraction need to be investigated.

To date, several all-optical and electro-optic techniques have been employed to achieve OTDM systems beyond 100 Gbit/s, with demonstrations at 160 Gbit/s [2-5], 320 Gbit/s [6, 7], 640 Gbit/s [8], and 1.28 Tbit/s [9], which are based on a tributary base rate of 10 or 20 Gbit/s. Due to advances in high-speed ETDM, it is inevitable that next generation OTDM systems will operate at an electronic tributary rate of 40 Gbit/s with optical multiplexing to 160 Gbit/s or more (Figure

4.1). The increase of the base rate and the consequent reduction in the number of optical channels will allow for more robust and stable high-speed OTDM systems.

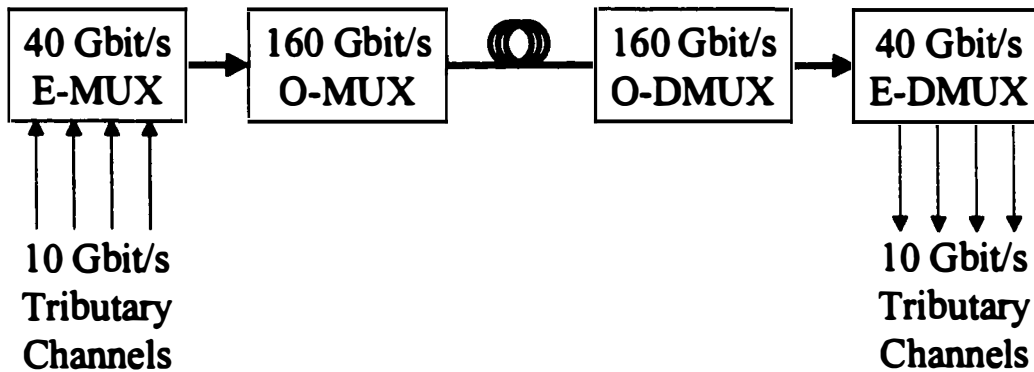


**Figure 4.1** Next-generation 160 Gbit/s OTDM systems based on 40 Gbit/s ETDM tributary channels at the transmitter and receiver.

In this chapter, a 120 Gbit/s OTDM system based on four 30 Gbit/s tributary channels is presented [10]. Electroabsorption (EA) modulators [11, 12], driven at modulation frequencies  $\geq 30$  GHz, are employed as stable and compact optical short pulse sources and demultiplexers. To the author's knowledge, this is the first demonstration of the feasibility of using EA modulators in conjunction with high-speed ( $> 20$  Gbit/s) electrical multiplexing and demultiplexing for greater than 100 Gbit/s OTDM systems.

## 4.2 OTDM System Requirements

In order to realize high-speed OTDM systems, several requirements need to be satisfied for the transmitter (optical pulse source and multiplexer) and receiver (optical demultiplexer and clock-recovery) subsystems. This section reviews the general OTDM requirements and the various technologies that are employed.

### **4.2.1 OTDM Transmitter Subsystem**

(1) *Optical Pulse Generator*: In high-speed OTDM systems, optical pulse sources need to satisfy several requirements including stable and reliable transform-limited pulse generation, high extinction ratio and signal-to-noise ratio (SNR), low insertion loss, tunable and controllable repetition rates and wavelength, and compact size. Since the pulse width of the optical signal determines the ultimate limit for the highest achievable multiplexed bit rate, the pulse width has to be less than the time slot of the desired bit rate. Transform-limited pulses are most suitable for OTDM applications since the optical pulses have the minimum spectral width for the given pulse width, which minimizes fiber dispersion effects. Several optical short pulse generation methods at 40 GHz repetition rates have been demonstrated using mode-locked semiconductor lasers [13, 14], non-linear pulse compression [15], mode-locked fiber ring lasers (ML-FRL) [16-19], and EA modulators [11, 12, 20-22]. Optical pulses as short as 1 ps have been achieved using ML-FRL's; however, due to the long fiber length within the pulse source, long-term stability is a critical issue. Similarly, the use of long lengths of fiber to non-linearly compress pulses may introduce unwanted phase and polarization drifts in the output pulse train due to temperature shifts in the fiber. On the other hand, sinusoidally driven EA modulators offer a compact and stable pulse source at the expense of broader pulses.

(2) *Optical Multiplexer*: Optical multiplexing, or bit-interleaving, of independently modulated and data encoded short pulses can be achieved in a parallel-type configuration by optical passive components (e.g. couplers), planar lightwave circuits [23], integrated semiconductor waveguides [24], and serial-type configuration by using a four-wave mixing (FWM) based multiplexer [25]. Even though optical multiplexing based on fiber delay lines and couplers is a common approach for laboratory experiments, the thermal drift in the multiplexer can lead to



interference between the multiplexed channels and degrade the overall system performance. Therefore, integrated multiplexers with timing precision better than 1 ps will become a key approach for future high-speed OTDM systems.

In the optical multiplexer, interference due to pulse tail overlap of adjacent channels and the overall finite background extinction ratio can result in significant system performance degradation if the crosstalk beat signal is within the receiver bandwidth. Defining the relative crosstalk power,  $\varepsilon$ , as the ratio of the total average crosstalk power to the average signal power, and following a similar analysis as in Section 2.4.2 for an optically preamplified receiver, the receiver sensitivity assuming Gaussian statistics for crosstalk contributions is given by,

$$\bar{P}_{rec} = h\nu F_n \Delta f \left( \frac{Q^2}{1 - \varepsilon Q^2} \right) \quad (4.1)$$

An optical power penalty,  $\delta_c$ , due to the relative crosstalk is then given by,

$$\delta_c = -10 \log(1 - \varepsilon Q^2) \quad (4.2)$$

Figure 4.2 shows the crosstalk induced power penalty for optically preamplified receivers at a BER of  $10^{-9}$ . It can be inferred from Eq. (4.2) that an error floor will be incurred due to high interference between the signal and crosstalk. The SNR due to incoherent interference on a single channel is given by [26],

$$SNR_n = \frac{\int P_n(t) dt}{\sum_{m \neq n} \int \sqrt{P_n(t) P_m(t)} dt} \quad (4.3)$$

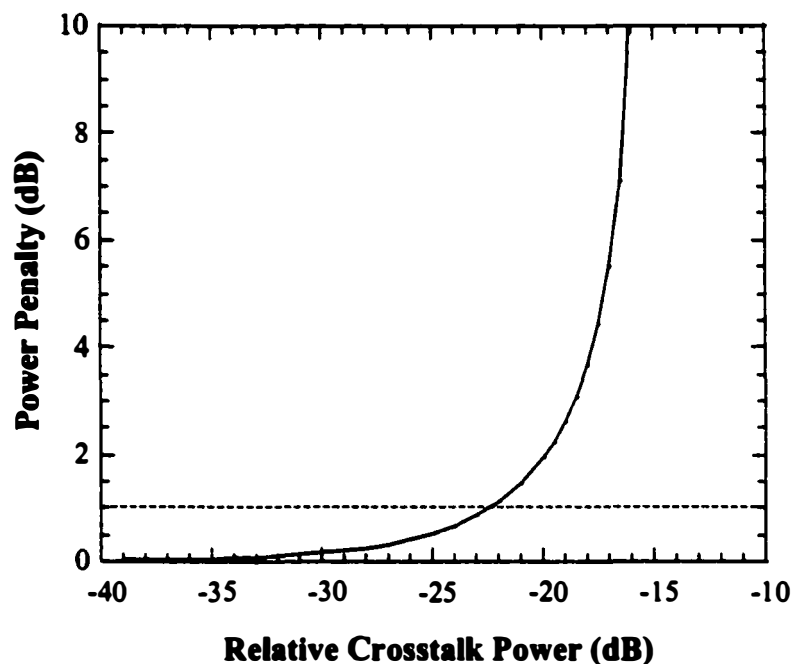


**Figure 4.2** Crosstalk-induced optical power penalty for optically pre-amplified OTDM systems for a BER of  $10^{-9}$ . An error floor is incurred for interference crosstalk levels higher than  $-16$  dB.

In order to achieve error-free operation (SNR of 18 dB for a BER of  $10^{-15}$ ), it can be easily calculated from Eq. (4.2) and (4.3) that for a four-channel 160 Gbit/s (120 Gbit/s) OTDM system with Gaussian pulses, an optical pulse extinction ratio higher than 35 dB is required with a maximum pulse width of 2 ps (2.7 ps). It should also be noted that for an OTDM system with more than four channels, the pulse extinction ratio requirement is higher as inferred from Eq. (4.3). Therefore, it is desirable to minimize the number of optical channels and increase the electronic base rate.

The stringent requirements on the extinction ratio and pulse width can be relaxed if both polarization and time multiplexing are employed. Polarization multiplexing of adjacent pulses reduces the beat noise due to the overlap of pulse tails, and therefore allows for the multiplexing of broader pulses than is required for the single polarization format. Several other advantages of polarization

multiplexing include a higher spectral efficiency and a decreased influence of fiber non-linearities such as intra-channel cross phase modulation and FWM [27].

#### **4.2.2 OTDM Receiver Subsystem**

For OTDM systems beyond 100 Gbit/s, high-speed optical demultiplexing is necessary to recover the tributary channels. For penalty-free optical demultiplexing, the effect of the demultiplexing window width, the window shape, and timing jitter must be considered. Crosstalk-induced power penalty analysis due to incomplete extinction of the undesired channels was discussed and presented in Section 3.4.4 (Eq. (3.5)). It has been also demonstrated that minimum optical power penalty is achieved when the window width is set to the bit slot width [28]. In order to ensure a BER less than  $10^{-12}$ , the rms value of the jitter must be less than 1/14.1 times the time slot [28]. Therefore, for 160 (120) Gbit/s to 40 (30) Gbit/s optical demultiplexing with less than 1 dB power penalty, a minimum dynamic extinction ratio of 20 dB with a square-like less than 6 ps (8 ps) wide switching window is required. It is also important that the demultiplexer is polarization insensitive in order to accommodate variable polarization states of incoming optical signals.

The most widely employed optical demultiplexing techniques for OTDM systems beyond 100 Gbit/s are non-linear optical loop mirrors (NOLM) [29], FWM in optical fiber [30, 31] and semiconductor optical amplifiers (SOA) [32, 33], LiNbO<sub>3</sub> modulator based Sagnac interferometers [34], SOA based Mach-Zehnder interferometers [35, 36], and EA modulators [4, 10]. Demultiplexing techniques based on optical fiber and SOA's not only require the generation of local optical clocks, but they are also susceptible to thermal drift, which can lead to SNR degradation in the demultiplexing process. Therefore, an OTDM receiver subsystem based on optical demultiplexing using stable and compact EA modulators currently seems to be the most practical technique.

### **4.2.3 Beyond 100 Gbit/s OTDM Demonstrations**

Single wavelength OTDM transmission experiments beyond 100 Gbit/s have been demonstrated in various research laboratories using the optical short pulse generation and demultiplexing techniques described in the preceding section over the past decade. The most significant system demonstrations are listed in Table 4.1. The first 100 Gbit/s optically multiplexed data stream was achieved at *NTT Laboratories*, Japan, in 1988 using a gain-switched laser with 6 ps optical pulses [37]. The ultra-high-capacity beyond 200 Gbit/s demonstrations at *NTT Laboratories* predominantly employed 10 GHz 3 ps pulses generated by a ML-FRL, which were compressed in supercontinuum fiber to less than 1 ps pulse widths, including the latest demonstration of 1.28 Tbit/s [9]. These experiments also employed NOLM's to demultiplex the high-speed data stream to the 10 Gbit/s base rate.

OTDM system experiments employing stable and compact EA modulators for both optical short pulse generation and demultiplexing were achieved at *Lucent Technologies*, USA [4] and at the *University of California, Santa Barbara* (this work) [10]. The optical pulse source EA modulator in [4] was followed by non-linear compression to achieve sub-2 ps transform-limited pulses. Both of these experiments are also the only demonstrations that employed pattern lengths of  $2^{31}-1$ . The optical pulse generator and demultiplexer EA modulators used in [10] are described in the next section while the 120 Gbit/s OTDM system, which is the only demonstration of the feasibility of using electrical multiplexers and demultiplexers beyond 20 Gbit/s in conjunction with EA modulators for high-speed OTDM, is presented in Section 4.4.

Company, Year	OTDM Bit Rate (Gbit/s)	Electrical Base Rate (Gbit/s)	Pulse Source & Pulse Width	Demultiplexer & Electrical Rate	Pattern Length (PRBS)	Ref.
NTT, 1988	100	3.125	GS-LD, 6 ps			[37]
NTT, 1993	100	6.3	ML-FRL, 3.5 ps	FWM, 6.3 Gbit/s		[38]
BT, 1998	100	10	ML-FRL, <3 ps	EA MOD, 10 Gbit/s	$2^7-1$	[39]
NTT, 1998	120	20	ML-FRL, 3.5 ps	EA MOD, 20 Gbit/s	$2^7-1$	[40]
UCSB, 2000	120 <sup>1</sup>	30	EA MOD, 3.7 ps	EA MOD, 30 Gbit/s	$2^{31}-1$	[10]
NTT, 1995	160 <sup>1</sup>	10	ML-FRL <sup>2</sup> , 1.5 ps	NOLM, 10 Gbit/s	$2^{15}-1$	[2]
NTT, 1999	160	10	ML-FRL <sup>2</sup> , 3 ps	FWM, 10 Gbit/s	$2^7-1$	[3]
Lucent, 1999	160	20	EA MOD <sup>2</sup> , 1.8 ps	EA MOD, 10 Gbit/s	$2^{31}-1$	[4]
H.-H. Ins., 2000	160	10	ML-FRL, 1.6 ps	MZI Switch, 10 Gbit/s	$2^7-1$	[5]
NTT, 1995	200 <sup>1</sup>	6.3	ML-FRL <sup>2</sup> , 2.1 ps	FWM, 6.3 Gbit/s		[41]
NRL, 2000	200 <sup>1</sup>	12.5	ML-FRL, 1.6 ps	NOLM, 12.5 Gbit/s	$2^{15}-1$	[42]
NTT, 1998	320	10	ML-FRL <sup>2</sup> , 0.4 ps	NOLM, 10 Gbit/s	$2^{15}-1$	[6]
NTT, 1996	400	10	ML-FRL <sup>2</sup> , 0.98 ps	FWM, 10 Gbit/s		[43]
NTT, 1998	640	10	ML-FRL <sup>2</sup> , 0.2 ps	NOLM, 10 Gbit/s	$2^{15}-1$	[8]
NTT, 2000	1280 <sup>1</sup>	10	ML-FRL <sup>2</sup> , 0.2 ps	NOLM, 10 Gbit/s	$2^{15}-1$	[9]

**Table 4.1** Summary of single-wavelength OTDM system demonstrations beyond 100 Gbit/s. Notes: <sup>(1)</sup> Polarization multiplexing of adjacent channels is employed; <sup>(2)</sup> the optical pulse source output was compressed by non-linear techniques. GS-LD: gain-switched laser diode; ML-FRL: mode-locked fiber ring laser; FWM: four-wave mixing; NOLM: non-linear optical loop mirror; MZI: Mach-Zehnder Interferometer.

### 4.3 High-Speed Optical Switching using EA Modulators

Sinusoidally driven EA modulators play a key role in OTDM systems as optical short pulse generators and optical demultiplexers (Chapter 3). The non-linear attenuation characteristic of EA modulators allows for the generation of optical pulses with less than 10% duty ratio under high reverse bias and large sinusoidal RF signal. According to the simulations in Section 3.2.3, it was determined that for a  $9.5 V_{pp}$  40 GHz modulation drive, optical pulses as short as 3 ps at a reverse bias of -8 V could be expected assuming an ideal EA modulator with no microwave dependence. However, since the optical loss depends strongly on the insertion loss and the duty ratio of the pulses, the average optical output power and consequently the SNR, especially at high frequencies, can be very low. Therefore, the EA modulator requires a high saturation input power to simultaneously satisfy short pulse widths and high optical output powers. Another limiting factor at modulation frequencies beyond 20 GHz is the available RF power as well as the EA modulator frequency response (microwave losses and reflections), which can result in broader pulses with degraded dynamic extinction ratios than is theoretically predicted. On the other hand, it has been shown that the walk-off effect between the electrical and optical pulses in traveling-wave EA modulators can be utilized to further compress optical short pulses [44].

In this section, the high-speed switching performance of traveling-wave EA modulators [45] for high capacity OTDM system applications is investigated. A novel dual-drive modulation of a single EA modulator is presented [11], which effectively doubles the RF drive to achieve less than 15% duty ratios at 40 GHz modulation. This is the smallest duty ratio ever achieved at these frequencies using a single EA modulator. Integrated tandem EA modulators with extinction ratios of 50 dB are also investigated for OTDM applications beyond 100 Gbit/s [12], and discussed in section 4.3.3.

### 4.3.1 Optical Short Pulse Demonstrations Beyond 30 GHz

Optical pulse generation at modulation frequencies of 20 GHz or lower has been widely demonstrated; however, the number of demonstrations beyond 20 GHz is currently limited. Table 2.2 summarizes the achieved pulse duty ratios and dynamic extinction ratios for all the published 30 and 40 GHz modulation of EA modulators. The shortest optical pulses (sub-4 ps) and highest dynamic extinction ratios (> 20 dB) have been achieved at the *University of California, Santa Barbara* (this work) [11, 12].

Company, Year	Modulation Frequency (GHz)	Pulse Width (ps)	Duty Ratio (%)	Dynamic Extinction Ratio (dB)	Ref.
NTT, 1993	30	9.5	28.5	< 10	[46]
NTT, 1997	30	12.3	36.9	14	[20]
	40	10.9	43.6	9	
NTT, 1998	40	5	20	> 15	[21]
OPTO+, 1998	40	6	24	12	[22]
UCSB, 2000	30	3.7	11.1	> 20	[11]
	40	3.6	14.4	> 20	
UCSB, 2000	30	4.2	12.6	> 20	[12]
	40	5.2	20.8	> 20	

**Table 4.2** Summary of optical short pulse generation at modulation frequencies > 30 GHz using electroabsorption modulators.

### 4.3.2 Dual-Drive Modulation

For the dual-drive modulation application, a traveling-wave EA modulator with two electrodes was used [45]. The fiber-to-fiber transmission characteristics of the 2- $\mu\text{m}$  wide, 300- $\mu\text{m}$  long EA modulator is shown in Figure 4.3. The insertion loss of the device at 1555 nm was 10.8 dB while the maximum extinction ratio was 36.4 dB and 40.3 dB at a reverse bias of -6 V for the TE and TM

polarization modes, respectively. The optical input power was +7.5 dBm for these measurements, which demonstrates the high saturation power characteristic of this 26 GHz bandwidth device.

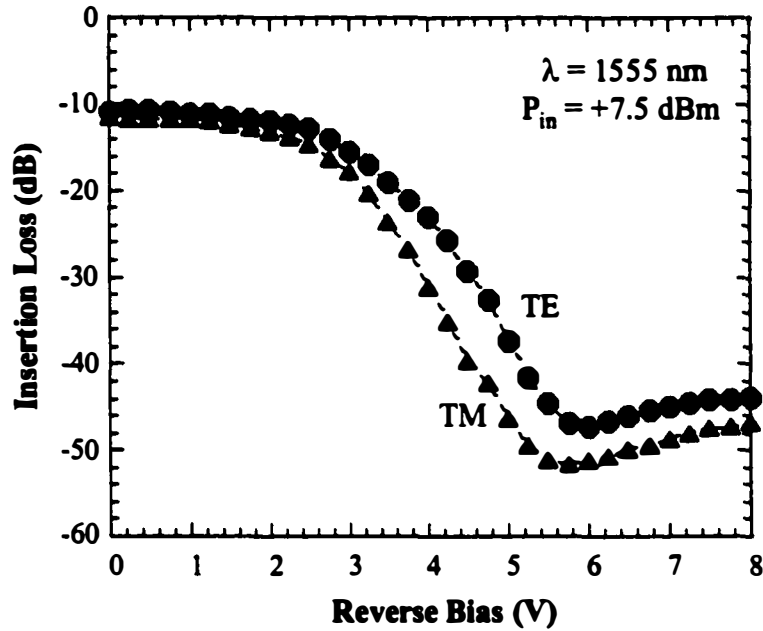


**Figure 4.3** Fiber-to-fiber transmission characteristics for an optical input power of +7.5 dBm at 1555 nm for the dual-drive EA modulator. The insertion loss of the device is 10.8 dB; the maximum extinction ratios are 36.4 dB and 40.3 dB for the TE and TM modes, respectively.

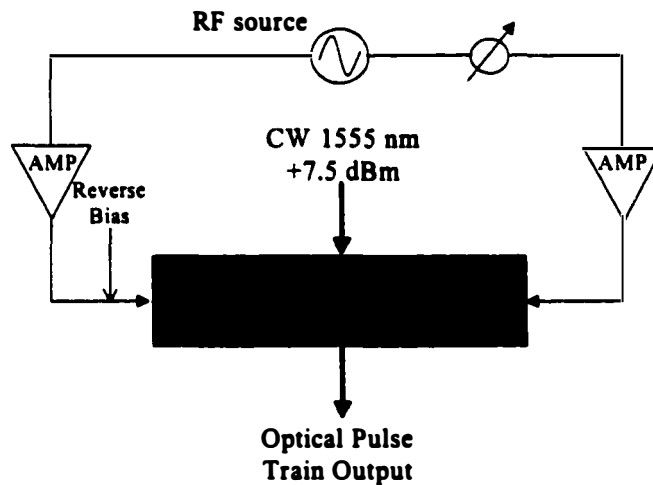


**Figure 4.4** Schematic of experimental set-up for the dual-drive operation of the EA modulator. The device is terminated by the amplifiers at both electrodes.



The dual-drive scheme operation is shown in Figure 4.4 [11]. Two RF signals, synchronized by an electrical delay line, were fed into the two electrodes of the modulator while a single reverse bias was applied. Since narrowband ac-coupled amplifiers effectively terminated both electrodes, impedance matching at the modulation frequency was ensured while heating effects were reduced and external temperature cooling was not employed. The optical pulse measurement set-up is shown in Figure 4.5. The optical output of the modulator was monitored using an in-line power meter and subsequently amplified by an optical amplifier, which was followed by a 1.9 nm optical bandpass filter. The output pulses were then measured on a second harmonic generation (SHG) autocorrelator and an optical spectrum analyzer (OSA). The width of the obtained pulses was deconvolved assuming a Gaussian pulse shape as inferred from the optical spectrum measurements. It is very important to note that the following criteria were used for the these measurements: (1) the average optical output power was higher than -25 dBm in order to ensure a high SNR, and (2) the dynamic extinction ratio was estimated to be greater than 20 dB from the autocorrelator and oscilloscope measurements.

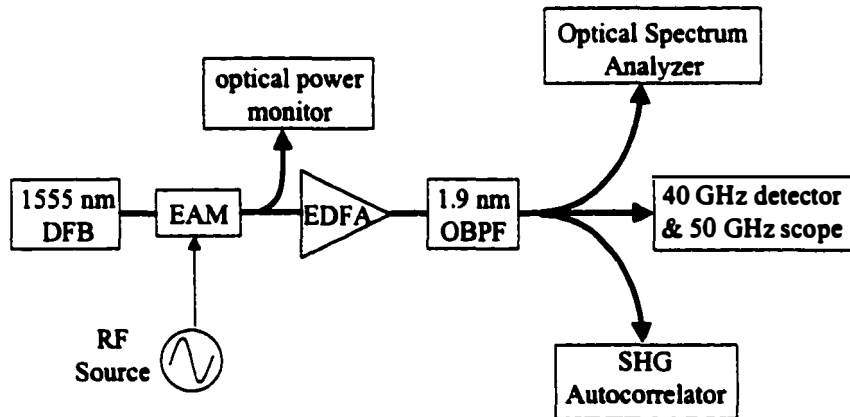


**Figure 4.5** Optical short pulse measurement set-up. OBPF: optical bandpass filter; SHG: second harmonic generation.

Figure 4.6 shows the obtained pulse widths as a function of reverse bias at 30 GHz for the TE polarization mode. The RF amplifiers generated 7 V<sub>pp</sub> into a 50 Ω load. Using only a single drive (the other electrode was terminated in 50 Ω), a minimum pulse width of 4.7 ps was achieved at a reverse bias of -5.5 V. Under the dual-drive modulation, an almost-transform-limited pulse width of 3.7 ps was obtained with a low polarization sensitivity of 0.3 ps. This result corresponds to a duty ratio of about 11% at 30 GHz. Further pulse compression was not observed when the EA modulator was followed by dispersion-compensating fiber (DCF). The advantage of dual-drive modulation is clearly demonstrated for allowing operation at higher reverse biases leading to shorter pulse generation.

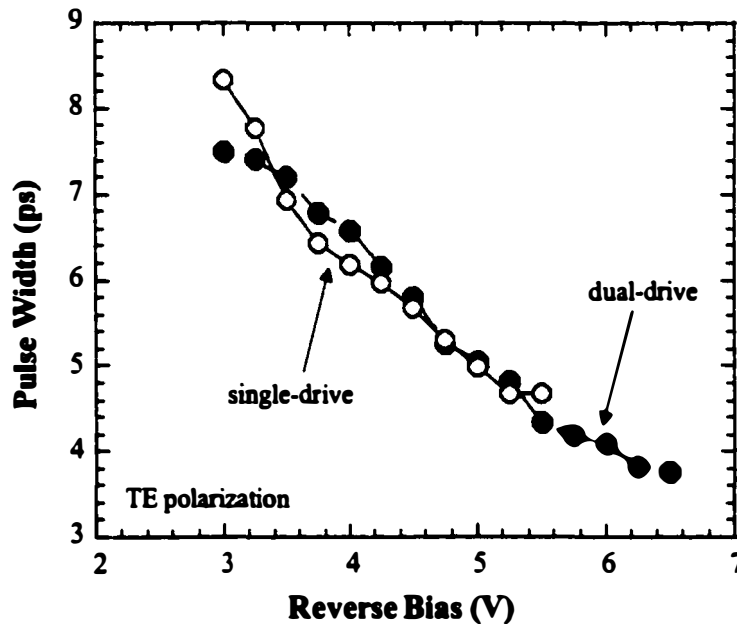


**Figure 4.6** Measured optical pulse widths as a function of reverse bias at 30 GHz single (open circles) and dual-drive (solid circles) modulation.

Figure 4.7 shows (a) the autocorrelation traces of the pulses achieved for single and dual modulation, and (b) the optical spectrum for the dual-drive operation. The optical bandwidth was 0.84 nm resulting in a transform-limited time-bandwidth product of 0.39. It is important to mention that shorter pulse

widths were obtained at higher reverse biases at the expense of degraded SNR and dynamic extinction ratio.

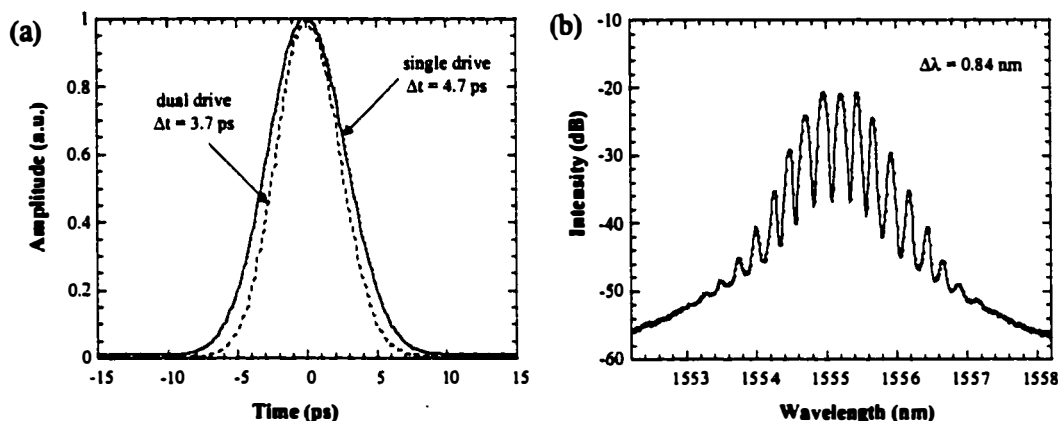


**Figure 4.7** (a) Measured autocorrelation trace for 30 GHz single (solid line) and dual-drive (dashed line) modulation, (b) measured optical spectrum for 30 GHz dual-drive modulation.

The EA modulator was also driven synchronously with 40 GHz 7 V<sub>pp</sub> dual RF signals. The pulse widths obtained as a function of reverse bias are shown in Figure 4.8. A minimum pulse width of 3.6 ps with an optical bandwidth of 0.83 nm was achieved at -5 V (Figure 4.9), which corresponds to a duty ratio of 14.4%. It should be noted that single drive modulation at 40 GHz did not satisfy either the dynamic extinction ratio or the average optical output power requirements, and therefore is not presented in Figure 4.8.

In summary, high-speed optical switching of the traveling-wave EA modulator with dual-drive modulation resulted in sub-4 ps pulses with low polarization sensitivity (0.3 ps), high dynamic extinction ratio (> 20 dB), high optical input power (+7.5 dBm), and high average optical output power (> -25 dBm). These results indicate that the dual-drive EA modulator can be used as a pulse source in polarization and time multiplexed 160 (120) Gbit/s OTDM systems. Similarly, the obtained switching windows and extinction ratios would satisfy penalty-free 160-to-40 Gbit/s (120-to-30 Gbit/s) optical demultiplexing. Further

compression of pulses to less than 2.5 ps is realizable by employing two concatenated dual-drive EA modulators with applications to single-polarization 160 Gbit/s OTDM systems.

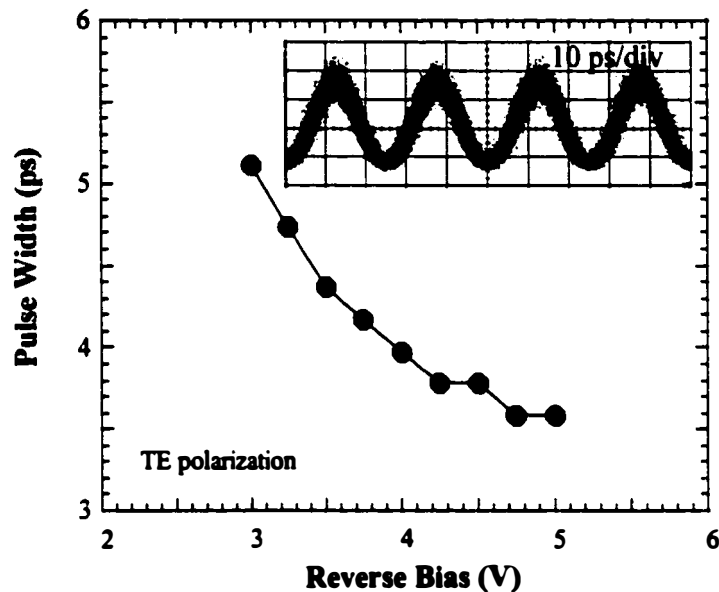


**Figure 4.8** Measured optical pulse widths as a function of reverse bias at 40 GHz dual-drive modulation. Inset: 40 GHz optical pulse waveform (10 ps/div).

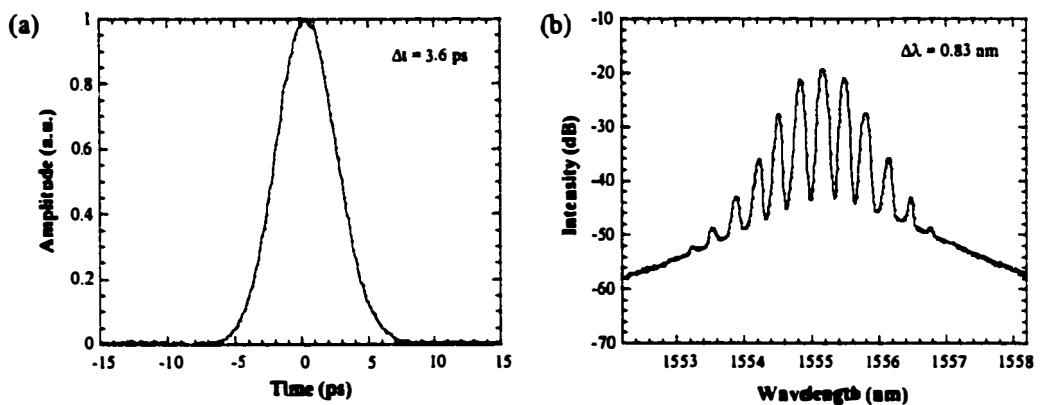


**Figure 4.9** (a) Measured autocorrelation trace and (b) optical spectrum for 40 GHz dual-drive modulation.

### ***4.3.3 Integrated Tandem EA Modulators***

Sinusoidally driven EA modulators are typically limited to a dynamic extinction ratio of about 20 dB, which is sufficient for demultiplexing purposes, but can lead to incoherent interference between multiplexed pulses in OTDM transmitters as discussed in Section 4.2.1. Therefore, a fiber-coupled pair of separate modulators was used for pulse generation in an 80 Gbit/s [47] and for demultiplexing in a 160 Gbit/s OTDM system [4]. This configuration not only effectively doubles the dynamic extinction ratio, but also reduces the switching window as discussed in Section 3.2.1. However, it is desirable to integrate the tandem on a single chip in order to eliminate the external optical amplifier, which compensates for the coupling losses between the modulators. This results in a compact and cost-effective transmitter (or demultiplexer) as well as an environmentally robust module to thermal fluctuations.

The integrated tandem EA modulators used for the high-speed optical switching application were previously introduced in Section 3.3 [12]. The 2- $\mu\text{m}$  wide, 300- $\mu\text{m}$  and 400- $\mu\text{m}$  long EA modulators were cleaved as a tandem (Figure 3.14), and the 20- $\mu\text{m}$  long optical waveguide between the two modulators was defined by  $\text{H}^+$  ion implantation. The ion implantation also extended about 50  $\mu\text{m}$  into each modulator, which reduced the absorption region for each modulator by 100  $\mu\text{m}$ . Both modulators were terminated in 50  $\Omega$  thin-film resistors and dielectric capacitors, which reduced heating effects and allowed for long-term operation of the tandem without any external temperature cooling.

The transmission characteristics of the tandem as a function of reverse bias are shown in Figure 4.10. An optical input power of +7 dBm was applied at 1555 nm. The insertion loss of the tandem was 14.1 dB and 15.3 dB for the TE and TM polarization modes, respectively. Each device was individually characterized

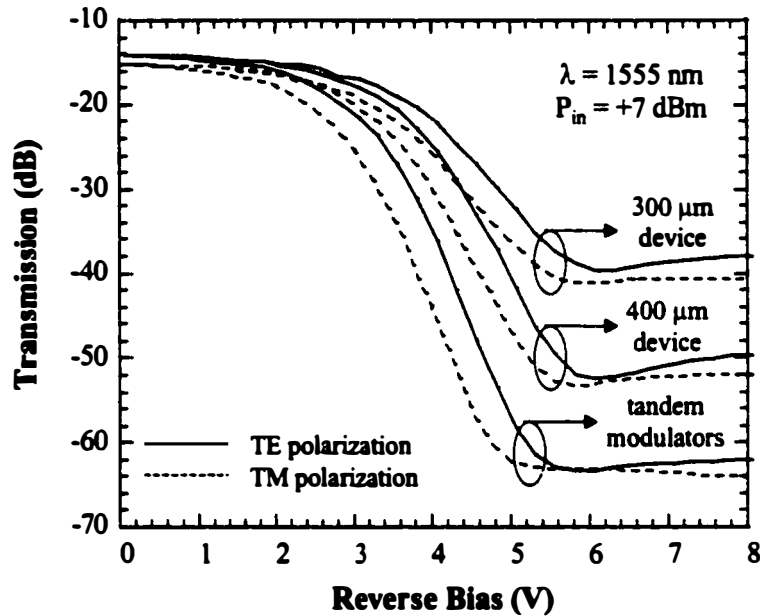


**Figure 4.10** Fiber-to-fiber transmission characteristics for an optical input power of +7 dBm at 1555 nm for the integrated tandem EA modulators.

by keeping the other modulator at zero bias. The 400- $\mu\text{m}$  device achieved a maximum extinction of 38 dB at -6 V while 26 dB of extinction was observed for the 300- $\mu\text{m}$  device. The difference in the maximum extinction ratios is due to the shorter absorption region of the 300- $\mu\text{m}$  device. It should also be noted that at high reverse biases, a saturation of absorption due to the quantum well excitonic peak is observed for both devices. Even though it is desirable to apply a high reverse bias in order to generate short switching windows using sinusoidal modulation, the absorption saturation will deteriorate the extinction ratio and generate significant wings. These wings are detrimental for OTDM applications since the resulting incoherent interference in the transmitter and the crosstalk in the receiver will significantly degrade system performance. On the other hand, the tandem configuration shows an improved extinction ratio of about 50 dB while the absorption saturation is well suppressed in comparison to single device operation.

A 14-dB reduction in the total expected extinction is observed, which is attributed to higher-order mode coupling.

The optical switching capability of the tandem was first characterized at 30 GHz. The experimental measurement set-up is as shown in Figure 4.5. Both modulators were driven with 7 V<sub>pp</sub> sinusoidal RF signals, which were synchronized by an electrical delay line. The widths of the optical pulses were measured using the SHG autocorrelator and deconvolved assuming a Gaussian pulse shape as inferred from the OSA measurements. The same average optical output power (> -25 dBm) and dynamic extinction ratio (> 20 dB) criteria as in the dual-drive measurements were enforced for the optical switching measurements. The pulse widths obtained from the individual devices by keeping the other device at zero bias are shown in Figure 4.11. At a reverse bias of -4.5 V, a minimum pulse width

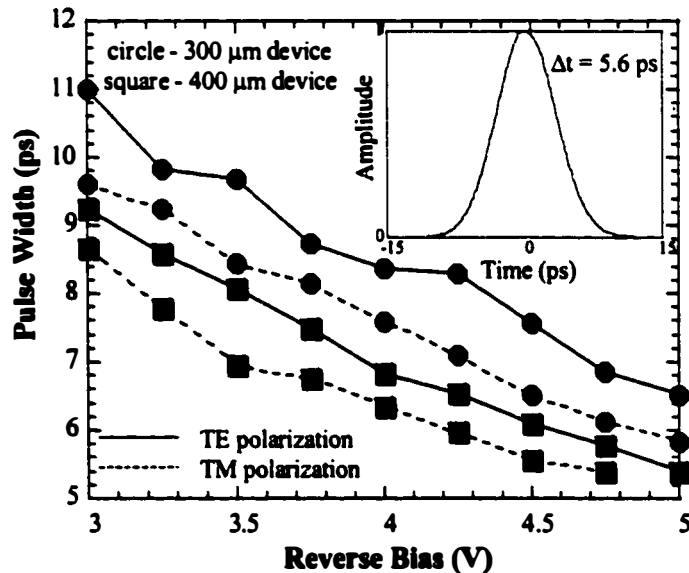
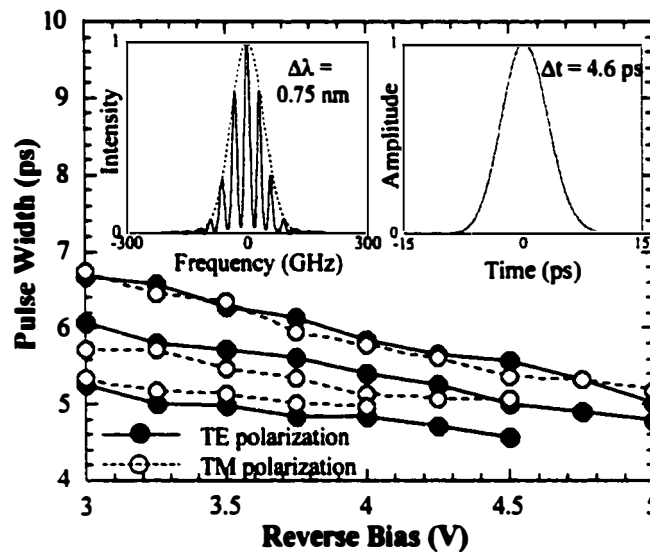


**Figure 4.11** Measured optical pulse widths at 30 GHz as a function of reverse bias for individual devices by keeping the other device at zero bias (circle: 300- $\mu\text{m}$  device; square: 400- $\mu\text{m}$  device). Inset: Autocorrelation trace of the 5.6 ps pulse generated by the 400- $\mu\text{m}$  device at -4.5 V.

of 6.5 ps and 5.6 ps were obtained for the 300- $\mu\text{m}$  and 400- $\mu\text{m}$  devices, respectively. Even though shorter pulses were achieved at higher reverse biases,

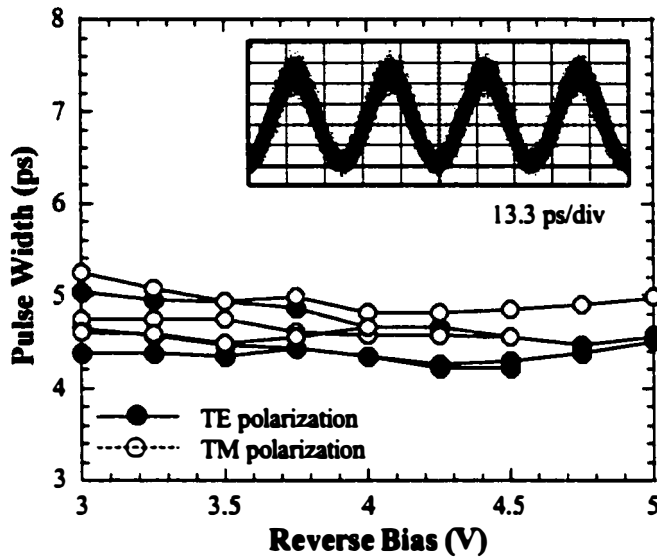
degradation in dynamic extinction ratio was observed due to the absorption saturation as discussed in the preceding section.

Figure 4.12 shows the obtained pulse widths as a function of reverse biases for the tandem configuration. A minimum pulse width of 4.6 ps (inset to Figure 4.12) was achieved with a fiber-coupled output power of -24.2 dBm while an average of 5-6 ps pulses were observed over a wide range of reverse biases and polarization states. This switching window is well suited for greater than 100 Gbit/s optical demultiplexing applications. The inset to Figure 4.12 also shows the optical spectrum of the modulated tandem of EA modulators, which has a Gaussian shape of 0.75 nm. The time-bandwidth product of 0.43 suggests that the pulses were slightly chirped. When the tandem was followed by DCF with a dispersion of about -6 ps/nm, the optical pulses were linearly compressed to a transform-limited pulse width of 4.2 ps (Figure 4.13). This pulse width suggests that the tandem is also suitable as an optical pulse source for simultaneous polarization and time division multiplexed systems in excess of 100 Gbit/s.



**Figure 4.12** Measured pulse width as a function of reverse biases at 30 GHz for the tandem device (x-axis: 400- $\mu$ m bias; symbols: 300- $\mu$ m bias). Closed symbols: TE polarization (top-to-bottom: -3.5 V, -4 V, -4.5 V); Open symbols: TM polarization (top-to-bottom: -3, -3.5 V, -4 V). Left inset: Optical spectrum; Right inset: Autocorrelation trace of 4.6 ps pulse.





**Figure 4.13** Measured pulse width as a function of reverse biases at 30 GHz for the tandem device followed by DCF (x-axis: 400- $\mu\text{m}$  bias; symbols: 300- $\mu\text{m}$  bias). Closed symbols: TE polarization (top-to-bottom: -3.5 V, -4 V, -4.5 V); Open symbols: TM polarization (top-to-bottom: -3, -3.5 V, -4 V). Inset: Oscilloscope trace of the 30 GHz pulses (13.3 ps/div).

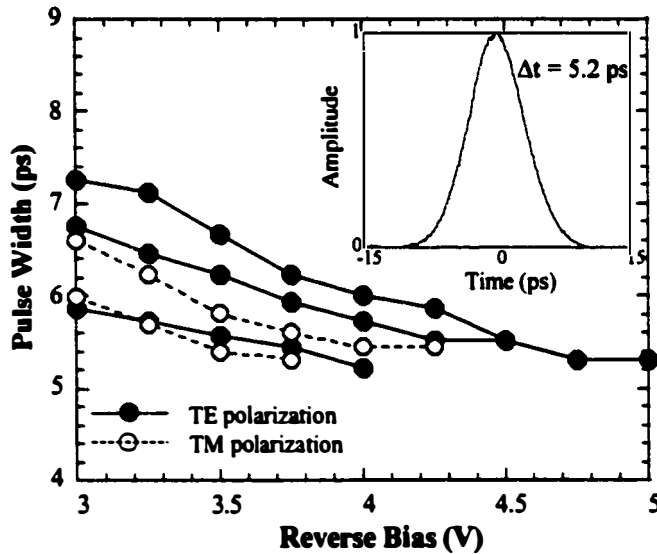


**Figure 4.14** Measured pulse width as a function of reverse biases at 40 GHz for the tandem device (x-axis: 400- $\mu\text{m}$  bias; symbols: 300- $\mu\text{m}$  bias). Closed symbols: TE polarization (top-to-bottom: -3.5 V, -4 V, -4.5 V); Open symbols: TM polarization (top-to-bottom: -3, -3.5 V). Inset: Autocorrelation trace of the 5.2 ps pulse.

The optical switching response of the tandem EA modulators was also performed at 40 GHz with RF drives of 7 V<sub>pp</sub>. The frequency response of the devices was estimated to be about 4 dB lower at 40 GHz (in comparison to the 30 GHz response), which resulted in a compromise between pulse width, dynamic extinction ratio and average optical output power. A minimum optical pulse width of 5.2 ps with an optical bandwidth of 0.59 nm was achieved (Figure 4.14). These results should improve when the tandem is driven with higher power RF amplifiers at 40 GHz and enable error-free optical demultiplexing of 160 Gbit/s OTDM data stream to 40 Gbit/s.

#### **4.4 Single Wavelength 120 Gbit/s (4 x 30 Gbit/s) OTDM System**

Optical fiber transmission beyond 100 Gbit/s OTDM has been demonstrated by various subsystem technologies as described in Section 4.2 (Table 2.1). All of these demonstrations have relied on electrical base rates of 10 or 20 Gbit/s, which require 16 or 8-fold optical multiplexing and demultiplexing paths to achieve 160 Gbit/s. The vast amount of optical channels not only complicates the transmitter and receiver subsystems, but also puts stringent requirements on the pulse sources and limits a practical system (Section 4.2). Therefore, it is desirable to minimize the number of optically multiplexed and demultiplexed channels by increasing the electrical base rate at the transmitter and receiver subsystems, which would allow for a more robust and stable OTDM system. Due to advances in high-speed ETDM, it is inevitable that next generation OTDM systems will operate at a base rate of 40 Gbit/s with optical multiplexing to 160 Gbit/s or more. More recently, a 160 Gbit/s OTDM data stream was optically demultiplexed to 40 Gbit/s using a nonlinear interferometer switch, and further electrically demultiplexed to 10 Gbit/s after photodetection [48]. In addition to using a high electrical base rate, it is also desirable to use compact and stable optical pulse sources and

demultiplexers, as discussed in Section 4.2. Sinusoidally driven EA modulators are good candidates for both of these OTDM applications [4].

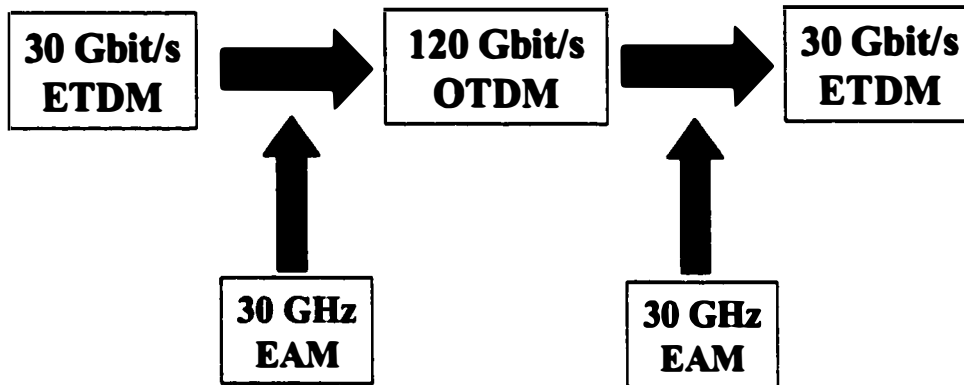


**Figure 4.15** Schematic of the investigated 120 Gbit/s OTDM system. High-speed 30 Gbit/s tributary ETDM channels are multiplexed to 120 Gbit/s by pulses generated from a 30 GHz driven EA modulator. A 30 GHz EA demultiplexer recovers the 30 Gbit/s ETDM channels at the receiver.

This section presents a 120 Gbit/s (4 x 30 Gbit/s) OTDM system with the intent of demonstrating the feasibility of EA modulators driven at 30 GHz as the optical pulse source and the demultiplexer in conjunction with a high-speed electrical base rate at the transmitter and receiver subsystems (Figure 4.15).

#### 4.4.1 Experimental Set-Up

The experimental set-up for the 120 Gbit/s OTDM system is schematically shown in Figure 4.16. The base rate of 30 Gbit/s was generated by electrically multiplexing two 7.5 Gbit/s channels with pattern lengths of  $2^{31}-1$ , followed by optical multiplexing to 30 Gbit/s (Figure 4.16(a)). The 30 Gbit/s optical signal of 2 dBm was then coupled into the dual-drive EA modulator (Section 4.3.2) [11], which has a maximum extinction ratio of 40.3 dB and a bandwidth of 26 GHz. The modulator was reverse biased at -6 V and driven by two 30 GHz RF amplifiers (7 V<sub>pp</sub> each), which were synchronized to the 30 Gbit/s data stream by electrical delay lines. Transform-limited 4 ps pulses were generated and external compression was

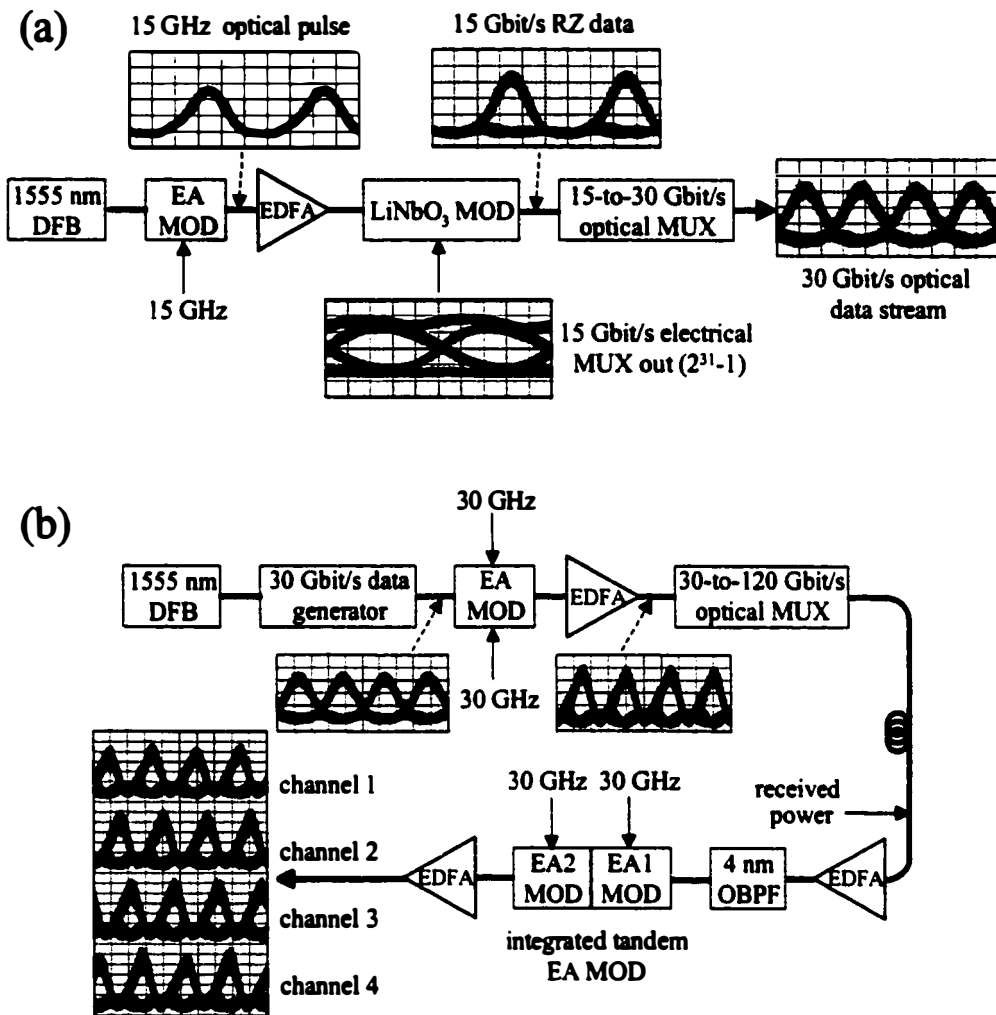
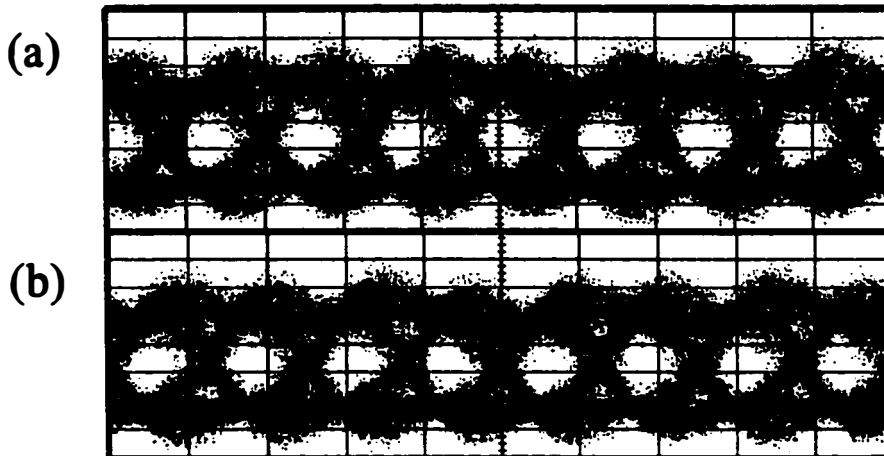


Figure 4.16 (a) The 30 Gbit/s data generator set-up (13.3 ps/div), and (b) the experimental 120 Gbit/s OTDM system set-up (13.3 ps/div). MUX: multiplexer; OBPF: optical bandpass filter.

not employed after the modulator, which minimizes the amount of environmentally induced timing variations before the optical multiplexer. The 30 Gbit/s signal was then passively multiplexed using fiber delay lines (with 200 bits of delay between channels) to generate the 120 Gbit/s OTDM data stream. Both polarization and time multiplexing were employed at the last stage of the multiplexer to minimize interference between adjacent channels due to pulse tail overlap. The two 60 Gbit/s orthogonal polarization channels are shown in Figure 4.17. The measured eye

diagrams are significantly deteriorated due to the limited 40 GHz photodetector bandwidth and the 7.5 GHz oscilloscope trigger.



**Figure 4.17** The alternate-polarization 60 Gbit/s eye diagrams (13.3 ps/div) measured with a 40 GHz photodetector.

In the receiver, the 120 Gbit/s data stream was optically pre-amplified followed by a 4 nm optical bandpass filter, and fed into the optical demultiplexer which consisted of the integrated tandem EA modulators (Section 4.3.3) [12]. The two modulators (EA1 and EA2) are 300- $\mu\text{m}$  and 400- $\mu\text{m}$  long respectively, and are separated by a 20- $\mu\text{m}$  long optical waveguide region. The insertion loss of the device was 14.2 dB while the maximum extinction ratio was about 50 dB. Both modulators were driven by 30 GHz RF signals and a switching window of 5-6 ps was achieved over a wide range of reverse biases. The output in Figure 4.16(b) shows the four demultiplexed 30 Gbit/s optical channels, which were individually selected by an electrical delay line. A polarization sensitivity of about 2 dB was observed which had a minimal impact on the 30 Gbit/s eye opening. The clean eye opening of the received 30 Gbit/s channels indicates that further high-speed electrical demultiplexing is feasible. It should also be noted that a similar dual-drive EA modulator used in the transmitter could have been employed as the optical demultiplexer.

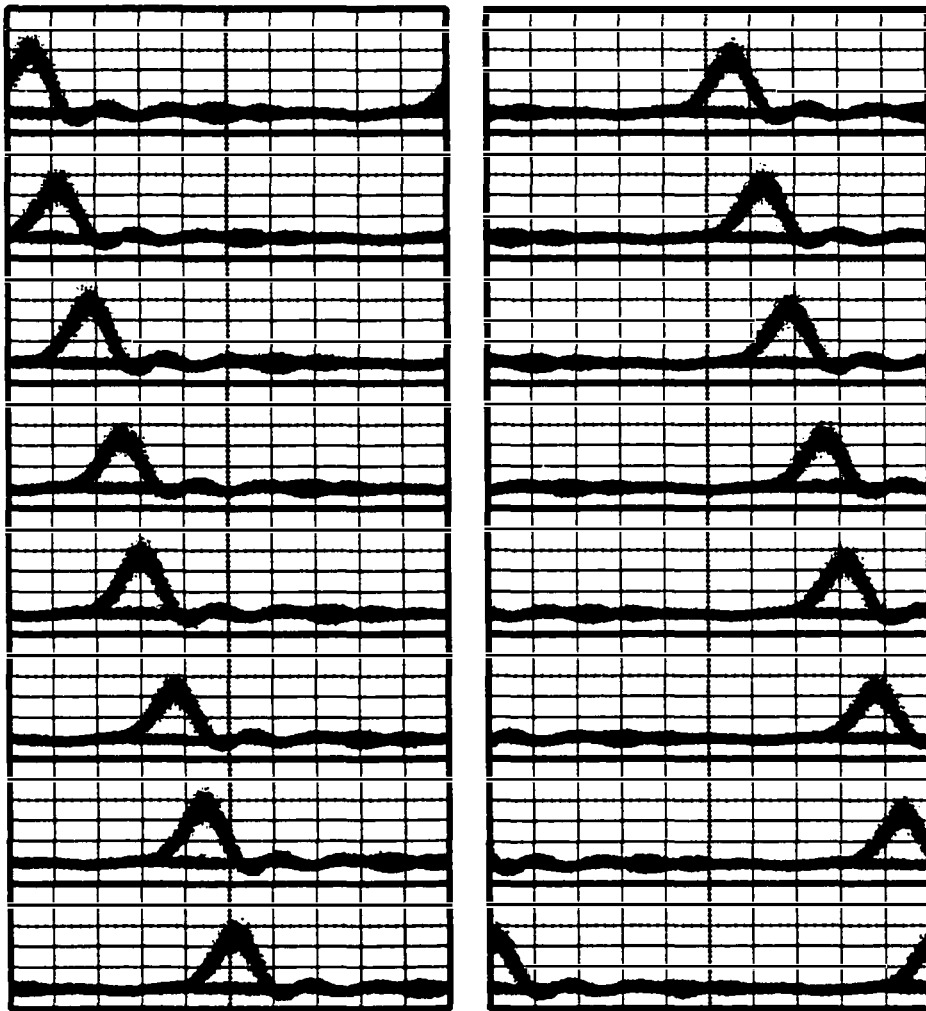
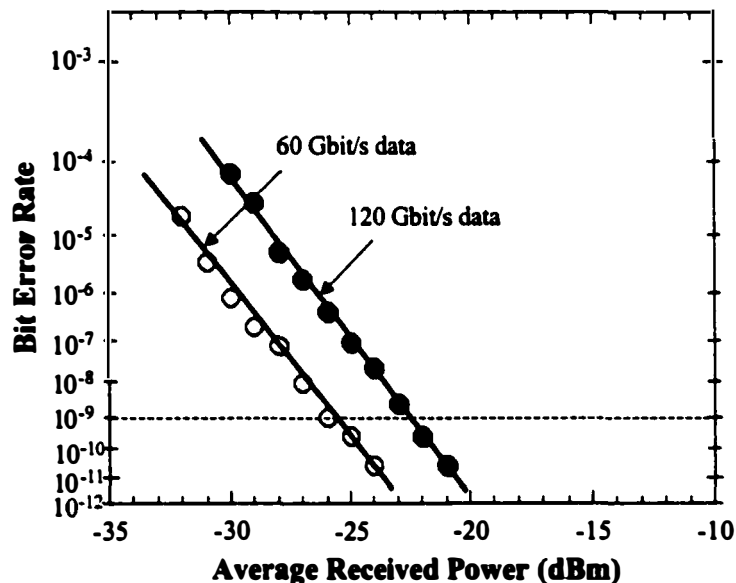


Figure 4.18 Eye diagrams for all 16 demultiplexed 7.5 Gbit/s channels (13.3 ps/div)

#### 4.4.2 Experimental Results and Discussion

Bit-error rate (BER) measurements were carried out in order to assess the performance of the 120 Gbit/s OTDM system based on EA modulators, where the received average power was determined at the input of the optical pre-amplifier. In order to simplify the BER measurements, EA2 was only driven by a 7.5 GHz RF signal and the 120 Gbit/s data stream was directly demultiplexed to 7.5 Gbit/s. The demultiplexed channel was then detected and electrically amplified using

commercial 10 Gbit/s components. The sixteen 7.5 Gbit/s channels are shown in Figure 4.18 with clear open eyes, which confirms the validity of the 120 Gbit/s data stream. The 120 Gbit/s and 60 Gbit/s BER measurements for an arbitrarily selected channel are shown in Figure 4.19. Error-free operation with 120 and 60 Gbit/s receiver sensitivities of -22.2 and -25.5 dBm, respectively, are achieved. The 3-dB difference in receiver sensitivities is due to the extra channels in the 120 Gbit/s data stream. These measurements indicate that no optical power penalty was incurred due to either optical multiplexing or demultiplexing. It should be also noted that no pattern length dependent power penalty was observed.



**Figure 4.19** BER measurements at 120 Gbit/s (solid) and 60 Gbit/s (open) for an arbitrarily selected channel with  $2^{31}-1$  pattern length.

The receiver sensitivities for a BER of  $10^{-9}$  for all 16 channels are shown in Figure 4.20 (mean sensitivity of -22.6 dBm). The slight sensitivity variations between channels are attributed to amplitude and timing alignment variations in the optical multiplexer. The successful error-free and penalty-free demonstration of the 120 Gbit/s OTDM system based on EA transmitters and demultiplexers driven

at 30 GHz confirms the future potential of EA modulators in high-speed OTDM applications.

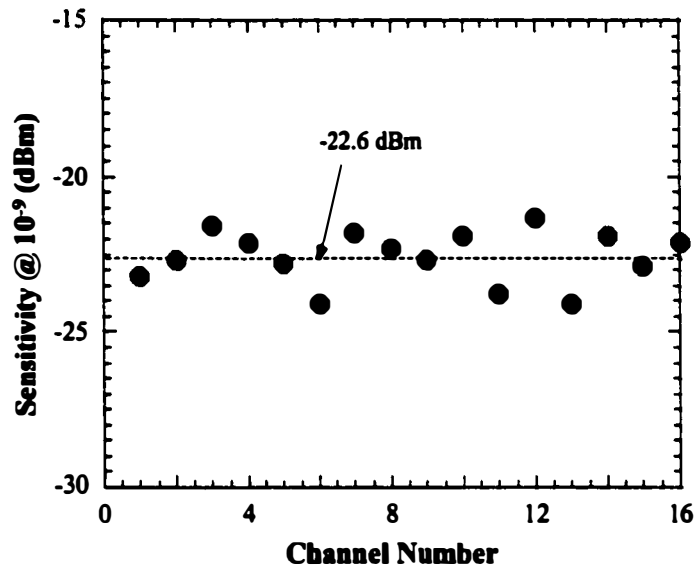


**Figure 4.20** 120 Gbit/s receiver sensitivities at a BER of  $10^{-9}$  for all 16 channels. A mean 120 Gbit/s sensitivity of  $-22.6$  dBm is achieved.

#### 4.5 Summary and Conclusions

In this chapter, a four-channel 120 Gbit/s OTDM system with reduced number of optical channels by increasing the electrical base rate was presented and investigated. This system was achieved by employing compact and stable EA modulators operating at 30 GHz for pulse generation and demultiplexing. A high saturation power dual-drive EA modulator realized less than 15% duty ratio pulses at frequencies beyond 30 GHz without any external pulse compression. Integrated tandem EA modulators with 50 dB extinction ratios were also presented for the suppression of incoherent interference between adjacent pulses in the transmitter and crosstalk in the receiver. Both of these EA modulator configurations were verified in the 120 Gbit/s OTDM system with error-free and penalty-free operation for pattern lengths of  $2^{31}-1$ . Further operation at an ETDM base rate of 40 Gbit/s



for an aggregate data rate of 160 Gbit/s was also shown to be feasible with these devices.

For high-speed OTDM systems beyond 100 Gbit/s, EA modulators offer significant advantages over fiber-based techniques due to their stable and simple operation as well as their potential for monolithic integration in realizing compact transmitter and receiver subsystems. The obtained optical pulse widths at 40 GHz currently limit OTDM systems to polarization multiplexing, which has the advantage of reduced interchannel interference and non-linearity suppression as well as offering a higher spectral efficiency for next-generation WDM systems. On the other hand, single polarization 160 Gbit/s OTDM signals can be realized by an improved EA modulator design with a high non-linear absorption characteristic.

## References

- [1] "Manufacturers and carriers prepare for OC-768," *Lightwave*, pp.74-80, June 2000.
- [2] M. Nakazawa, K. Suzuki, E. Yoshido, E. Yamada, T. Kitoh, and M. Kawachi, "160 Gbit/s soliton transmission over 200 km," *Electron. Lett.*, vol. 31, pp. 565-566, 1995.
- [3] S. Kawanishi, H. Takara, K. Uchiyama, I. Shake, and K. Mori, "3 Tbit/s (160 Gbit/s\*19 channel) optical TDM and WDM transmission experiment," *Electron. Lett.*, vol. 35, pp. 826-827, 1999.
- [4] B. Mikkelsen, G. Raybon, R. J. Essiambre, K. Dreyer, Y. Su, L. E. Nelson, J. E. Johnson, G. Shtengel, A. Bond, D. G. Moodie and A. D. Ellis, "160 Gbit/s single-channel transmission over 300 km non-zero-dispersion fiber with semiconductor based transmitter and demultiplexer", *ECOC '99 Technical Digest*, PD2-3, 1999.
- [5] R. Ludwig, U. Feiste, S. Diet, C. Schubert, C. Schmidt, H. J. Ehrke, and H. G. Weber, "Unrepeated 160 Gbit/s RZ single-channel transmission over 160 km of standard fibre at 1.55  $\mu\text{m}$  with hybrid MZI optical demultiplexer," *Electron. Lett.*, vol. 36, pp. 1405-1406, 2000.
- [6] E. Yoshida, T. Yamamoto, A. Sahara, and M. Nakazawa, "320 Gbit/s TDM transmission over 120 km using 400 fs pulse train," *Electron. Lett.*, vol. 34, pp. 1004-1005, 1998.
- [7] G. Raybon, B. Mikkelsen, R. J. Essiambre, A. J. Stentz, T. N. Nielsen, K. Dreyer, J. E. Johnson, L. Hsu, D. W. Peckham, and L. Gruner-Nielsen, "320 Gbit/s single-channel pseudo-linear transmission over 200 km non-zero-dispersion fiber", *OFC '00 Technical Digest*, PD29, 2000.
- [8] M. Nakazawa, E. Yoshida, T. Yamamoto, E. Yamada, and A. Sahara, "TDM single channel 640 Gbit/s transmission experiment over 60 km using 400 fs pulse train and walk-

- off free, dispersion flattened nonlinear optical loop mirror," *Electron. Lett.*, vol. 34, pp. 907-908, 1998.
- [9] M. Nakazawa, T. Yamamoto, and K. R. Tamura, "1.28 Tbit/s – 70 km OTDM transmission using third- and fourth-order simultaneous dispersion compensation with a phase modulator," *ECOC '00*, PD 2.6, 2000.
- [10] V. Kaman, and J. E. Bowers, "120 Gbit/s OTDM system using electroabsorption transmitter and demultiplexer operating at 30 GHz," *Electron. Lett.*, vol. 36, pp. 1477-1479, 2000.
- [11] V. Kaman, Y. J. Chiu, S. Z. Zhang, and J. E. Bowers, "3.7 ps pulse generation at  $\geq 30$  GHz by dual-drive electroabsorption modulator," *Electron. Lett.*, vol. 36, pp. 1130-1132, 2000.
- [12] V. Kaman, Y. J. Chiu, T. Liljeberg, S. Z. Zhang and J. E. Bowers, "Integrated tandem traveling-wave electroabsorption modulators for  $> 100$  Gbit/s OTDM applications", *IEEE Photonics Tech. Lett.*, vol. 12, November 2000.
- [13] S. Arahira, Y. Matsui, T. Kunii, S. Oshiba, and Y. Ogawa, "Transform-limited optical short-pulse generation at high repetition rate over 40 GHz from a monolithic passive mode-locked DBR laser diode," *IEEE Photonics Tech. Lett.*, vol. 5, pp. 1362-1365, 1993.
- [14] K. Sato, A. Hirano, and H. Ishii, "Chirp-compensated 40-GHz mode-locked lasers integrated with electroabsorption modulators and chirped gratings," *IEEE J. of Selected Topics in Quantum Electron.*, vol. 5, pp. 590-595, 1999.
- [15] E. Swanson, and S. R. Chinn, "40-GHz pulse train generation using soliton compression of a Mach-Zehnder modulator output," *IEEE Photonics Tech. Lett.*, vol. 7, pp. 114-116, 1995.
- [16] T. Pfeiffer, and G. Veith, "40 GHz pulse generation using a widely tunable all-polarisation preserving erbium fibre ring laser," *Electron. Lett.*, vol. 29, pp. 1849-1850, 1993.
- [17] A. D. Ellis, R. J. Manning, I. D. Phillips, and D. Nasset, "1.6 ps pulse generation at 40 GHz in phaselocked ring laser incorporating highly nonlinear fibre for application to 160 Gbit/s OTDM networks," *Electron. Lett.*, vol. 35, pp. 645-646, 1999.
- [18] E. Yoshida, N. Shimizu, and M. Nakazawa, "A 40-GHz 0.9-ps regeneratively mode-locked fiber laser with a tuning range of 1530-1560 nm," *IEEE Photonics Tech. Lett.*, vol. 11, pp. 1587-1589, 1999.
- [19] B. Bakhshi, and P. A. Andrekson, "40 GHz actively modelocked polarisation-maintaining erbium fibre ring laser," *Electron. Lett.*, vol. 36, pp. 411-413, 2000.
- [20] H. Takeuchi, K. Tsuzuki, K. Sato, M. Yamamoto, Y. Itaya, A. Sano, M. Yoneyama, and T. Otsuji, "Very high-speed light-source module up to 40 Gb/s containing an MQW electroabsorption modulator integrated with a DFB laser," *IEEE J. of Selected Topics in Quantum Electron.*, vol. 3, pp. 336-343, 1997.
- [21] K. Wakita, K. Yoshino, A. Hirano, S. Kondo, and Y. Noguchi, "Very-high-speed and low driving-voltage modulator modules for a short optical pulse generation," *IEICE Trans. on Electron.*, vol. E81-C, pp. 175-179, 1998.
- [22] J. R. Burie, J. F. Cadiou, O. Le Gouezigou, M. Goix, and A. Bodere, "Transform limit optical pulse at 40 GHz from a 1.55  $\mu\text{m}$  module with an integrated DFB laser/electroabsorption modulator," *ISLC '98 Technical Digest*, pp. 91-92, 1998.

- [23] H. Takara, I. Shake, S. Kawanishi, Y. Yamabayashi, K. Magari, Y. Tohmori, K. Takiguchi, I. Ogawa, and A. Himeno, "Integrated optical time division multiplexer based on planar lightwave circuit," *Electron. Lett.*, vol. 35, pp. 1263-1264, 1999.
- [24] F. Zamkotsian, K. Sato, H. Okamoto, K. Kishi, I. Kotaka, M. Yamamoto, Y. Kondo, H. Yasaka, Y. Yoshikuni, and K. Oe, "Monolithic integration of MQW modulators on an optical multiplexer on InP for 100 Gb/s transmission," *J. of Lightwave Tech.*, vol. 14, pp. 2344-2352, 1996.
- [25] S. Kawanishi, K. Okamoto, M. Ishii, O. Kamatani, H. Takara, and K. Uchiyama, "All-optical time-division-multiplexing of 100 Gbit/s signal based on four-wave mixing in a travelling-wave semiconductor laser amplifier," *Electron. Lett.*, vol. 33, pp. 976-977, 1997.
- [26] A. D. Ellis, T. Widdowson, I. D. Phillips, and W. A. Pender, "High speed OTDM networks employing electro-optic modulators," *IEICE Trans. on Electron.*, vol. E81-C, pp. 1301-1308, 1998.
- [27] R. J. Essiambre, B. Mikkelsen, and G. Raybon, "Intra-channel cross-phase modulation and four-wave mixing in high-speed TDM systems," *Electron. Lett.*, vol. 35, pp. 1576-1578, 1999.
- [28] M. Jinno, "Effects of crosstalk and timing jitter on all-optical time-division demultiplexing using a nonlinear fiber Sagnac interferometer switch," *IEEE J. of Quantum Electron.*, vol. 30, pp. 2842-2853, 1994.
- [29] K. Uchiyama, H. Takara, S. Kawanishi, T. Morioka, M. Saruwatari, and T. Kitoh, "100 Gbit/s all-optical demultiplexing using nonlinear optical loop mirror with gating-width control," *Electronics Lett.*, vol. 29, pp. 1870-1871, 1993.
- [30] T. Morioka, S. Kawanishi, K. Uchiyama, H. Takara, and M. Saruwatari, "Polarisation-independent 100 Gbit/s all-optical demultiplexer using four-wave mixing in a polarisation-maintaining fibre loop," *Electron. Lett.*, vol. 30, pp. 591-592, 1994.
- [31] O. Kamatani, Y. Katagiri, and S. Kawanishi, "100-Gbit/s optical TDM add/drop multiplexer based on photonic downconversion and four-wave mixing," *OFC '98 Technical Digest*, pp. 112-113, 1998.
- [32] T. Morioka, H. Takara, S. Kawanishi, K. Uchiyama, and M. Saruwatari, "Polarisation-independent all-optical demultiplexing up to 200 Gbit/s using four-wave mixing in a semiconductor laser amplifier," *Electron. Lett.*, vol. 32, pp. 840-842, 1996.
- [33] S. Kawanishi, T. Morioka, O. Kamatani, H. Takara, J. M. Jacob, and M. Saruwatari, "100 Gbit/s all-optical demultiplexing using four-wave mixing in a travelling wave laser diode amplifier," *Electron. Lett.*, vol. 30, pp. 981-982, 1994.
- [34] M. L. Dennis, W. K. Burns, T. F. Carruthers, and I. N. Duling, "Eight-to-one demultiplexing of 100-Gbit/s TDM data using LiNbO<sub>3</sub> Sagnac interferometer modulators," *OFC '98 Technical Digest*, pp. 110-112, 1998.
- [35] S. Nakamura, Y. Ueno, K. Tajima, J. Sasaki, T. Sugimoto, T. Kato, T. Shimoda, M. Itoh, H. Hatakeyama, T. Tamaoki, and T. Sasaki, "Demultiplexing of 168-Gb/s data pulses with a hybrid-integrated symmetric Mach-Zehnder all-optical switch," *IEEE Photonics Tech. Lett.*, vol. 12, pp. 425-427, 2000.

- [36] S. Diez, C. Schubert, R. Ludwig, H. J. Ehrke, U. Feiste, C. Schmidt, and H. G. Weber, "160 Gbit/s all-optical demultiplexing using hybrid gain-transparent SOA Mach-Zehnder interferometer," *Electron. Lett.*, vol. 36, pp. 1484-1486, 2000.
- [37] A. Takada, and M. Saruwatari, "100 Gbit/s optical signal generation by time-division multiplication of modulated and compressed pulses from gain-switched distributed feedback (DFB) laser diode," *Electron. Lett.*, vol. 24, pp. 1406-1408, 1988.
- [38] S. Kawanishi, H. Takara, K. Uchiyama, M. Saruwatari, and T. Kitoh, "Fully time-division-multiplexed 100 Gbit/s optical transmission experiment," *Electron. Lett.*, vol. 29, pp. 2211-2212, 1993.
- [39] A. D. Ellis, J. K. Lucek, D. Pitcher, D. G. Moodie, and D. Cotter, "Full 10\*10 Gbit/s OTDM data generation and demultiplexing using electroabsorption modulators," *Electron. Lett.*, vol. 34, pp.1766-1767, 1998.
- [40] S. Kawanishi, Y. Miyamoto, H. Takara, M. Yoneyama, K. Uchiyama, I. Shake, and Y. Yamabayashi, "120 Gbit/s OTDM system prototype," *ECOC '98 Technical Digest*, pp. 43-45, 1998.
- [41] S. Kawanishi, H. Takara, T. Morioka, O. Kamatani, and M. Saruwatari, "200 Gbit/s, 100 km time-division-multiplexed optical transmission using supercontinuum pulses with prescaled PLL timing extraction and all-optical demultiplexing," *Electron. Lett.*, vol. 31, pp. 816-817, 1995.
- [42] W. I. Kaechele, M. L. Dennis, T. F. Carruthers, and I. N. Duling, "Dispersion-managed 200 Gb/s polarization-multiplexed transmission over 160 km," *ECOC '00 Technical Digest*, paper 6.1.4, 2000.
- [43] S. Kawanishi, H. Takara, T. Morioka, O. Kamatani, K. Takiguchi, T. Kitoh, and M. Saruwatari, "Single channel 400 Gbit/s time-division-multiplexed transmission of 0.98 ps pulses over 40 km employing dispersion slope compensation," *Electron. Lett.*, vol. 32, pp. 916-918, 1996.
- [44] Y. J. Chiu, V. Kaman, S. Z. Zhang, and J. E. Bowers, "Distributed effects model for traveling-wave electroabsorption modulator design", submitted to *IEEE Photonics Tech. Lett.*, 2000.
- [45] S. Z. Zhang, Y. J. Chiu, P. Abraham, J. E. Bowers, "25 GHz polarization-insensitive electroabsorption modulators with traveling-wave electrodes", *IEEE Photonics Tech. Lett.*, vol. 11, pp. 191-193, 1999.
- [46] E. Yamada, K. Wakita, and M. Nakazawa, "30 GHz pulse train generation from a multi-quantum well electroabsorption intensity modulator," *Electron. Lett.*, vol. 29, pp. 845-847, 1993.
- [47] D. D. Marcenac, A. D. Ellis, and D. G. Moodie, "80 Gbit/s OTDM using electroabsorption modulators," *Electron. Lett.*, vol. 34, pp. 101-103, 1998.
- [48] U. Feiste, R. Ludwig, C. Schubert, J. Berger, S. Diez, C. Schmidt, H. G. Weber, A. Munk, and B. Schmauss, "160 Gbit/s transmission using 160 to 40 Gbit/s OTDM and 40 to 10 Gbit/s ETDM DEMUX-techniques," *ECOC '00 Technical Digest*, PD 1.10, 2000.



## CHAPTER 5

### Conclusions and Future Work

#### 5.1 Summary

The rapid development of optical fiber communication technologies in conjunction with the exponentially growing demand for Internet access over the past decade has resulted in a prompt need to utilize the available optical bandwidth by extending the capacity of time division multiplexed (TDM) channels. For these high-capacity systems to be commercially viable, the high-speed transmitter and receiver subsystems technologies need to be reproducible as well as being compact and stable. This motivation was the driving force behind the investigation and demonstration of various high-speed electrical and optical TDM subsystems, primarily based on electroabsorption (EA) modulators, for this dissertation.

Optical systems based on high-speed electrical TDM (ETDM) systems beyond 20 Gbit/s was the focus of Chapter 2. A 30 Gbit/s ETDM optical system, which predates all of the 40 Gbit/s ETDM demonstrations, with full electrical multiplexing and demultiplexing was presented. A traveling-wave EA modulator was also investigated at 30 Gbit/s as a low drive voltage and polarization insensitive high-speed data encoder. This was also the first optical modulation demonstration of a traveling-wave EA modulator. The most significant problems of high-speed ETDM subsystems were determined to be microwave reflections between electrical-to-optical (E/O) and optical-to-electrical (O/E) interfaces, long electrical amplifier chains, and saturated operation of modulator drivers. The experimental analysis also revealed that monolithic integration of various electronic and opto-electronic devices is required for future high-speed ETDM systems, where EA modulators will be strong candidates.

In Chapter 3, various optical processing techniques primarily intended for high-speed OTDM system applications using simple sinusoidal modulation of EA modulators were investigated and demonstrated. Due to its non-linear attenuation characteristic, a reverse biased EA modulator can generate various optical gates for optical short pulse generation and demultiplexing. While optical pulses with duty ratios less than 10% and extinction ratios greater than 20 dB were achieved, the EA modulator's high-speed OTDM demultiplexing capability was also demonstrated. Due to the high optical insertion loss of these devices, a novel compact and stable 40 Gbit/s OTDM receiver subsystem based on integrated tandem EA modulators was presented. The chapter concluded with another novel application of an EA modulator in which a single channel was simultaneously demultiplexed and detected from a high-speed OTDM data stream. The analysis revealed that four-channel 40 Gbit/s operation of the simultaneous demultiplexer and detector could be employed for realizing compact future add/drop multiplexers and OTDM demultiplexing receivers.

Chapter 4 focused on next generation OTDM systems with capacities beyond 100 Gbit/s based on high-speed EA transmitters and demultiplexers. A high saturation power dual-drive EA modulator was demonstrated as an optical short pulse source with less than 15% duty ratios at frequencies beyond 30 GHz while integrated tandem EA modulators achieved 50 dB extinction ratios. These devices were employed in the demonstration of a 120 Gbit/s OTDM system based on 30 Gbit/s tributary base rates. It was shown that for future robust and stable ultra-high-speed OTDM systems, the number of optical channels needs to be reduced by increasing the electrical base rate.

## 5.2 Electroabsorption Modulator Improvements

For next generation commercially viable high-speed ETDM and OTDM systems, EA modulators have the strongest potential for satisfying the data modulation, optical short pulse generation and optical demultiplexing applications. This is due to several advantages EA modulators possess, including their simple and stable operation, compact size and potential for monolithic integration. For all three applications, the EA modulator requires (1) high electro-optic bandwidth, (2) high dynamic extinction ratio, (3) fast non-linear absorption onset for low drive voltage, (4) low polarization sensitivity, (5) high optical power saturation, (6) low chirp, and (7) low optical insertion loss. The intrinsic device design improvements for some of these requirements have previously been presented in detail in [1]. In this section, some of the externally controlled improvements are discussed.

(1) *Bandwidth Improvements*: The traveling-wave EA modulator has the advantage of overcoming the  $RC$ -limited bandwidth; however, its bandwidth is limited by microwave insertion losses as well as impedance mismatch induced reflection losses [1]. Therefore, an optimum external termination needs to be designed according to the measured S-parameters of the device. In this design, the parasitic effects of the input and output ribbon bonds need to be considered as well. Flip-chip bonding the EA modulator can further reduce microwave insertion losses. On the other hand, for high-speed optical switching applications, the EA modulator is usually driven by a single RF frequency. Therefore, the device and the external circuitry designs can be optimized for the specific frequency. A simple impedance matching circuit [2], or microwave resonators [3], can significantly improve the return losses at the desired RF frequency. Recently, a matching circuit based on microstrip double open stubs decreased the return losses from -5 dB to less than -30 dB at 60 GHz for a 75- $\mu\text{m}$  long 40 GHz EA modulator [2].



(2) *Optical Insertion Loss Improvements*: In any application involving EA modulators, optical insertion losses as low as possible are desired from signal-to-noise ratio (SNR) and fiber transmission power budget issues. EA modulators typically have 8-12 dB of optical insertion loss, which is mainly due to the high fiber-to-device coupling losses. The intrinsic propagation losses are usually less than 2 dB; therefore, the optical coupling to EA modulators need to be improved without sacrificing bandwidth or drive voltage requirements. Several techniques have been demonstrated for reduced optical coupling losses. A packaged EA modulator module with high coupling efficiency has been demonstrated by employing an aspheric lens system [4]. Optical insertion losses as low as 5 dB were achieved for a 200- $\mu\text{m}$  long device with less than 1 dB polarization dependent loss. The optical coupling losses can also be reduced by employing integrated spot-size converters, or beam expanders [5, 6]. The spot-size converters on both sides of the device can be designed such that the frequency response of the EA modulator is not affected [6]. Due to the 300- $\mu\text{m}$  long spot-size converter sections, the longer EA modulator is also easier to handle and package.

Depending on the application, EA modulators can also be integrated with DFB lasers [7], semiconductor optical amplifiers (SOA) [8-10], and photodetectors [11]. Integrating the photodetector with the EA demultiplexer not only provides a compact receiver, but also allows for efficient coupling and reduction of external optical components [11]. On the other hand, a fiber-to-fiber gain of 14 dB was measured for a tandem of EA modulators integrated with SOA's [9], which indicates the potential of monolithic integration for high-speed optical switching applications. In consideration of integrating EA modulators with SOA's, there are two intrinsic limitations imposed by the SOA. For low optical input powers, the SNR degrades by the amplified spontaneous emission (ASE) noise introduced by the SOA. Therefore, the EA modulator optical output has to be considerably higher than the ASE limit and the SOA should be followed by an optical filter [12]. The

second limitation arises at high optical input powers to the SOA, in which the dynamic gain saturation effect leads to a degradation of the extinction ratio. Both the ASE noise and the gain saturation limits should be considered in the design of an integrated EA modulator and SOA module. Furthermore, with a proper active layer design, the positive chirp of the EA modulator can be compensated by the phase modulation of the SOA and converted into negative chirp [13, 14], which is ideal for transmission in the anomalous dispersion regime of standard single mode fibers (SMF).

(3) *Dynamic Extinction Ratio Improvements*: A dynamic extinction ratio of 15-20 dB, which a single EA modulator is capable of, is generally suffice for less than 1 dB of optical power penalty for the optical data modulator and the optical demultiplexer applications. However, as discussed in Chapter 4, the optical short pulse source in a four-channel single-polarization OTDM system requires greater than 30 dB of dynamic extinction ratio in order minimize interference induced power penalties and error floors. A single EA modulator is typically limited to a 20-dB dynamic extinction ratio; therefore, an external improvement is required for pulse generation applications using an EA modulator. Synchronized EA modulators in a tandem configuration, either with two separate fiber coupled devices [15] or integrated EA modulators [16, 17], not only improves the extinction ratio, but also shortens the optical pulses as discussed in Chapter 3. Recently, an automatic time delay control unit was proposed to avoid SNR degradation due to environmentally induced timing variations for two separate concatenated EA modulators [18]. However, from a system perspective, it is preferable to integrate the tandem devices on a single chip for a compact and environmentally stable optical pulse generator module. As discussed in the preceding section, it would also be desirable to incorporate SOA's in the module to overcome optical insertion losses.

Another method for improving the dynamic extinction ratio is by employing self phase modulation (SPM) in a non-linear medium with subsequent optical filtering [19]. This method not only generates transform-limited pulses with pulse widths determined by the optical filter spectral width, but also increases the dynamic extinction ratio dramatically by suppressing finite signal and noise in the zero level. This technique has been implemented in 8 km of dispersion-shifted fiber (DSF) for pulse compression and extinction ratio improvement of an EA modulator pulse source in a 160 Gbit/s OTDM experiment [20]. Similarly, a dispersion-imbalanced fiber loop mirror (DILM), with 3 km of fiber in the loop, was employed as a non-linear filter by transmitting only the pulse component with the appropriate peak power and pulse duration [21]. However, both of these methods are not practical since they require long lengths of fiber before the optical multiplexer, which can introduce instability due to polarization and temperature variations. Recently, a pulse extinction ratio improvement of 20-25 dB using SPM was also demonstrated in a SOA, which has the potential for a compact and reliable optical transmitter by monolithic integration with an EA modulator [22].

### **5.3 Next-Generation Traveling-Wave Electroabsorption Modulator**

A next-generation traveling-wave EA modulator was recently fabricated in order to satisfy optical system requirements such as high saturation input power and low drive voltage [23]. The design of the device is similar to the modulators described in Chapter 1 [1]; however, the active region material was modified with a photoluminescence peak of higher than 1500 nm. Figure 5.1 shows the static fiber-to-fiber transmission characteristic of the device at a wavelength of 1555 nm (the facets were not antireflection-coated). The onset of the non-linear absorption is very fast with a 10-dB extinction at 0.55 V, and a 20-dB extinction at 1.3 V for the TM polarization. The high-degree of non-linearity of this device is ideal for optical short pulse generation applications. The device also exhibits a very high optical

input saturation power due to proper bandgap engineering; the frequency response of the EA modulator at an optical input of +14 dBm shows no degradation (inset to Figure 5.1).

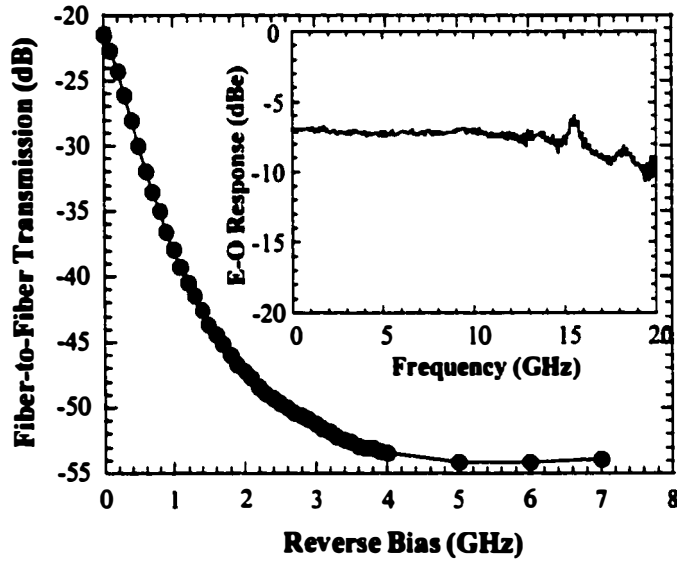


**Figure 5.1** Fiber-to-fiber transmission characteristic of the next-generation traveling-wave EA modulator at 1555 nm. Inset: Frequency response of device for an optical input of +14 dBm.

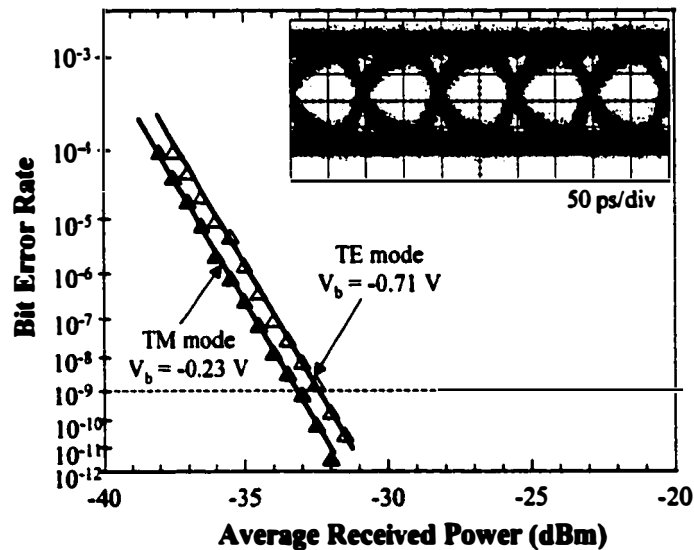


**Figure 5.2** BER measurements at 10 Gbit/s for the next-generation traveling-wave EA modulator. Inset: Eye diagram at 10 Gbit/s (50 ps/div).

The next-generation traveling-wave EA modulator was also used as a low drive 10 Gbit/s optical data modulator. The measured bit error rate (BER) curves at 10 Gbit/s for a pattern length of  $2^{31}-1$  and an optical input of +9 dBm is shown in Figure 5.2. Both the TE and the TM polarization modes required reverse biases less than -1 V while the 10 Gbit/s drive signal was 1 V<sub>pp</sub>. Error-free operation with a receiver sensitivity of -33 dBm was achieved for the TM mode. The device exhibited some polarization dependence; however, its potential for future high-speed applications with low drive voltages and high optical input powers is clearly demonstrated.

#### **5.4 High-Speed TDM for High-Capacity WDM**

This dissertation has mainly focused on demonstrating compact and reliable transmitter and receiver configurations for next generation ETDM and OTDM bit rates of 40 and 160 Gbit/s without discussing optical transport issues in detail. As a conclusion to this dissertation, it would be appropriate to comment on fiber transmission and wavelength division multiplexing (WDM) applications at these data rates.

Over the past decade, there were a few misconceptions on high-speed return-to-zero (RZ) format transmission that should be cleared. Due to the higher spectral bandwidth and optical peak power of the RZ format, fiber dispersion and fiber non-linearities would be enhanced for single-wavelength transmission while WDM capacity would be reduced; therefore, the non-return-to-zero (NRZ) format has been considered as the appropriate modulation form. However, with the advances in optical fiber technology, second-order dispersion and the dispersion slope can be well compensated through properly managed fiber links. Secondly, since short pulses disperse quite rapidly in the beginning of the optical link, SPM-induced degradation is mitigated and high launch powers are allowed; this is in contrast to the NRZ format, which is strongly affected by SPM due to its longer

dispersion length and thus higher peak power. For example at 40 Gbit/s, a nearly doubled SMF transmission of 432 km was achieved using the RZ format [24]. In regards to WDM transmission, the NRZ format does have a higher spectral efficiency than the RZ format. However, by employing alternate polarization multiplexing of the RZ data stream at the expense of slightly more complicated transmitter and receiver configurations, the spectral bandwidth of the RZ format can be reduced to the NRZ bandwidth.

Several advantages are also achieved by employing high-speed channel rates in high-capacity WDM systems. Firstly, the available optical bandwidth is utilized effectively by decreasing the number of guard bandwidths between adjacent wavelength channels. Secondly, since the wavelength channel spacing is on the order of 100 GHz or more, non-linear interaction between WDM channels are reduced and the limitations are due to single-channel effects. This will be especially evident in the next-generation 160 Gbit/s per wavelength WDM systems.

At a line rate of 40 Gbit/s, over 10 Tbit/s WDM transmission will be possible in the very near future. Employing both polarization interleaving of adjacent wavelength channels and optical duobinary modulation can increase the spectral efficiency by a factor of three. Therefore, the 0.4-bit/s/Hz spectral efficiency of a conventional 40 Gbit/s NRZ based WDM system with 100 GHz wavelength spacing could be increased to 1.2 bit/s/Hz. This would correspond to a total capacity of over 10 Tbit/s for the C- and L-bands. Considering the vast available bandwidth of optical fiber and the trend of rapid development of advanced technologies over the past decade, it is quite likely that tens of Terabit per second capacity transmission will be demonstrated in the coming decades.

**References**

- [1] S. Z. Zhang, "Traveling-wave electroabsorption modulators," *ECE Technical Report*, Ph. D. Dissertation, University of California, Santa Barbara, 1999.
- [2] N. Mineo, K. Yamada, K. Nakamura, S. Sakai, and T. Ushikubo, "60-GHz band electroabsorption modulator module, *OFC '98 Technical Digest*, pp. 287-288, 1998.
- [3] H. Tanaka, and Y. Matsushima, "Novel method for optical short pulse generation using an EA modulator incorporating microwave resonators with 3<sup>rd</sup> harmonic sinusoidal voltage," *ECOC '96 Technical Digest*, pp. 4.67-4.69, 1996.
- [4] K. Yoshino, T. Takeshita, I. Kotaka, S. Kondo, Y. Noguchi, R. Iga, and K. Wakita, "Compact and stable electroabsorption modulator modules," *J. of Lightwave Tech.*, vol. 17, pp. 1700-1707, 1999.
- [5] F. Devaux, L. Menigaux, J. Brandon, C. Ramus, M. Carre, F. Huet, P. Legay, and M. Juhel, "Polarization-independent electroabsorption modulator integrated with spot-size converters," *OFC '96 Technical Digest*, pp. 208-209, 1996.
- [6] A. E. Bond, G. Shtengel, Y. Akulova, and C. L. Reynolds, "43 GHz modulation bandwidth packaged InGaAsP MQW EA modulators with integrated mode converters," *ECOC'99 Technical Digest*, pp.14-15, 1999.
- [7] H. Takeuchi, K. Tsuzuki, K. Sato, M. Yamamoto, Y. Itaya, A. Sano, M. Yoneyama, and T. Otsuji, "NRZ operation at 40 Gb/s of a compact module containing an MQW electroabsorption modulator integrated with a DFB laser," *IEEE Photonics Tech. Lett.*, vol.9, pp. 572-574, 1997.
- [8] J. R. Burie, F. Dumont, O. le Gouezigou, S. Lamy, D. Cornec, and P. Andre, "50 Gb/s capability of a new zero loss integrated SOA/EA modulator," *ECOC '00 Technical Digest*, paper 1.3.3, 2000.
- [9] F. Devaux, N. Souli, A. Ougazzaden, F. Huet, and M. Carre, "High-speed tandem of MQW modulators for coded pulse generation with 14-dB fiber-to-fiber gain," *IEEE Photonics Tech. Lett.*, vol. 8, pp. 218-220, 1996.
- [10] A. Ramdane, F. Devaux, N. Souli, D. Delprat, and A. Ougazzaden, "Monolithic integration of multiple-quantum-well lasers and modulators for high-speed transmission," *IEEE J. of Selected Topics in Quantum Electron.*, vol. 2, pp. 326-335, 1996.
- [11] V. Kaman, Y. J. Chiu, T. Liljeberg, S. Z. Zhang, and J. E. Bowers, "A compact 40 Gbit/s demultiplexing receiver based on integrated tandem electroabsorption modulators," to be published in *Electron. Lett.*, 2000.
- [12] E. Legros, T. Barrou, S. Vuye, L. Giraudet, C. Joly, F. Blache, T. Ducellier, and M. Goix, "High-sensitivity high-gain SOA-filter-PIN-PHEMT 40-Gb/s photoreceiver," *ECOC '98 Technical Digest*, pp.69-70, 1998.
- [13] T. Watanabe, N. Sakaida, H. Yasaka, and M. Koga, "Chirp control of an optical signal using phase modulation in a semiconductor optical amplifier," *IEEE Photonics Tech. Lett.*, vol. 10, pp. 1027-1029, 1998.

- [14] M. Koch, B. Stegmüller, and W. Harth, "Integrated laser-modulator-amplifier in an identical layer with two different multiquantum wells," *Electron. Lett.*, vol. 34, pp. 2330-2331, 1998.
- [15] D. D. Marcenac, A. D. Ellis, and D. G. Moodie, "80 Gbit/s OTDM using electroabsorption modulators," *Electron. Lett.*, vol. 34, pp. 101-103, 1998.
- [16] F. Devaux, D. Jahan, F. Alexandre, A. Ougazzaden, E. Vergnol, and M. Carre, "Tandem of modulators for high on/off pulse generation (-55 dB)," *Electron. Lett.*, vol. 33, pp. 1491-1492, 1997.
- [17] V. Kaman, Y. J. Chiu, T. Liljeborg, S. Z. Zhang and J. E. Bowers, "Integrated tandem traveling-wave electroabsorption modulators for > 100 Gbit/s OTDM applications", *IEEE Photonics Tech. Lett.*, vol. 12, November 2000.
- [18] K. Shimizu, T. Komiya, N. Takemura, K. Matsushita, and T. Kitayama, "A study on 10 Gb/s RZ transmitter with automatic time delay control circuits for bit-synchronous modulation," *ECOC '97 Technical Digest*, pp. 243-246, 1997.
- [19] P. V. Mamyshev, "All-optical data regeneration based on self-phase modulation effect," *ECOC '98 Technical Digest*, pp. 475-476, 1998.
- [20] B. Mikkelsen, G. Raybon, R. -J. Essiambre, K. Dreyer, Y. Su, L. E. Nelson, J. E. Johnson, G. Shtengel, A. Bond, D. G. Moodie and A. D. Ellis, "160 Gbit/s single-channel transmission over 300 km nonzero-dispersion fiber with semiconductor based transmitter and demultiplexer", *ECOC '99 Technical Digest*, PD2-3, 1999.
- [21] I. Y. Khrushchev, I. D. Phillips, A. D. Ellis, R. J. Manning, D. Nisset, D. G. Moodie, R. V. Penty, and I. H. White, "OTDM applications of dispersion-imbalanced fibre loop mirror," *Electron. Lett.*, vol. 35, pp. 1183-1185, 1999.
- [22] M. L. Nielsen, B. -E. Olsson, and D. J. Blumenthal, "Pulse extinction ratio improvement using SPM in an SOA for OTDM systems applications," *ECOC '00 Technical Digest*, paper 1.1.6, 2000.
- [23] Y. -J. Chiu, V. Kaman, P. Abraham, S. Z. Zhang, J. E. Bowers, "Low-bias and high-saturation-power traveling-wave electroabsorption modulator by using InGaAsP/InGaAsP MQW," to be presented at *LEOS '00*, paper TuX4, 2000.
- [24] R. Ludwig, U. Feiste, E. Dietrich, H. G. Weber, D. Breuer, M. Martin, and F. Kuppers, "Experimental comparison of 40 Gbit/s RZ and NRZ transmission over standard singlemode fibre," *Electron. Lett.*, vol.35, pp. 2216-2218, 1999.





## APPENDIX A

### Microwave Packaging Technology for 40 Gbit/s Applications

For electrical time division multiplexed (ETDM) systems operating at speeds of 40 Gbit/s, high-speed integrated circuits (IC) need to be packaged into modules that can handle frequencies up to 40 GHz without introducing excess parasitics and hence degrade device performance. Therefore, the overall package design should be designed according to the specific IC characteristics and simultaneously consider the transmission line type, the microwave substrate, the IC-to-transmission line and module interconnections as well as the module type.

Microstrip and coplanar waveguide (CPW) transmission lines are the most commonly utilized transmission lines for high-speed microwave applications [1]. The primary advantage of the CPW structure is that the ground plane is readily available at the surface of the substrate. This allows for an efficient and low-inductance flow of the ground from the high-speed connector interface to the IC. Furthermore, since the high-speed IC's provided by *Rockwell Science Center* had on-chip ground-signal-ground pad structures, the CPW transmission line was the fundamental choice. A typical CPW transmission line cross section is shown in Figure A1.

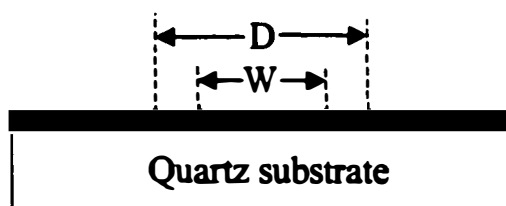


**Figure A1** Schematic of coplanar waveguide cross section.  $D$  is the ground-to-ground width and  $W$  is the signal line width.

Losses on CPW transmission lines mainly consist of skin,  $\alpha_{skin}$ , and radiation losses,  $\alpha_{rad}$ , which are related to the essential design parameters of frequency,  $f$ , material dielectric constant,  $\epsilon_r$ , and ground-to-ground spacing,  $D$ , by [2],

$$\alpha_{skin} \propto (\epsilon_r + 1)^{1/2} f^{1/2} D^{-1} \tag{A.1a}$$

$$\alpha_{rad} \propto \epsilon_r^{3/2} f^3 D^2 \tag{A.1b}$$

From Eq (A.1), it can be inferred that both losses increase with the relative material dielectric constant; therefore, a low dielectric constant material is required. Furthermore, the radiation loss becomes dominant at high frequencies compared to skin losses while it decreases with narrower signal-to-ground gaps. Figure A2 shows the frequency dependence of quartz ( $\epsilon_r = 3.8$ ) and alumina ( $\epsilon_r = 9.8$ ) CPW structures for various signal widths.

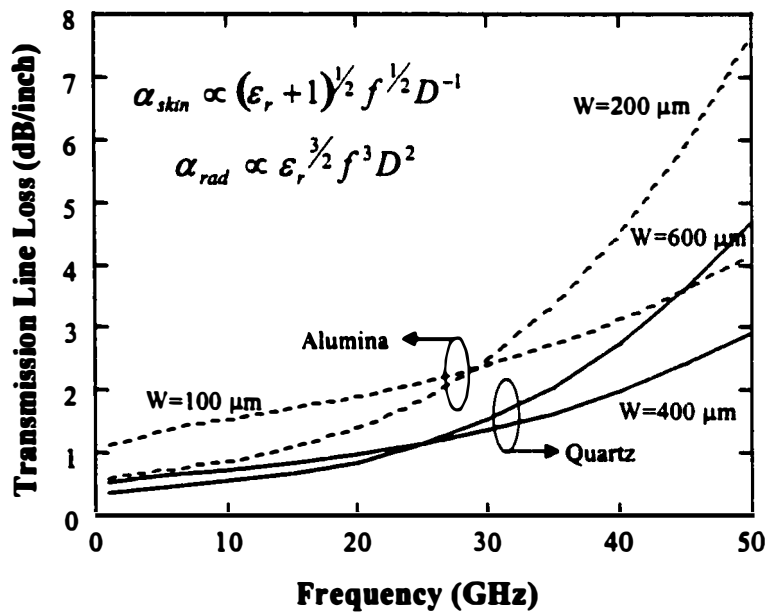


Figure A2 Frequency dependence of total microwave losses of quartz ( $\epsilon_r = 3.8$ ) and alumina ( $\epsilon_r = 9.8$ ) CPW structures for various signal widths.

From the outcome of the preceding analysis, CPW structures on quartz substrate were chosen as the transmission line substrate for the high-speed microwave packages. The CPW lines were designed for lowest loss up to 40 GHz, which resulted in 300- $\mu\text{m}$  wide lines and 40  $\mu\text{m}$  gaps on 25 mil thick quartz substrates. Since the on-chip bond pads were typically 100- $\mu\text{m}$  wide, the CPW lines were linearly tapered to 100- $\mu\text{m}$  width and 10  $\mu\text{m}$  gaps. The ability to taper transmission line width while preserving a 50  $\Omega$  impedance is another reason for the choice for the CPW structure over microstrip lines.

An important package parasitic comes from the wire bond connection between the chip and the CPW transmission line, which introduces inductance for both the signal and the ground connections. To minimize the length and the inductance of the wire bond connections, the bonding pads of the IC were aligned with the top surface of the substrate by mounting the IC in a recessed hole. Conventionally, the interconnection between the IC and the substrate are achieved by employing wire bonds. However, due to its lower inductance (in comparison to wire bonding), gold ribbon bonds were employed for the high-speed interconnections between the IC and the quartz substrate (signal and ground). The inductance (nH) for gold ribbon ribbon with length  $l$ , width  $w$ , and thickness  $t$ , is given by [2]

$$L = 0.0051 \left[ \ln \left( \frac{l}{w+t} \right) + 0.22 \left( \frac{w+t}{l} \right) + 1.19 \right] \quad (A.2)$$

For a typical length of 6 mil, width of 3 mil, and thickness of 0.25 mil, the inductance is less than 0.1 nH. Therefore, in all of the high-speed interconnections between the IC and the quartz substrate (signal and ground), gold ribbons with lengths less than 150  $\mu\text{m}$  were used.

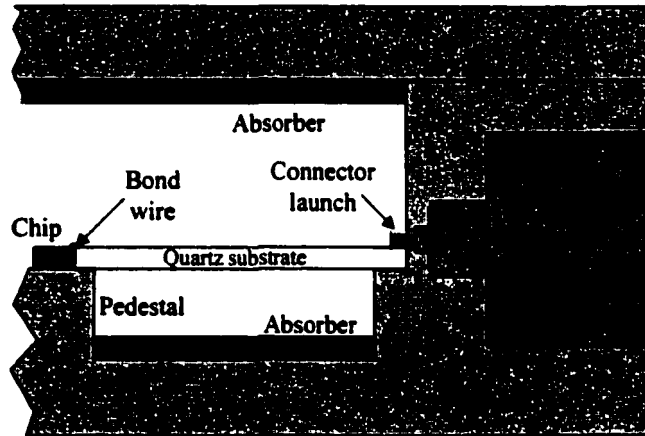


**Figure A3** Cross section of the microwave package. The chip is mounted on a pedestal while the quartz substrate is suspended over an air gap in the brass housing.

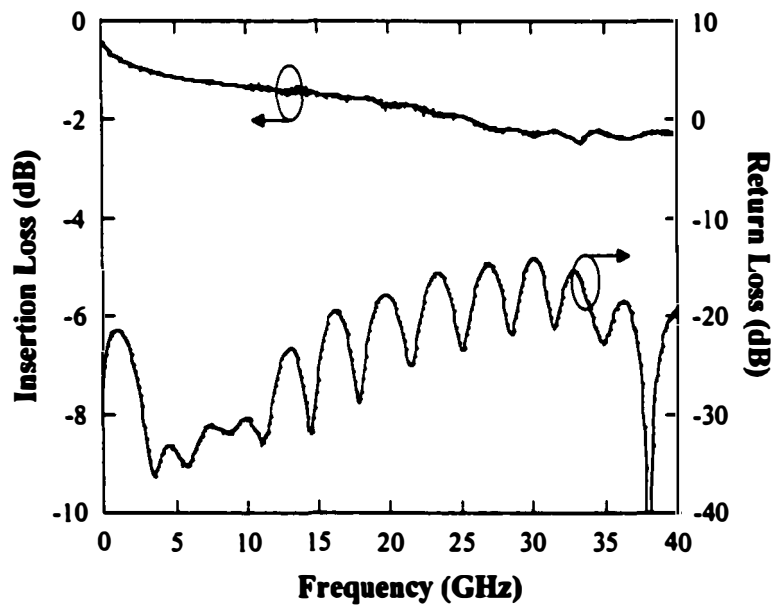


**Figure A4** Measured insertion and return losses of a microwave package with 300- $\mu\text{m}$  wide and 1-inch long CPW line on a quartz substrate.

A brass housing was used to attach the substrate and IC for good thermal conduction (Figure A3). The package dimension tolerances were within 1 mil to reduce air gaps between the housing and quartz substrate. Conductive epoxy was used to attach the IC and the substrate to the brass body. Due to the CPW structure,

the quartz substrate was suspended over an air gap with microwave absorbing material to suppress cavity resonances and parasitic microstrip modes. For the outer interconnection, K-connectors with 46 GHz bandwidths were employed. The frequency response of a packaged 300- $\mu\text{m}$  wide and 1-inch long CPW transmission line on a quartz substrate is shown in Figure A4. The measured loss is less than 2.5 dB/inch at 40 GHz while the return loss is less than  $-14$  dB.

The described microwave packaging technology was employed for the packaging of 30 Gbit/s multiplexers [3] and demultiplexers (Chapter 2) [4], 26 GHz AGC amplifiers [5], 20-kHz to 50-GHz amplifiers (Appendix B) [6], 20-kHz to 46-GHz bias-tees and a variety of low-pass filters (Appendix C). Recently, some of these modules have become commercially available.

## References

- [1] R. K. Hoffman, *Handbook of Microwave Integrated Circuits*, Boston, MA: Artech House, Inc., 1987.
- [2] R. Y. Yu, M. Reddy, J. Puzl, S. T. Allen, M. Case, and M. J. W. Rodwell, "Millimeter-wave on-wafer waveform and network measurements using active probes," *IEEE Trans. on Microwave Theory Tech.*, vol. 43, pp. 721-729, 1995.
- [3] A. K. Petersen, R. Yu, K. Runge, J. E. Bowers, and K. C. Wang, "Microwave packages for 30 Gbit/s analog and digital circuits," *Proc. of EPEP '95*, pp. 152-154, 1995.
- [4] K. Runge, P. J. Zampardi, R. L. Pierson, P. B. Thomas, S. M. Beccue, R. Yu, and K. C. Wang, "High speed AlGaAs/GaAs HBT circuits for up to 40 Gb/s optical communication," *Technical Digest GaAs IC Symposium*, pp. 211-214, 1997.
- [5] R. Yu, S. Beccue, P. J. Zampardi, R. L. Pierson, A. Peterson, K. C. Wang, and J. E. Bowers, "A packaged broad-band monolithic variable gain amplifier implemented in AlGaAs/GaAs HBT technology," *IEEE J. of Solid-State Circuits*, vol. 31, pp. 1380-1387, 1996.
- [6] V. Kaman, T. Reynolds, A. Peterson, and J. E. Bowers, "A 100-kHz to 50-GHz traveling-wave amplifier IC module," *IEEE Microwave and Guided Wave Lett*, vol. 9, pp. 416-418, 1999.



## APPENDIX B

### Design of 20-kHz to 50-GHz Amplifier IC Modules

Baseband amplifiers used as modulator drivers, receiver pre-amplifiers and post-amplifiers are key components for the currently considered 40 Gbit/s electrically time division multiplexed (ETDM) multi-wavelength optical communications systems. A linear response with little magnitude variation and a constant group delay over a broad bandwidth is essential for low bit error rates with long pattern lengths. Amplifiers with these characteristics have been demonstrated in various integrated circuit (IC) technologies (see for example [1-3]). The packaging of high-speed IC's is a real challenge since the overall package parasitics (the transmission line, discontinuities, wire bonds and lumped elements used in the module) become significant at high frequencies and can severely limit the performance of the broadband IC being packaged. Some very impressive high-speed modules have been demonstrated for in-house IC's, either by optimizing the module for the given IC [4-6], or by designing the IC according to the known package parasitics [7, 8].

This Appendix describes packaging techniques for reducing the overall insertion losses as well as the design of the external drain bias circuitry to extend the low-frequency cutoff of a commercially available traveling-wave amplifier [9] down to 20 kHz while maintaining gain-flatness over a broad bandwidth. These packaged modules were used as modulator drivers and receiver amplifiers in the 30 Gbit/s ETDM optical transmission system described in Chapter 2 [10].

#### ***B.1 IC Characteristics***

The frequency response for on-wafer measurements and other characteristics for the commercial 2-to-50 GHz amplifier are given in [11].



Bonding pads are provided to allow the amplifier to operate at frequencies lower than 2 GHz and to supply the drain and gate biases by means of external circuit components. However, since the output of the amplifier is directly connected to the drain bias pad, any parasitic coupling in the drain bias circuitry reflects as resonances and frequency response deterioration. In addition to these constraints, the input and the output of the amplifier need to be externally ac-coupled without introducing excess insertion loss.

### ***B.2 Package Design***

A coplanar waveguide (CPW) transmission line was chosen for the ease of providing a low-inductance ground between the chip and the surface ground of the substrate. The details of the quartz substrate as well as general microwave packaging are presented in Appendix A. The 3350- $\mu\text{m}$  long identical substrates used at the input and the output of the amplifier were designed to have minimum insertion and return losses. The photograph of the packaged IC is shown in Figure 2.6 (Chapter 2).

An important package parasitic comes from the wire bond connection between the chip and the CPW transmission line, which introduces inductance for both the signal and the ground connections. It was shown in [7] that this parasitic could be reduced by designing the IC according to the outer bonding wire inductance. However, this technique is not possible for the packaging of a commercial IC; therefore, an optimization of this interconnection is required. It was experimentally observed that gold ribbon with a width of 75  $\mu\text{m}$  has less inductance than the conventionally used wire bonds. The bonding pads of the IC were aligned with the top surface of the substrate to minimize the length and the inductance of the ribbon. The length of the ribbons was approximately 150  $\mu\text{m}$  long with an estimated inductance of less than 1 nH/mm.

The ac-coupling of the input and the output of the amplifier are conventionally achieved by mounting a surface mount dielectric (SMD) capacitor across a gap on the signal line. However, since broadband (20 kHz to 50 GHz) SMD's are currently commercially unavailable, a parallel combination of a 180 pF dielectric capacitor (di-cap) and a 100 nF SMD was chosen (Figure B1(a)). In order to simulate the input and output substrates simultaneously, a pair of the capacitor combination was epoxied on a 7-mm long CPW line. Frequency response measurements showed that there was about 2.4 dB extra insertion loss due to the two gaps and the capacitor combinations at 40 GHz. In order to eliminate the discontinuities on the CPW, the module was designed such that the capacitors would be placed directly under the K-connector launch (Figure B1(b)). This new design improved the insertion loss by 1 dB at 40 GHz and allowed for slightly shorter CPW lines.

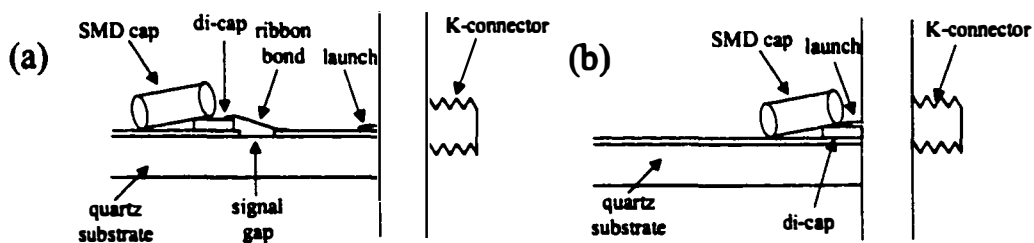


**Figure B1** Illustrative schematic diagrams of different ac-coupling schemes: (a) capacitor combination mounted on the signal line next to a gap. Ribbon bonds are used to connect the capacitor and the signal line over the gap. (b) Capacitor combination mounted under the K-connector launch, thereby eliminating the gap (signal line discontinuity) and the ribbon bonds.

A similar parallel configuration of capacitors was connected to the low-frequency extensions of the amplifier. The parasitics of the capacitors or the gold ribbon were not seen to be significant on the frequency response of the amplifier. However, at frequencies below 2 GHz, a gain rise was caused due to the increase in the drain termination resistor value from 50  $\Omega$  to 65  $\Omega$  (Figure 1 in [11]). This is overcome in the drain bias circuitry as will be described in the following section.

### B.3 Drain Bias Circuit Design

The challenge of the drain bias circuit design is to use commercial components (with limited bandwidth and uncertain parasitics) while also incorporating an external resistor to reduce the low-frequency gain; it is essential that the whole circuit looks like an open from the output pad up to 50 GHz. This design turned out to be the most crucial aspect of the package since any coupling of the parasitics resulted in huge resonances in the frequency response of the module. The circuit schematic that gave a consistent flat response for a broad bandwidth is shown in Figure B2. The inductor/resistor combination L1/R1 through L4 ensures gain-flatness from 20 kHz to 2 GHz. The components were chosen by simulation to minimize any resonance between a pure inductor and the preceding parasitic capacitance. In order to minimize the coupling between the ribbon inductance (L6) and its preceding parasitic capacitance (which resonates strongly in the GHz range), an inductor with a high self-resonating frequency and a thin-film resistor with minimal parasitics and a small bonding pad were used. The purpose of the R5 thin-film resistor was to reduce the low-frequency gain described in the preceding section. The ribbon length of 2.5 mm was very critical for the high frequency (>2 GHz) response of the module. It was chosen to be long enough to act as a broadband high-frequency inductor, but short enough to shift the resonance due to the preceding parasitic capacitance out of the operational bandwidth.

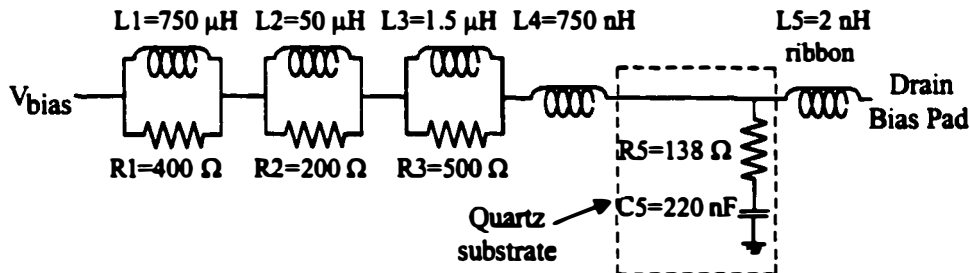


**Figure B2** Drain bias circuitry used for biasing the amplifier. R5 is the low-frequency gain reduction thin-film resistor patterned on a quartz substrate.

### ***B.4 Performance of Packaged Amplifiers***

The measured gain and return losses for the module are shown in Figure 2.7 (Chapter 2). The gain is at an average of 8.5 dB with a gain-flatness within  $\pm 1.5$  dB from 20 kHz to 50 GHz. The packaged amplifier's response is in good agreement with the chip performance with the exception of a resonance at 45 GHz and a deterioration of the return losses. The resonance around 45 GHz is due to the bandwidth limit of the K-connectors used, which will be improved by using V-connectors. The return loss should also be improved once broadband capacitors for ac-coupling are available. The amplifier modules were used as modulator drivers and receiver post-amplifiers in the 30 Gbit/s ETDM transmission experiment [10]. The 30 Gbit/s eye diagrams for the input and the  $3 V_{pp}$  output of three cascaded amplifier modules are shown in Figure 2.8 (Chapter 2). No significant degradation of the eye is observed. Bit error rate measurements confirmed this with error-free operation for input signals above - 22 dBm.



**Figure B3** Picture of a 20-kHz to 50-GHz amplifier module.

### **References**

- [1] S. Kimura, Y. Imai, S. Yamaguchi and K. Onodera, "0-56 GHz GaAs MESFET gate-line-division distributed baseband amplifier IC with 3D transmission lines," *Electron. Lett.*, vol. 33, pp. 93-95, 1997.

- [2] Z. Lao, A. Thiede, U. Nowotny, H. Lienhart, V. Hurm, M. Schlechtweg, J. Hornung, W. Bronner, K. Kohler, A. Hulsmann, B. Raynor and T. Jakobus, "40-Gb/s high-power modulator driver IC for lightwave communication systems," *IEEE J. of Solid-State Circuits*, vol. 33, pp. 1520-1526, 1998.
- [3] C. J. Madden, R. L. Van Tuyl, M. V. Le and L. D. Nguyen, "A 17 dB gain, 0.1-70 GHz InP HEMT amplifier IC," *ISSCC '94 Technical Digest*, pp. 178-179, 1994.
- [4] A. K. Petersen, R. Yu, K. Runge, J. E. Bowers and K. C. Wang, "Microwave packages for 30 Gbit/s analog and digital circuits," *EPEP '95 Technical Digest*, pp. 152-154, 1995.
- [5] R. Yu, S. Beccue, P. J. Zampardi, R. L. Pierson, A. Petersen, K. C. Wang and J. E. Bowers, "A packaged broad-band monolithic variable gain amplifier implemented in AlGaAs/GaAs HBT technology," *IEEE J. of Solid-State Circuits*, vol. 31, pp. 1380-1387, 1996.
- [6] Y. Imai, T. Otsuji, E. Sano and Y. Umeda, "40-Gb/s IC and packaging technologies for future lightwave communications," *Proc. SPIE*, vol. 3038, pp. 186-197, 1997.
- [7] R. Ohhira, Y. Amamiya, T. Niwa, N. Nagano, T. Takeuchi, C. Kurioka, T. Chuzenji and K. Fukuchi, "A high-sensitivity 40-Gbit/s optical receiver using packaged GaAs HBT-IC's," *OFC '98 Technical Digest*, pp. 155-156, 1998.
- [8] H. M. Rein and M. Moller, "Design considerations for very-high-speed Si-bipolar IC's operating up to 50 Gb/s," *IEEE J. of Solid-State Circuits*, vol. 31, pp. 1076-1090, 1996.
- [9] V. Kaman, T. Reynolds, A. Peterson, and J. E. Bowers, "A 100-kHz to 50-GHz traveling-wave amplifier IC module," *IEEE Micro. and Guided Wave Lett.*, vol. 9, pp. 416-418, 1999.
- [10] V. Kaman, S. Z. Zhang, A. J. Keating and J. E. Bowers, "High-speed operation of travelling-wave electroabsorption modulator," *Electron. Lett.*, vol. 35, pp. 993-995, 1999.
- [11] Hewlett Packard Co., "2-50 GHz Distributed Amplifier Technical Data", *Communication Components Designer's Catalog*, pp. 6-40 – 6-46, 1997.

## APPENDIX C

### High-Speed Microwave Package Examples

The microwave packaging technology described in Appendix A was also used for the packaging of various electrical devices, such as 20-kHz to 46-GHz bias-tees, low-pass filters, and 20 Gbit/s 2:1 multiplexers as well as opto-electronic devices including prototype 30 GHz receivers and electroabsorption (EA) modulator modules.

#### *C.1 20-kHz to 46-GHz Bias-Tees*

High-speed bias-tees are required for supplying external bias in various parts of electrical time division multiplexed (ETDM) systems, such as at the input of EA modulators and output of receivers. It is imperative that the device supplies bias without attenuating or deteriorating the high-speed RF signal. Therefore, low-loss 0.5-inch long coplanar waveguide (CPW) transmission lines on quartz substrate were employed (Appendix A). A parallel combination of a 180 pF dielectric capacitor (di-cap) and a 100 nF SMD was used for ac-coupling (Figure B1(a)). The packaged bias-tee module is shown in Figure C1 while its frequency



**Figure C1** Photograph of a packaged 20-kHz to 46-GHz bias-tee module. The white dashed area is shown as a close up on the right.

response is presented in Figure C2. The 3-dBe bandwidth of the bias-tee was limited by the input and output K-connectors, but should be improved beyond 50 GHz using V-connectors.

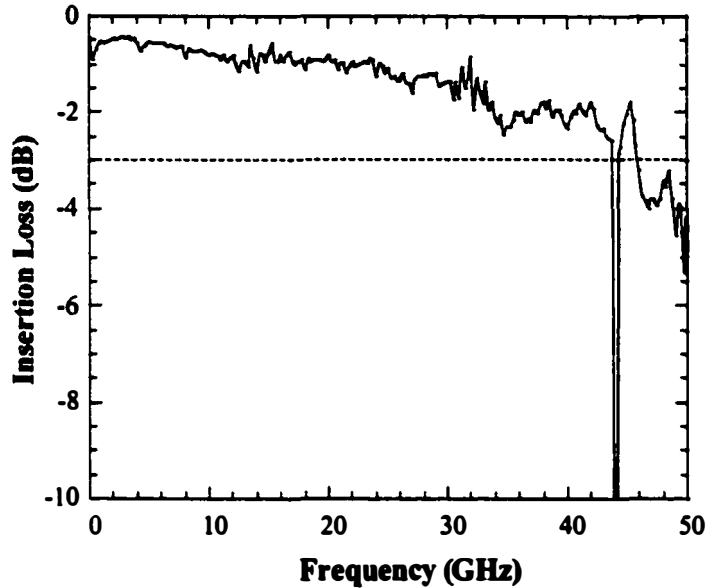


Figure C2 Measured frequency response of the packaged bias-tee module.

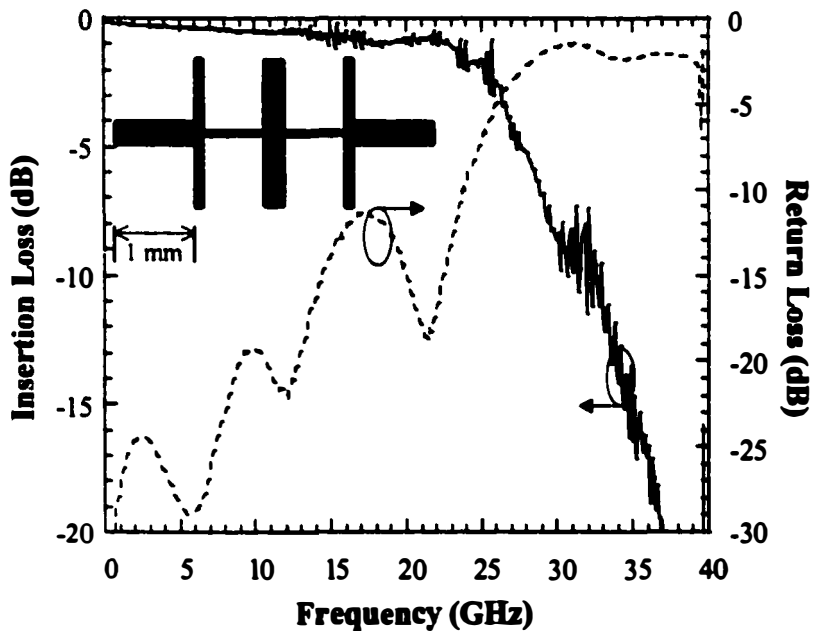


Figure C3 Measured frequency response of the packaged 26 GHz low-pass filter.

### ***C.2 Microwave Low-Pass Filters***

Several open-stub low-pass filters based on the Butterworth design [1] with 3-dBe bandwidths ranging from 5 to 26 GHz were designed and packaged. The high cutoff frequency of the 26 GHz low-pass filter requires its dimensions to be very small (inset to Figure C3). The smallest feature size is 40  $\mu\text{m}$  while the quartz substrate is 125- $\mu\text{m}$  thick. The measured insertion and return losses for the packaged 26 GHz filter are shown in Figure C3.

### ***C.3 20 Gbit/s 2:1 Multiplexer***

A 20 Gbit/s 2:1 multiplexer chip was packaged in a square module, where the chip was recessed and CPW lines on a quartz substrate were employed (Figure C4). The multiplexer requires two 10 Gbit/s inputs and a differential 10 GHz clock source. The measured 20 Gbit/s eye diagrams and data patterns are shown in Figure C5. This multiplexer was used in the 120 Gbit/s OTDM experiment in Chapter 4.

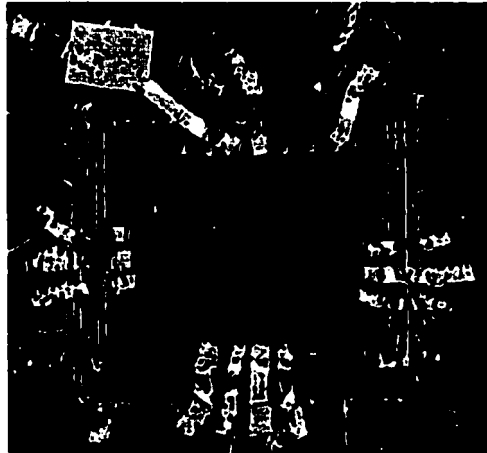


**Figure C4** Close-up picture of a packaged 2:1 20 Gbit/s multiplexer. The chip is recessed in a hole in the quartz substrate and ribbon bonding is employed for the interconnections.



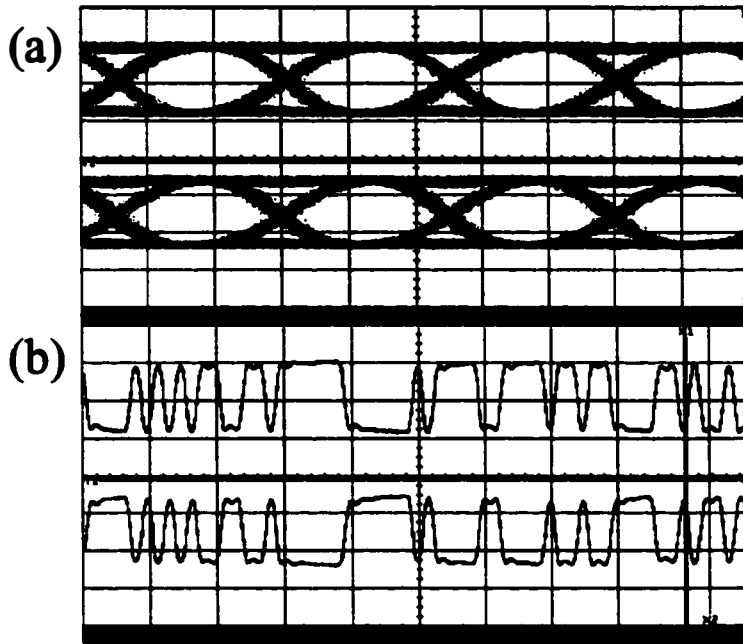


**Figure C5** Measured 20 Gbit/s (a) eye diagrams (20 ps/div), and (b) data pattern (300 ps/div) for the complementary outputs of the packaged 2:1 multiplexer.

#### ***C.4 100-kHz to 30-GHz Receiver***

A traveling-wave front-end receiver, based on a backside illuminated InGaAs/InP pin photodiode integrated with an on-chip CPW line [2], capable of operating in high-speed digital and analog optical communication systems was packaged [3]. The absorption thickness of the photodiode is 900 nm while the active area is 10  $\mu\text{m}$  in diameter. A dark current of 13 nA at the operating bias of -2.5 V was measured while the series resistance and capacitance are 30  $\Omega$  and 20 fF, respectively. The photodiode is flip-chip mounted on two capacitors and connected to a traveling-wave monolithic amplifier using a short ribbon wire (Figure C6). The output of the amplifier is ac-coupled through a surface mount dielectric capacitor. The measured bandwidth of the receiver is 30 GHz while the responsivity is 0.5 A/W at a wavelength of 1.5  $\mu\text{m}$ .

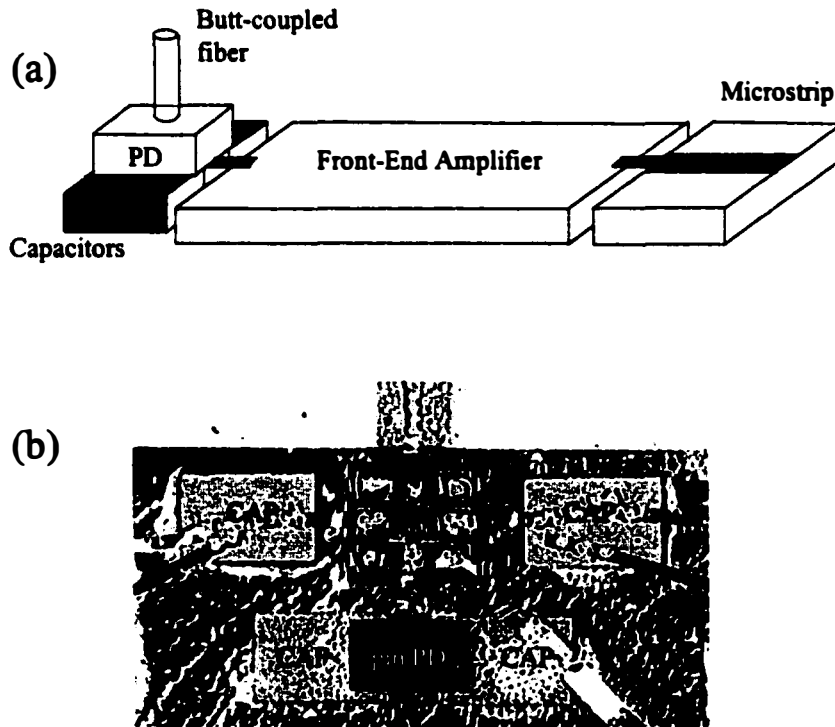


Figure C6 (a) Schematic diagram and (b) close-up picture of a packaged 30 GHz receiver.

### C.5 Electroabsorption Modulator Modules

Several prototype EA modulator [4] modules were also implemented. Figure C7 shows an example of a packaged EA modulator, where the RF signal is supplied to the EA modulator using tapered CPW lines on quartz substrate.

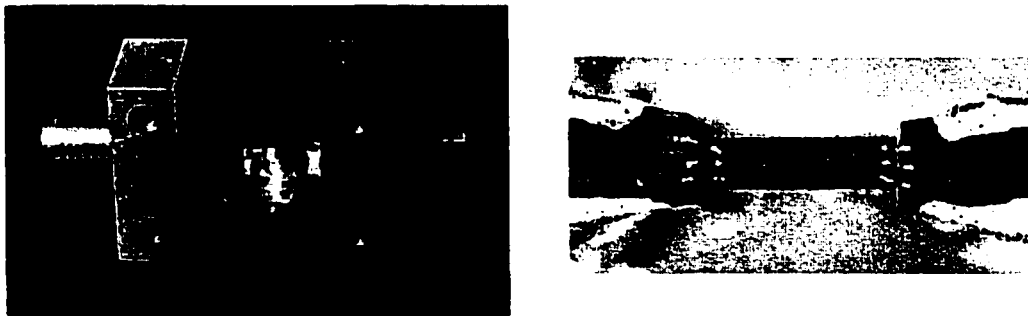


Figure C7 Photograph of a packaged electroabsorption modulator module. Tapered CPW lines are employed for the RF input and output to the modulator.

**References**

- [1] P. A. Rizzi, *Microwave Engineering Passive Circuits*, Prentice Hall, 1988.
- [2] Y. G. Wey, K. S. Giboney, J. E. Bowers, M. J. W. Rodwell, P. Silvestre, P. Thiagarajan, and G. Y. Robinson, "108-GHz GaInAs/InP p-i-n photodiodes with integrated bias tees and matched resistors," *IEEE Photonics Tech. Lett.*, vol. 5, pp. 1310-1312, 1993.
- [3] A. K. Petersen, T. Reynolds, R. Nagarajan, Y. G. Wey, J. E. Bowers, and M. Rodwell, "3-MHz-30-GHz traveling-wave optical front-end receiver," *OFC '95 Technical Digest*, pp. 157-158, 1995.
- [4] S. Z. Zhang, Y. -J. Chiu, P. Abraham, and J. E. Bowers, "25 GHz polarization-insensitive electroabsorption modulators with traveling-wave electrodes." *IEEE Photonics Tech. Lett.*, vol. 11., pp. 191-193, 1999.